Tectono-metamorphic evolution of western Maine, Northern Appalachians, USA

Volume 1

Thesis submitted by
Ioan Vasile Sanislav BSc, MSc UAIC (Romania)
in July 2009

for the degree of Doctor of Philosophy
in the School of Earth and Environmental Sciences
James Cook University, Australia

CONTENT OF VOLUME 1

STATEMENT OF ACCESS

I, the undersigned, the author of this thesis, understand that James Cook University will make it available of use within the University Library and, by microfilm or other means, allow access to other users in other approved libraries.

All users consulting this thesis will have to sign the following statement:

> *In consulting this thesis, I agree not to copy closely or paraphrase it in whole or in part without the written consent of the author; and to make proper public written acknowledgement for any assistance that I have obtained from it.*

Beyond this, I do not wish to place any restrictions on access to this thesis.

_____ _____

Ioan Vasile Sanislav July 2009

STATEMENT OF SOURCES

DECLARATION

I declare that this thesis is my own work and has not been submitted in any form for another degree or diploma at any university or other institution of tertiary education. Information derived from the published and unpublished work of others has been acknowledged in the text and a list of references is given

_____ _____

Ioan Vasile Sanislav July 2009

ELECTRONIC COPY

DECLARATION

I, the undersigned, the author of this thesis, declare that the electronic copy of this thesis provided to the James Cook University Library is an accurate copy of the print thesis submitted, within the limits of the technology available.

_____ _____

Ioan Vasile Sanislav July 2009

ACKNOWLEDGMENTS

Firstly, I would like to thank Professor Tim Bell for his seemingly boundless energy and enthusiasm in his role as supervisor. Tim gave me the opportunity to freely explore my own ideas, and has created a fantastic research environment within the SAMRI group at James Cook University. My thanks go also to dr. Mike Rubenach for all the help with monazite dating and for many discussions about metamorphic petrology. Many thanks are due to my colleagues in SAMRI for providing a very stimulating and enjoyable workplace. In particular, I would like to thank Afroz Shah, Ahmed Abu Sharib, Asghar Ali, Clement Fay, Chris Fletcher, Hui Cao, Jyotindra Sapkota, Matt Bruce, Mark Rieuwers, Raphael Quentin de Gromard and Shyam Ghimire, with whom I enjoyed countless lively discussions about various aspects of geology.

I wish to express my gratitude to the all the wonderful people that I met during my fieldwork in Maine.

Funding for this project was provided by a James Cook University Earth Sciences Scholarship, and an ARC grant awarded to Tim Bell.

The staff at the Advanced Analytical Centre at James Cook University provided superb technical assistance in data collection. In particular, I would like to thank Dr Kevin Blake for his support on the electron microprobe. Darren Richardson is thanked for his help in preparing thin sections.

I would also like to thank my mum, Mariana, my dad, Viorel, and my brother, Claudiu, for their constant support and encouragement throughout my somewhat extended stay in Townsville. Finally, I would like to thank to two special people, my wife, Oana, for the love, patience and inspiration she has given to me during the course of this work and to my grandmother, Georgina, who was always with me.

INTRODUCTION AND THESIS OUTLINE

This thesis investigates the tectono-metamorphic evolution of a portion of the Northern Appalachians, located in Western Maine, USA. The region under study is located in the contact aureole of the Mooselookmeguntic pluton, which is one of the best-documented areas in the literature on the Northern Appalachians. Although, the region under study is quite small, the results presented in this thesis have considerable significance for the Maine-New Hampshire portion of the Northern Appalachians as well as for similar terranes in other parts of the world. The thesis integrates results from detailed microstructural measurements with electron microprobe analysis (EPMA) dating of monazite grains preserved as inclusions in staurolite porphyroblasts (and the matrix), thermobarometry and phase diagram modeling. This reveals a lengthy tectono-metamorphic history tightly associated with plutonism.

The thesis consists of four sections, each a stand-alone body of work intended for publication in international journals. The sections are ordered such that they progress in a logical fashion. Volume 1 contains the text and reference list, whilst Volume 2 contains the figures and appendices. The first section provides a detailed description of the porphyroblast microstructures in the contact aureole of the Mooselookmeguntic pluton. It uses foliation inflection/intersection axis measurements in garnet and staurolite porphyroblasts (FIAs) to show that without 3D measurements of these microstructures, it is impossible to accurately correlate deformation and metamorphism across a region. Sections B and C use EPMA dating of the monazite grains included in staurolite porphyroblasts to reveal longer tectono-metamorphic histories in Western Maine and the

Colorado Front Range than was previously believed. The last section integrates the results obtained from the previous chapters with thermobarometry and phase diagram modeling to constrain the PT evolution of the region under study. This is part of a larger research project in the Northern Appalachians undertaken by the Structural and Metamorphism Research Institute (SAMRI) at James Cook University. Shyam Ghimire, another PhD student in the SAMRI group at James Cook University is working on rocks collected from an area located about 3 kms south of the region under study. So far, he has obtained similar results to those presented in this thesis.

Porphyroblast inclusion trails provide a unique opportunity to examine how the small-scale geometries that form prior to porphyroblast growth begin to partition through the rock because these large crystals nucleate and/or grow at the initiation of deformation (Spiess and Bell, 1996). Bell (1981) suggested that porphyroblasts commonly nucleate and grow in sites of progressive coaxial shortening. Anastomosing zones of combined non-coaxial shortening and shearing develop around these zones and when they intensify and interact with the growing porphyroblasts, growth ceases. He further argues that growth does not recommence until a new deformation occurs at high angle to the earlier one allowing new growth to occur in porphyroblast strain shadows (e.g., Bell and Rubenach, 1983; Bell et al., 1986; Bell and Hayward, 1991).

If this is correct then porphyroblasts trap and preserve as inclusion trails microstructures that are destroyed in the matrix by the same event or during subsequent deformations. Therefore, examining the geometry of the inclusion trails in porphyroblasts and their relationship to the surrounding matrix should provide important information on the processes occurring early in the local deformation history of multiply deformed

metamorphic terranes and reveal a tectonic record that is much more complete than that preserved in the matrix (e.g. Cihan and Parsons, 2005; Rich, 2006). This thesis seeks to test this hypothesis.

Identification of porphyroblast micro-fabrics using conventional methods has been accomplished by many studies (e.g., Zwart, 1962; Vernon et al., 1993). Such methods usually provide a very simple history because, thin sections cut perpendicular to the matrix foliation reveal very little inclusion trail complexity (e.g., Cihan, 2004). Studies using the relatively new approaches described herein provide much more extensive deformation and metamorphic histories and show that deformation processes are much more complex than previously believed (e.g., Bell et al., 2004; Bell and Newman, 2006). Measuring FIAs (Bell et al., 1995) and the concept of "*reactivation of bedding during successively formed foliations*" (Bell et al., 2004) provide the backbone of this thesis. Measuring FIAs involves cutting 8 to 10 vertically-oriented thin sections per sample. Although this requires a lot of effort, it allows an order of magnitude more rock to be observed in 3-D. This approach proves to be vital for understanding how to integrate deformation and metamorphic processes, as their inter-relationship cannot be quantitatively accessed in any other way.

Through FIA analysis the same generation of porphyroblasts can be correlated across a region. FIAs form at high angle to the direction of main bulk shortening so that studying the orientation of the inclusion trails has regional-scale significance. EPMA dating of monazite grains included in staurolite porphyroblasts that contain one or a succession of different FIA trends allows the absolute timing of a specific deformation and metamorphic event to be accurately constrained. In this way mineral associations that

characterize a FIA event can be discerned and the PT conditions responsible for forming these mineral associations can be deducted.

Section A of the thesis is mainly meant as an introduction to the complex deformation and metamorphic history of the region under study as revealed by porphyroblast inclusion trails microstructures. The FIAs were measured in both garnet and staurolite porphyroblasts and their relative timing were established based on microstructural and textural relationships. The orientations of foliations preserved as inclusion trails in staurolite porphyroblasts were measured as pitches and plotted on stereo nets to obtain 3D orientations from which similar trends with FIAs were obtained. These data are discussed in terms of their significance for the regional deformation and metamorphic history as well as the effect of partitioning of deformation on porphyroblast microstructures and their relationship to the surrounding matrix.

Section B uses EPMA dating of monazite grains included in staurolite porphyroblasts to constrain the absolute timing of the development of the succession of FIAs. The results presented in this part of the thesis have an extraordinary impact on the regional tectono-metamorphic history by suggesting that tectonism and plutonism in the Northern Appalachian extended over a much larger period of time than previously believed. The implications for deformation, metamorphism, and plutonism are discussed.

Section C of the thesis provides an example from two spatially and temporally separated terranes, the Paleozoic West Central Maine and the Proterozoic Colorado Front Range, where multiple periods of staurolite growth occurred over a lengthy period of time.

The similarities between the two regions indicate that such processes may be common for most of the orogenic belts. My contribution to this section is 50% in both data collection and concepts.

Section D of the thesis combines the results obtained from the previous sections with phase diagram modeling and thermobarometry to infer PT-d-t paths in Western Maine. The computer software Thermocalc was used to model mineral stability fields for the mineral assemblages present in the contact aureole of the Mooselookmeguntic pluton. The effect of changing bulk composition on the phase diagram topology was also investigated.

References

Bell, T. H., and Hayward, N., 1991. Episodic metamorphic reactions during orogenesis: the control of deformation partitioning on reaction sites and reaction duration. *Journal of Metamorphic Geology*, **9**, 619–640.

Bell, T. H., and Johnson, S. E., 1989. Porphyroblast inclusion trails: the key to orogenesis. *Journal of Metamorphic Geology*, **7**, 279–310.

Bell, T. H., and Newman, R., 2006. Appalachian orogenesis: the role of repeated gravitational collapse. In: *Butler, R., Mazzoli, S. (Eds.), Styles of Continental Compression. Special Papers of the Geological Society of America*, **414**, 95-118.

Bell, T. H., and Rubenach, M. J., 1983. Sequential porphyroblast growth and crenulation cleavege developement during progressive deformation. *Tectonophysics*, **92**, 171–194.

Bell, T. H., 1986. Foliation development and refraction in metamorphic rocks: reactivation of earlier foliations and decrenulation due to shifting patterns of deformation partitioning. *Journal of Metamorphic Geology*, **4**, 421–444.

Bell, T. H., Fleming, P. D., and Rubenach, M. J., 1986. Porphyroblast nucleation, growth and dissolution in regional metamorphic rocks as a function of deformation partitioning during foliation development. *Journal of Metamorphic Geology*, **4**, 37–67.

Bell, T. H., Forde, A., and Wang, J., 1995. A new indicator of movement direction during orogenesis: measurement technique and application to the Alps. *Terra Nova*, **7**, 500–508.

Bell, T. H., Ham, A. P., and Kim, H. S., 2004. Partitioning of deformation along an orogen and its effects on porphyroblast growth during orogenesis. *Journal of Structural Geology*, **26**, 825-845.

Bell, T.H., 1981. Foliation development: the contribution, geometry and significance of progressive bulk inhomogeneous shortening. *Tectonophysics*, **75**, 273–296.

Cihan, M., 2004. The drawbacks of sectioning rocks relative to fabricorientations in the matrix: a case study from the Robertson River Metamorphics (North Queensland, Australia). *Journal of Structural Geology*, **26**, 2157–2174.

Cihan, M., and Parsons, A. 2005, The use of porphyroblasts to resolve the history of macro-scale structures: An example from the Robertson River Metamorphics, north-eastern Australia: *Journal of Structural Geology*, 27 p. 1027– 1045

Rich, B.H., 2006. Permian bulk shortening in the Narrangansett Basin of southeastern New England, USA. *Journal of Structural Geology*, **28**, 682-694.

Spiess, R., and Bell, T. H., 1996. Microstructural controls on sites of metamorphic reaction: a case study of the inter-relationship between deformation and metamorphism. *European Journal of Mineralogy*, **8**, 165-186.

Vernon, R.H., Paterson, S.R., and Foster, D., 1993. Growth and deformation of porphyroblasts in the Foothills terrane, central Sierra Nevada, California: negotiating a microstructural minefield, *J. Metamorph. Geol.* **11**, 203–222.

Zwart, H. J., 1962. On the determination of polymetamorphic mineral associations, and its application to the Bosost area (Central Pyrenees). *Geologische Rundschau*, **52**, 38-65.

- SECTION A -

PARTITIONING OF DEFORMATION IN THE CONTACT AUREOLE OF THE MOOSELOOKMEGUNTIC PLUTON (WESTERN MAINE, USA) AND ITS EFFECT ON PORPHYROBLAST GROWTH AND INCLUSION TRAIL/MATRIX RELATIONSHIPS

- SECTION A -

PARTITIONING OF DEFORMATION IN THE CONTACT AUREOLE OF THE MOOSELOOKMEGUNTIC PLUTON (WESTERN MAINE, USA) AND ITS EFFECT ON PORPHYROBLAST GROWTH AND INCLUSION TRAIL/MATRIX RELATIONSHIPS

ABSTRACT

Multiply-deformed schists in Western Maine were multiply metamorphosed under lower-amphibolite-facies conditions during the Acadian orogeny. Most of the many deformations were partitioned on a regional scale into zones dominated by coaxial bulk shortening and surrounded by anastomosing zones of non-coaxial shortening and shearing. Protection provided by plutons emplaced at different times during this history resulted in the matrix foliation orientation varying with respect to pluton proximity as well as to the regional-scale structures. Garnet and staurolite porphyroblasts grew episodically many times as deformation was partitioned and repartitioned during successive tectonic events. A succession of five FIAs trending ESE-WNW, N-S, E-W, ENE-WSW and NE-SW were measured from both garnet and staurolite porphyroblasts. Thus at least five periods of growth are inferred for these phases, in contrast with only two periods of growth as was previously believed. Pitch measurements of inclusion-trail orientation in staurolite porphyroblasts revealed that the foliations preserved as inclusion trails have similar trends with FIAs and are steeply dipping. Well-defined inclusion trails revealed complex porphyroblast-matrix relationships resulting from deformation and porphyroblast growth both being partitioned very heterogeneously across the region. The deformation and metamorphism were totally synchronous, and the partitioning of the deformation at the scale of a porphyroblast always controlled the location of its growth.

Keywords: deformation partitioning; porphyroblasts; inclusion trails; FIAs; foliations.

1. INTRODUCTION

Consistent successions of FIAs (foliation inflection/intersection axes preserved in porphyroblasts) across large-scale regions have revealed that well-developed matrix foliations are multiply reused and reactivated many times during deformation (Bell et al., 2004, 2005; Ham and Bell, 2004). Consequently, such foliations generally preserve very little of the total deformation and metamorphic history (e.g., Bell and Newman, 2006; Sayab, 2006, 2007). In the vicinity of the Mooselookmeguntic Pluton in Maine, deformation was partitioned very heterogeneously. This suggests that some portions of the many foliations are preserved locally within the matrix due to the strain-shadow effects of plutons, local competency contrasts and fold hinges. Seven tectono-metamorphic zones have been discerned based on differences in matrix foliation orientations, microstructural features, prograde mineral assemblages, and retrogressive effects that match regional changes in structural trend. Discernment of these zones suggests that there has been variation with time in the partitioning of the deformation on a regional scale and that relics of different periods in this process have been preserved from zone to zone. Occurrences of large outcrops containing several different FIAs from a regional succession that lie in proximal samples suggest that deformation partitions very heterogeneously at the scale of a porphyroblast (Bell et al., 1998). Regional changes in total FIA distribution suggest that partitioning occurs at this scale as well (e.g., Bell et al., 2004). Therefore, it should come as no surprise that such variations are also preserved at a macro scale in the matrix across a mapped area. This paper examines examples of this phenomenon and their significance for both deformation and metamorphic processes.

2. GEOLOGICAL SETTING

The Central Maine Belt of north central Maine, USA (Fig. 1), it is bordered to the NW by Neoproterozoic basement rocks of the Bronson Hill Belt. To the SE, there is a transition from the Central Maine Belt through the Norumbega Shear Zone into the Avalon Composite Terrane. The Central Maine Belt of north central Maine, USA, is composed of a succession of Siluro-Devonian turbidites that form the Rangeley Stratigraphic Sequence. It was metamorphosed and deformed during the Acadian orogeny (Bradley et al., 1998). Two types of structural zones have been identified within this belt: NE-SW-trending zones of apparent flattening or high strain, and zones of apparent constriction or low strain (Brown and Solar, 1998a,b, 1999; Solar and Brown, 1999; Solar and Brown, 2001a).

The metamorphism occurred at low pressures and high temperatures with partial melting at higher grades forming migmatites within the Tumbledown and Weld anatectic domains (Brown and Solar, 1998a). The metamorphic grade increases from greenschist-facies in the central part of the region, to upper-amphibolite facies in the south and north east (Guidotti, 1989). Three metamorphic events have been described. Two of them, M1 and M2, are regional-scale events and the third one, M3, was regarded as pluton-driven metamorphism (Holdaway et al., 1988; De Yoreo et al., 1989; Guidotti and Holdaway, 1993; Guidotti and Johnson, 2002; Johnson et al., 2003). In the study area (Fig. 2), rocks affected by M2 are also affected by the M3 event, which occurred at higher pressure than M2 (Guidotti and Johnson, 2002). The time difference between M2 and M3 was estimated as ~30 m.y. (Solar et al., 1998). Staurolite, andalusite, and garnet pseudomorphs are common and were attributed to the M3 thermal event that postdated the last deformation in the region (Guidotti and Johnson, 2002). Based on U-Pb data from metamorphic monazite

in staurolite schists, the age of regional metamorphism was assessed at 405 to 399 ± 2 Ma (Smith and Barreiro, 1990). The metasedimentary suites of the Rangeley Stratigraphic sequence were intruded syntectonically by Devonian plutons (Solar et al., 1998). Deformation, metamorphism, and granite crystallization were contemporaneous (Brown and Solar, 1998a, 1998b, 1999; Solar and Brown, 2001). The area described herein (Fig. 2) contains rocks of the Rangeley and Perry Mountain Formations from the Rangeley Stratigraphic Sequence. These rocks were intruded by the 389 to 370 Ma Mooselookmeguntic pluton.

3. SAMPLE DESCRIPTION

Ninety-six oriented samples were collected from the contact aureole of the Mooselookmeguntic pluton, as shown in Fig. 2. From each of these samples at least eight vertically-oriented thin sections were cut and studied under the microscope. Matrix foliations were measured in the field and from the thin sections. Table 1 shows the mineralogy of each sample and the relative timing between porphyroblasts. Seven zones were defined based on mineralogy and foliation trends.

3.1. Distribution of foliation trends

Two main types of foliation trend, with local variations, occur across Fig. 3. A steeply ESE-dipping schistosity with a pronounced NE strike is characteristic of Zone 2. Brown and Solar (1998a, 1998b) interpreted this structural fabric to result from zones of higher strain. The foliation is strongly developed and is oriented sub-parallel to the compositional layering. Relative to Zone 2 the foliation trends in Zones 1 and 7 are near orthogonal to each other; that in Zones 3 and 4 oblique, and that in zones 5 and 6 a mixture

of sub-parallel and near-orthogonal. All zones have a more gently dipping foliation than Zone 2 that might correspond to the lower strain zones of Brown and Solar (1998a, 1998b). In these zones, the foliation is less intense, usually crosscuts the layering, and has more variable strikes.

3.2. Zone 1

This zone is characterized by the mineral assemblage St+Bt+Grt±And±Crd. Staurolite is present as randomly-oriented, poikilitic, anhedral to subhedral, porphyroblasts whose size varies within and between different compositional layers in the same rock. Based on core to rim and porphyroblast-matrix relationships two generations of staurolite growth can be recognized in many samples, with some containing three stages of growth (Fig. 4) or even more. The inclusion trails preserve crenulation corresponding to stages 2 and 3 of Bell and Rubenach (1983). Garnet occurs in small amounts as anhedral to subhedral, poikilitic porphyroblasts in most samples. Andalusite is present in a few samples as large poikilitic porphyroblasts overgrowing the matrix foliation. Cordierite is almost entirely replaced by large biotite or muscovite grains that are aligned with the matrix foliation. Close to the granite, the matrix foliation has a strong WSW-ENE trend and dips moderately towards the N. Further away, it swings NNW-SSE until it strikes approximately N-S and dips toward the E (Fig. 3). Crenulations are preserved as a function of the composition of the layering rather than proximity to the pluton. Pelite-rich layers show moderate crenulation of the main foliation whereas psammitic layers exhibit little effect from this event. Elongate blades of muscovite define the matrix foliation whereas biotite mainly occurs as porphyroblasts. Straight and sigmoidal inclusion trails are also preserved throughout the zone in staurolite porphyroblasts.

3.2.1. Timing of porphyroblast growth and foliation development

Staurolite porphyroblasts commonly show two and/or three stages of growth while garnet porphyroblasts overgrew sub-horizontal and/or sub-vertical fabric. The term sub-horizontal fabric will refer to inclusion trails that have an orientation of less than 45° in thin section whereas the term sub-vertical fabric will be used for inclusion trails with an orientation higher than 45°. The true dip (in 3D) could be much higher (see the next chapters). Figure 4 shows the complex relationships between matrix and porphyroblasts inclusion trails. Following the microstructural models of Bell and Johnson (1989) and Hayward (1992), early garnet growth would have included a sub-horizontal fabric (S_{i1} in Fig. 4). The foliation labels in all figures are just informative, apply only at the scale of the thin section, and do not represent regional or local correlations.

Staurolite porphyroblasts that overgrew a similar fabric show a different asymmetry, suggesting growth over a different foliation (S_{i2}). Most staurolite and garnet growth occurred over a sub-vertical fabric (S_{i3}). This second generation of staurolite growth consistently overgrows a differently-oriented foliation (S_{i4}). Some of these foliations are preserved in the porphyroblast strain shadows (S_{e3}, S_{e4}, and S_{e5}) whereas the main matrix foliation (S_{e6}) anastomoses around pods rich in porphyroblasts. The many fabrics shown in Fig. 4 could be the result of different fabrics that successively transposed and obliterated each other, but most probably they represent the same early-formed fabric, subsequently reactivated and reoriented in superposed deformation fields.

3.3. Zone 2

This zone is characterized by considerable retrogression that culminates in perfectly pseudomorphed staurolite and/or garnet porphyroblasts, although the degree and extent of this varies greatly and randomly across this zone. The mineral assemblages in these rocks are characterised by the presence of St+Grt+Bt+Ms+Chl. No traces of andalusite and/or cordierite have been found. Complete or incipient pseudomorphs after staurolite can be found proximal and distal to the granite. The types of staurolite replacement consist of:

1. Incipient – staurolite is present as large euhedral to subhedral porphyroblasts. The margins are slightly replaced (Fig. 5) by fine-grained Ms + Bt aggregates. The original crystallographic faces can be easily recognized.
2. Partial pseudomorphs – the mineral is present only as a remnant of a poikilitic core. No crystallographic faces are preserved (Fig. 6a).
3. Blocky remains – this type of pseudomorph consists of blocky remains without any crystal shape or with a well-defined crystal shape. Both types are present as pseudomorphs in a fine-grained Ms+Bt±Chl aggregate.
4. Total pseudomorphs – little or no trace of the original mineral is preserved (Fig. 6b). Commonly, only the shape of the pseudomorph identifies the pseudomorphed mineral.

Garnet porphyroblasts are less affected by retrogression than staurolite. Usually, garnet is present in the matrix as subhedral to anhedral crystals. Partial pseudomorphs of garnet are common, but only a few complete pseudomorphs have been identified. Garnet is replaced by chlorite, which grows preferentially parallel to dodecahedral faces (Fig. 6c,d).

Biotite is present in the matrix as a porphyroblastic phase or replaces staurolite porphyroblasts together with muscovite and chlorite. Matrix biotite in some samples is almost entirely replaced by chlorite. Chlorite is present in all samples from this zone in variable proportions. It grew randomly across the matrix foliation and/or participated in retrograde reactions with staurolite, garnet and biotite. Muscovite is present in the matrix as elongate blades and in pseudomorphs after staurolite as fine-grained crystals. All samples show a strong foliation sub-parallel to the bedding (Fig.7). The schistosity in this zone has a SSW-NNE trend with a slight change to NNW-SSE towards the pluton. The dip direction is generally ESE to E. Weak crenulation of the regional foliation is present in micaceous layers. The matrix foliation is deflected at porphyroblasts margins (Fig. 5). The continuity of the inclusion trails in staurolite porphyroblasts with the matrix foliation is uncertain in many samples because the margin of the mineral has been pseudomorphed by Ms+Bt±Chl.

3.3.1. Timing of porphyroblast growth and foliation development

The pervasive regional foliation in this zone can be used as a reference frame to assess the relative timing of porphyroblast growth and foliation development. Figure 8a and 8b shows the relationship between garnet porphyroblasts that overgrew a sub-horizontal foliation S_{i1} and the regional foliation marked here as S_{e2}. The truncation between S_{i1} and S_{e2} suggests that garnet porphyroblasts grew early relative to S_{e2} over a foliation that predates the regional foliation. A second generation of garnet porphyroblast (Fig. 8c,d) showing sub-vertical inclusion trails S_{i2}, which were possibly synchronous with S_{e2}, is more common. In samples showing the second generation of garnet growth the

regional foliation S_{e2} is slightly crenulated by a sub-horizontal axial plane cleavage S_{e3}. Near the porphyroblast margins this crenulation intensifies and differentiates.

3.4. Zone 3

Retrograde reactions in this zone are less common than in zone 2. These rocks are dominated by the assemblage Grt+Bt±St,Chl. Garnet is the main porphyroblastic phase and only a few remains of staurolite are present as pseudomorphs. Garnet is normally poikilitic with subhedral to anhedral shapes and is locally partially altered to chlorite. An increase in modal chlorite occurs towards zone 2. Irregular aggregates of coarse-grained Bt+Ms+Chl can be found throughout this zone. Some of these aggregates preserve patches of staurolite but most do not. Ragged, irregular coarse-grained patches of muscovite could be remains of andalusite (Guidotti and Johnson, 2002), but no traces of this mineral have been observed in these rocks. Foliation in this zone is consistently NNW-SSE trending, dips NE, and is sub-parallel to the compositional layering. The matrix foliation (S_R) is well-defined and is strongly deflected against porphyroblast margins. The relationship between inclusion trails in staurolite remains and S_R was impossible to determine, but inclusion trails preserved in garnet are mainly truncated by the matrix foliation. Crenulations are present in the matrix, and the development of crenulation cleavage varies with the compositional layering.

3.4.1. Timing of porphyroblast growth and foliation development

The earliest phase of growth of garnet contains a sub-vertical S_{i1} fabric (Fig. 9a,b) truncated by a shallow dipping matrix foliation S_{e2}. A second generation of garnet overgrew a sub-horizontal S_{i2} that is sub-parallel to the matrix foliation (Fig. 9c,d). The

inclusion trails S_{i2} appear to be restricted to the garnet core, and, therefore, they may be older than the matrix foliation. The relative timing of growth of staurolite porphyroblasts could not be determined with certainty, but most probably it overgrew a sub-horizontal foliation. Locally the matrix foliation is crenulated by a weakly developed sub-vertical axial plane crenulation cleavage. In the strain shadows of some of the early porphyroblasts, a sub-vertical fabric is preserved.

3.5. Zone 4

This zone contains graphite-rich quartz lenses 3 to 10 cm long and 1 to 3 cm wide, parallel to the principal foliation. Their sigmoidal shape suggests a top-to-the-west shearing component during development of a late crenulation cleavage (visible in the bottom half of Fig. 10). The rocks are characterized by the assemblage St+Grt+Bt±And,Sill,Chl. Poikilitic, subhedral to anhedral, staurolite porphyroblasts show the effects of prograde and retrograde reactions. Both reactions appear to have occurred in the same sample. Prograde breakdown of staurolite to large Ms+Bt was followed by fine- to medium-grained Ms+Bt replacement of staurolite. The resulting pseudomorphs contain two types of staurolite relics:

1. poikilitic remains in a groundmass of Ms+Bt and/or
2. euhedral blocky remnants in a similar groundmass.

In some rocks, a second generation of staurolite overgrows cores with differently oriented and truncated inclusion trails (Figs. 11 and 12). In some of these samples, poikilitic andalusite replaces the second generation of staurolite, leaving the cores unaltered. This andalusite is very poikiloblastic and overgrows the matrix foliation. Partial

and complete pseudomorphs of medium grained Ms+Bt after andalusite are common. Sillimanite needles have subsequently grown though andalusite and/or biotite porphyroblasts. Garnet is present in all samples as subhedral to anhedral porphyroblasts. Chlorite is present in the matrix as randomly-oriented crystals, but locally replaces biotite and staurolite. The matrix foliation varies from NNW-SSE to SW-NE trends, and dips towards the NE and SE respectively. Crenulations are well-developed and are asymmetric. Inclusion trails in staurolite porphyroblasts are truncated and/or curve strongly into the matrix.

3.5.1. Timing of porphyroblast growth and foliation development

A sub-horizontal foliation S_{i1} is locally preserved in garnet and staurolite porphyroblasts (Fig. 11). This first generation of staurolite shows growth rims with a steeply-dipping internal fabric (S_{i2}) that appears to be continuous with the external foliation (S_{e2}). To the NW, these steeply-dipping foliations (S_{e2}) may have been overgrown by a second generation of garnet and cores of staurolite porphyroblasts (Fig. 12) surrounded by rims with different trending inclusion trails (S_{i3}).

3.6. Zone 5

Very little retrogression has occurred in zone 5. Chlorite is the only mineral phase that indicates the presence of any retrogression. This zone is characterized by the assemblage St+Grt+Bt±Sill,And,Chl. Staurolite porphyroblasts have a poikilitic, irregular, subhedral to anhedral aspect. They are locally present as blocky irregular crystals in a groundmass of coarse-grained Ms+Bt. The texture and morphological character of the latter minerals suggests a prograde breakdown of staurolite. The appearance of sillimanite

in association with these Ms+Bt aggregates in some samples further supports prograde breakdown of the staurolite. The presence of chlorite, as an irregular intergrowth with biotite in the matrix and rarely in contact with staurolite, suggests a retrograde path for this zone after reaching the sillimanite zone. Garnet is subhedral to anhedral and locally has a poikilitic aspect. Some garnet porphyroblasts are surrounded by biotite flakes, suggesting prograde breakdown to biotite. Unaltered andalusite is present in a few samples as large anhedral, poikilitic porphyroblasts overgrowing the matrix foliation. The matrix foliation in this zone has a strong NW-SE trend and dips NE. It is sub-parallel to the compositional layering and is cross-cut by an axial-plane crenulation cleavage (Fig. 13). Crenulations are very common in mica-rich layers. Inclusion trails in staurolite porphyroblasts appear to be truncated by the matrix foliation; many inclusion trails preserve weak crenulations.

3.6.1. Timing of porphyroblast growth and foliation development

The matrix foliation has a consistent NW-SE trend and dips gently NE. Locally a steeper dipping foliation with a similar trend is preserved (Fig. 13). There is no core-rim relationship preserved in this zone, which makes it difficult to establish a growth succession for same-phase porphyroblasts. Figure 14 shows garnet and staurolite porphyroblasts that overgrew a shallow-dipping foliation. Both phases have inclusion trails that appear continuous with the external matrix foliation. The opposite asymmetry preserved in garnet (anti-clockwise) compared to staurolite (clockwise) indicate that these phases grew at different times over different foliations (Fig. 14). A similar situation is shown in Fig. 13, where garnet and staurolite porphyroblasts overgrew a steeply-dipping foliation. The relative timing between foliations and porphyroblasts from Figs. 13 and 14 is difficult to determine.

3.7. Zone 6

This zone shows the largest variety of microstructures and mineral species. Complete retrograde pseudomorphs of fine-grained Ms+Bt after staurolite, and partial prograde pseudomorphs of andalusite after staurolite are common. Staurolite varies from large euhedral crystals, to large anhedral crystals that are partially replaced by Ms+Bt, to highly poikilitic crystals; two generations can be identified. The second generation of staurolite occurs as growth rims and, locally, these can be replaced by andalusite. Andalusite has two different textural forms. Poikilitic examples overgrow the matrix foliation. Large Ms+Bt clots appear to have replaced andalusite porphyroblasts that were inclusion free. Sillimanite grew as randomly-oriented needles in biotite porphyroblasts. Garnet is always present, usually with a rim of coarse biotite grains. Porphyroblastic biotite is locally totally replaced by chlorite, as is staurolite. The matrix foliation orientation varies, but a NW-SE trend that dips NE is dominant. Crenulation-cleavage development varies across the zone, with stages 3, 4, and 5 from Bell and Rubenach (1983) being present. In the matrix, two different crenulations are present that overprint each other. Inclusion trails in staurolite porphyroblasts preserve crenulations (Figs. 15) and normally are truncated by the matrix foliation.

3.7.1. Timing of porphyroblast growth and foliation development

The complex nature of the porphyroblast-matrix relationships and the variety of the geometries preserved as inclusion trails makes it difficult to establish a crystallization order for garnet and staurolite without 3D measurements. Figure 15 shows two foliations, a sub-vertical foliation (S_{i1}) that was crenulated by a sub-horizontal differentiated cleavage (S_{i2}) overgrown by staurolite porphyroblasts. In other samples from the same zone

staurolite porphyroblasts that contain core inclusion trails truncated by rim inclusion trails are common. Usually, the inclusion trails in garnet porphyroblasts have similar orientations with early-formed inclusion trails in staurolite, or are truncated by them.

3.8. Zone 7

This zone contains the highest-grade metamorphic assemblages. Fibrolitic sillimanite is present everywhere in the matrix, in biotite, and andalusite. Staurolite is replaced by coarse-grained muscovite, and all such pseudomorphs contain a small amount of biotite. Staurolite relics occur as poikilitic cores with crenulated inclusion trails (Fig. 16) or as a few scattered small grains in muscovite pseudomorphs that are commonly deformed. Andalusite overgrew the matrix foliation and is replaced by randomly-oriented muscovite and sillimanite. Some andalusite contains small, irregular staurolite grains. Garnet is pseudomorphed by coarse biotite in which sillimanite has nucleated. Locally, sillimanite has almost totally replaced these biotite pseudomorphs. The matrix foliation has a general NW-SE trend and dips NE. An asymmetric, differentiated, crenulation cleavage is always present at stage 3 or 4 of development (Bell and Rubenach, 1983). Traces of an older, steeper, differentiated crenulation cleavage can be observed locally.

3.8.1. Timing of porphyroblast growth and foliation development

All staurolite and garnet porphyroblasts are variably replaced by coarse grained micas. They mainly preserve a sub-vertical foliation that shows a weak crenulation cleavage in staurolite porphyroblasts (Fig. 16). These porphyroblasts are located in the hinges of a sub-horizontal, axial-planar, differentiated crenulation cleavage.

4. TIMING OF PSEUDOMORPHS

Of considerable importance for deciphering the deformation and metamorphic history of this region is establishing whether or not the pseudomorphs have been deformed. Pseudomorphs are more easily deformable than the replaced mineral because of their finer grain-size. That is, Ms+Bt±Chl pseudomorphs are much less competent than single large porphyroblasts. If any deformation had occurred during and/or after pseudomorph formation, a preferential alignment of mica laths would be expected, and this indeed was observed in all zones of the study area. In zones with a well-developed sub-horizontal crenulation cleavage (e.g., Zones 7 and 6), the pseudomorphs have been deformed twice. Sub-vertical muscovite blades appear truncated or crenulated by the younger sub-horizontal foliation (Fig. 17). Staurolite cores reveal that these minerals were pseudomorphed during the earlier event that produced sub-vertical foliation. A sub-horizontal fabric is dominant in some samples containing both deformed and undeformed pseudomorphs. In the former the mica laths show a strong tendency to align parallel to the matrix cleavage (Fig. 18a), whereas in the latter, they are randomly-oriented (Fig. 18b) and the cleavage intensifies against the pseudomorph margins.

Pseudomorphs in zones of higher strain with sub-vertical matrix foliation (e.g., Zone 2) are straight in rocks where this foliation was subsequently crenulated to only stage 2 of Bell and Rubenach (1983). Mica laths are strongly-aligned parallel with the matrix foliation in both complete and partial pseudomorphs (Figs. 5 and 19), but the matrix foliation is slightly deflected against pseudomorph margins. Inclusion trails are still recognizable in the pseudomorphs and slightly curve into the matrix (Fig. 5), indicating formation of these pseudomorphs late during foliation development. However, the

coexistence of pseudomorphs containing oriented versus randomly-oriented mica in the same zone, outcrop or sample, suggests that another important factor in interpreting these microstructures is the absence of deformation of many of the pseudomorph shapes. If the shape is undeformed there was no internal deformation so mica laths should be un-oriented. If they still appear oriented (despite preserved shape) another mechanism could have been involved, such as syntaxial overgrowth of inclusion trails. In Zone 7, the shape of the previous mineral can be difficult to recognize, but in all other zones where pseudomorphs are present, the shape of the previous mineral is normally very well preserved. Where the pseudomorph shape has been deformed, deformation is present that is similar in character to the deflection of inclusion trails at the margins of porphyroblasts.

Did the undeformed pseudomorphs form at the same time as the deformed pseudomorphs? An obvious explanation for the former is that they formed after any deformation ceased or very late when the stress was too weak to produce any new microstructures. If a volume change occurred, one could expect the shape of the pseudomorph to have been deformed. After two deformation events any relics of the previous porphyroblast shape should have been lost and all mica recrystallised and aligned as part of the matrix foliation. This is not the case. In Zone 7, where the original shapes of the replaced porphyroblasts are not preserved, all muscovite grains in pseudomorphs are randomly aligned. The resulting aggregate is coarser-grained than the matrix minerals and easy to identify.

5. FIA DATA

Eighty-five spatially-oriented samples collected from the contact aureole of the Mooselookmeguntic pluton (Fig. 2) were reoriented in the laboratory, and horizontal rock

slabs were marked and cut. Six vertical blocks were cut 30° apart around the compass from these slabs, and thin sections were prepared. FIA in both garnet and staurolite porphyroblasts were measured as described by Hayward (1990) and Bell et al., (1995, 1998). Where a change in the curvature of the inclusion trails asymmetry occurred (clockwise/anticlockwise), when viewed from the same direction, two thin sections were prepared at 10° intervals to increase the accuracy of the FIA reading for one sample to ±5°. The FIAs were determined as lying between the 10° sections where the asymmetry changed (Fig. 20). A total of 77 FIA for staurolite and 75 for garnet porphyroblasts were measured. FIA data are shown in Table 2, and FIA sets plotted on rose diagrams are shown in Fig. 21.

5.1. Interpretation of FIA succession

A succession of 5 different FIA sets for garnet and staurolite porphyroblasts can be interpreted using samples that preserve changes in FIAs trend from core to rim that trend successively NNW-SSE, ESE-WNW, E-W, ENE-WSW, and NE-SW. FIA set 3 is not obvious for garnet porphyroblasts alone (Fig. 22a) but is apparent in staurolite porphyroblasts or when these two phases are combined (Figs. 21b and 21c).

Samples, that contain staurolite porphyroblasts with complex inclusion trail geometries and distinct microstructural domains (e.g., core-to-rim; crenulation cleavages) were used to establish the relative FIA succession. Differing FIA trends have been preserved by porphyroblasts (e.g., garnet and staurolite) formed during discrete periods of mineral growth or as different minerals that grew during a single phase of progressive metamorphism (Tab. 2). Analysis of multi-FIA samples can determine the relative timing between successive consistent FIA trends. Episodically-grown porphyroblasts showing

different growth-timing relationships relative to the surrounding foliations provide good relative-timing criteria.

Many staurolite porphyroblasts preserve a core-to-rim relationship, which can be used to determine the relative FIA succession. A FIA trend from the core of a porphyroblast must be older than a FIA from the rim. A consistent succession of trends allows a paragenesis of FIAs to be established (Bell et al., 1998). For example, in Fig. 4 three distinct generations of staurolite growth can be observed. FIA measurements for the inclusion trails marked as S_{i2} in Fig. 4 show an E-W trend for this foliation; for the inclusion trails marked as S_{i3} in Fig. 4, FIA measurements show a ENE-WSW trend, and for inclusion trails marked as S_{i4}, FIA measurements show a NE-SW trend. Figure 22 shows how the relative timing for FIAs in staurolite porphyroblasts was determined by using core-to-rim transitions and different stages of crenulation cleavage development. Staurolite cores with NW–SE trending FIAs are succeeded by N-S-, E-W-, and ENE-WSW-trending rims. N-S-trending FIA cores and pre-FIAs are succeeded by NE-SW-trending rims. E-W trending FIAs cores are succeeded by ENE-WSW-trending medians/rims and NE-SW rims. ENE-WSW-trending cores are succeeded by NE-SW-trending rims.

Most samples contain both garnet and staurolite porphyroblasts. Table 3 shows FIA readings for garnet and staurolite porphyroblasts for those samples that contain both phases. The microstructural relationships between garnet and staurolite porphyroblasts indicate that garnet grew simultaneously or earlier than staurolite. Therefore, garnet FIAs must follow a similar succession to staurolite FIAs.

6. PITCH DATA

Inclusion-trail pitches in staurolite porphyroblasts were measured from the same thin sections used for FIA readings. The pitches were measured only in those porphyroblasts where the foliation orientation defined by inclusion trails was very clear. Where the inclusion trails were sigmoidal in shape only the straight part of the inclusions from the middle of the porphyroblast was measured. Figure 23 shows an example of how the pitches were measured in a staurolite porphyroblast containing core and rim inclusion trails. Following the procedure described above, 30 to 140 pitches per sample were measured from at least eight vertically-oriented thin sections with different strikes, yielding a total of 2350 measurements. The results were plotted on stereograph projections with the computer software GEOrient v.9.4.0 of Rod Holcombe (http://www.holcombe.net.au/software) for each sample and microstructural domain (core, median, or rim inclusion trails), so that the strike and dip for the foliations preserved in staurolite porphyroblasts could be determined (Fig. 24). The strikes of the inclusion trail foliations were plotted on a rose diagram (Fig. 25a) from which five major trends could be defined. Most of the data strikes NE-SW (30%), with the bulk of the measurements between 20° and 50°. Another major peak (26% of the data) strikes NW-SE. Almost 12% of the data strikes N-S, 15% strikes ENE-WSW, and 8% strikes E-W.

Inclusion-trail orientations in thin section have sub-horizontal or sub-vertical pitches. Figure 25b shows that in 3-D the foliations preserved in staurolite porphyroblasts are predominantly steep although some of them are oblique. Matrix foliations (Fig. 25c) are mainly oblique to steep, suggesting that there should always be present a deflection of the inclusion trails from the porphyroblasts into the matrix. This suggests that sub-

horizontal-foliation-forming events are much more weakly developed than sub-vertical ones and form crenulations rather than axial-planar foliations.

The five FIA trends (Fig. 20b) measured from staurolite correlate very well with the foliations preserved inside the porphyroblasts (Fig. 25a). At least two foliations are needed to define a FIA, a pre-existing one (preserved in the core of the porphyroblasts) and a newly-developed one (preserved as the curvature in the rim of the porphyroblasts). The intersection axes between these two foliations represent the FIA trend. When a steep foliation intersects a gently-dipping one, the FIA trend is controlled by the steep foliation (Fig. 26a). Therefore, the foliation preserved in staurolite should have about the same trend as the FIA. When two steep foliations intersect, the FIA is defined by the newly-formed foliation, which is preserved as the curvature in the rim of the porphyroblasts (Fig. 26b). Therefore, the foliation in the core of the porphyroblast may have orientations of any of the previous fabrics. For the youngest FIA the foliations from the core of the porphyroblasts may have any of the previous FIAs orientations. If most of the foliations preserved in porphyroblasts are steep, then a rose diagram of their strikes must result in similar trends to the FIAs (Fig. 25a). FIAs can be determined from pitches by using the computer software "FitPitch" (Aerden, 2003) if the orientation of the inclusion trails curvature, as measured from one horizontal thin section, is determined.

7. DISCUSSION

7.1. Timing of porphyroblasts growth in the contact aureole of the Mooselookmeguntic pluton

There are many methods used to assess the relative timing of porphyroblast growth and its relationship to the matrix foliation. The most common are:

- truncated versus continuous inclusion trails
- sub-horizontal versus sub-vertical inclusion trails
- crenulations preserved in porphyroblast
- core-to-rim relationships

7.1.1. Previous interpretations

Metamorphic history and timing of porphyroblast growth in the contact aureole of the Mooselookmeguntic pluton are well documented in the literature (e.g., Guidotti, 1970; 1974; 1989; 2000; Holdaway et al., 1982; 1988; DeYoreo et al., 1989; Guidotti and Holdaway, 1993; Guidotti and Johnson, 2002; Henry and Guidotti, 2002; Johnson et al., 2003; Johnson et al., 2006) and can be summarized as follows:

- a first metamorphic event occurred prior to 400 Ma and produced large-scale chlorite-zone metamorphism; this metamorphic event was syn-kinematic (D1), and produced the regional-scale, NE-trending folds and slaty cleavage (e.g., Guidotti, 2000; Henry and Guidotti, 2002);

- a second metamorphic event occurred at about 400 Ma and produced the low amphibolite-facies assemblage And+St+Bt±Grt. This event occurred late during the second deformation event, which produced locally-developed folds similar in trend to the regional structures, and an axial-planar crenulation cleavage (e.g., Guidotti, 2000; Henry and Guidotti, 2002); the first generation of staurolite (M2) porphyroblasts overgrew this cleavage.
- the last metamorphic event was regarded as post-kinematic, related to the intrusion of the Mooselookmeguntic pluton, and produced a second generation of staurolite (M3) as growth rims of the M2 staurolite, which overgrew a pluton-emplacement-related foliation (e.g., Guidotti, 2000; Johnson et al., 2006).

As a result of the above history all staurolite cores and rims should have overgrown a similar fabric, and should show similar relationships to the matrix, plus should correlate well across the region.

Johnson et al. (2006) claimed that the spread of inclusion trails in the staurolite porphyroblasts from the Mooselookmeguntic pluton aureole contact is due to variable porphyroblast rotation relative to one another. They measured inclusion-trail pitches in staurolite porphyroblasts in 2 thin sections at a high angle to the matrix foliation. They plotted these on stereo-nets and found in 3-D a range in dip from 16° to 75° with increasing strain in the aureole (their Fig. 5). They also show a large range in strikes but did not comment on them. A simple analysis of the data shown in their Fig. 5 reveals 4 peaks in foliation trend, the largest of which strikes NE (Fig. 27). These 4 peaks coincide almost exactly with both the FIA-trend peaks and the foliation-strike peaks (Fig. 27). Rotation such as they claim should produce a progressive spread of foliation strikes away

from a main trend, as well as a range of dips. Their data show a series of peaks in the foliation strikes at moderate to high angles to one another and not a progressive spread. In fact, their data accord very well with that presented herein. The difference is the control on relative timing gained from core-rim transitions, which they ignored possibly because they used too few thin sections.

7.1.2. Truncated versus continuous inclusion trails

Inclusion trails that are continuous with the matrix can be interpreted in terms of relatively late growth of porphyroblasts while truncated inclusion trails as early formed ones. Cihan (2004) has shown that inclusion trails that appear continuous with foliations in thin sections cut orthogonal to the matrix foliation may not be continuous with it in 3D and in that case represent earlier foliations (Bell and Johnson, 1989; Bell and Hayward, 1991; Passchier and Speck, 1994; Bell at al., 1997). Therefore, to determine weather or not the inclusion trails that appear continuous with the matrix foliation are indeed continuous, a 3D study of the inclusion trail orientation is needed. For this study, the thin sections used for FIA measurements were also used to study the orientation of the inclusion trails in 3D. Figure 28 shows, for most of the samples, the microstructural relationships between the inclusion trails preserved in porphyroblasts and the matrix foliation. Most of the porphyroblasts have truncated inclusion trails, but some of them have inclusion trails that appear to be continuous with the matrix. For example, in Zone 2 it can be inferred that at least two generations of garnet growth occurred. It can be assumed that garnet porphyroblasts that are continuous with the matrix represent the youngest phase of growth, but no reliable assumptions can be made about the truncated ones. In Zone 3 there is a similar situation, but when compared with Zone 2 the garnet porphyroblasts that have

continuous inclusion trails in both zones may be truncated by the matrix foliation in the other zone. Whether or not the continuous garnet porphyroblasts from these two zones represent the same generation of growth cannot be accurately determined without a 3D measurement (FIAs) of their inclusion trails orientations. FIA measurements (Tab. 2) shows that garnet porphyroblasts from these zones could have grown during any of the five FIA events; therefore at least five different generations of garnet growth occurred.

If all continuous/truncated porphyroblasts grew at the same time across a region, porphyroblast/matrix relationships could be successfully used to correlate foliations and the timing of deformation. If that is not the case, then no more than two generations of porphyroblasts can be distinguished and different generations can be interpreted as one.

7.1.3. Sub-horizontal versus sub-vertical inclusion trails

The importance of cycles of successively developed sub-vertical and sub-horizontal foliations during Appalachian orogenesis has been well documented by Bell and Newman (2006). While sub-vertical fabric is generally accepted as being the result of bulk horizontal shortening, various theories have been proposed for the development of sub-horizontal fabrics. Gravitational collapse (Stipska et al., 2001; Bell and Newman, 2006; Duclaux et al., 2007) in a contractional environment accompanied by sub-horizontal shearing (Stipska et al., 2001) or compresional nappe style tectonics (Matte and Mattauer, 1987) have been investigated as possible solution. Soula et al. (1986) and De Bresser et al. (1986) argued that this foliation may be result of a localized extensional attribute above granitoid diapirs in a compressional regime. Many authors have attributed flat-lying foliation to extensional tectonics (e.g., Gibson, 1991; Pavlis and Sisson, 1993; Harris et al., 2002; Fergusson et al., 2007). An orogenic belt can undergo alternating episodes of

contraction and extension or can experience both at the same time. Dewey (1988) put forward that most orogenic belts experience lithospheric thickening followed by extensional collapse, which is activated by thinning of the thickened lithospheric-mantle root of the orogen.

Alternating episodes of contraction and extension are widely-recognized processes associated with convergent margins (Hall, 2002). Bell and Newman (2006) suggested that indirect coupling between plates throughout the period of collision resulted in horizontal shortening, followed by crustal instability and collapse, repeated over and over until orogenesis ceased. Contemporaneity of alternating extensional and contractional episodes could be a characteristic of many orogenic belts (Foster et al., 2005; Squire and Wilson, 2005; Fergusson et al., 2007).

The principal movement direction has a strong influence on strain/fabric orientation during coaxial deformation. In shear zones, the non-coaxial component of deformation might be dominant (e.g., on a fold limb) and a sub-vertical fabric might develop independent of direction of maximum strain. In such zones, any record of most of the previous deformation history is lost, and a consistent orientation of the fabric over large areas may appear as the result of a single event. Foliation tends to be parallel with the fold limbs due to decrenulation and rotation during reactivation of the foliation being folded (Bell et al., 2003). In contrast, zones dominated by coaxial deformation (e.g., fold hinges) can show a larger variety of fabric orientations, which can be the result of multiple events that have been erased by shearing and reactivation on the fold limbs. Most porphyroblasts in the contact aureole of the Mooselookmeguntic pluton have steeply-dipping foliations preserved as inclusion trails (Fig. 25b). If only two thin sections were cut (N and P

sections) then most of them probably would appear oblique. In western Maine, matrix foliations are normally steeply-dipping (e.g., Brown and Solar, 1998; Solar et al., 1998), therefore most porphyroblasts overgrew a steeply-dipping foliation. Taking into consideration the Brown and Solar (1998) model for western Maine (Fig. 1) that shows alternating zones of lower strain (with moderate- to steeply-dipping foliation) between zones of higher strain (with steeply-dipping foliations) then the region under study would be located in a zone of predominantly lower strain. Therefore, one may expect to find previous deformation events better preserved than in zones of higher strain. Even so, just by considering only porphyroblast-matrix relationships, correlations beyond the scale of a thin section are difficult to make without detailed 3D measurements. The transition from a sub-horizontal fabric to a sub-vertical fabric and back to sub-horizontal due to crenulation events can locally erase any trace of previous foliations. Porphyroblasts that grew over a sub-horizontal foliation S_1 could preserve its orientation and appear synchronous with a much later sub-horizontal fabric S_3 (Fig. 29).

7.1.4. Crenulations inside staurolite porphyroblasts

Crenulation cleavage is one of the most common features found in deformed metamorphic rocks. Many authors have tried to understand the deformation mechanisms that control crenulation cleavage development. Most have agreed that in the early stages of crenulation development pressure- or shear-controlled dissolution, solution transfer, rotation, and differentiation are important factors (Williams, 1972; Marlow and Etheridge, 1977; Bell and Rubenach, 1983). Bell and Rubenach (1983) identified six stages of crenulation-cleavage development. The main deformation mechanism at lower temperature is differentiation by solution transfer and rotation, and at higher temperatures

recrystallisation and grain growth. Porphyroblasts commonly appear to grow in crenulation hinges prior to crenulation-cleavage development (Bell and Rubenach, 1983; Spiess and Bell, 1996; Johnson, 1999; Bell et al., 2003), with this geometry playing an important role in porphyroblast nucleation and growth (Bell and Bruce, 2007). Kisch (1998) showed that crenulation cleavages start to develop as early as incipient metamorphism occurs if deformation is present. In this way a porphyroblast can nucleate as soon as metamorphic conditions are favourable if the bulk composition is appropriate. The structural fabric is recorded as inclusion trails.

Porphyroblasts that overgrew similarly developed crenulation cleavage could or could not nucleate during the same event. Zones 4, 5 and 7 contain staurolite porphyroblasts in which the inclusion trails are slightly crenulated (Fig. 17) rather than being fully differentiated crenulation cleavages at stage 4. Such crenulations are present as symmetrical and/or asymmetrical undulations of the inclusion trails. Zones 1 and 6 show more-differentiated crenulations preserved as inclusion trails (Fig. 15). For example, staurolite porphyroblast from sample IS104, which contain slightly crenulated inclusion trails (Fig. 17), grew during FIA 1, whereas staurolite porphyroblasts from samples IS73 and IS74, which overgrew a differentiated crenulation cleavage, grew during FIA 5. Although, the later samples both grew during FIA 5, their crenulated cleavage shows different timing. For example, in sample IS73 the crenulated cleavage shows FIA 2, whereas in sample IS74 the crenulated cleavage shows FIA 4.

7.1.5. Core-to-rim relationships

Inclusion trails in porphyroblasts have been used for decades to decipher complex metamorphic and deformation histories. Where a core-to-rim relationship is present, the

core-inclusion trails are interpreted as synchronous with an earlier S_{i1} foliation, whereas the rim S_{i2} foliation can be interpreted as more or less contemporaneous with the later matrix foliation. Bell (1981) suggested that porphyroblasts commonly nucleate and grow in sites of progressive coaxial shortening. Developing anastomosing zones of combined non-coaxial shortening and shearing surround these zones, and when they interact with the growing porphyroblasts growth ceases. It does not recommence until a new deformation occurs at high angle to the earlier one and repartitions around the porphyroblast margins allowing new growth to occur in their strain shadows (e.g., Bell and Rubenach, 1983; Bell et al., 1986; Bell and Hayward, 1991). The resulting geometry reflects the relationship between two sets of inclusion trails, or two foliations, and can be interpreted as the result of two separate deformation events. Cihan (2004) showed that timing of porphyroblast growth relative to deformation events could be misinterpreted if not enough care is taken in interpreting these types of microstructures.

Core-to-rim relationships between differing foliations have been found in zones 1, 2, 4, and 6. Core-to-rim relationships are only preserved in the SW of Zone 2 because most staurolite porphyroblasts in this zone are affected by retrogression. In most of Zone 6 only a few samples contain staurolite porphyroblasts that preserve a core-to-rim relationship. Prior to the work of Bell et al. (1986), the rims in these samples may have been interpreted as resulting from a later growth of this porphyroblastic phase during the same deformation event in which the core formed. However, the differentiated cleavage truncating the core-inclusion trails locally shows curvature on the porphyroblast rim, indicating that the rim grew during a younger, near-orthogonal deformation event. It has been assessed that all cores grew at the same time and represent one generation of growth whereas the rims were

the result of a later event (e.g., Guidotti, 2000; Guidotti and Johnson, 2002; Johnson et al., 2006). Such an argument cannot be upheld without detailed 3D measurements. For example, samples IS17 and IS86 both have staurolite porphyroblasts with core and rim growth, and both samples show FIA 1 for core inclusion and FIA 4 for rim inclusion trails, but other samples may have different timing for there core and/or rim growth. In the case of sample IS85, the core-inclusion trails show FIA 4 and the rim inclusion trails show FIA 5. Other samples, like IS91, IS94, and IS95 can have as many as three generations of staurolite growth. For all three samples the oldest generation of staurolite growth shows FIA 3, followed by FIA 4, and the last generation is FIA 5. Correlating such microstructures across a small area like the one shown in Fig. 2 may be difficult without 3D measurements, and misinterpretations can easily occur.

The many deformation events experienced by the matrix and preserved only in porphyroblasts as inclusion trails can be easily visualised in Fig. 30, which shows four staurolite porphyroblasts and their microstructures from sample IS91. At least five different generations of inclusion trails can be interpreted from Fig. 30, from which it was possible to measure three FIAs. The inclusion trails marked as S_{i2} in St contain FIA 3. The inclusion trails marked as S_{i3} in St 2 contain FIA 4. The inclusion trails marked as S_{i4} in ST 3 contain FIA 5. Staurolite 1 overgrew at least two different foliations during FIA 3. The first is represented by the inclusion trails marked as S_{i1} (see detail 1 in Fig. 31a). The second generation of inclusions, marked as S_{i2} and the curvature of which defines FIA 3, truncates S_{i1} inclusion trails. The inclusion trails S_{i4} in St 4 truncate those in St 1 and are the same generation as those truncating S_{i2} in the LH rim of St 1 shown in Fig. 31d. They are parallel with the matrix, but predate it because they are not continuous with it. They are

continuous into the strain shadow (Fig. 31b). St 2 grew during FIA 4 and preserves inclusion trails, S_{i3}. These inclusion trails appear to be continuous with the matrix in the strain shadow above St 2 but are truncated below by S_{i5}. The matrix foliation actually wraps around St 2. St 3 contains inclusion trails, S_{i4}, that truncate the inclusion trails, S_{i2}, in St 1. St 1, St 2, and St 3 show growth rims, for which FIAs could not be determined because they are not present in all thin sections. The inclusion trails marked with S_{i5} in both St 2 and St3 appear to have similar orientation and may represent the same event. Since none of the rim-growth inclusion trails were consistent in all thin sections cut from this sample they cannot be accurately correlated and their relative timing remains uncertain. Without FIA measurements they cannot be correlated, with similar microstructures from other samples across the region. Where samples from different locations contain different types of inclusion-trail geometries, the problem of correlating the timing of porphyroblast growth, even for samples that contain core to rim relationships, can be misinterpreted (Fig. 32).

REFERENCES

Bell, T.H., 1981. Foliation development: the contribution, geometry and significance of progressive bulk inhomogeneous shortening. *Tectonophysics*, **75**, 273-296.

Bell, T. H., 1986. Foliation development and refraction in metamorphic rocks: reactivation of earlier foliations and decrenulation due to shifting patterns of deformation partitioning. *Journal of Metamorphic Geology*, **4**, 421-444.

Bell, T. H., and Forde, A., 1995. On the significance of foliation patterns preserved around folds by mineral overgrowths. *Tectonophysics*, **246**, 171-181.

Bell, T. H., and Hayward, N., 1991. Episodic metamorphic reactions during orogenesis: the control of deformation partitioning on reaction sites and reaction duration. *Journal of Metamorphic Geology*, **9**, 619-640.

Bell, T. H., and Hickey, K. A., 1997. Distribution of pre-folding linear indicators of movement direction around the Spring Hill Synform, Vermont: significance for mechanism of folding in this portion of the Appalachians. *Tectonophysics*, **274**, 274-294.

Bell, T. H., and Johnson, S. E., 1989. Porphyroblast inclusion trails: the key to orogenesis. *Journal of Metamorphic Geology*, **7**, 279-310.

Bell, T. H., and Rubenach, M. J., 1983. Sequential porphyroblast growth and crenulation cleavege developement during progressive deformation. *Tectonophysics*, **92**, 171-194.

Bell, T. H., and Hickey K. A., 1999. Complex microstructures preserved in rocks with a simple matrix: significance for deformation and metamorphic processes. *Journal of Metamorphic Geology*, **17**, 521-535.

Bell, T. H., and Mares V. M., 1999. Correlating deformation and metamorphism around orogenic arcs. *American Mineralogist*, **84**, 1727-1740

Bell, T. H., Fleming, P. D., and Rubenach, M. J., 1986. Porphyroblast nucleation, growth and dissolution in regional metamorphic rocks as a function of deformation partitioning during foliation development. *Journal of Metamorphic Geology*, **4**, 37-67.

Bell, T. H., Forde, A., and Wang, J., 1995. A new indicator of movement direction during orogenesis: measurement technique and application to the Alps. *Terra Nova*, **7**, 500-508.

Bell, T. H., Ham, A. P., Hayward, N., and Hickey, K. A., 2005. On the development of gneiss domes. *Australian Journal of Earth Sciences*, **52**, 183-204.

Bell, T. H., Ham, A. P., and Hickey, K. A., 2003. Early formed regional antiforms and synforms that fold younger matrix schistosities: their effect on sites of mineral growth. *Tectonophysics*, **367**, 253-278.

Bell, T. H., Ham, A. P., and Kim, H. S., 2004. Partitioning of deformation along an orogen and its effects on porphyroblast growth during orogenesis. *Journal of Structural Geology*, **26**, 825-845.

Bell, T. H., Hickey, K. A., and Upton, G. J. G., 1998. Distinguishing and correlating multiple phases of metamorphism across a multiply deformed region using the axes of spiral, staircase and sigmoidal inclusion trails in garnet. *Journal of Metamorphic Geology*, **16**, 767-794.

Bell, T. H., Hickey, K. A., and Wang, J., 1997. Spiral and staircase inclusion trail axes within garnet and staurolite porphyroblasts from the schists of the Bolton Syncline, Connecticut: timing of porphyroblast growth and the effects of fold development. *Journal of Metamorphic Geology*, **15**, 467-478.

Bell, T. H., Johnson, S. E., Davis, B., Forde, A., Hayward, N., and Wilkins, C., 1992. Porphyroblast inclusion-trail orientation data: eppure non son girate! *Journal of Metamorphic Geology*, **10**, 295-307.

Bell, T. H., and Newman, R., 2006. Appalachian orogenesis: the role of repeated gravitational collapse. In: *Butler, R., Mazzoli, S. (Eds.), Styles of Continental Compression. Special Papers of the Geological Society of America*, **414**, 95-118.

Bradley, D. C., Tucker, R. D., Lux, D. R., Harris, A. G., and McGregor, D. C., 1998. Migration of the Acadian orogen and foreland basin across the northern Appalachians. *U.S. Geological Survey, Open-File Report*, 98-770, 79 p.

Brown, M., and Solar, G. S., 1998a. Shear zone systems and melts: feedback relations and self organization in orogenic belts. *Journal of Structural Geology*, **20**, 211-227.

Brown, M., and Solar, G. S., 1998b. Granite ascent and emplacement during contractional deformation in convergent orogens. *Journal of Structural Geology*, **20**, 1365-1393.

Brown, M., and Solar, G. S., 1999. The mechanism of ascent and emplacement of granite magma during transpression: a syntectonic granite paradigm. *Tectonophysics*, **312**, 1-33.

Cihan, M., 2004. The drawbacks of sectioning rocks relative to fabricorientations in the matrix: a case study from the Robertson River Metamorphics (North Queensland, Australia). *Journal of Structural Geology*, **26**, 2157-2174.

De Bresser, J. H. P., Majoor F. J. M., and Ploegsma M., 1986. New insights in the structural and metamorphic history of the western Lys. Caillauas massif (Central Pyrenees, France). *Geologie en Mijnbouw*, **65**, 177-187.

Dewey, J., 1988. Extensional collapse of orogens. *Tectonics*, **7**, 1123-1139.

DeYoreo, J. J., Lux, D. R., Guidotti, C. V., Decker, E. R., and Osberg, P. H., 1989. The Acadian thermal history of western Maine. *Journal of Metamorphic Geology*, **7**, 169-190.

Duclaux, G., Rey, P., Guillot, S., and Ménot, R. P., 2007. Orogen-parallel flow during continental convergence: Numerical experiments and Archean field examples. *Geology*, **35**, 715-718.

Fergusson, C. L., Henderson, R. A., Withnall, I. W., Fanning, C. M., Phillips, D., and Lewthwaite, K. J., 2007. Structural, metamorphic, and geochronological constraints on alternating compression and extension in the Early Paleozoic Gondwanan Pacific margin, northeastern Australia. *Tectonics*, **26.**

Foster, D. A., Gray, D. R., and Spaggiari, C., 2005. Timing of subduction and exhumation along the Cambrian East Gondwana margin, and the formation of Paleozoic backarc basins. *Geological Society of America Bulletin*, **117**, 105-116.

Gibson, R. L., 1991. Hercynian low-pressure – high-temperature regional metamorphism and subhorizontal foliation development in the Canigou massif, Pyrenees, France—Evidence for crustal extension. *Geology*, **19**, 380-383.

Guidotti, C. V., 1989. Metamorphism in Maine: an overview: In: Studies in Maine *Geology*, **3**, 1-19.

Guidotti, C. V., and Holdaway, M. J., 1993. Petrology and field relations of successive metamorphic events in pelites of west-central Maine. In: *Cheney, J.T., Hepburn, J.C. (Eds.), Field Trip Guidebook for the Northeastern United States*, **1**. Geological Society of America, pp. L1-L23.

Guidotti, C. V., and Johnson, S. E., 2002. Pseudomorphs and associated microstructures of western Maine, USA. *Journal of Structural Geology*, **24**, 1139-1156.

Hall, R., 2002. Cenozoic geological and plate tectonic evolution of SE Asia and the SW Pacific: Computer-based reconstructions, model and animations, *Journal of Asian Earth Science*, **20**, 353-431.

Ham, A. P., Bell, T. H., 2004. Recycling of foliations during folding. *Journal of Structural Geology*, **26**, 1989-2009.

Harris, L. B., Koyi, H. A., and Fossen, H., 2002. Mechanisms for folding of high-grade rocks inextensional tectonic settings. *Earth Science Review*, **59**, 163-210.

Hayward, N., 1990. Determination of early fold-axis orientations in multiply deformed rocks using porphyroblast inclusion trails. *Tectonophysics*, **179**, 353-369.

Johnson, S. E., Dupee M. E., and Guidotti C. V., 2006. Porphyroblast rotation during crenulation cleavage development; an example from the aureole of the Mooselookmeguntic Pluton, Maine, USA. *Journal of Metamorphic Geology*, **24**, 55-73.

Johnson, S. E., 1999a. Back-rotation during crenulation cleavage development: implications for structural facing and cleavage - forming processes. *Journal of Structural Geology*, **21**, 139-145.

Johnson, T. E., Brown, M., and Solar, G. S., 2003. Low-pressure subsolidus and suprasolidus phase equilibria in the MnNCKFMASH system: constraints on conditions of regional metamorphism in western Maine, northern Appalachians. *American Mineralogist*, **88**, 624-638.

Kisch, H. J., 1998. Criteria for incipient slaty and crenulation cleavage development in Tertiary flysch of the Helvetic zone of the Swiss Alps. *Journal of Structural Geology*, **20**, 601-615.

Marlow, P. C., and Etheridge, M. A., 1977. Development of a layered crenulation cleavage in mica schists of the Kanmantoo Group near Macclesfield, South Australia. *Geological Society of America Bulletin*, **88**, 873-882.

Matte, Ph., and Mattauer M., 1987. Hercynian orogeny in the Pyrenees was not a rifting event. *Nature*, 739-740.

Moench, R. H., 1970. Premetamorphic down-to-basin faulting, folding, and tectonic dewatering, Rangeley area, western Maine. *Geological Society of America Bulletin*, **81**, 1463-1496.

Passchier, C. W., Trouw, R. A. J., Zwart, H. J., and Vissers, R. L. M., 1992. Porphyroblast rotation: eppur si muove? *Journal of Metamorphic Geology*, **10**, 283-294.

Pavlis, T. L., and Sisson, V. B., 1993. Mid-Cretaceous extensional tectonics of the Yukon-Tanana terrane, Trans-Alaska Crustal Transect (TACT), east-central Alaska. *Tectonics*, **12**, 103-122.

Ramsay, J. G., 1962. The geometry and mechanics of formation of 'similar' type folds. *Journal of Geology*, **70**, 309-327.

Rosenfeld, J. L., 1970. Rotated garnets in metamorphic rocks. *Geological Society of America Special Paper*, **129**, 105p.

Sayab, M., 2005. Microstructural evidence for N–S shortening in the Mount Isa Inlier (NW Queensland, Australia): the preservation of early W–E trending foliations in porphyroblasts revealed by independent 3D measurement techniques. *Journal of Structural Geology*, **27**, 1445-1468.

Sayab, M., 2006. Decompression through clockwise P–T path: implications for early N–S shortening orogenesis in the Mesoproterozoic Mt Isa Inlier (NE Australia). *Journal of Metamorphic Geology*, **24**, 89-105.

Sayab, M., 2007. Correlating multiple deformation events across the Mesoproterozoic NE Australia using foliation intersection axes (FIA) preserved within porphyroblasts. *Gondwana Research*, **13**, 331-351.

Smith, H. A., and Barreiro, B., 1990. Monazite U-Pb dating of staurolite grade metamorphism in pelitic schists. *Contributions to Mineralogy and Petrology*, **105**, 602-615.

Solar, G. S., and Brown, M., 2001a. Deformation partitioning during transpression in response to Early Devonian oblique convergence, northern Appalachian orogen, USA. *Journal of Structural Geology*, **22**, 1043-1065.

Solar, G. S., and Brown, M., 1999. The classic high-T – low-P metamorphism of west-central Maine, USA: Is it post-tectonic or syn-tectonic? Evidence from porphyroblast-matrix relations. *Canadian Mineralogist*, **37**, 311-333.

Soula, J. C., Debat, P., Déramond, J., and Pouget, P., 1986a. A dynamic model of the structural evolution of the Hercynian Pyrenees. *Tectonophysics*, **129**, 29-51.

Spiess, R., Bell, T. H., 1996. Microstructural controls on sites of metamorphic reaction: a case study of the inter-relationship between deformation and metamorphism. *European Journal of Mineralogy*, **8**, 165-186.

Squire, R., and Wilson, C. J. L., 2005. Interaction between collisional orogenesis and convergent margin processes: Evolution of the Cambrian proto-Pacific margin of East Gondwana, *Journal of the Geological Society* (London), **162**, 749-761.

Stallard, A. R., Hickey, K. A., and Upton, G. J., 2003. Measurement and correlation of microstructures: the case of foliation intersection axes. *Journal of Metamorphic Geology*, **21**, 241-252.

Stipska, P., Schulmann, K., Thompson, A. B., Jezek, J. and Kroener, A., 2001. Thermo-mechanical role of a Cambro-Ordovician paleorift during the Variscan collision; the NE margin of the Bohemian Massif. *Tectonophysics*, **332**, 239-253.

Williams, P. F., 1972. Development of metamorphic layering and cleavage in low grade metamorphic rocks at Bermagui, Australia. *American Journal of Science*, **272**, 1-47.

Williams, P. F., and Jiang, D., 1999. Rotating garnets. *Journal of Metamorphic Geology*, **17**, 367-378.

Worley, B. A., and Wilson C. J. L., 1996. Deformation partitioning and foliation reactivation during transpressional orogenesis, an example from the Central Longmen Shan, China. *Journal of Structural Geology*, **18**, 395-411.

- SECTION B -

70 MILLION YEARS OF TECTONO-METAMORPHISM REVEALED BY STAUROLITE GROWTH ADJACENT TO THE MOOSELOOKMEGUNTIC PLUTON

- SECTION B –

70 MILLION YEARS OF TECTONO-METAMORPHISM REVEALED BY STAUROLITE GROWTH ADJACENT TO THE MOOSELOOKMEGUNTIC PLUTON

ABSTRACT

Emplacement of the Mooselookmeguntic pluton, located in the western Maine region of the Northern Appalachians, was thought to have occurred towards the end of the Acadian deformation at around 370 Ma. Foliation inflection/intersection axes within porphyroblasts (FIAs) from its aureole reveal at least five periods of garnet and staurolite growth. EPMA dating of monazite grains included in staurolite porphyroblasts containing one of these five periods of FIA development reveals a succession of aparrent ages from 410 Ma to 345 Ma. This succession indicates that deformation and metamorphism outlasted the Acadian orogeny and continued into Alleghanian, the thermal structure of the orogen progressively evolved to enable pluton emplacement, and it continued to develop afterwards with magmatic fluids still forming at depth.

Keywords: FIAs; staurolite; monazite dating; plutonism; orogenic heat.

1. INTRODUCTION

The development of techniques such as the characterisation of (1)-FIAs (foliation inflection/intersection axes preserved in porphyroblasts) and their derivative shear senses, (2)-successions of porphyroblast growth, and (3)-pressure-temperature paths relative to deformation and time, has led to important advances in resolving complex histories in multiply deformed and metamorphosed rocks. A major benefit of this technique is that a succession of changes in FIA trend allows access to a sequence of progressively formed monazite grains that can be used for dating by EPMA (electron probe microanalysis), leading to absolute age constraints. Most deformed terranes contain a schistosity parallel

layering (S_0//S_1). The bulk of the deformation and metamorphic history undergone by such rocks has generally been lost from the matrix (Davis, 1995; Cihan and Parson, 2005). Early-formed deformation events are obliterated, erased, or rotated into parallelism with S_0 by younger ones due to reactivation of the compositional layering (Bell, 1986). This lengthy part of the deformation history is only preserved by inclusion trails in porphyroblasts (Reinhardt and Rubenach, 1989; Bell et al., 1998).

FIA measurement provides extraordinary access to a large amount of information that is not accessible by other means. Changes in FIA trend directly reflect changes in the direction of horizontal bulk shortening (relative plate motion) with time. The succession of foliation orientations and their shear senses can be quantitatively accessed with ease once the FIA succession has been determined. The PT history of development of each FIA is trapped within the porphyroblasts that grew as they formed. Monazite grains, which grow in matrix foliations as garnet and staurolite begin to form in the rocks, are preserved amongst the inclusion trails and can be dated within a well-defined framework of relative time (e.g., Bell and Welch, 2002; Sayab, 2008). Without this framework, monazite ages from a sequence of metamorphic rocks yield a large range of ages that are ambiguous and difficult to interpret.

A succession of five different FIA trends has been determined for both staurolite and garnet porphyroblasts in a multiply deformed and metamorphosed region in west central Maine. These FIAs range in total-Pb age from 411.3±8.5 Ma to 352.5±4 Ma, accounting for 60 m.y. of active deformation and metamorphism in West Central Maine. These data and its implications for deformation, metamorphism, and pluton emplacement are described herein.

2. REGIONAL GEOLOGICAL SETTING

The Central Maine Belt, a major regional unit (Fig. 1), is bordered to the NW by Neoproterozoic basement rocks of the Bronson Hill Belt. To the SE, there is a transition from the Central Maine Belt through the Norumbega Shear Zone into the Avalon Composite Terrane. The Central Maine Belt is composed of a succession of Siluro-Devonian turbidites that form the Rangeley Stratigraphic Sequence. It was metamorphosed and deformed during the Acadian orogeny (Bradley et al., 1998). Two types of structural zones, trending NW-SW, have been identified within this belt; zones of apparent flattening or high strain, and zones of apparent constriction or low strain (Brown and Solar, 1998 a, b; 1999; Solar and Brown, 1999; Solar and Brown, 2001).

The metamorphism occurred at low pressures and high temperatures, with partial melting at higher grades forming migmatites within the Tumbledown and Weld anatectic domains (Fig. 2; Brown and Solar, 1998a). The metamorphic grade increases from greenschist facies in the central part of the region shown in Fig. 1, to upper-amphibolite facies in the south and northeast (Guidotti, 1989). Three metamorphic events have been described. Two of them, M1 and M2, are regional-scale events and the third one, M3, was regarded as pluton driven metamorphism (Guidotti, 1989; Guidotti and Holdaway, 1993; Guidotti and Johnson, 2002). In the study area (Fig. 2), rocks affected by M2 were also affected by the M3 event, which experienced a higher pressure than M2 (Guidotti and Johnson, 2002). The time difference between M2 and M3 was estimated as ~30 m.y. (DeYoreo et al., 1989; Solar et al., 1998). Staurolite, andalusite, and garnet pseudomorphs are common and were attributed to a later M3 thermal event that postdated the last deformation in the region (Guidotti and Johnson, 2002). Based on U-Pb isotopic data from

metamorphic monazite from staurolite schists the age of regional metamorphism was assessed at 405 to 399±2 Ma (Smith and Barreiro, 1990). The metasedimentary suites of the Rangeley Stratigraphic sequence were intruded syntectonically by Devonian plutons (Solar et al., 1998). Deformation, metamorphism, and granite crystallization were regarded as contemporaneous (Brown and Solar, 1998a, 1998b, 1999; Solar and Brown, 2001).

3. FIA DATA

The asymmetry approach provides a method for determining the FIA trend preserved by inclusion trails in staurolite and constrains the timing of porphyroblast growth to a specific period of tectonism. This method distinguishes successions of porphyroblast growth and foliation development. FIAs in both garnet and staurolite were measured using the asymmetry method developed by Hayward (1990) and Bell et al. (1995, 1998). This is shown in Fig. 3 and consists of cutting initially 6 vertical thin sections 30° apart around the compass and then 2 more 10° apart where the inclusion trail asymmetry flips. A total of 76 FIA for staurolite and 75 for garnet porphyroblasts were measured from samples collected from the contact aureole of the Mooselookmeguntic pluton. FIA data are shown in Table 1, and FIA sets plotted on rose diagrams are shown in Fig. 4. Figure 5 shows the sample locations on the map grouped by FIA trend.

Most of the samples selected for analysis contain both garnet and staurolite porphyroblasts. Garnet porphyroblasts typically range in size from 0.2 to 5 mm with larger ones occurring in highly graphitic layers. Inclusion trails in garnet porphyroblasts consist of quartz, graphite, ilmenite, and relict chlorite. Porphyroblasts can have inclusion-rich cores with inclusion-free rims or vice versa. In quartz-rich layers garnet is usually

xenoblastic and poikilitic whereas in more graphite rich layers it is idioblastic and can exhibit sector zoning. Inclusion trails in garnet porphyroblasts are typically straight and sigmoidal-shaped and in most occurrences they are truncated by the matrix foliation (Fig. 6). The inclusion trails are either smoothly-curving across the porphyroblasts or straight with the curvature restricted to the porphyroblast rims. In the southeastern part, garnet porphyroblasts were retrograde-pseudomorphosed by chlorite, whereas in the northwestern part they were prograde-pseudomorphosed by biotite and sillimanite in the rims.

Staurolite porphyroblasts range in size from 3 to 30 mm, and cross twins are common. Inclusion trails consist mainly of quartz and opaque minerals with relict chlorite and biotite preserved locally. Where garnet porphyroblasts are included within staurolite grains, they are usually idioblastic with sharp intimate contacts, and their inclusion trails are truncated and/or continuous with the staurolite inclusion trails (Figs. 6 and 7). The inclusion trails in staurolite porphyroblasts are more complex than those in garnet. Sigmoidal and straight inclusion trails are the most common, and they can be continuous and/or truncated by the matrix foliation. In the proximity of the granite and especially in the northern part, crenulation cleavages in different stages of development are well-preserved (Fig. 8). Staurolite porphyroblasts with core inclusion trails truncated by those in the rim are common, and locally three different generations of inclusion trails are preserved (Fig. 9) that correspond with three distinct FIA trends. In the southeastern part of the area, staurolite porphyroblasts have been retrograde-pseudomorphosed and replaced by fine-grained mica and chlorite, whereas in the northern and northwestern part they are replaced by coarse-grained muscovite and biotite and/or andalusite.

3.1. Interpretation of FIA succession

A succession of 5 different FIA sets for garnet and staurolite porphyroblasts can be interpreted using samples that preserve core-to-rim changes in FIA, trending successively from NNW-SSE, ESE-WNW, E-W, ENE-WSW, to NE-SW. FIA set 3 is not obvious for garnet porphyroblasts alone (Fig. 4a) but is apparent in staurolite porphyroblasts or when these two phases are combined (Figs. 4b and 4c).

Samples containing staurolite porphyroblasts with complex inclusion-trail geometries and distinct microstructural domains (e.g., core and rim foliations; crenulation cleavages) were used to establish the relative FIA succession. Differing FIA trends have been preserved by porphyroblasts through separate periods of mineral growth or as different minerals that grew during progressive metamorphism such as garnet and then staurolite (Table 2). Analysis of multi-FIA samples can determine the relative timing between successive consistent FIA trends. Episodically-grown porphyroblasts showing clear growth-timing relationships relative to the surrounding foliations provide good relative-timing criteria.

Many staurolite porphyroblasts preserve a core-to-rim relationship, which can be used to determine the relative FIA succession. A FIA trend from the core of a porphyroblast must be older than a FIA from the rim. A consistent succession of trends allows a paragenesis of FIAs to be established (Bell et al., 1998). Figure 10 shows how the relative timing for FIAs in staurolite porphyroblasts was determined by using core-to-rim transitions and different stages of crenulation cleavage development. Staurolite cores with NW–SE-trending FIAs are succeeded by N-S-, E-W-, and ENE-WSW-trending rims. N-S-trending FIA cores and pre-FIAs are succeeded by NE-SW-trending rims. E-W-trending

FIAs cores are succeeded by ENE-WSW-trending medians/rims and NE-SW-trending rims. ENE-WSW-trending cores are succeeded by NE-SW-trending rims.

Most samples contain both garnet and staurolite porphyroblasts. Table 2 shows FIA readings for garnet and staurolite porphyroblasts for those samples that contain both phases. The microstructural relationships between garnet and staurolite porphyroblasts indicate that garnet grew simultaneously or earlier than staurolite (Figs. 6 and 7). Therefore, garnet FIAs must follow a similar succession to staurolite FIAs. The relative timing between FIA sets determined as described above was used to select samples for monazite dating of FIAs.

4. SAMPLES DATED

Although 20 polished thin sections (four per FIA set) were used to find monazite grains included in porphyroblasts, only eight samples contained sufficiently large monazite grains to make dating worthwhile. Monazite inclusions in garnet porphyroblasts were too small and did not provide enough analytical surface for the electron beam to perform acceptable measurements. Most of the dated monazite grains come from samples showing FIA sets 3, 4, and 5. A couple of monazite grains from samples containing FIA set 2 were also dated and provided acceptable results for constraining the timing of this FIA set. No sample preserving FIA set 1 contained monazite grains that could be dated; they were all too small and only matrix monazites were analyzed.

Matrix monazites were really of no interest for this study because they cannot be placed into a FIA reference frame. However, most matrix monazite was still analyzed for comparison with the ages obtained from staurolite porphyroblasts. All analyzed grains appeared homogeneous in BSE images without evidence of cores with rim overgrowths.

Multi-FIA samples were of special interest to test whether or not they yielded different ages.

4.1. Sample description

IS23

This sample contains the mineral assemblage St+Grt+Bt+Ms and retrograde chlorite. Both garnet and staurolite porphyroblasts show FIA set 3. Staurolite partially breaks down to coarse Bt+Ms. Garnet porphyroblasts are typically idioblastic to subidioblastic and appear to be stable. Chlorite overgrows randomly the matrix foliation. Only few monazite grains were large enough to make dating worthwhile.

IS71

This sample contains the mineral assemblage And+St+Grt+Bt+Ms+Sill and retrograde chlorite overgrowing randomly the matrix. Both staurolite and garnet porphyroblasts contain FIA set 5. Andalusite porphyroblasts are large, poikilitic, and overgrew almost the entire matrix. Staurolite porphyroblasts were partially replaced by coarse Bt+Ms or andalusite. Garnet porphyroblasts usually are idioblastic to subidioblastic. Sillimanite is fibrolitic where it nucleated in biotite, and prismatic where it occurs in andalusite. There is evidence that staurolite locally broke down to coarse-grained Ms+Bt and garnet to biotite (Fig. 11a) prior to the growth of andalusite porphyroblasts. Most monazite grains were found in the staurolite porphyroblasts, but a few matrix monazite could also be dated.

IS74

This sample contains the mineral assemblage St+Grt+And+Bt+Ms+Sill. Staurolite porphyroblasts overgrew a differentiated crenulation cleavage that shows FIA set 4 for the

crenulated cleavage and FIA set 5 in the differentiated cleavage (Fig. 8). Garnet porphyroblasts show FIA set 4. Locally garnet porphyroblasts were surrounded by blades of biotite that grew parallel to the dodecahedral faces. Andalusite is present in small modal proportions and locally pseudomorphosed staurolite. Sillimanite is present as needles in biotite and andalusite. All dated monazite grains from staurolite porphyroblasts were located in the crenulated cleavage that shows FIA set 4. A few of monazite grains from the matrix could also be dated.

IS77

This sample contains the mineral assemblage St+Grt+Bt+Ms and chlorite that grows randomly in the matrix. Staurolite is present as large poikilitic porphyroblasts, with a core that contains FIA set 2 and a rim corresponding to FIA set 5. Garnet is idioblastic to subidioblastic and contains FIA set 2. Most of the dated monazite grains from the staurolite porphyroblasts were less than 10 μm in size and they all come from the core of the porphyroblasts. A few small monazite grains from the matrix could be dated as well.

IS88

This sample contains the mineral assemblage St+Bt+Ms. Staurolite porphyroblasts contain FIA set 3 in the core, and FIA set 5 in the rim. Usually the core of the porphyroblasts contains crenulated inclusion trails. All dated monazite grains were less than 10 μm in size. No monazite grains were found in the rims of the porphyroblasts.

IS94 and IS95

These samples show similar textural and mineralogical features. They contain the mineral assemblage St+Grt+Bt+Ms+Sill. Staurolite porphyroblasts are large with three stages of growth corresponding to FIA sets 3, 4 and 5 (Fig. 9). Garnet porphyroblasts show

FIA set 3 only. Locally garnet is surrounded by biotite blades that grew parallel to the crystallographic faces. Sillimanite nucleated as needles in biotite. These samples are rich in monazite grains of variable size. Only monazite grains included in staurolite porphyroblasts showing FIA set 4 and 5 could be dated. Three matrix monazites in sample IS94 were analyzed as well.

IS104

This sample shows the highest metamorphic grade. It contains the mineral assemblage Sill+And+St+Grt+Bt+Ms. Both garnet and staurolite porphyroblasts show FIA set 1. Sillimanite is present in high modal proportions nucleating in biotite and andalusite. Andalusite is large, poikilitic, and overgrew the matrix foliation and/or replaced staurolite. Staurolite breaks down to large Ms+Bt. Garnet was partially and/or completely replaced by biotite and sillimanite (Fig. 11b). No monazite grains were found in staurolite porphyroblasts, but a couple of matrix monazites were analyzed.

5. ANALYTICAL METHODS

Monazite ages were determined using a Jeol JXA8200 EPMA housed at the Advanced Analytical Centre, James Cook University. The analytical set-up is given in Table 3. The measurements were taken at an accelerating voltage of 15kV, probe current of 200nA, and spot size at 1-2 microns. The PAP (Pouchou and Pichoir, 1984; 1985) method was used to undertake matrix corrections. Background positions were chosen to minimize curvature and peak overlaps based on wavelength scans from eight monazites of known and varied composition. For each analysis, phi-rho-z matrix corrections were applied to the measured intensities of the full major and trace elements analyzed (see table 3). Interference

corrections of Th and Y on Pb Mα and Th on U Mβ were applied as in Pyle et al. (2002). Monazite from Manangotry, Madagascar (545±2 Ma; Paquette et al., 1994) was analyzed as internal age standard 5 times before and after each analytical session. The ages were calculated by using the weighted-average method and compiled with Isoplot 3 (Ludwic, 2003). Dates were calculated for each analytical spot using the matrix and interference-corrected concentrations of Pb, U, and Th by solving the monazite age equation of Montel et al. (1996). The statistical precision on each point was determined via counting statistics. For each point was calculated the relative standard deviation of the net peak count rate of the unknown (Pyle et al., 2005) for each of the three elements ($\varepsilon_{unknown}$). This value was then combined with the equivalent for the respective standards (ε_{std}), such that a value for the relative standard deviation of the *k*-ratio ($\varepsilon_{k\text{-ratio}}$) is determined, i.e.,

$$\varepsilon_{k\text{-ratio}} = \sqrt{\varepsilon^2_{std} + \varepsilon^2_{unknown}}$$

This is then assumed to be representative of the relative error in precision for the concentration of Pb, U, and Th. The concentration errors were then propagated through the age equation (Lisowiec, 2006). Once single-point dates and errors were determined at a 2σ level, data were grouped separately by grain, textural setting, and intragrain location (core, rim, etc.). Age groups between grains in similar textural settings (i.e., FIA set) were formed, and dates from the individual analyses comprising these groups were weighted and averaged to reduce errors on estimated age of the geological event recorded in a single FIA set.

6. RESULTS AND INTERPRETATION

A total of 383 analyses on monazites from the matrix (177 analyses) and staurolite porphyroblasts (206 analyses) were performed. For each analytical spot chemical ages were calculated (Tab. 4). These ages were grouped per grain, textural location (e.g. core, median, and rim; crenulated and crenulation cleavage) and FIA (Tabs. 5 and 6). All monazite grains from the same sample and textural setting for which less than four analytical spots were performed were grouped as one grain.

6.1. Monazite ages and FIAs

Monazite grains from staurolite porphyroblasts showing the same FIA set were grouped, and a single weighted-average age was calculated (Fig. 12). For FIA set 2 all monazite grains come from the cores of the staurolite porphyroblasts in sample IS77. The weighted-average age calculated for this FIA is 408±10 Ma (Fig. 12a and e). Previous work in the region identified a pre-400 Ma regional scale thermal event that produced the mineral assemblage And+St+Bt+Chl±Sill,Grt (e.g., Guidotti, 1989; DeYoreo et al., 1989; Smith and Barreiro, 1990; Guidotti and Holdaway, 1993; Guidotti and Johnson, 2002). Figure 5 (b and g) shows the distribution of garnet and staurolite porphyroblasts containing this FIA set. The event responsible for FIA set 2, developed during a period of W-E shortening, produced abundant garnet porphyroblasts; staurolite appears to be dominant in the SSE part of the region. In contrast, FIA set 1 porphyroblasts that formed during NE-SW shortening appear to be more evenly distributed on the map (Fig. 5a and f). Based upon relative FIA distributions it is likely that the event that produced FIA set 1 porphyroblasts had a regional extent, whereas FIA set 2 porphyroblasts were produced

more locally as a result of a thermal event related to the emplacement of the Emsian belt of plutons as the Acadian orogenic front was advancing westward (Bradley et al., 1998). If the observed distribution of garnet and staurolite porphyroblasts for this FIA set was produced as the result of the thermal event associated with the emplacement of the Emsian plutons, then an approximate age for the staurolite isograd for this event can be inferred. Staurolite growth around 400 Ma was documented in the literature as the result of an extensive regional thermal event (e.g., DeYoreo et al., 1989; Guidotti, 1989; Guidotti and Holdaway, 1993; Guidotti and Johnson, 2002). Taking into consideration the distribution of the garnet and staurolite porphyroblasts for this FIA set (Fig. 5b and g), and the regional staurolite isotherm, we suggest that staurolite growth at c. 400 Ma at a regional scale was restricted to the vicinity of the plutons emplaced at this time. From the regional distribution of the c. 400 Ma plutons in Fig. 2 we suggest that the heat source responsible for the formation of this FIA set was located to the south, within the migmatite domain, rather than towards east and northeast, where the Philips and Redington plutons are located.

For FIA set 3, monazite grains come from the cores of staurolite porphyroblasts in sample IS88 and from the staurolite porphyroblasts in sample IS23. The weighted-average age calculated for this FIA is 388.0±8.8 Ma (Figs. 12b and f). It has been proposed that between the regional-scale thermal event (≥ 400 Ma) and the emplacement of the Mooselookmeguntic pluton (c. 370 Ma) the rocks in the region cooled at the ambient temperature (DeYoreo et al., 1989). Figure 5 (c and h) shows that this FIA set is poorly represented and that the N-S shortening associated with this event did not produce extensive metamorphism. In relation to Bradley et al's (1998) work, the model age of this FIA set postdates the advancing of the orogenic front over that location. The age obtained

from FIA 3 porphyroblasts correlates well with the oldest age reported for the Mooselookmeguntic pluton, a biotite granite with a U-Pb zircon age of 389±2 Ma (Solar et al., 1998). A similar age, calculated for a chemically distinct matrix monazite grain (see bellow) from sample IS94 that shows FIA set 3 in the cores of the staurolite porphyroblasts, confirms that, around 388 Ma thermal activity in the region was renewed in close association with episodic emplacement of the Mooselookmeguntic pluton. The presence of this FIA set and the strong relationship with the oldest age for the Mooselookmeguntic pluton may have significant implications for its emplacement history. Smith and Barreiro (1990) suggested that the pluton might have been emplaced during multiple pulses. Brown and Solar (1998a, 1998b, 1999) and Solar et al., (1998) proposed that the emplacement of the Mooselookmeguntic pluton was deformation-controlled. Possibly the N-S shortening associated with this FIA set was responsible for the initiation of the pluton emplacement.

Monazite grains constraining the age of FIA set 4 come from samples IS74, IS94, and IS95. In sample IS74, FIA set 4 is represented by the crenulated cleavage in the staurolite porphyroblasts, whereas in samples IS94 and IS95 it is represented by the median growth of the staurolite porphyroblasts. The calculated model age for this FIA set is 372.1±5.5 Ma (Fig. 12c and g), which is in good agreement with the emplacement age of c. 370 Ma (Solar et al., 1998) for the main body of the Mooselookmeguntic pluton. The metamorphic event associated with the emplacement was described as static and produced mineral assemblages similar to those produced by the regional thermal event but experienced a slight increase in pressure (Guidotti and Holdaway, 1993; Guidotti and Johnson, 2002; Johnson et al., 2003). The NNW-SSE shortening associated with FIA set 4 and the thermal event related to the emplacement of the Mooselookmeguntic pluton

produced garnet and staurolite porphyroblasts (Fig. 5 d and i) as a result of positioning relative to the thermal gradient (e.g., Guidotti, 1989; Guidotti and Holdaway, 1993; Guidotti and Johnson, 2002). If the transition from garnet to staurolite is due to their relative position with respect to the heat source, then a staurolite isograd for this FIA set could be drawn (in preparation). According to the Bradley et al. (1998) model for Acadian orogenic front migration, the emplacement of the Mooselookmeguntic pluton was late-syntectonic (Solar and Brown, 2001).

The model age for FIA set 5 was calculated from monazite grains from samples IS71, IS94, and IS95. Staurolite porphyroblasts from sample IS71 show only one period of growth, whereas samples IS94 and IS95 show three distinct periods of growth, as discussed above. FIA set 5 staurolite, are present in samples IS94 and IS95, mainly as rim overgrowths (Figs. 13 and 14) of FIA 3-4 staurolite and/or overgrowth of a flat-lying matrix foliation (Fig. 9). The calculated model age for this FIA set is 352.7±4.2 Ma. This FIA set corresponds with a NW-SE shortening direction and has a similar orientation to the regional-scale structures (e.g., folds, schistosity). Figure 13 shows that this event produced extensive garnet and staurolite porphyroblasts. The heat source for this event could have been provided by the remnant heat that resulted from the emplacement of the Mooselookmeguntic pluton. The closest pluton with a similar age to FIA 5 is located in the Presidential Range (Eusden et al., 2000) about 150 km southwest of the Mooselookmeguntic pluton.

6.2. The absolute timing of porphyroblast growth

Different generations of porphyroblast growth can be separated and correlated at regional scale by using FIAs (e.g., Bell et al., 1998; Bell and Mares, 1999; Bell et al.,

2004). The relative timing between distinct generations of porphyroblasts can be determined by using microstructural relationships. Every FIA in a succession represents a specific tectono-metamorphic event during which the direction of bulk shortening was constant and orthogonal to the FIA trend (Bell and Welch, 2002). Tables 5 and 6 show the weighted-average model ages calculated for individual monazite grains and grouped by FIAs and monazite location textural location. Figure 15a shows the ages of individual grains grouped in ascending order and their relationships with the FIAs ages. Monazite grains included in staurolite porphyroblasts are isolated from the matrix so that during subsequent metamorphic events they will not be able to participate in new reactions. This is provided that fluid will not have access to the monazite location along cracks or other defects in the host crystal structure. Therefore, individual monazite grains included in staurolite porphyroblasts can give an age coeval and/or older, and/or younger than the time of the porphyroblast growth if the assumption has been violated. By using the textural location of the monazite grains in the matrix and staurolite porphyroblasts, as well as the relative timing determined for FIAs, approximate time duration for each FIA set can be deduced.

Data presented in Fig. 15a show that monazite growth in the interval 410 – 340 Ma was episodic but continuous. Most of the monazite data comes from samples showing FIA sets 3, 4, and 5, which makes these samples better suited for inferring the time extent of these FIAs, and, therefore, of a FIA in general. Samples IS94 and IS95 show a similar FIA history. They both grew garnet during FIA 3 and staurolite during FIA 3, 4, and 5. All monazite grains included in staurolite porphyroblasts come from cores showing FIA 4 and rims showing FIA 5 (Tab. 5). Monazite grains from FIA 5 staurolites show consistently

younger ages than those from FIA 4 staurolites (Figs. 13 and 14). The youngest age in FIA 4 staurolites is c. 360 Ma whereas in FIA 5 staurolites the youngest age is c. 353 Ma. Matrix monazites from sample IS94 (Tab. 6) were located in the crenulated cleavage, grains is94-m-2 and is94-m-3, which was overgrown by FIA 4 staurolites and in the crenulation cleavage, grain is94-m-1, overgrown by FIA 5 staurolites. Grains is94-m-1 and is94-m-2 show similar ages (Tab. 6 and Fig. 16). Grain is94-m-1 (Fig. 16a) has an elongated shape with its margins dissolved by progressive shearing during crenulation cleavage development, which indicates that this grain predates the crenulation cleavage. Grain is94-m-2 (Fig. 16b) does not show any evidence of deformation controlled dissolution suggesting that this grain might be coeval with the development of the foliation in the crenulated cleavage. Grain is94-m-3 is compositionally distinct (Fig. 17a) and shows a different age (Fig. 16). Therefore, it appears to predate the foliation in the crenulated cleavage and FIA 4 staurolites. Based on these data the growth of FIA 4 staurolites most probably occurred in the 360-380 Ma interval whereas growth of FIA 5 staurolites post-dated 360 Ma.

Sample IS71 grew staurolite and garnet porphyroblasts during FIA 5. Monazite grains from this sample have ages in the interval 344-378 Ma (Tabs. 5 and 6). Staurolite porphyroblasts were partially replaced by coarse-grained Ms+Bt and garnet porphyroblasts were broken down to biotite (Fig. 11a). The yttrium budget in a rock may be controlled by reactions involving garnet and accessory phases (Pyle and Spear, 1999), whereas the yttrium content in monazite has been directly linked to garnet-in and -out reactions (Pyle and Spear, 2003; Gibson et al., 2004). Fig. 17b shows the average yttrium content for all monazite grains coming from sample IS71. Note that matrix monazite is71-m-2 has a

distinctively higher yttrium content than all the other grains. The age of this grain is marginally younger than the youngest monazite grain included in FIA 5 staurolite and has significantly higher yttrium content. We suggest that this monazite grain formed shortly after the staurolite growth ceased and that the changed metamorphic conditions caused the staurolite and garnet to break down. As a consequence of the garnet breaking down to biotite, the yttrium budget in the rock was reset and the new monazites became yttrium enriched. Based on these arguments we suggest that FIA 5 porphyroblasts most probably grew in the interval 345-360 Ma.

The time duration for FIA 2 and 3 porphyroblasts is less certain, taking into consideration the lower number of monazite grains coming from samples showing these FIA sets. In the case of FIA 3 porphyroblasts, a number of arguments can be considered. No monazite grain included in these porphyroblasts shows an age younger than 385 Ma (Tab. 5). In the case of sample IS88, monazite grains from the core of the staurolite porphyroblasts yield a weighted-average model age of 385±9.7 Ma whereas the weighted average age for the matrix monazites is 371±10 Ma. Sample IS94 shows FIA 3 in garnet porphyroblasts and FIA 3, 4, and 5 in staurolite porphyroblasts. Although no monazite grain was found in FIA 3 porphyroblasts from this sample, one matrix monazite, is94-m-3, gives an age of 386±12 Ma, which is coeval with the development of FIA 3. Figure 17a shows the average yttrium content for all monazite grains from sample IS94. Note that grain is94-m-3 has a significantly lower yttrium content than all the other monazite grains in the rock. The age of this grain suggests that it grew during FIA 3 when garnet was produced; therefore, the monazite was involved in a competing reaction with garnet for the yttrium. Most probably yttrium partitioned preferentially in garnet so that yttrium-depleted

monazites were formed. The breakdown of FIA 3 garnet to produce FIA 4 and 5 staurolites released yttrium, which in turn was incorporated in the newly-formed monazites. Taking into consideration these arguments we suggest that the growth of FIA 3 porphyroblasts ceased at about 380 Ma when yttrium enrichment in new monazite began to occur (e.g., is94-st3) during FIA 4. An upper limit for the initiation of FIA 3 is difficult to ascertain taking into consideration the small areal extent and the small number of porphyroblasts containing this FIA (Fig. 5 c and h). Based on other monazite ages in the region (Smith and Barreiro, 1990), however one can suggest the interval 395-380 Ma for this FIA set.

Monazite ages in the range of FIA 2 (408±10 Ma) have previously been reported in the region by Smith and Barreiro (1990); they are 398-406 Ma. Using the comparator of the age extent of the other FIAs we can suggest that FIA 2 extended over the 395-415 Ma interval.

6.3. Monazite growth conditions

Smith and Barreiro (1990) suggested that monazite growth in the region occurred at staurolite-grade conditions. The change in chemistry for different monazite grains in sample IS94 with time indicates that monazite grain is94-m-3 in this sample was produced at garnet-grade conditions rather than staurolite grade conditions. FIA data in sample IS71 clearly indicate that this sample produced garnet and staurolite during FIA 5 (345-360 Ma), whereas the ages of the monazite grains is71-m-4 and is71-st3 indicate that they formed before garnet. Sample IS74 produced garnet during FIA 4 and staurolite during FIA 5. Staurolite porphyroblasts overgrew a differentiated crenulation cleavage where the inclusion trails representing the crenulated cleavage have a similar orientation and FIA with the inclusion trails in garnet porphyroblasts (Fig. 8). All monazite grains from

staurolite porphyroblasts were located in the crenulated cleavage and gave a weighted-average model age (371±13 Ma) synchronous with the age of FIA 4 porphyroblasts. Two monazite grains from the matrix, is74-m-1 and is74-m-6, although situated in different textural settings, yield similar ages (Tab. 6) reflecting FIA 4. However, monazite growth in this sample also occurred at garnet-grade conditions.

6.4. Comparison with previous metamorphic geochronology in the region

Previous geochronological work on the Acadian deformation and metamorphism of the Northern Appalachian employed a variety of techniques and methods (e.g., in-situ isotopic and EPMA dating – Pyle et al., 2005; in-situ isotopic dating – Gerbi and West, 2007; U-Pb chemical extraction – Eusden et al., 2000). Accurate correlations are difficult. Figure 18 shows the location of the metamorphic ages cited in this paper. The available metamorphic ages spread over the 430-350 Ma interval with major peaks around 400 Ma and 370 Ma. Smith and Barreiro (1990) separated two distinct monazite populations from schists of the Perry Mountain Formation in the contact aureole of the Mooselookmeguntic pluton. The first population dates at about 400 Ma and the second one at about 370 Ma. They did not exclude the possibility of multiple generations of monazite due to several pulses of igneous emplacement. Eusden et al. (2000) reported monazite ages of c. 400 Ma from schists and migmatites of the Presidential Range, New Hampshire. Bell and Welch (2002) based on a consistent succession of five different FIA trends measured in garnet porphyroblasts from the metamorphic rocks in the Chester Dome region of Vermont, separated five different monazite ages with peaks at: 425, 405, 387, 367, and 352 Ma. Pyle et al. (2005) separated four age-compositionally-distinct monazite domains in schists from

southwestern New Hampshire with peaks at 400±10 Ma – domain 1, 381±8 Ma – domain 2, 372±6 Ma – domain 3 and 352±14 Ma domain 4. Gerbi and West (2007) reported monazite ages from schist in the south-central Maine that showed an age spread from 430 to 350 Ma with peaks at 430, 410, 390, 370, and 350 Ma.

7. DISCUSSION

7.1. The age of FIA 1

Sample IS104 contains FIA set 1 in both garnet and staurolite porphyroblasts. All monazite grains from this sample lie in the matrix. They have ages in the 360 – 370 Ma interval (Tab. 6), which are contemporaneous with the development of FIA set 4. Microstructural evidence suggests that FIA 1 porphyroblast growth predates the growth of all the other porphyroblasts in the region. However, younger monazite ages in the matrix than in porphyroblasts are common (e.g., Bell and Welch, 2002; Gibson et al., 2004), yet this sample shows no evidence of any age older than FIA set 4 porphyroblasts. These young ages in the matrix monazites can be explained by:

- This sample did not produce monazite until c. 370 Ma;
- Monazite ages were reset under upper-sillimanite-zone conditions (Smith and Barreiro, 1990) due to the emplacement of the Mooselookmeguntic pluton at 370 Ma;
- The growth of many c. 370 Ma monazite grains obliterated any older ones in the statistics and EPMA dating can not differentiate between different populations in the absence of isotopic measurements;

Combined isotopic measurements and EPMA dating revealed that careful separation of chemically-distinct domains is reflected in concordant isotopic and chemical ages (e.g., Gibson et al., 2004; Pyle et al., 2005; Dahl et al., 2005; Williams et al., 2006). From all the elements responsible for chemical zoning in monazite, yttrium zoning shows the best correlation with different age domains. Two distinct populations can be separated based on yttrium statistics (Fig. 19), both of them giving the same age within error. The presence of small monazite inclusions in staurolite and garnet porphyroblasts indicates that this sample did produce monazite at the time of porphyroblast growth. If the monazite growth was synchronous with the growth of garnet porphyroblasts then competing reactions for yttrium between garnet and monazite, and possibly xenotime, (Pyle and Spear, 1999), would have favored the partitioning of yttrium into garnet and smaller monazite grains were produced. Monazite grains that grew simultaneously with the garnet porphyroblasts in sample IS94 have a distinctively lower yttrium content (Fig. 17a). Matrix coarsening during high-grade metamorphism related to intrusion of the Mooselookmeguntic pluton (c. 370 Ma) would have dissolved the small matrix monazites located on the grain boundaries, while the consumption of garnet (Fig. 11b) released yttrium so that new younger monazite grains were formed at the expense of the previously developed ones.

Figure 15b shows emplacement ages for plutons in Maine and adjacent areas. Pluton ages spread over the interval 430-350 Ma which correlates with metamorphic monazite ages determined from the same rocks (Smith and Barreiro, 1990; Eusden et al., 2000; Bell and Welch, 2002; Pyle et al., 2005; Gerbi and West, 2007). Based on these ages

and the microstructural relationships between porphyroblasts from different FIA sets (Tab. 2 and Fig. 10), we suggest that the age of FIA 1 could be around 420 Ma.

7.2. Implications for the metamorphic history of west-central Maine

At least three different metamorphic events (M1, M2, and M3) have affected the region (e.g., Guidotti, 1989; Guidotti and Holdaway, 1993; Guidotti and Johnson, 2002). Metamorphism was syn-tectonic during M1 when an areally large chlorite-zone was produced. Following M1 two high temperature, largely static events affected the region. Around 400 Ma a regional thermal event produced St+And+Bt+Chl±Grt and possibly Sill+Kfs at higher grades. Most of the M2 was overprinted by the late post-tectonic contact metamorphism, M3, related with the intrusion of Devonian plutons. The age of the M3 was determined to be around 370 Ma (Smith and Barreiro, 1990), post-dating the peak regional metamorphism, M2, by c. 30 Ma. During M3 mineral assemblages similar to those of M2 were produced as well as prograde and retrograde pseudomorphs of M2 porphyroblasts. It was proposed that between M2 and M3 the rocks cooled to the ambient temperature before being overprinted by M3 (DeYoreo et al. 1989).

Figures 13, 14, and 20 show examples of "typical" staurolite porphyroblasts from the contact aureole of the Mooselookmeguntic pluton. The cores of these staurolites, which contain FIA 4, were referred in the literature as M2 staurolites (Guidotti and Johnson, 2002; Johnson et al., 2006) that post-kinematically overgrew the regional foliation S_2 (e.g., Guidotti, 2000, Guidotti and Johnson, 2002; Johnson et al., 2006). The staurolite rims, which contain FIA 5, were referred to as M3 staurolites that overgrew a foliation related to pluton emplacement. Figures 13, 14, and 20 and the ages of FIAs 4-5

show that M2 staurolites (e.g., FIA 4 staurolites in this study), which were previously thought to be around 400 Ma (e.g. Smith and Barreiro, 1990; Johnson et al. 2006) in age, are actually about 370 Ma old or younger and contemporaneous with the intrusion of the main body of the Mooselookmeguntic pluton at 370 Ma (Solar and Brown, 1998). The rims, called M3 staurolites by these earlier workers (FIA 5 staurolites in this study), were thought to have formed around 370 Ma. The ages calculated for the monazite grains included in the "M3" rims (Figs. 13, 14 and 20) indicate that this generation of staurolites formed later than 353 Ma. The microstructural relationships between FIA sets distinguished these younger garnet and staurolite porphyroblasts, which along with the andalusite and cordierite porphyroblasts (no FIA data are available for the latter) indicate that the later phases of porphyroblast growth postdate all the FIA sets described in this study (in preparation).

7.3. Staurolite isograds in the contact aureole of the Mooselookmeguntic pluton

The staurolite isograd in Fig. 5 was drawn after Guidotti and Johnson (2002) and shows an accurate representation of the field transition from garnet-zone to staurolite-zone. Obvious questions, in the light of the data presented above are to which event does this staurolite isograd relate, and can isograds be accurately distinguished for different events (e.g., different FIA sets)? As shown above, the timing of metamorphism in the region was largely misinterpreted, and porphyroblasts belonging to different tectono-metamorphic events were considered the result of one event. The situation of five different successive periods of garnet and staurolite growth during different tectono-metamorphic events opens

the possibility of tracing the evolution of the staurolite isograds with time. Although at the moment speculative this possibility, remains open for future work.

7.4. Acadian orogeny

Recent studies in the Northern Appalachian orogen reported metamorphic and pluton crystallization ages for the Acadian orogeny in the 430-350 Ma interval (e.g., Solar et al., 1998; Bradley et al., 1998; Eusden et al., 2000; Bell and Welch, 2002; Pyle et al., 2005; Gerbi and West, 2007). Three distinct periods of pluton emplacement can be separated based on data shown in Fig. 15b. Two of them concentrate around 420 Ma and 405 Ma whereas the third one spreads over the 400-350 Ma interval. Porphyroblast-matrix relationships suggest that deformation and metamorphism were synchronous (e.g., Bell et al., 1998; Solar and Brown, 1999; Bell and Welch, 2002; Bell and Newman, 2006), whereas pluton emplacement was deformation-controlled (e.g., Solar et al., 1998; Brown and Solar, 1999; Solar and Brown, 2001). The two distinct peaks, prior to 400 Ma probably indicate that the deformation was more intense and evenly partitioned across the orogen. Bradley et al. (1998) suggested that the Acadian orogenic deformation front reached the current level during early Emsian. Following the advance of the Acadian orogenic front perhaps the partitioning of deformation and metamorphism were more heterogeneous and localized around plutons (DeYoreo et al., 1989), so that they variably modified and overprinted previous events. Similar metamorphic age ranges in different parts of the Northern Appalachian orogen (Smith and Barreiro, 1990; Eusden et al., 2000; Bell and Welch, 2002; Pyle and Spear, 2005; Gerbi and West, 2007; this study) confirm the Bell and Welch (2002) hypothesis that the orogenesis in the Northern Appalachians was continuous from the Taconic through the Acadian to $\leq$ 350 Ma.

7.5. The heat source

Figures 15a and 15b show that pluton emplacement and metamorphism in the Central Maine Belt occurred with little interruption from 430 to 350 Ma. Solar et al. (1998) and Solar and Brown (1999, 2000) determined that deformation, metamorphism, and pluton emplacement were synchronous. Although the idea of pluton-driven metamorphism (DeYoreo et al., 1989) has support in predominantly localized high-grade metamorphism around the plutons, the new metamorphic ages (Fig. 18 and this study) suggest that the metamorphic high was more regional than local, and superimposed by pluton-driven thermal pulses (Brown and Solar, 1999). Bradley et al. (1998), based on pluton emplacement ages and foreland basin analysis, suggested that the Acadian orogenic front migrated inboard during Devonian. Solar and Brown (2001) interpreted the Central Maine Belt to have developed as a thrust system during dextral-transpressive deformation in response to the Acadian oblique convergence. They argued that this resulted in large-scale belts of high strain separated by intervening zones of low strain. This suggests a strong inter-relationship and a feed-back system between melting, pluton emplacement, deformation, and metamorphism.

The metamorphic grade in the region (lower-amphibolite facies) cannot have generated conditions for melting at 3 to 4 kbars. An additional heat source is required to generate the thermal perturbation responsible for melting and metamorphism over the 430-350 Ma interval. Robinson et al. (1998) and Pyle et al. (2005) proposed a model of sub continental lithospheric detachment of the lower plate, followed by asthenospheric mantle upwelling responsible for heat advection into the lower crust and consequent melting. Murphy et al. (1999) proposed flattening of the subduction zone, which they attributed to

overriding of a plume by the convergent margin, thermally eroded the overlying lithosphere and exposed continental lithosphere to a hot asthenosphere. Their model fits well with the Bradley et al. (1998) model for the Acadian evolution of the orogen and the Solar and Brown (2001) structural model for the Central Maine Belt and gives a viable explanation for melting and metamorphism. Both of these models, that is, lithospheric mantle delamination and/or flattening of the subduction zone, accounts for the presence of mantle components in pluton compositions. Tomascak et al. (2005) showed that mafic melts from the mantle were not important in the genesis of the Devonian plutons or the Carboniferous Sebago batholith (Tomascak et al., 1996).

Schoonmaker et al. (2005) explained the extensive plutonism by slab breakoff, when the leading edge of the subducting continental margin was still in the far-foreland or outer-trench position, by failure of the mechanically weak pseudo-passive margin containing large strike parallel faults during Acadian underthrusting. Although this model might explain the lack of mantle material in the isotopic signature of the Devonian plutons, it does not explain continuous deformation and metamorphism from before 410 Ma to c. 340 Ma. This model (see also Bradley et al., 1998; and Robinson et al., 1998) proposes that the position of the Acadian deformation (Fig. 21) front reached the present level by early Emsian (c. 407 Ma), which is confirmed by FIA 2 porphyroblasts at 408 Ma. The presence of FIA 1 porphyroblasts indicates that deformation took place at least 10 m.y. prior to the emplacement of the Emsian plutons and continued up to c. 340 Ma and possibly later into the Alleghanian.

An example of a low-pressure high-temperature terrane where high temperature regimes were sustained for more than 100 m.y. is the western Mount Isa Inlier, Australia.

McLaren et al. (1999) attributed the high thermal gradients to the burial of granite batholiths enriched in radiogenic elements beneath the thick insulating sedimentary succession of the Mount Isa Group. However, in the Maine region of the Northern Appalachian the situation is quite different and syn-metamorphic plutonism at shallow crustal levels is very common, while absent in the Mount Isa inlier. The thermal gradients in Maine must have been higher since they were responsible not only for the metamorphism, but also for melting large amounts of crust.

Hyndman et al. (2005) proposed a model to explain long-lived orogenic belts and the origin of the heat where, they argue, continental back-arcs have hot and thin lithosphere, because of shallow asthenosphere convection facilitated by water rising from the underlying subducting slab. In this model continental collision and orogenic shortening are concentrated in back arcs that are much weaker than the adjacent stable areas. The inherited high temperatures provide an explanation for widespread orogenic plutonism, high-temperature regional-metamorphism and ductile-crustal deformation. In western Maine and adjacent areas, although plutonism is widespread, high-temperature metamorphism is closely related to pluton proximity. This may suggest that plutonism is the cause of high-temperature metamorphism, but high regional geothermal gradients are required to cause plutonism.

High temperature-low pressure terranes associated with plutonism are very common in most orogenic belts. In most cases the main question that arises from such a combination is what actually caused the plutonism and the associated metamorphism. Is it the pre-existence of a high regional heat flow the cause of plutonism or is the plutonism responsible for the high geothermal gradients? The intimate association of metamorphic

grades with the plutons contours suggests that the plutonism was responsible for the high heat flow and associated metamorphism (DeYoreo et al., 1989). The succession of at least five high-grade metamorphic events in the contact aureole of the Mooselookmeguntic pluton and the close relationship with the pluton proximity indicate that the pluton was built up in steps during subsequent deformation events. The intimate association of high-grade metamorphism and plutonism in Maine suggest that plutonism was not generated by high regional geothermal gradients and that something else was responsible for melting in the lower crust. Brown and Solar (1998) proposed that the deformation in Maine was partitioned between larges-scale shear zones and intervening zones of low strain. If mylonitization at depths associated with fluids due to dehydration reactions and shear heating and melting (Weertman, 1971) at the base of crust was responsible for magma generation, then the ascending melt along dilatation sites would be emplaced in the upper crust at a rate controlled by the partitioning of deformation and the intensity of the regional stress field. Every new deformation event will trigger melting in the lower crust, and therefore heat transfer by advection in discrete magmatic episodes, which will result in high temperature-low pressure metamorphism in the upper crust during contractional deformation (Sandiford et al., 1992; Stüwe et al., 1993).

REFERENCES

Bell, T. H., 1986. Foliation development and refraction in metamorphic rocks: reactivation of earlier foliations and decrenulation due to shifting patterns of deformation partitioning, *Journal of Metamorphic Geology,* **4**, 421-444.

Bell, T. H., and Mares, V. M., 1999. Correlating deformation and metamorphism around arcs in orogens. *American Mineralogist*, **84**, 1727-1740.

Bell, T. H., and Newman, R., 2006. Appalachian orogenesis: the role of repeated gravitational collapse. In: *Butler, R., Mazzoli, S. (Eds.), Styles of Continental Compression. Special Papers of the Geological Society of America*, **414**, 95-118.

Bell, T. H., and Welch, P. W., 2002. Prolonged Acadian Orogenesis: revelations from FIA controlled monazite dating of foliations in porphyroblasts and matrix. *American Journal of Science* **302**, 549-581.

Bell, T. H., Forde, A., and Wang, J., 1995. A new indicator of movement direction during orogenesis: measurement technique and application to the Alps. *Terra Nova*, **7**, 500-508.

Bell, T. H., Ham, A. P., and Kim, H. S., 2004. Partitioning of deformation along an orogen and its effects on porphyroblast growth during orogenesis. *Journal of Structural Geology*, **26**, 825-845.

Bell, T. H., Hickey, K. A., and Upton, G. J. G., 1998. Distinguishing and correlating multiple phases of metamorphism across a multiply deformed region using the axes of spiral, staircase and sigmoidal inclusion trails in garnet. *Journal of Metamorphic Geology*, **16**, 767-794.

Bell, T. H., Hickey, K. A., and Wang, J., 1997. Spiral and staircase inclusion trail axes within garnet and staurolite porphyroblasts from the schists of the Bolton Syncline, Connecticut: timing of porphyroblast growth and the effects of fold development. *Journal of Metamorphic Geology*, **15**, 467-478.

Bradley, D. C., Tucker, R. D., Lux, D., Harris, A. G., and McGregor, D. C., 1998. Migration of the Acadian orogen and foreland basin across the northern Appalachians. U.S. Geological Survey Open File Rep. 98-770, 79 p.

Brown, M., and Solar, G. S., 1998a. Shear zone systems and melts: feedback relations and self organization in orogenic belts. *Journal of Structural Geology*, **20**, 211-227.

Brown, M., and Solar, G. S., 1998b. Granite ascent and emplacement during contractional deformation in convergent orogens. *Journal of Structural Geology*, **20**, 1365-1393.

Brown, M., and Solar, G. S., 1999. The mechanism of ascent and emplacement of granite magma during transpression: a syntectonic granite paradigm. *Tectonophysics*, **312**, 1-33.

Cihan, M., and Parsons, A., 2005. The use of porphyroblasts to resolve the history of macro-scale structures: an example from the Robertson River Metamorphics, North-Eastern Australia, *Journal of Structural Geology,* **27**, 1027-1045.

Dahl, P. S., Hamilton, M. A., Jercinovic, M. J., Terry, M. P., Williams, M. L. and Frei R., 2005. Comparative isotopic and chemical geochronometry of monazite, with implications for U–Th–Pb dating by electron microprobe: an example from metamorphic rocks of the eastern Wyoming (U.S.A.). *American Mineralogist* **90** , 619–638.

Davis, B. K., 1995. Regional-scale foliation reactivation and re-use during formation of a macroscopic fold in the Robertson River Metamorphics, north Queensland, Australia. *Tectonophysics,* **242**, 293-311.

DeYoreo, J. J., Lux, D. R., Guidotti, C. V., Decker, E. R., and Osberg, P. H., 1989. The Acadian thermal history of western Maine. *Journal of Metamorphic Geology*, **7**, 169-190.

Eusden, J. D., Jr., Guzovski, C. A., Robinson, A. C., and Tucker, R. D., 2000. Timing of the Acadian orogeny in northern New Hampshire. *Journal of Geology*, **108**, 219-232.

Gerbi, C., and West, D. P., Jr., 2007. Use of U-Pb geochronology to identify successive, spatially overlapping, tectonic episodes during Silurian-Devonian orogenesis in south-central Maine, USA. *Geological Society of America Bulletin*, **119**, 1218-1231.

Gibson, H. D., Carr, S. D., Brown, R. L. and Hamilton, M. A., 2004. Correlations between chemical and age domains in monazite, and metamorphic reactions involving major pelitic phases: an integration of ID-TIMS and SHRIMP geochronology with Y–Th–U X-ray mapping. *Chemical Geology,* **211**, 237-260.

Guidotti, C. V., 1989. Metamorphism in Maine: an overview: In: Studies in Maine. *Geology*, **3**, 1-19.

Guidotti, C. V., 2000. The classic high-T–low-P metamorphism of west-central Maine, USA: Is it post-tectonic or syntectonic? Evidence from porphyroblast-matrix relations: Discussion. *Canadian Mineralogist*, **38**, 1007-1026.

Guidotti, C. V., and Holdaway, M. J., 1993. Petrology and field relations of successive metamorphic events in pelites of west-central Maine. In: *Cheney, J.T., Hepburn, J.C. (Eds.), Field Trip Guidebook for the Northeastern United States*, **1**. Geological Society of America, L1-L23.

Guidotti, C. V., and Johnson, S. E., 2002. Pseudomorphs and associated microstructures of western Maine, USA. *Journal of Structural Geology*, **24**, 1139-1156.

Hayward, N., 1990. Determination of early fold-axis orientations in multiply deformed rocks using porphyroblast inclusion trails. *Tectonophysics*, **179**, 353-369.

Hyndman, R. D., Currie, C. A., and Mazzotti, S. P., 2005. Subduction zone backarcs, mobile belts, and orogenic heat. *GSA Today*, **15**, 4-10.

Johnson, S. E., Dupee, M. E., and Guidotti, C. V., 2006. Porphyroblast rotation during crenulation cleavage development: an example from the aureole of the Mooselookmeguntic pluton, Maine, USA. *Journal of Metamorphic Geology,* **24**, 55-73.

Johnson, T. E., Brown, M. and Solar, G. S. 2003. Low-pressure subsolidus and suprasolidus phase equilibria in the MnNCKF-MASH system: constraints on conditions of regional metamorphism in western Maine, northern Appalachians. *American Mineralogist*, **88**, 624-638.

Lisowiec, N., 2006. Precision estimation in electron microprobe monazite dating: Repeated measurements versus statistical (Poisson) based calculations. *Chemical Geology*, **234**, 223-235.

Ludwig, K., 2003. User's Manual for Isoplot 3.00, A Geochronological Toolkit for Microsoft Excel: Berkeley Geochronology Center, No. 4a, Berkeley, California.

McLaren, S., Sandiford, M., and Hand, M., 1999. High radiogenic heat-producing granites and metamorphism; an example. *Geology,* **27**, 679-682.

Murphy, J. B., van Staal, C. R., and Keppie, J. D., 1999. Middle to late Paleozoic Acadian orogeny in the northern Appalachians: A Laramide-style plume-modified orogeny?. *Geology*, **27**, 653-656.

Paquette, J. L., Nedelec, A., Moine, B. and Rakotondrazafi, M., 1994. U-Pb, Single Zircon Pb-Evaporation, and Sm/Nd Isotopic Study of a granulite domain in SE Madagascar, *Journal of Geology,* **102**, 523-538.

Pouchou, J. L., and Pichoir, F., 1984. A new model for quantitative X-ray microanalysis. I: Application to the analysis of homogeneous samples. *La Recherche Aerospatiale,* **3**, 13-38.

Pouchou, J. L., and Pichoir, F., 1985. "PAP" (ϕ-ρ-Z) procedure for improved quantitative microanalysis. In: J. T. Armstrong, Editor, *Microbeam Analysis*, San Francisco Press Inc, San Francisco, 104-106.

Pyle, J. M., and Spear, F. S., 1999. Yttrium zoning in garnet: coupling of major and accessory phases during metamorphic reactions. *Geological Materials Research*, **1**, 1-49.

Pyle, J. M., and Spear, F. S., 2003. Four generations of accessory-phase growth in low-pressure migmatites from SW New Hampshire, *American Mineralogist,* **88**, 338-351.

Pyle, J. M., Spear, F. S., and Wark, D.A., 2002. Electron microprobe analysis of REE in apatite, monazite and xenotime: protocols and pitfalls, *Reviews in Mineralogy and Geochemistry,* **48**, 337-362.

Pyle, J. M., Spear, F. S., Cheney, J. T., and Layne, G., 2005. Monazite ages in the Chesham Pond Nappe, SW New Hampshire, U.S.A.: implications for assembly of central New England thrust sheets. *American Mineralogist*, **90**, 592-606.

Pyle, J. M., Spear, F. S., Wark, D.A., Daniel, C. G., and Storm, L. C., 2005. Contributions to precision and accuracy of chemical ages of monazite, *American Mineralogist,* **90**, 547-577.

Reinhardt, J., and Rubenach, M. J., 1989. Temperature–time relationships across metamorphic zones: evidence from porphyroblast–matrix relationships in progressively deformed metaplites, *Tectonophysics,* **158**, 141-161.

Robinson, P., Tucker, R. D., Bradley, D. C., Berry, H. N., and Osberg, P. H., 1998. Paleozoic orogens in New England, U.S.A. *Geologiska Föreningens I Stockholm Förhandlingar*, **120**, 119-148.

Sandiford, M. A., Foden, J. D., Zhou, S., and Turner, S. P., 1992. Granite genesis and the mechanics of convergent orogenic belts with application to the southern Adelaide fold belt. *Royal Society of Edinburgh Transactions*, **83**, 83-93.

Sayab, M., 2007. Correlating multiple deformation events across the Mesoproterozoic NE Australia using foliation intersection axes (FIA) preserved within porphyroblasts. *Gondwana Research*, **13**, 331-351.

Schoonmaker, A., Kidd, W. S. F., Bradley, D. C., 2005. Foreland-forearc collisional granitoid and mafic magmatism caused by lower-plate lithospheric slab breakoff: The Acadian of Maine, and other orogens. *Geology,* **33**, 961-964.

Smith, H. A., and Barreiro, B., 1990. Monazite U-Pb dating of staurolite grade metamorphism in pelitic schists. *Contributions to Mineralogy and Petrology*, **105**, 602-615.

Solar, G. S., and Brown, M., 1999. The classic high-T – low-P metamorphism of west-central Maine, USA: Is it post-tectonic or syn-tectonic? Evidence from porphyroblast-matrix relations. *Canadian Mineralogist*, **37**, 311-333.

Solar, G. S., and Brown, M., 2000. The classic high-*T*–low-*P* metamorphism of west–central Maine, USA: is it post-tectonic or syn-tectonic? Evidence from porphyroblast–matrix relations. Reply. *Canadian Mineralogist,* **38**, 1007-1026.

Solar, G. S., and Brown, M., 2001. Deformation partitioning during transpression in response to Early Devonian oblique convergence, northern Appalachian orogen, USA. *Journal of Structural Geology*, **22**, 1043-1065.

Solar, G. S., Pressley, R. A., Brown, M., and Tucker, R. D., 1998. Granite ascent in convergent orogenic belts: Testing a model. *Geology*, **26**, 711-714.

Stüwe, K., Sandiford, M., and Powell, R., 1993. Episodic metamorphism and deformation in low-pressure, high-temperature terranes. *Geology,* **21,** 829-832.

Tomascak, P. B., Brown, M., Solar, G. S., Becker, H. J., Centorbi, T. L., and Tian, J., 2005. Source contributions to Devonian granite magmatism near the Laurentian border, New Hampshire and western Maine, U.S.A. *Lithos*, **80**, 75-99.

Tomascak, P. B., Krogstad, E. J., and Walker, R. J., 1996. Nature of the crust in Maine, U.S.A.: evidence from the Sebago batholith, *Contributions to Mineralogy and Petrology*, **125**, 45-59.

Weertman, J., 1971. Theory of water-filled crevasses in glaciers applied to vertical magma transport beneath ocean ridges. *Journal of Geophysical Research,* **B76**, 1171-1183.

Williams, M. L., Jercinovic, M. J., Goncalves, P., and Mahan, K. H., 2006. Format and philosophy for collecting, compiling, and reporting microprobe monazite ages. *Chemical Geology*, **225**, 1-15.

– SECTION C –

THE PROBLEM, SIGNIFICANCE, AND METAMORPHIC IMPLICATIONS OF 60 MILLION YEARS OF POLYPHASE STAUROLITE GROWTH

- SECTION C –

THE PROBLEM, SIGNIFICANCE, AND METAMORPHIC IMPLICATIONS OF 60 MILLION YEARS OF POLYPHASE STAUROLITE GROWTH

ABSTRACT

Microstructural measurements of FIAs (foliation intersection/inflection axes preserved in porphyroblasts) in staurolite reveal at least 3 periods of growth in the Proterozoic Colorado front range and 5 in the Palaeozoic of western Maine. Monazite inclusions in staurolite have an absolute age of 1760±12 Ma (FIA 1), 1720.4±6.8 Ma (FIA 2), and 1682±18 Ma (FIA 3) in Colorado, and 408±10 Ma (FIA 2), 388±8.8 Ma (FIA 3), 372.1±5.5 Ma (FIA 4), and 352.7±4.2 Ma (FIA 5) in Maine, confirming the multiple periods of deformation and metamorphism indicated by the FIA succession in each region. Thermodynamic modeling in the NCMnKFMASH system reveals that this episodic growth of staurolite occurred over a similar bulk compositional range and PT path. Multiple phases of growth by one reaction in the same and adjacent rocks in both regions strongly suggest that PT and X are not the only factors controlling the commencement and cessation of metamorphic reactions. The FIAs preserved by the staurolite porphyroblasts indicate that each stage of growth in both areas occurred during deformation and indicate that the local partitioning of deformation at the scale of a porphyroblast was the controlling factor on whether or not the reaction took place.

Keywords: FIAs; staurolite; monazite dating; metamorphism; Thermocalc.

1. INTRODUCTION

The basis of quantitative metamorphic petrology is the inference that the prograde mineral assemblages within a rock are in chemical equilibrium (Bickle and Baker, 1990).

This conclusion, though difficult to prove absolutely, seems a logical consequence of the enormous amounts of geological time available for individual deformation/metamorphism events. The extraordinary lengths of time available for reactions means that for a certain bulk composition and PT environment, once local equilibrium is achieved, it ought to go to completion. Thus bulk composition, PT, fluids, and time are generally assumed to be the only controls on whether or not a reaction will take place. Workers such as Carlson et al. (1995), Baxter and DePaolo (2000, 2002, and 2004) and Baxter (2003) have shown that several problems exist with this approach. However, newly developed approaches to studying the metamorphic and structural interrelationships have revealed another significant problem.

It is known that deformation affects fluid and heat flow (Lasaga et al., 2000) and can control porphyroblast nucleation. It does this by reducing the nucleation energy barrier to a reaction (Carlson et al., 1995; Hirsch, 2007) and by providing rapid access and removal of materials to a reaction site (Bell at al., 1986). However, existing models for most orogenic terranes commonly lack detailed time constraints on direct links between deformation and metamorphism. The measurement of foliation intersection/inflection axes in porphyroblasts (FIAs) allows detailed access to the timing of growth of the same as well as different mineral phases. Multiple generations of garnet growth over lengthy time periods have been recognized and dated via monazite grains preserved within the inclusion trails that have been used to define a succession of FIAs (Bell and Welch, 2002).

Garnet is a mineral that can grow from a variety of reactions over a large range of TP conditions and so the recognition of multiple phases of growth of this phase did not cause any conceptual problems. However, staurolite is not, because staurolite-forming

reactions typically have a lower variance than those producing garnet. This study demonstrates that the same behavior that occurs for garnet can occur for staurolite in rocks where there is little or no change in bulk composition. This has considerable implications for the current assumptions used by most metamorphic petrologists. To demonstrate the widespread nature of this problem, two differently aged and located fold belts in the Precambrian rocks in the Rocky Mountain Foothills in Colorado and the Palaeozoic rocks of the Appalachians in western Maine are used.

2. LOCATION AND SETTING

2.1. Northern Appalachians

The western Central Maine Belt (Fig. 1) was deformed and metamorphosed at lower amphibolitic facies during the Acadian orogeny. At least three different metamorphic events affected the region with peak metamorphic conditions occurring around 400 Ma (Guidotti and Johnson, 2002). The first event produced chlorite, the second And+St+BtGrt, and the third St+Grt+Sill plus pro and retrograde pseudomorphs of earlier-formed porphyroblasts (Guidotti and Johnson, 2002). The Siluro–Devonian metasediments were intruded syn-tectonically by the 389 to 370 Ma Mooselookmeguntik pluton. A strong pervasive matrix foliation striking NE is crosscut by an axial plane crenulation cleavage.

2.2. Colorado Front Range

The Colorado front (Fig. 2) contains Early Proterozoic schists and gneisses that record multiple episodes of deformation and metamorphism that varied on a regional scale during two main periods of orogeny around 1700 and 1400 Ma with associated igneous intrusions (Selverstone et al., 1997). In the northern Front Range most of the rocks reached

the amphibolite facies and extensive migmatization occurred at higher grades. Peak metamorphic conditions produced Grt+St+And±Sill and have been broadly constrained between 1.75-1.70 Ga (Nesse, 1984). A second metamorphic event was associated with regional heating throughout the Front Range and locally produced new growth of garnet, andalusite, and staurolite (Shaw et al., 1999). The metasedimentary sequence was affected by two main plutonic events, one around 1.7 Ga and the second one around 1.4 Ga (Cavosie and Selverstone, 2003).

3. DATA

3.1. FIA

Garnet and staurolite FIAs were measured by the asymmetry method described in Hayward (1991) and Bell et al. (1995, 1998). A relative succession through time was obtained using both garnet and staurolite core to rim changes in FIA trend that were consistent for each area. The FIAs and monazite ages in staurolite porphyroblasts from the Colorado Front Range were measured by Afroz Shah as part of his PhD thesis at James Cook University. A detailed description of FIAs measured in staurolite porphyroblasts from the Western Maine is provided in Section A and B of the thesis. The trends for each staurolite FIA in the succession are shown on the rose diagram in Fig. 3.

3.2. Monazite data

A minimum of two samples containing one of each of the FIAs in staurolite from the succession was used to measure the U, Th, Pb, and Y contents of monazite grains. The ages were determined using a JEOL JXA8200 microprobe housed at the Advanced Analytical Centre, James Cook University. Table 1 shows the trace-element analyses of the

monazite grains included in staurolite porphyroblasts from Colorado Front Range used to calculate the ages. Section B of the thesis provides a detailed description of the monazite dating of the staurolite porphyroblasts from west-central Maine. Figure 4a-h and Fig. 5a-f show the probability curve and calculated age for west central Maine and Colorado Front Range respectively, as weighted averages for each FIA set as determined using ISOPLOT 3 (Ludwig, 2003).

3.3. Thermocalc

A pseudosection was modeled in the NCMnKFMASH (Fig. 6) system for each area by using the computer software Thermocalc (Holland and Powell, 1998) and the average composition of the pelites from both regions as determined from XRF analyses. Table 2 shows the bulk composition determined by XRF at the Advanced Analytical Centre, James Cook University for seven samples and their average from the Colorado Front Range. The bulk composition for the west-central Maine pelites were determined as described in Section D of the thesis.

4. INTERPRETATION

The rocks from each area have gone through a similar reaction history, as shown by the pseudosections, in reaching the regional PT conditions. In rocks from the Colorado Front Range staurolite stability extends to lower pressures, about 0.3 kbars less than in western Maine, whereas the St+And stability field is slightly larger. Garnet and staurolite in both areas appear to be in textural and chemical equilibrium. They have sharp intimate contacts with one another, and when garnet is included within staurolite it has euhedral boundaries with no signs of retrogression prior to being included. In some samples,

cordierite and andalusite have locally replaced and/or partially pseudomorphosed staurolite. In those few samples where sillimanite is present, staurolite porphyroblasts are replaced by coarse muscovite and biotite. This suggests that staurolite mainly grew at the expense of chlorite and that little biotite was consumed during the reaction. Thermodynamic modeling in the NCMnKFMASH system confirms this, with the reactions being:

$$Ms+Chl+Qtz = St+Bt+H_2O \text{ (1)},$$

if Grt was not consumed during St growth, or:

$$Ms+Chl+Grt+Qtz = St+Bt+H_2O \text{ (2)}$$

if Grt was partially consumed during St growth. Synchronous growth of Grt and St can be explained by the following reaction:

Chl+Ms = Mg-St+Mg-richer Bt+Mg-richer Chl+Grt+Na-richer Ms+H_2O (3),

proposed by Guidotti (1974), which describes the petrological observations.

At 3-4kb and ~520 ºC these reactions imply the coexistence of the metastable mineral assemblage Grt+St+Bt+Chl (Fig. 6). In many samples staurolite porphyroblasts preserve chlorite as inclusions suggesting that this reaction did not go entirely to completion.

Monazite dating shows that the succession of FIA sets accords with a progression in ages from 1760 to 1700 Ma in the Rockies and 410 to 350 Ma in the Appalachians. The consistency of this progression with the microstructurally-determined FIA succession confirms the value of FIA successions for accessing the combined structural and metamorphic history of an orogen (e.g., Aerden, 1994; Bell et al., 1998; Sayab, 2005; Yeh, 2007). Thus, 5 periods of staurolite growth occurred in the Palaeozoic rocks of western Maine and 3 in the PaleoProterozoic rocks of Colorado.

It appears that many rocks in both regions did not grow staurolite during the first or even second period of growth of this phase. Furthermore, some grew staurolite at one time and then grew it again up to 60 million years later. This does not accord with current concepts of reaction progress whereby once the P-T conditions for mineral growth occur for a particular bulk composition, the reaction goes to completion. The only variables outside of P-T-x that can explain this are the timing of growth relative to deformation and the role of deformation in nucleation and growth itself. Bell et al. (2003) showed that porphyroblasts commonly nucleate and grow into sites of progressive coaxial shortening surrounded by anastomosing zones of predominantly non-coaxial shortening. When the growing porphyroblasts reach the surrounding shear zones their growth ceases. It does not recommence until a new deformation occurs at high angle to the earlier one and repartitions around the porphyroblast margins, allowing new growth to occur in the strain shadow (e.g., Spiess and Bell, 1996). This suggests that staurolite growth did not occur unless the succession of deformation events that formed a specific FIA had taken place. That is, partitioning of deformation through an outcrop at the scale of a porphyroblast is a controlling factor on determining sites of metamorphic reaction and whether it occurs (Bell et al., 2004).

5. DISCUSSION AND SIGNIFICANCE

This is the first quantitative demonstration that staurolite can grow episodically by one reaction in rocks of similar bulk composition. Interpretations of metamorphic reactions are commonly based on laboratory experiments, which suggest that reaction rates at high temperature are very fast (Walther and Wood, 1984) and that local equilibrium is achieved (Bickle et al., 1997). However, field measurements of reaction rates indicate that the

speeds of reactions in metamorphic rocks are orders of magnitude lower (Baxter and DePaolo, 2000; 2002). They also suggest that disequilibrium is a common phenomenon during mineral growth even for reactions that went to completion (Carlson, 2002). These results require the existence of a factor that controls porphyroblast nucleation and growth that is distinct from bulk chemistry, PT, fluids, and time. A number of studies have pointed to the role of deformation in determining sites of metamorphic reaction and whether or not a particular reaction will take place (e.g., Spiess & Bell, 1996). Bell (1981) showed that deformation is partitioned into zones of lower strain, dominated by coaxial deformation, surrounded by anastomosing, higher strain zones, where the non-coaxial component is dominant. Porphyroblasts preferentially nucleate in zones of lower strain (e.g., crenulation hinges) prior to crenulation cleavage development (Bell et al., 2003). A similar conclusion was reached by Baxter and DePaolo (2004), who pointed out that certain reactions may occur within discrete portions of the rock, while others react little or not at all. These studies reveal that the reactions involved in the formation of metamorphic minerals are episodic during prograde metamorphism, starting or stopping, as a function of deformation partitioning and strain localization (e.g., Etheridge and Hobbs, 1974; Wintsch, 1985; Bell and Hayward, 1991; Dempster and Tanner, 1997; Whitmeyer and Wintsch, 2005). It has been proposed that chemical and textural equilibrium during metamorphism can occur locally (e.g., Bickle and Baker, 1990; Cartwright and Valley, 1991), while the overall rock matrix was not in equilibrium (Kretz, 1973). This would allow reactions to go to completion locally, but overall, the potential for new reactions to take place could be preserved until the deformation repartitioned and new reactive sites were created.

Until recently, porphyroblast-matrix relationships were mainly used to define the

timing of porphyroblast growth relative to the matrix fabric (e.g., Zwart, 1962). Such an approach is simplistic and ignores the fact that the matrix can be re-used and reactivated many times during orogenesis (Bell et al., 2003; Worley and Wilson, 1996). It also only allows one or two generations of growth of the same porphyroblastic phase to be recognized. The FIA method provides a quantitative tool to distinguish and correlate multiple generations of porphyroblasts over large distances (Bell and Mares, 1999). Combined with in situ dating of the inclusion trails that define a FIA set, this provides detailed insights into tectono-metamorphic histories that were previously inaccessible. Similar monazite ages to those recorded in Maine have been determined by Pyle et al., (2005) in the southwestern New Hampshire region of the Northern Appalachians. Their ages (400±10, 381±8, 372±6, and 352±14 Ma), combined with our data from western Maine, confirm the ~60 m.y. of continuous tectono-metamorphism for this portion of the Appalachians. Peak-metamorphic conditions have commonly been regarded as being contemporaneous along an orogen and late polymetamorphism was interpreted to result from local pluton-driven thermal activity (e.g., De Yoreo et al., 1989). However, orogeny is not the result of a single event that culminates with peak metamorphic conditions, but rather, a series of continuous but episodic events driven by tectonic plate motion (e.g., Bell and Newman, 2006).

Available age data from metamorphic terranes is commonly derived from accessory minerals that are present in the matrix. Such ages provide limited information and are difficult to precisely integrate with the tectono-metamorphic history because of reactivation of compositional layering plus local protection of grains in the strain shadows of large competent minerals. More recent studies using other approaches (Bell and Welch,

2002; Pyle et al., 2005) have revealed that accessory minerals such as monazite can grow episodically during metamorphism. They showed that distinct populations yielding significantly different ages can be separated, and this work confirms their approach. The episodic growth of staurolite porphyroblasts revealed by this study is significant for metamorphism and reveals a significant role for deformation that needs to be taken into account.

REFERENCES

Aerden, D. G. A. M., 1994. Kinematics of orogenic collapse in the Variscan Pyrenees deduced from microstructures in porphyroblastic rocks from the Lys-Caillaouas Massif. *Tectonophysics*, **236**, 139-160.

Baxter, E. F., 2003. Natural Constraints on Metamorphic Reaction Rates. In Vance D, Muller W, Villa I (eds) Geochronology: Linking the Isotopic Record with Petrology and Textures. *Geological Society, London, Special Publication*, **220**, 183-220.

Baxter, E. F., and DePaolo, D. J., 2000. Field measurement of slow metamorphic reaction rates at temperatures of 500-600°C. *Science*, **288**, 1411-1414.

Baxter, E. F., and DePaolo, D. J., 2002. Field measurement of high temperature bulk reaction rates II: Interpretation of results from a field site near Simplon Pass, Switzerland. *American Journal of Science*, **302**, 465-516.

Baxter, E. F., and DePaolo, D. J., 2004. Can metamorphic reactions proceed faster than bulk strain?. *Contributions to Mineralogy and Petrology*, **146**, 657-670.

Bell, T. H., 1981. Foliation development: the contribution, geometry and significance of progressive bulk inhomogeneous shortening. *Tectonophysics*, **75**, 273-296.

Bell, T. H., and Hayward, N., 1991. Episodic metamorphic reactions during orogenesis: the control of deformation partitioning on reaction sites and duration. *Journal of Metamorphic Geology*, **9**, 619-640.

Bell, T. H., and Mares, V. M., 1999. Correlating deformation and metamorphism around orogenic arcs. *American Mineralogist*, **84**, 1727-1740.

Bell, T. H., and Newman, R., 2006. Appalachian orogenesis: the role of repeated gravitational collapse. *In: Butler, R., Mazzoli, S. (Eds.), Styles of Continental Compression. Special Papers of the Geological Society of America*, **414**, 95-118.

Bell, T. H., and Welch, P. W., 2002. Prolonged Acadian Orogenesis: Revelations from FIA controlled monazite dating of foliations in porphyroblasts and matrix. *American Journal of Science*, **302**, 549-581.

Bell, T. H., Fleming, P. D., and Rubenach, M. J., 1986. Porphyroblast nucleation, growth and dissolution in regional metamorphic rocks as a function of deformation partitioning during foliation development. *Journal of Metamorphic Geology*, **4**, 37-67.

Bell, T. H., Forde, A. and Wang, J., 1995. A new indicator of movement direction during orogenesis: measurement technique and application to the Alps. *Terra Nova*, **7**, 500-508.

Bell, T. H., Ham, A. P., and Hickey, K. A., 2003. Early formed regional antiforms and synforms that fold younger matrix schistosities: their effect on sites of mineral growth. *Tectonophysics*, **367**, 253-278.

Bell, T. H., Ham, A., and Kim, H. S., 2004, Partitioning of deformation along an orogen and its effects on porphyroblast growth during orogenesis. Journal of Structural

Geology, v. 26, p. 825–845.

Bell, T. H., Hickey, K. A., and Upton, G. J. G., 1998. Distinguishing and correlating multiple phases of metamorphism across a multiply deformed region using the axes of spiral, staircase and sigmoidally curved inclusion trails in garnet. *Journal of Metamorphic Geology*, **16**, 767-794.

Bickle, M. J., and Baker, J., 1990. Advective-diffusive transport of isotopic fronts: An example from Naxos, Greece. *Earth and Planetary Science Letters*, **97**, 78-93.

Bickle, M. J., Chapman, H. J., Ferry, J. M., Rumble, D., and Fallick, A. E., 1997. Fluid flow and diffusion in the Waterville Limestone, south-central Maine: Constraints from strontium, oxygen and carbon isotopic profiles. *Journal of Petrology*, **38**, 1489-1512.

Carlson, W. D., 2002. Scales of disequilibrium and rates of equilibration during metamorphism. *American Mineralogist*, **87**, 185-204.

Carlson, W. D., Denison, S., and Ketcham, R. A., 1995. Controls on the nucleation and growth of porphyroblasts: Kinetics from natural textures and numerical models. *Geological Journal*, **30**, 207-225.

Cartwright, I., and Valley, J. W., 1991. Steep oxygen-isotope gradients at marble-metagranite contacts in the northwest Adirondack Mountains, New York, USA: products of fluid-hosted diffusion. *Earth and Planetary Science Letters*, **107**, 148-163.

Cavosie, A., and Selverstone., J., 2003. Early Proterozoic oceanic crust in the northern Colorado Front Range: Implications for crustal growth and initiation of basement faults. *Tectonics*, **22**, 10-1-10-23.

De Yoreo, J. J., Lux, D. R., Guidotti, C. V., Decker, E. R., and Osberg, P. H., 1989. The Acadian thermal history of western Maine. *Journal of Metamorphic Geology*, **7**, 169-190.

Dempster, T. J., and Tanner, P. W. G., 1997. The biotite isograd, Central Pyrenees: a deformation-controlled reaction. *Journal of Metamorphic Geology*, **15**, 531-548.

Etheridge, M. A., and Hobbs, B. E., 1974. Chemical and deformational controls on recrystallization of mica. *Contributions to Mineralogy and Petrology*, **43**, 111-124.

Guidotti, C. V., and Johnson, S. E., 2002. Pseudomorphs and associated microstructures of western Maine, USA. *Journal of Structural Geology*, **24**, 1139-1156.

Hayward, N., 1991. Orogenic processes, deformation and mineralization history of portions of the Appalachian orogen, USA, based on microstructural analysis. Unpublished PhD thesis, James Cook University.

Hirsch, D. M., 2007. Controls on porphyroblast size along a regional metamorphic field gradient. *Contributions to Mineralogy and Petrology*, **155**, 401-415.

Holland, T. J. B., and Powell, R., 1998. An internally consistent thermodynamic data set for phases of petrological interest. *Journal of Metamorphic Geology*, **16**, 309-343.

Kretz, R., 1973. Kinetics of the crystallisation of garnet at two localities near Yellowknife. *The Canadian Mineralogist*, **12**, 1-20.

Lasaga, A. C., Luttge, A., Rye, D. M., and Bolton, E. W., 2000. Dynamic treatment of invariant and univariant reactions in metamorphic systems. *American Journal of Science*, **300**, 173-221.

Ludwig, K. R., 2003. Isoplot 3.0 – A geochronological toolkit for Microsoft Excel. Berkeley Geochronology Center Special Publication No. 4

Nesse, W. D., 1984. Metamorphic petrology of the northeast Front Range, Colorado: The Pingree area. *Geological Society of America Bulletin*, **95**, 1158-1167.

Pyle, J. M., Spear, F. S., Cheney, J. T., and Layne, G., 2005. Monazite ages in the Chesham Pond Nappe, SW New Hampshire, U.S.A.: implications for assembly of central New England thrust sheets. *American Mineralogist*, **90**, 592-606.

Sayab, M., 2005. Microstructural evidence for N–S shortening in the Mount Isa Inlier (NW Queensland, Australia): the preservation of early W–E-trending foliations in porphyroblasts revealed by independent 3D measurement techniques. *Journal of Structural Geology*, **27**, 1445-1468.

Selverstone, J., Hodgins, M., Shaw, C., Aleinikoff, and J. N., Fanning, C. M., 1997. Proterozoic tectonics of the northern Colorado Front Range. In *Geologic history of the Colorado Front Range* (Bolyard, D.W., and Sonnenberg, S. A., eds.). Denver, Rocky Mountain Association of Geologists, 9-18.

Shaw, C. A., Snee, L. W., Selverstone, J., and Reed, J. C., Jr., 1999. $^{40}Ar/^{39}Ar$ thermochronology of Mesoproterozoic metamorphism in the Colorado Front Range. *Journal of Geology*, **107**, 49-67.

Spiess, R., and Bell, T. H., 1996. Microstructural controls on sites of metamorphic reaction: a case study of the inter-relationship between deformation and metamorphism. *European Journal of Mineralogy*, **8**, 165-186.

Walther, J. V., and Wood, B. J., 1984. Rate and mechanism in prograde metamorphism. *Contributions to Mineralogy and Petrology*, **88**, 246-259.

Whitmeyer, S. J., and Wintsch, R. P., 2005. Reaction localization and softening of texturally hardened mylonites in a reactivated fault zone, central Argentina. *Journal*

of Metamorphic Geology, **23**, 411-424.

Wintsch, R. P., 1985. The possible effects of deformation on chemical processes in metamorphic fault zones. *Advances in Physical Geochemistry*, **4**, 251-268.

Worley, B. A., and Wilson, C. J. L., 1996. Deformation partitioning and foliation reactivation during transpressional orogenesis, an example from the Central Longmen Shan, China. *Journal of Structural Geology*, **18**, 395-411.

Yeh, M. W., 2007. Deformation sequence of Baltimore gneiss domes, USA, assessed from porphyroblast Foliation Intersection Axes. *Journal of Structural Geology*, **29**, 881-897.

Zwart, H. J., 1962. On the determination of polymetamorphic mineral associations, and its application to the Bosost area (Central Pyrenees). *Geologische Rundschau*, **52**, 38-65.

– SECTION D –

P-T-d-t EVOLUTION IN THE CONTACT AUREOLE OF THE MOOSELOOKMEGUNTIC PLUTON: PROGRESSIVE PLUTON CONSTRUCTION OVER 70 MILLION YEARS

- SECTION D –

P-T-d-t EVOLUTION IN THE CONTACT AUREOLE OF THE MOOSELOOKMEGUNTIC PLUTON: PROGRESSIVE PLUTON CONSTRUCTION OVER 70 MILLION YEARS

ABSTRACT

Tectonic activity took place virtually continuously from before 420 Ma to less than 345 Ma in the vicinity of the Mooselookmeguntic Pluton. Field observations, petrological studies, foliation intersection/inflection axis (FIA) measurements, monazite dating of FIAs, and phase diagram modeling reveal at least five periods of growth of garnet and staurolite porphyroblasts over most of this period. At least one period of andalusite growth followed, before decompression into the cordierite field led eventually to retrogression. Peak metamorphic conditions of ~4 kbars and 600 °C were attained after the five periods of garnet and staurolite growth in the sillimanite field, although, locally, some fibrolite formed very early. The syn-kinematic Mooselookmeguntic pluton was progressively constructed at approximately the same structural level during successive deformations and over a long period of time rather than being the result of one discrete event as it has been previously proposed.

Keywords: FIAs; porphyroblasts; Thermocalc; PT evolution; pluton emplacement.

1. INTRODUCTION

Low pressure-high temperature terranes associated with granite intrusion are common in orogenic belts (Pattison et al., 1999). Most contain evidence for regional metamorphism that was variably overprinted and partially erased by later thermal events associated with the intrusion of plutons into the country rock. Insights into the early history are provided by porphyroblasts, which commonly preserve past deformation and

metamorphic history within their inclusion trails (e.g., Bell and Johnson, 1989; Bell and Welch, 2002). Metastable preservation of early-grown porphyroblasts through subsequent high grade metamorphic events is favored by partitioning of deformation from the regional scale to that of a porphyroblast. This is done by controlling the distribution of heat and fluids into the country rocks as well as the sites where metamorphic reactions take place (Bell and Hayward, 1991). By measuring FIAs (foliation intersection/inflexion axes in porphyroblasts) a close relationship between deformation and metamorphism can be established. Therefore, correlation with the pluton-emplacement history can be accomplished. In-situ monazite dating of FIAs allows absolute correlation between the many deformation and metamorphic events and the timing of pluton emplacement.

Changes in the PT conditions with time can be documented by detailed field and petrological studies integrated with microstructural measurements (FIAs) and isotopic dating. The stability field of mineral assemblages for pelites can be realistically predicted by modeling with the computer software Thermocalc (Holland and Powell, 1998) in the NCMnKFMASH system (e.g. Tinkham et al., 2001; Johnson et al., 2003; Tinkham et al., 2003). The results can be compared with field, petrological, and microstructural observations to accurately quantify the PT evolution through time. Garnet-core isopleths can be used to determine the PT conditions of garnet growth (e.g., Vance and Mahar, 1998; Evans, 2004; Tinkham and Ghent, 2005). This is especially important where more than one generation of garnet is present and overlapping metamorphic events have obstructed any information about their PT conditions of growth. The area located in the contact aureole of the Mooselookmeguntic pluton in western Maine, Northern Appalachians, provides a perfect location to study the interaction between deformation, metamorphism, and pluton

emplacement. The structural and magmatic history of this part of the Appalachians is well constrained by recent studies (e.g., Brown and Solar, 1998a, 1998b; Solar et al., 1998; Solar and Brown, 1999, 2001a, 2001b) and the metamorphic history has been a subject of detailed studies for decades (e.g., Guidotti, 1968, 1970. 1974, 2000; Holdaway et al., 1982; 1988; Guidotti and Johnson, 2002; Henry and Guidotti, 2002; Johnson et al., 2006). Recent studies (e.g., Solar et al., 1998; Tomascak et al., 2005) provided important geochemical and geochronological data for the Mooselookmeguntic pluton. Accurately documenting the deformation and metamorphic evolution in such terranes is very important for our understanding of the processes that take place during granite emplacement and the interaction between magma generation, melt migration, and tectonism. This study documents aspects of PT evolution in the contact aureole of the Mooselookmeguntic pluton by combining field data, petrological observations, microstructural measurements, monazite dating, and phase diagram modeling, and reveals a much longer and more complicated history than previously considered possible.

2. GEOLOGICAL SETTING

The area of study is located within the Central Maine Belt, which was metamorphosed and deformed during the Acadian orogeny (e.g., Smith and Barreiro, 1990; Solar et al., 1998; Bradley et al., 1998). This belt is bordered to the west by the rocks of the Bronson Hill Belt which were metamorphosed and deformed during the Taconian orogeny (Robinson et al., 1998) and to the east by the Avalon Composite Terrane (Fig. 1). The Central Maine Belt was interpreted to have developed as a thrust system during dextral - transpressive deformation in response to Acadian oblique convergence (Solar and Brown, 2001). Bradley et al. (1998), based on pluton crystallization ages and basin analysis,

suggested that the Acadian orogenic front migrated inboard during the Devonian. This suggests that the deformation front reached its current position at about 407 Ma. Structural, microstructural, and petrological evidence indicate that deformation, plutonism, and metamorphism were contemporaneous (Solar et al., 1998; Solar and Brown., 2001).

The metasedimentary sequence consists of a Silurian to early Devonian succession called the Rangeley Stratigraphic sequence, which was intruded by plutons ranging in age from c. 408 Ma to 363 Ma (Bradley et al., 1998). The Rangeley Stratigraphic sequence was multiply deformed and metamorphosed. The close spatial relationship between the metamorphic isograds and the pluton contours led to the idea of pluton-driven metamorphism (DeYoreo et al., 1989). The metamorphic grade increases along strike to the southwest, from biotite-zone conditions to upper-sillimanite-zone conditions (Guidotti, 1989). To the southeast of the study area, the metamorphic high produced migmatites within the Tumbledown and Weld anatectic domain. The metamorphic conditions within the migmatitic area have been interpreted to be above the contemporary solidus (Brown and Solar, 1999). The poly-metamorphic history of the area under study (Fig. 2) and the western Maine region has been well-documented in the literature (e.g., Guidotti, 1970, 1974, 1989, 2000; Holdaway et al., 1982, 1988; DeYoreo et al., 1989; Guidotti and Holdaway, 1993; Guidotti and Johnson, 2002; Henry and Guidotti, 2002; Johnson et al., 2003; Johnson et al., 2006). Three different metamorphic events have been distinguished. The first event, M1, produced regional greenschist-facies metamorphism. This was followed by a regional thermal event, M2, which produced the assemblage And+St+Bt±Grt (e.g., Guidotti, 2000; Henry and Guidotti, 2002). The intrusion of late-syntectonic plutons (e.g., the Mooselookmeguntic pluton) was interpreted to be responsible

for the M3 event, which erased most of the M2 assemblages and produced St+Bt and Sill at higher grades (e.g., Guidotti, 2000; Henry and Guidotti, 2002). This event occurred at higher pressure and was spatially associated with the plutons. As a function of the M3 thermal gradient, prograde pseudomorphs of the M2 porphyroblasts have been produced at higher grades and retrograde pseudomorphs at lower grades (Guidotti and Johnson, 2002).

3. THE MOOSELOOKMEGUNTIC PLUTON AUREOLE

All the rocks in this study come from the contact aureole of the Mooselookmeguntic pluton (Fig. 2). The pluton consists mainly of two types of rock: granite and monzodiorite (Tomascak et al., 2005). The granite contains enclaves of monzodiorite. The pluton has a tabular shape and dips shallowly in the north, versus moderately and shallow in the south (Moench and Zartman, 1976). On the southeast side, the monzodiorite was interpreted as a thin sub-horizontal sheet (Brown and Solar, 1998), which is discordant with the terrane boundaries and the foliation pattern. The granite is about 4 km thick on the northern and eastern side, wedging out in country rock to the north, east and south, and thinning to the southwest above a shallow NE-dipping floor (Brown and Solar, 1998). Solar et al. (1998) reported crystallization ages of 389±2 Ma and 370±1 Ma from the southern part of the pluton, whereas Tomascak et al. (2005) reported an age of 377 Ma for the western part, which is similar to the 378±2 Ma age published by Moench and Aleinkoff (2002).

4. SAMPLE DESCRIPTION

All samples are of staurolite grade with abundant sillimanite at higher grades. The pelites are fine- to medium-grained and the mineral assemblages and the grain size vary with the compositional layering. Biotite becomes coarser-grained with increasing grade whereas coarse muscovite is present only within staurolite pseudomorphs. Major mineral phases are represented by Ms-Bt-Pl-Grt-St-And-Crd-Sill and retrograde chlorite. Common accessory minerals consist of ilmenite, apatite, tourmaline, monazite, xenotime, graphite, and rutile as needles in biotite. Prograde pseudomorphs of the porphyroblastic phases occur at higher grades, whereas at lower grades retrograde pseudomorphs are common.

Table 1 presents the mineral assemblages contained in each sample collected from the contact aureole of the Mooselookmeguntic pluton. The locations of the samples are shown in Fig. 2. The mineral succession was established using textural and microstructural relationships. In the case of garnet and staurolite porphyroblasts, the same generation of growth was correlated across the region using FIA measurements (Table 2**)**. For andalusite and cordierite porphyroblasts no FIA measurements were made. Their local timing was established based on textural and microstructural characteristics for each sample, with regional correlations being speculative.

Based on data presented in Table 1 five zones containing differing mineral assemblages and recording changing PT conditions have been separated, and a distinction between the relative stability of the porphyroblastic phases (prograde vs. retrograde pseudomorphs) with respect to the metamorphic grade has been made (Fig. 3). Garnet porphyroblasts are small to medium in size, with the largest ones being around 2 mm in diameter. Most of them are subhedral to euhedral, although anhedral grains are not

uncommon. Inclusion trails in garnet porphyroblasts vary from straight, with curvature restricted to the margin of the porphyroblasts, to sigmoidal in shape. Garnet cores rich in inclusions with inclusion-free rims are also common. Other important microstructural and textural characteristics of garnet (although less common) are: textural zoning (Fig. 4a), inclusion free-cores surrounded by an inclusion-rich median zone bordered by an inclusion-free rim (Fig. 12a), and clusters of small grains (Fig. 4b). Ilmenite inclusions are common in all porphyroblasts. Other types of inclusions detected with EDS from back-scattered images consist of tourmaline, monazite, zircon, sulphides, and apatite.

Staurolite porphyroblasts can be up to three centimeters long. Inclusion-trail geometries are more complex than in garnet porphyroblasts. Sigmoidal inclusion trails (Fig. 5) are the most common, but straight inclusion trails with the curvature restricted to the margins are also found. Staurolite porphyroblasts that overgrew a well-defined crenulation cleavage (Fig. 6) are common in the northern part. Porphyroblasts containing cores with a rim overgrowth can be found throughout the region. Some samples can contain up to four different generations of inclusion trails from which at least three (Fig. 7) were of good quality for FIA measurements. Mineral inclusions in staurolite consist mainly of quartz; others include muscovite, biotite, chlorite, ilmenite, monazite, zircon, and apatite. Locally, garnet porphyroblasts are present as inclusions, and their microstructural and textural relationships always indicate that staurolite was coeval with or postdated garnet growth.

Andalusite porphyroblast usually are poikilitic, have overgrown the matrix foliation, and can be larger than the scale of a thin section. In most occurrences andalusite was partially replaced staurolite porphyroblasts (Fig. 6), indicating that in all samples andalusite growth postdated the staurolite.

Cordierite porphyroblasts can be up to three centimeters in size and always have an ovoidal shape in thin sections. Their microstructural and textural relationship with staurolite indicates that cordierite grew later. Their inclusion trails curve into the matrix indicating syn-kinematic growth (Fig. 5). In samples that contain staurolite, andalusite, and cordierite porphyroblasts, andalusite in most cases has partly replaced staurolite (Fig. 7) and cordierite has overgrown the foliation that wraps around staurolite porphyroblasts. This indicates that cordierite growth postdated andalusite. Two samples collected from about 2 km north of the region shown in Fig. 2 have andalusite relicts in cordierite porphyroblasts, indicating a clear succession in that area.

4.1. Mineral assemblages

Five mineral assemblages have been separated into five different zones as shown in Fig. 3. These are the Grt+St, Grt+St+Crd, Grt+St+And, Grt+St+And+Crd, and Grt+St+And+Sill zones. Muscovite, biotite, and plagioclase are common to all these assemblages. There is no clear change in the appearance of the minerals from one assemblage to another. Theoretically, such a small region (Fig. 2) would experience the same PT conditions during regional metamorphism and the mineral occurrences and modes would be dictated mainly by the bulk composition. Although, the importance of the bulk composition cannot be ignored, this region underwent multiple deformational, metamorphic, and thermal events. The metastable preservation of minerals with changing PT conditions is well known and any change in the mineral occurrences will contribute to the overall history of the region. The map pattern in Fig. 3 suggests that each mineral assemblage equilibrated at slightly different PT conditions. Another important observation

is the correlation of these mineral assemblages with the mineral isograds (Fig. 2) described by Guidotti (1974) and the pluton proximity. These suggest that at least the last part of the metamorphic history was closely linked with the pluton history.

4.2. Prograde and retrograde pseudomorphs

Although it was not the purpose of this study to investigate the various pseudomorph types found in the region, a brief description is necessary because of their abundance and significance for establishing conditions during metamorphism. Pseudomorphs in the region are well described in the literature with emphasis on muscovite pseudomorphs after staurolite (e.g., Guidotti 1968, 1970, 1974; Foster, 1977, 1981; Dutrow et al., 1999, 2008; Guidotti and Johnson, 2002). Guidotti (1968) demonstrated that pseudomorphs formed as a function of metamorphic grade with prograde pseudomorphs within and retrograde pseudomorphs away from the sillimanite zone. Prograde and retrograde pseudomorphs formed by different reaction mechanisms (Guidotti, 1968), at constant volume, limited by the bulk composition and the pseudomorphing process closely approached chemical equilibrium (e.g., Guidotti, 1970, 1974; Guidotti and Johnson, 2002). Sillimanite nucleation triggered chemical potential gradients between it, pre-existing staurolite, and the matrix minerals, enabling local mass transfer via diffusion that led to the pseudomorphing of staurolite by micas at the expense of the matrix phases (Foster, 1977, 1981). Recent work (Dutrow et al., 1999, 2008) showed that bulk composition and fluid infiltration play an important role in the formation of muscovite-rich pseudomorphs after staurolite, and that some are the result of a multistage process. Figure 3 strongly suggests that the type of pseudomorphs (prograde or retrograde) is a function of pluton proximity. There is a small buffer zone between the prograde and

the retrograde zone where porphyroblastic phases appear to be relatively stable and no clear prograde or retrograde pseudomorphs have been observed. A common feature for both prograde and retrograde situations is the presence of deformed pseudomorphs, suggesting that the pseudomorphing process began prior to the latest tectonic event.

4.2.1. Prograde pseudomorphs

In this study, the term prograde pseudomorphs refers to the prograde replacement of the major porphyroblastic phases by coarse-grained mica in the presence of sillimanite. Pseudomorphs after staurolite, andalusite, and garnet have been recognized in almost all samples coming from this zone. Usually, the prograde pseudomorphs after staurolite consist of coarse-grained muscovite and biotite. At the most advanced stages of replacement only a small relict of staurolite is present in a groundmass consisting mainly of muscovite. Most of the biotite lies on the pseudomorph margins where sillimanite is also present. Everywhere there is evidence for staurolite being pseudomorphed, andalusite, which usually contains staurolite inclusions, is also present. Andalusite inside such pseudomorphs is mainly replaced by coarse-grained muscovite; sometimes sillimanite needles nucleated in the andalusite. Garnet porphyroblasts are surrounded by biotite grains that nucleated parallel to the crystallographic faces at lower grade, and in which fibrolitic sillimanite started to nucleate. At the highest grades, the entire garnet porphyroblast was replaced by biotite and sillimanite.

4.2.2. Buffer zone

In what was designated as a buffer zone, all porphyroblastic phases appear to be in relative stability. Maybe a better description for this would have been a transition zone

between prograde and retrograde pseudomorphs, but this was avoided in order to not create confusion with the methodology used by Guidotti (1974) for describing the transition from the staurolite to the sillimanite zone.

4.2.3. Retrograde pseudomorphs

In this study the term retrograde pseudomorph is applied to any reaction where fine-grained white mica in the presence of chlorite partially or totally replaced major porphyroblastic phases. Staurolite porphyroblasts can be replaced by fine-grained white mica and, although chlorite may or may not be present in the pseudomorph mass, it is always found in the matrix. Where complete replacement occurred, a small rim of graphite formed at the pseudomorph margins. Complete and partial retrograde pseudomorphs of chlorite after garnet are common. Cordierite porphyroblasts were replaced on their margins by a rim of chlorite. No evidence of andalusite and/or pseudomorphs after andalusite was found in this zone.

5. FIA DATA

FIAs in both garnet and staurolite were measured using the asymmetry method developed by Hayward (1991) and Bell et al. (1995, 1998). This is shown in Fig. 8 and consists of cutting initially 6 vertical thin sections 30° apart around the compass and then 2 more 10° apart where the inclusion trail asymmetry flips. A total of 77 FIA for staurolite and 75 for garnet porphyroblasts were measured from samples collected from the contact aureole of the Mooselookmeguntic pluton. FIA data is shown in Table 2 and FIA sets plotted on rose diagrams are shown in Fig. 9.

5.1. Interpretation of FIA succession

A succession of 5 different FIA sets for garnet and staurolite porphyroblasts can be interpreted using samples that preserve changes in FIA trends from core to rim (see section A of thesis). These trend successively NNW-SSE, ESE-WNW, E-W, ENE-WSW, and NE-SW (Fig. 10; Tab. 2). Figure 7 shows an example where three generations of inclusion trails from staurolite porphyroblasts, corresponding to three different FIA sets, could be separated. FIA set 3 is not obvious for garnet porphyroblasts alone (Fig. 9a), but is apparent in staurolite porphyroblasts or when these two phases are combined (Fig. 9b and c). The prograde transition from garnet to staurolite from sample to sample was used as well to establish a relative FIA succession (Table 3), and gave similar results to the FIA succession established by using core-to-rim transitions in staurolite porphyroblasts.

5.2. The absolute timing of FIAs

Smith and Barreiro (1990) used monazite ages from schist located in the contact aureole of the Mooselookmeguntic pluton to resolve two high-temperature metamorphic events around 400 Ma and 370 Ma. The first high-temperature event was interpreted to represent peak conditions due to regional metamorphism, whereas they related the second event to the emplacement of the Mooselookmeguntic pluton (e.g., Smith and Barreiro, 1990; Guidotti and Johnson, 2002; Henry and Guidotti, 2002; Johnson et al., 2003; Johnson et al., 2006). Monazite dating of FIAs and matrix monazites ages indicate the existence of five discrete but continuous periods of monazite growth associated with FIAs. The age of FIA 1 was resolved at around 420 Ma, the age of FIA 2 between 415-395 Ma, the age of FIA 3 between 395-380, the age of FIA 4 between 380-360, and the age of FIA

5 between 360-345 Ma (see Section C of Thesis). This suggests that FIA 1 and FIA 2 formed earlier than the pluton during regional-style metamorphism, FIA 3 and FIA 4 were synchronous with the pluton and of contact-type metamorphism, and FIA 5 formed later than pluton emplacement, but was probably still related to pluton thermal activity.

6. MINERAL CHEMISTRY

6.1. Analytical method

Major elements in muscovite, biotite, plagioclase, garnet and staurolite were determined by spot analyses. For each grain, several spots were analyzed and the average determined composition was considered to be representative. Data were collected using the JEOL JXA – 8200 SuperProbe housed at the Advance Analytical Centre, James Cook University. Operating conditions for spot analyses were 15kV and 20nA, with a beam diameter of 3μm. For the garnet rim a beam diameter of 1μm was used. Natural materials were used as standards. X-ray compositional maps of garnet were collected by using a 2μm beam diameter, a beam current of 200-250 nA, and a dwell time of 100 ms.

6.2. Micas

Structural formulae for both muscovite and biotite were calculated on a 22 oxygen basis (Tables 4 and 5). Both muscovite and biotite show no significant variation in Si and therefore Al^{IV} content, which was defined as the difference between 8.0 and the number of Si atoms. All micas are saturated with respect to Ti because of their coexistence with ilmenite and sagenitic rutile. Because of the presence of aluminous phases (garnet, staurolite, andalusite, sillimanite) all micas are saturated in Al. Fe^{3+} was not determined although the presence of ilmenite and graphite would restrict its participation to a minimum level (Guidotti and Dyar, 1991; Guidotti and Sassi, 1998a, 1998b). The end-

member calculation was done by following the procedure described in Holdaway et al., (1988).

The compositional variation of muscovite and biotite with metamorphic grade in the region is well documented in the literature (e.g., Cheney and Guidotti, 1973; Guidotti, 1978; Holdaway et al. 1988; Henry and Guidotti, 2002; Henry et al., 2005). It can be summarized as follows: (i) in tetrahedral sites Si decreases and Al^{IV} increases; (ii) in octahedral sites Al^{VI} decreases, Ti increases and ΣVI decreases; (iii) in the twelve-fold sites in muscovite, the paragonite content first increases and then decreases, while in biotite ΣXII increases with grade; (iv) Fe/(Fe+Mg) in biotite increases slightly.

6.2.1. Muscovite

Al^{VI} content of muscovite varies very little, from 3.911 to 4.002 atoms per formula unit (p.f.u.), with the lowest value occurring in a matrix muscovite from the highest-grade sample (IS104 – with high modal sillimanite) and the largest value from sample IS77 (a garnet-staurolite schist). Al comprises 95% of the ions on average in the octahedral sites. The remainder contain approximately equal amounts of Fe and Mg (between 1.5-2.1%) and Ti (between 0.5-1.3%). The Mn content of all muscovites studied is very low (≤ 0.01 cations p.f.u.). The octahedral sites occupancy (ideally 4.00 atoms p.f.u.) varies from 4.115 to 4.166 atoms p.f.u., indicating slight deviation from dioctahedral micas in all analyses.

The twelve-fold interlayer site in white mica is filled predominantly by K (1.158-1.365 atoms p.f.u.) and by lesser amount of Na (0.196-0.309 atoms p.f.u.). The calcium content is negligible with a maximum of 0.002 atoms p.f.u. in sample IS77. The total occupancy of the interlayer site ranges from 1.480 to 1.646 atoms p.f.u.. Deficiencies in the twelve-fold sites in muscovite, even when trace elements are included in the analyses,

may be partially explained by the H_3OK_{-1} and NH_4K_{-1} substitutions and by vacancies in the twelve-fold sites due to charge balance constraints caused by other substitutions in tetrahedral, octahedral, and twelve-fold sites (Guidotti and Sassi, 1998a; Guidotti and Sassi, 1998b). The analyzed muscovites have less than 0.01 atoms of Cl p.f.u..

6.2.2. Biotite

The majority of octahedral sites are filled by Fe_{total} (2.34-2.90 atoms p.f.u.) and Mg (1.838-2.356 atoms p.f.u.). X_{Mg} of biotite, ranging from 0.388 to 0.500, reflects variation both in the bulk composition and temperature. Octahedral Al in biotite, defined as the difference between Al_{total} and Al^{IV}, is almost constant with an average of 0.96±0.02 atoms p.f.u., suggesting operation of Al-Tschermaks substitution (Fe, Mg)$SiAl^{VI}_{-1}Al^{IV}_{-1}$. All biotite is saturated in Al_{total} due to coexistence with aluminous phases (garnet, staurolite, andalusite, sillimanite). Ti contents in biotite range from 0.135 to 0.182 atoms p.f.u., with no clear correlation with the contents of Fe and Mg, but increasing with the metamorphic grade. Concentrations of Mn are typically low, between 0.008 and 0.015 atoms p.f.u. In all of the biotites studied, the sum of the octahedral cations is below the theoretical value of six atoms p.f.u., but is always above 5.70, implying no significant amount of Fe^{3+} in the biotites.

Theoretically, two atoms p.f.u. are allocated to the twelve-fold site in biotite. The interlayer site in the analyzed biotite is dominated by K (1.581-1.680 atoms p.f.u.) with small amounts of Na (0.071-0.102 atoms p.f.u.) and Ca (less than 0.03 atoms p.f.u.). Cl content is uniformly low (less than 0.003 atoms p.f.u.). The amount of interlayer-site vacancy, ranging from 0.212 to 0.322 atoms p.f.u. can be attributed to the incomplete analyses.

6.3. Garnet

The composition and the stoichiometry of garnet cores and rims from six samples are provided in Table 6. All analyzed garnet grains lie in the matrix, and in the case of sillimanite rich samples, care was taken to analyze only garnet situated away from sillimanite grains. Although all analyzed garnet comes from a narrow metamorphic grade (staurolite- to lower-sillimanite-zone), care has been taken to ensure that the mineralogy of the samples reflects a prograde path. Relative to the regional metamorphic field gradient (Fig. 2) the prograde succession will be as follows: staurolite zone (IS77)→transition zone (IS94 and IS28A)→lower sillimanite zone (IS2, IS74 and IS104). Based on the mineral assemblages preserved by individual samples the succession will look like this: IS28A (Grt+Bt+Ms) → IS77 and IS95 (Grt+St+Bi+Ms) → IS2 and IS74 (Grt+St+And+Bt+Ms+low modal sillimanite) → IS104 (Grt+St+And+Bt+Ms+high modal sillimanite).

Six garnet analyses for core and rim, with the calculated end-member and structural formulae based on 12 oxygens, are given in Table 6. The edge zone from the outermost layers of the porphyroblast is reported as rim compositions. The oxide totals are close to 100 weight per cent with a few analyses having values higher than 101 weight percent. The cation sums generally approach the ideal value of 8. The Al^{VI} values, usually close to 2, indicate that garnet can be considered as a solid solution of almandine-pyrope-spessartine-grossular end-members. The almost constant Al^{VI} participation of 2.013±0.008 atoms p.f.u. suggests that the amount of Fe^{3+} is insignificant. Ti contents in garnet are very low, with less than 0.003 atoms p.f.u.

From Table 6 some general features of garnet composition can be derived. The almandine content of garnet cores decreases from staurolite- to the transition-zone and then increases in the lower sillimanite zone. In the rim, the almandine content increases and decreases independent of the metamorphic zone. The grossular content increases in both cores and rims with increasing grade then decreases sharply in sample IS104. Pyrope decreases in the cores and rims of the garnet with increasing grade, except for sample IS104 where it increases in the rim. Spessartine increases in the cores from the staurolite zone to the transition zone, then decreases in the lower sillimanite zone. In the rims the spessartine content has a zig-zag pattern opposed to that of almandine.

Fe/(Fe+Mg) increases from staurolite to the lower sillimanite zone in both cores and rims except sample IS104 where it decreases in the rim, while Mg/(Mg+Fe) has the exactly the opposite behavior. The overall chemistry of the analyzed garnets reflects a typical prograde zoning with Mn- and Ca-rich cores and Fe- and Mg-rich rims. The absolute compositional variations from cores to rims are small; unless they represent initial zoning, some internal diffusion may have occurred.

6.3.1. Garnet compositional zoning

Compositional zoning patterns in garnet have been used for decades to infer metamorphic conditions during and after their growth (e.g., Hollister, 1966; Loomis, 1975; Tracy et al., 1976; Tracy, 1982; Spear et al., 1990; Carlson, 1999). The absolute variations in the major components in garnet from the contact aureole of the Mooselookmeguntic pluton are minor. The size of the garnet porphyroblasts (less than 2 mm; usually around 1 mm) makes them susceptible to homogenization during subsequent metamorphic events and/or during high-grade or retrograde metamorphism. Three garnet porphyroblasts from

samples IS28A, IS77 and IS104 were selected for X-ray mapping (Fig. 11) and line profile analyses (Fig. 12).

Although all garnets are highly almandinic (at least 74 mole percent almandine), discrete but consistent zoning patterns can be observed for all components. Samples IS28A and IS77 show typical zoning patterns for pelitic garnets that grew during prograde metamorphism at peak temperatures of 450-550°C (Hirsch et al., 2003). They have overall Mn- and Ca-rich cores, which decrease from core to rim as Mg and Fe increases. Discrete variations in this pattern are present in both garnets.

In the garnet porphyroblasts from sample IS28A, four discrete, roughly concentric, domains can be identified. The first domain represents an inclusion-free core which corresponds with the maximum concentrations in Mn and Ca and the minimum Fe and Mg concentrations. The second domain corresponds with an inclusion-rich zone which surrounds the inclusion-free core. This zone coincides with a significant drop in Mn and Ca concentrations followed by the corresponding increase in Fe. The variations in Mg concentration are less obvious. The third zone, which roughly corresponds with the outer part of the inclusion-rich zone, is characterized by a further decrease in Mn, increase in Ca and a slight increase in Fe and Mg. The fourth zone corresponds with an inclusion-free rim with the lowest Mn and Ca concentrations and the highest Fe values. A small decrease in Mg can be observed at the outer edge of this zone. The sharp transition for Fe, Mn, and Ca zoning, from the inclusion-free core to the surrounding inclusion-rich zone, may reflect not only a change in the metamorphic conditions and nutrient availability due to evolving bulk chemistry. It may also indicate a change in the tectonic regime as well, which reflects a transition from static to a dynamic growth coinciding with the onset of a new deformation

event. Once deformation ceased, growth was controlled by post-kinematic factors such as local diffusion and fluid infiltration. Ca zoning at the edge of the inclusion rich domain with "dendritic"-like shapes indicates fluid-assisted growth during chemical disequilibrium (Chernoff and Carlson, 1997, 1999; Wilbur and Ague, 2006) rather than diffusion effects, since the diffusion coefficients of Ca in garnet are much lower than those for Fe, Mg, and Mn (e.g., Tuccillo et al., 1990; Spear and Kohn, 1996; Chernoff and Carlson, 1999). Chemical disequilibrium during growth induced by Ca-rich metamorphic fluids (Skelton et al., 2002) appears to be the only valid explanation because there is no evidence that these "dendritic"-like shapes are connected with cracks, inclusion patterns, or crystal faces; no crystallographic measurements are available. In the rim this pattern disappears and a more homogenous Ca zoning is present indicating that probably the "chemical disequilibrium" was induced by a brief pulse of Ca-rich metamorphic fluid.

Sample IS77 shows a quite consistent normal prograde growth zoning for Mn and Fe where the Mn decreases from core to rim and Fe increases. Somewhat similar to sample IS28A, the Mg content in sample IS77 shows the lowest values in the core, increases towards the rim, and then decreases in the rim. Ca shows an overall normal growth pattern where its concentration decreases from core to rim. An irregular zoning pattern is superimposed on the normal growth zoning with a central and median-rich domain characterized by sector-like crystallographic structures delimited by compositional variations. This zone is surrounded by a Ca-poorer zone which is divided in two parts by a thin line of Ca enrichment. The Ca zoning in the core and median region with sector-like crystallographic structures shows high-Ca rims that delimit cores of low Ca. The entire domain is surrounded by a low-Ca zone consistent with a hypothesis of multiple nucleation

and coalescence during garnet growth (e.g., Daniel and Spear, 1998; Spiess et al., 2001; Whitney et al., 2008). Backscatter images (Fig. 12) and thin-section study shows that this zoning is not consistent with the presence of cracks or the orientation of the inclusion trails. The zoning pattern for Fe, Mn, and Mg does not resemble Ca zoning, or, if such a connection exists, it must be beyond the detection limits of the microprobe. The regular pattern of almost perfectly polygonal grain boundaries is consistent with the explanation of Whitney et al. (2008) of close initial nucleation spacing of crystals and early coalescence before growth zoning occurred, although the hypothesis of Spiess et al. (2001), where coalescing nuclei physically rotate towards a single orientation, cannot be disproved. The latter explanation require temperatures in excess of 600°C (Spiess et al., 2001) which are not consistent with the published metamorphic temperatures in this part of the region (e.g., Guidotti, 1974; Guidotti and Johnson, 2002; Henry and Guidotti, 2002). The small thin line of Ca enrichment that surrounds the porphyroblast may be a retrogressive feature due to Ca-rich fluid infiltration (Skelton et al., 2002), which coincided with late retrograde growth of the garnet rim by the fluid-driven retrograde AFM reaction:

$$St+Bt+H_2O \rightarrow Grt+Chl \quad (1)$$

This reaction may be associated with the breakdown of staurolite porphyroblasts to fine grained white mica and chlorite in the adjacent rocks. This suggests that, although, there is no evidence of retrogression in the matrix, metamorphic fluids responsible for retrogression in the nearby rocks circulated throughout the region. These fluids may be related to a pulse of metamorphic fluid flow that, as a function of temperature, produced prograde pseudomorphs at higher grades and retrograde pseudomorphs at lower grades.

There is no evidence that the inner zone of the garnet porphyroblasts was affected by fluid infiltration and/or by retrograde metamorphism.

Sample IS104 shows no distinct compositional zoning for Fe, reverse zoning for Mn with the opposite behavior for Mg and three distinct compositional domains for Ca. The network of fractures that are visible in both back-scattered images and X-ray compositional maps as well as in thin section does not appear to influence, at least in 2D, the elemental zoning. The interpretation of the chemical zoning in this specimen has to be closely related to Ca zoning. In contrast with the other two garnets grains studied in this sample, the Ca zoning corresponds with three distinct but uniform compositional domains. The first domain localized in the core of the actual garnet is confined to the crystallographic shape of a supposedly "initial crystal." This core is surrounded by a relatively uniform zone of Ca enrichment that appears to mimic the shape of the core. The third zone corresponds with the lowest Ca content and surrounds the previous two domains. Such zoning cannot be correlated with continuous growth accompanied by changes in the availability of Ca due to matrix reactions or fluid infiltration. The shape of the first domain and of the mimicking zone of enriched Ca indicates prograde growth and that the "initial crystal" was partially dissolved before new growth occurred. The first two zones may correspond with continuous growth during which the availability of Ca has changed as a result of discontinuous change in the mineralogy of the rock due to changing metamorphic conditions (Franceschelli et al., 1982; Spear and Kohn, 1996). The almost flat profile for X_{Alm}, the increase in X_{Sp} from core to rim and the high X_{Py} cores are consistent with diffusion controlled homogenization (Yardley, 1977; Tracy, 1982; Tuccillo et al., 1990). Diffusion of Ca in garnet is much slower than the diffusion of Fe, Mg, and Mn (e.g.,

Tuccillo et al., 1990; Spear and Kohn, 1996; Chernoff and Carlson, 1999). Therefore, Ca zoning is interpreted to reflect the original growth zoning.

6.4. Staurolite

Representative compositions of staurolite with the calculated structural formula are presented in Table 7. The structural formula has been calculated on the basis of 46 oxygens. For the Si-O tetrahedra Al^{IV} was assigned by making the difference between 8 and Si. It can be observed a decrease in Si from sample IS77, (7.722 atom p.f.u.) with increasing grade, to sample IS104 (in average 7.426 atoms p.f.u.) and the corresponding increase in Al^{IV}. The octahedral sites were filled with Al^{VI} (calculated as the difference between the Al_{total} and Al^{IV}), Ti and Mg. The octahedral Al increases from sample IS77 (17.289 atom p.f.u.) to sample IS104 (in average 17.623 atoms p.f.u). The majority of the Fe-O tetrahedra are occupied by Fe (in average 3.213 atoms p.f.u.) and the remaining Mg after filling the octahedral sites. The Mn content usually is low, with the highest value of 0.073 atoms p.f.u. in a staurolite relict from a muscovite pseudomorph. Ca is very low, counting for less than 0.002 atoms p.f.u. The X_{Mg} decreases with increasing grade, while X_{Fe} increases. A similar trend can be observed in biotite, garnet for both cores and rims, and in muscovite (Fig. 13).

6.5. Plagioclase

Representative core and rim composition of plagioclases with the calculated atomic proportion and end-members are shown in Table 8. The structural formula has been calculated on the basis of 8 oxygens.

The oxide totals generally are around 99 weight per cent and the cation sums are always close to the ideal value of 5. The small deviations from the ideal NaSi=CaAl

substitution shown by some analyses may depend on inaccuracy of the analyses and/or reflect the effect of alteration.

Plagioclase can be considered a solid solution of albite and anorthite. The K content is generally very low (≤ 0.003 atoms p.f.u.). In all samples, plagioclase is an oligoclase, with An contents from An22 to An18. The maximum compositional variation in each specimen is very small with a maximum of about 2 % An in sample IS104.

7. PHASE-RELATION MODELING WITH THERMOCALC AND PT ESTIMATION

7.1. General considerations

Any phase-relation modeling and PT estimation for the pelites in the contact aureole of the Mooselookmeguntic pluton has to take into consideration the possibility that the actual composition of the rocks may have been modified by fluids, and that at least at one stage, chemical disequilibrium during mineral growth was common. The extensive area occupied by pseudomorphs suggests that all rocks in the contact aureole were subject of fluid infiltration whether or not pseudomorphs were formed. Further, the polymetamorphic history of the region indicates that earlier metamorphic events may have been erased from the matrix and/or overprinted by younger ones. The presence of deformed pseudomorphs with un-deformed ones indicates that pseudomorphism occurred at least twice and/or reflects the effect of partitioning of deformation at the scale of a porphyroblast. FIA measurements and monazite dating of FIAs preserved in staurolite porphyroblasts indicate that deformation and metamorphism occurred at least five times in the region. If each of these events were accompanied by metamorphic fluid flow and retrogression, than we might expect that the bulk-rock composition had been changed from

one event to another. Therefore, adjacent rocks may reflect different PT conditions due to shifting into bulk-rock composition. Another factor that can contribute to changes in the effective bulk-rock composition is the fractionation of zoned minerals, such as garnet (Spear et al., 1990; Vance and Mahar, 1998; Evans, 2004; Tinkham and Ghent, 2005). The effect of garnet fractionation on the bulk composition and the pseudosection topology was not investigated for the following reasons: 1) uncertainty in evaluating how much of the garnet was removed from the bulk composition; 2) garnet modes vary greatly from one sample to another and any such estimates must take into account individual samples; 3) polymetamorphism; 4) evidence of fluid rock interaction and mass transfer processes; 5) garnet zoning patterns indicate discontinuous changes in the rock mineralogy and fluid infiltration during garnet growth.

To investigate the effect of changing bulk composition on the mineral stability fields we chose to use individual rock compositions. Changes in composition from one sample to another should account for both mass transfer during fluid infiltration and the effect of garnet fractionation on the effective bulk rock chemistry. 14 samples (Table 9) were selected for XRF analysis at the Advance Analytical Centre, James Cook University. At least eight thin sections from each sample were studied under the microscope to determine whether the amount of retrogressive chlorite and/or alteration was insignificant or not present. Only layers of similar mineralogy were probed. For each sample five different zones were probed (approximately 200g of fresh rock from each zone), then crushed individually and the resulting powder was mixed and homogenized. From the homogenized rock powder 50g were selected for XRF analyses. To obtain an approximate

average composition for the pelites in the region from each of the 14 samples, 50g of powder were selected, then mixed, homogenized, and analyzed by XRF.

Individual pseudosections were modeled in the Na_2O – CaO – MnO - K_2O – FeO – MgO - Al_2O_3 - SiO_2 - H_2O system (NCMnKFMASH) by using the computer software THERMOCALC 3.25 (Powell and Holland., 1988), dataset of Holland and Powell (1998; with the update tcds55.txt produced at 19:29:59 on 22 Nov 2003) and mixing models after Tinkham et al. (2001) and White et al. (2001). The calculations considered the following phases: chlorite, zoisite, muscovite, plagioclase, biotite, garnet, staurolite, andalusite, sillimanite, kyanite, cordierite, and H_2O. The average composition was modeled in the 1-10 kilobar range and 430-650°C intervals for comparison with similar work in the region. Individual samples were modeled in 2-6 kilobars and 430-650°C intervals which fully describe the PT conditions in the study area. The advantages and the limitations of using the NCMnKFMASH system to model mineral stability fields for pelites have been well documented in the literature and will not be discussed here (e.g., Johnson et al., 2003; Tinkham et al., 2003; Johnson and Brown, 2004; Martinez et al., 2004; Zuluaga et al., 2005).

7.2. Phase relationships in the contact aureole of the Mooseelookmeguntic pluton

Figure 14 shows mineral phase equilibria for the average composition determined for the pelites in the contact aureole of the Mooselookmeguntic pluton as described above. The mineral assemblages in the contact aureole of the Mooselookmeguntic pluton for the area under study (Fig. 3) contain the following mineral associations (see above for a detailed description): Grt+St; Grt+St+And; Grt+St+Crd; Grt+St+And+Crd; Grt+St+And+Sill.

All assemblages contain biotite, muscovite, plagioclase, and retrograde chlorite. Bellow 5 kbars the stability of Grt+St in the presence of Chl is predicted to occur at pressures above 2.7 kbars and in a narrow temperature range (≈ 545-555°C). In the absence of chlorite, Grt+St is stable above 3 kbars and at a minimum of 555°C. An increase in pressure will expand the staurolite stability field at higher temperatures. In the field, the stability of this assemblage is restricted to a narrow area between Grt+St+And and Grt+St+Crd and the retrograde pseudomorph zone (Fig. 3). That sets the upper pressure limit for the Grt+St assemblage at 4 kbars, the lower pressure limit at 2.7 kbars and a temperature interval between 534-578°C.

The assemblage Grt+St+And, in the absence of chlorite, is predicted to occur at pressures between 3.2 and 4 kbars and in the temperature range 547-578°C. In the presence of chlorite, the stability field of coexisting Grt+St+And is restricted to a narrow divariant field, which will be crossed quickly if the prograde metamorphic conditions imply isobaric heating or isothermal compression. In all samples where Grt+St+And+Bt+Ms+Pl coexists with chlorite there is evidence that chlorite is a retrograde phase. The stability field predicted by Thermocalc for this assemblage is too narrow to be stable in common metapelites unless some unusual compositions are present. In all samples, microstructural and textural relationships indicate that staurolite predates andalusite, which is consistent with initial metamorphism in the Grt+St+Bt+Ms+Pl field before andalusite entered in the system. The upper pressure limit of 4 kbars, imposed by the neighboring assemblages Grt+St and Grt+St+And (Fig. 3) for the Grt+St assemblage, may represent the maximum equilibration pressure for the Grt+St assemblage in the field. The fact that andalusite is never present in the rocks without staurolite indicates that the minimum pressure in

St+Grt+And rocks was around 3 kbars. Also, the appearance of andalusite coincides with the first signs of staurolite instability, which was partly replaced in all samples by andalusite. The appearance of the sillimanite in the system corresponds with the polymorphic transition andalusite→sillimanite and further breakdown of staurolite and garnet. Andalusite is present as a metastable phase in all sillimanite-bearing assemblages. The minimum temperature predicted by Thermocalc for the onset of sillimanite is about 578°C at 4 kbars. The assemblage Grt+St+And+Sill represents the peak metamorphic conditions recorded in the rocks, although peak conditions may have changed with time. Whether or not the rocks experienced higher peak metamorphic conditions is difficult to prove since most of the previous metamorphic history has been erased from the matrix.

Of considerable importance for the metamorphic history of the region are cordierite-bearing assemblages. Most of the previous studies in the region (e.g., Guidotti, 1966, 1968, 1970, 1974, 2000; Guidotti and Johnson, 2002) focused mainly on what was described as M3 metamorphism (Grt+St+And+Sill) and neglected and/or ignored this phase. Indeed from the 96 samples included in this study cordierite is present in only 10, and its distribution cannot really be related to important field relationships. Important constraints on whether or not cordierite was formed may have been dictated by the bulk composition and fluid activity. If the appearance of cordierite was controlled by variation in the bulk composition, then we could expect that the PT conditions responsible for cordierite formation had a more regional significance, even in the absence of this phase from the rock mineralogy. The cordierite history and its metamorphic significance will be investigated in detail in another study. For now the discussion will be restrict to aspects relevant to this study.

Firstly, cordierite appears in two distinct mineral associations, Grt+St+Crd and Grt+St+And+Crd. Secondly, and very important for any further interpretation, in all cases cordierite is the result of polymetamorphism. The succession in the paragenesis is clearly delimited by textural, microstructural, and FIA measurements. In both assemblages cordierite is the last phase to have formed. The PT pseudosection modeled by using the average composition does not predict the assemblage Grt+St+Crd if andalusite is included in the calculations. Sample IS77 comes from the Grt+St+Crd zone and did not predict the appearance of andalusite when modeled with Thermocalc. Therefore, it was used to predict the stability field of the Grt+St+Crd+Bt+Ms assemblage (Fig. 15). The stability field for the assemblage Grt+St+Chl in cordierite-bearing rocks, as predicted by Thermocalc, appears to extend to lower pressures around 2.2 kbars, than in andalusite-bearing assemblages, while the lower pressure limit for Grt+St in the absence of chlorite remains unchanged. The stability field for the Grt+St+Crd extends over the 2.2-3.4 kbars and 530-565°C intervals. In the presence of chlorite, the divariant field Grt+St+Crd+Chl is stable over less than 1°C interval at constant pressure. Unless the chlorite is retrograde (which is the case in this study), the assemblage Grt+St+Crd+Chl will indicate an increase in pressure at constant temperature, which is unrealistic for the region under study, or isothermal decompression if retrograde chlorite is present.

The assemblage Grt+St+And+Crd occurs in few samples and is always present in the absence of chlorite. In the presence of chlorite, this assemblage would be represented on the phase diagram in the NCMnKFMASH system as an invariant point from where divariant reaction lines diverge and delimit the stability of the non-chlorite fields. The stability field for Grt+St+And+Crd in the absence of chlorite is predicted by Thermocalc

as a small divariant field below 1.6 kbars and to less than 480°C (Fig. 16). The effect of extra components may allow the stable co-existence of St+And+Crd in Zn and/or Mn rich metamorphic rocks (e.g., Pattison and Tracy, 1991; Pattison et al., 1996; Patisson et al., 1999).

7.3. The effect of changing bulk composition on mineral stability fields

Of special interest for this study was the effect of changing bulk composition on garnet and staurolite stability fields. The main change in the bulk composition that may affect the stability of these phases involves variation in the aluminum, iron, magnesium (for staurolite and garnet) and manganese (for garnet) content. The absolute changes in the bulk chemistry of the samples considered for this study are minor and therefore no significant changes on the pseudosection topology are expected. Figure 17 shows that the rocks in the contact aureole of the Mooselookmeguntic pluton became progressively aluminum enriched with decreasing iron and magnesium. The rocks tend to become aluminum-rich toward the NW, and iron and magnesium rich in the opposite direction (Fig. 18). It is difficult to assess with the available data if these changes reflect variations due to initial composition of the pelites or are the result of allochemical metamorphism induced by fluid flow. The complete replacement of staurolite by coarse-grained muscovite indicates that, at least locally, mass transfer reaction occurred (Foster, 1977). If regional-scale mass transfer took place during fluid flow, the rocks would become aluminum-rich by removing iron and magnesium from the system. The easiest way to do that is by dissolving ferromagnesian minerals (biotite, garnet, staurolite) and replacing them with aluminum-rich minerals (sillimanite, andalusite, muscovite). Recent studies in similar terranes indicate that allochemical metamorphism associated with shear zones may be

quite common (Gates and Speer, 1991; Selverstone et al., 1991; Ague, 1994a, 1994b). Although mineralogical evidence in the field may support such an idea, more detailed work is required to prove it.

The main influence of changing bulk composition on the pseudosection topology can be observed for the garnet-in reaction line, which is mainly affected by the manganese concentration in the rock (Fig. 19). It has been suggested for a long time that MnO stabilizes garnet at lower temperature and pressures in the NCMnKFMASH system relative to KFMASH (Spear and Cheney, 1989; Droop and Harte, 1995; Mahar et al., 1997; Tinkham et al., 2001). According to Henry and Guidotti (2002) the rocks in the region were metamorphosed under isobaric conditions at 3.3 kbars. Based on this pressure and by using the Spear and Cheney (1989) petrogenetic grid, the temperatures in the garnet zone were assigned at 500°C for the lower garnet zone, at 520°C for the middle garnet zone, and at 540°C for the upper garnet zone (Henry and Guidotti, 2002). Figure 19 shows that garnet-in line shifts to lower temperature with increasing bulk MnO. On this Figure is also shown the garnet core FIA for each sample. At 3.3 kbars there is almost a perfect correlation between the temperature at which garnet reacts in and the bulk MnO. Taking into consideration the minimum temperature value as given in Henry and Guidotti (2002) for the garnet isograd, then the garnet–in reaction must have occurred to at least 500°C. If that occurred, then, for most samples considered in this study, the garnet-in reaction must have been temperature-overstepped. In the case of sample IS28B, that will account for at least 70°C of reaction overstep. Tinkham et al., (2001) noticed that garnet stability at low temperature is strongly increased by decreasing MgO/(MgO+FeO), while the bulk Al_2O_3 has little effect on garnet stability at low temperatures. If we take into consideration that in

the present case, the decrease in MgO/(MgO+FeO) correlates with the increase in the bulk Al_2O_3, then increased Al must have a stabilizing effect on garnet at lower temperatures. Although FIAs 4 and 5 show a consistency in temperature increase via the garnet-in line, in Fig. 19, FIAs 1 and some degree 2 tend to spread across the plot. Therefore, there is no clear-cut relationship between apparent temperature overstepping, FIA trend, and relative timing supporting the bulk composition as being the root cause of this linear relationship.

The effect of variable bulk composition appears to be less pronounced for the staurolite stability field (Fig. 20). At 4 kbars the staurolite-in line varies from 549°C to 565°C, while the staurolite-out line lies between 580°C and 590°C. The stability field of coexisting St+And at fixed temperature varies within about 0.3 bars. A significant change in the sillimanite stability field for St+And bearing assemblages was not observed here in contrast with those considered in Tinkham et al. (2001). The bulk Al_2O_3 varies less than 5% for all samples included in this study.

Sample IS71 (Fig. 2) is an important sample. It contains the lowest Mn-content garnet (0.5%, Fig. 19), and these porphyroblasts formed in FIA 5 at the highest temperature (~540°C). Some garnet porphyroblasts are included in staurolite that also contains FIA 5, and the youngest monazite grains dated from this area (345 Ma). Matrix monazite yielded ages of 344 Ma. This was the sample that did not produce staurolite in a pseudosection from the Bt+Grt assemblage. Yet it contains staurolite (Grt+St+And+Bt+Ms+Pl) and prograde muscovite rich pseudomorphs after staurolite and andalusite. It has the highest $Al_2O_3/(Al_2O_3+Fe_2O_3+MgO)$ value (0.683) from all samples, showing a significant enrichment in Al_2O_3 relative to Fe_2O_3 and MgO. Biotite and garnet inclusions in staurolite and andalusite porphyroblasts, chlorite inclusions in garnet

porphyroblasts, and andalusite replacing staurolite clearly indicate the PT path followed by this sample. This mineralogy suggests that the chemistry of this sample was modified during high grade metamorphism (or possibly late retrogression) by fluid flow and this is supported by the attempts shown in Fig. 21 to produce staurolite.

The only way to produce staurolite on a pseudosection is to start with the association Chl, Pl, St (line number 1 in Fig. 21) and set staurolite to zero modal proportions. Andalusite (line number 2 in Fig. 21) is produced in a similar manner. The high-temperature part of the pseudosection has a similar topology to the other samples and appears to not be affected by these changes in bulk composition. Increasing the bulk MnO shifts the garnet-in line to lower temperatures. For example, when the bulk MnO was changed to 0.15% (like sample IS2 and IS23) the garnet-in reaction at 3.3 kbars occurred at 493°C, at 0.23% MnO (like sample IS28A) the reaction occurred at 462°C and at 0.33% MnO (like sample IS28B) the reaction occurred at 424°C. These values differ up to 10°C from the values obtained by using those samples, which suggest interference of the other components on the garnet stability at low temperature. The biotite-in reaction (line number 4 if Fig. 21) occurred at temperatures at least 30°C higher than in all the other samples consistent with the results of Tinkham et al. (2001), showing that biotite is destabilized at lower temperatures with increasing bulk Al_2O_3. If high bulk Al_2O_3 stabilizes staurolite and destabilizes biotite at lower temperatures, then we may expect staurolite to grow before biotite (like in Fig. 21). Therefore, changes due to increasing Al_2O_3 and decreasing Fe_2O_3 and MgO could be significant enough to modify the mineral stability fields in the NCMnKFMASH system. Although mineralogical evidence suggests that most of the rocks were affected by mass transfer reactions, there is no clear effect on the pseudosection

topology except for sample IS71. The amount of mass transfer for most of the rocks in the region was not significant enough to produce changes on the pseudosection topology. The consistency of the mineral stability fields modeled with Thermocalc with the petrological observations for most of the samples support the idea of insignificant mass transfer beyond the scale of a porphyroblast. More work is required to detail the extent of mass transfer and fluid rock interaction in the region before any significant conclusions can be reached.

Alternatively, this sample (IS71) did have a lower Mn content originally the others and, therefore, could not grow garnet until the temperature got high enough late in FIA 5. Staurolite then grew very late in the development of FIA 5 and thus contains the youngest monazite inclusions.

8. THERMOBAROMETRY

Thermobarometric estimations were done using four different methods to infer the equilibration conditions for the observed mineral assemblages; average PT via Thermocalc (Holland and Powell, 1998), conventional geothermobarometers (computer software GTB v.2.1 of Spear and Kohn, http://ees2.geo.rpi.edu/MetaPetaRen/Software/GTB_Prog/GTB.html) and pseudosections. The stability field for different mineral assemblages from the contact aureole of the Mooselookmeguntic pluton in the PT space by using the pseudosection approach was discussed in a previous section. Garnet isopleth thermobarometry was used to obtain PT conditions for garnet nucleation.

8.1. Average PT with Thermocalc

The mineral activities were calculated with the computer software AX (http://rock.esc.cam.ac.uk/astaff/holland/ax.html) and the average PT was determined

using option 2 in Thermocalc. In the case of zoned minerals (garnet and plagioclase) only the rim compositions were used (Tables 6 and 8). The calculations were performed for $aH_2O=1$ with andalusite and sillimanite as the only aluminosilicate phases. To optimize the results, a two step procedure was used:

1. End-members activity compositions were first calculated with the starting guesses (P and T) following Henry and Guidotti (2002) values for the middle of the lower sillimanite zone and for the peak conditions in the lower sillimanite zone. These were 3.3 kbars and 610°C for the middle of the lower sillimanite zone and 3.3 kbars and 630°C for the peak conditions. The average PT was calculated with Thermocalc for each sample with these activities.
2. The final results were calculated by using the PT values obtained from the previous step as starting guesses to recalculate the end-member activity compositions.

Two samples were selected for average PT determinations with Thermocalc (IS74 and IS104). Both come from the lower sillimanite zone and theoretically should represent peak metamorphic conditions. The mineral assemblage in both samples is represented by the association Ms+Pl+Bt+Grt+St+And+Sill. Sample IS104 has a much higher amount of modal sillimanite and contains prograde muscovite rich pseudomorphs after andalusite and staurolite and prograde biotite pseudomorphs after garnet. The mineral chemistry is presented in Tables 4, 5, 6, 7 and 8, and the end members included in the calculations and the results are shown in Tables 10 and 11. The results plotted on the phase diagram for the average composition is shown in Fig. 22. The average P and T calculated for sample IS104 is 3.9±0.2 kbars and 592±10°C and for sample IS74 the average P and T is 4±0.3 kbars and 589±12°C.

8.2. Conventional geothermobarometry

Conventional thermobarometry involving the intersection of the temperature sensitive garnet-biotite equilibrium and the pressure sensitive garnet-aluminosilicate-plagioclase-quartz (GASP) equilibrium were also used for sample IS74 and IS104. For samples IS2 and IS77 only the garnet-biotite thermometer was used for the following reasons: (i) sample IS2 comes from the lower sillimanite zone and should record similar conditions with samples IS74 and IS104 and (ii) there is clear evidence (Fig. 11) that in the case of sample IS77 the calcium equilibrium in the rim of the garnet and possibly in plagioclase as well was disturbed by retrogression. The results are presented in Figs. 23 and 24. The shaded areas in Fig. 23 delimitated by the minimum and maximum values obtained with different calibrations are considered to represent the errors associated with the uncertainties in the PT conditions where equilibration occurred. The equilibration conditions for samples obtained this way are 580-635°C and 2.7-5.6 kbars for sample IS104, and 485-530°C and 2.1-5.2 kbars for sample IS74. The PT range for both samples is about $\Delta T=\pm 26$°C and $\Delta P=\pm 1.5$ kbars. All temperatures obtained for samples IS2, IS74, and IS77 are below 520°C, which put them into the chlorite stability field. That is not surprising for sample IS77, which is located in a zone affected by retrogression and some retrogressive chlorite was found in the matrix. The temperature results for samples IS2 and IS74 are surprising taking into consideration that both samples come from the sillimanite zone and no retrogression effects were observed during thin section studies. This may suggest that retrogression was subtle but strong enough to affect the Fe-Mg partitioning between coexisting garnet and biotite.

The average PT conditions calculated with Thermocalc for sample IS74 are consistent with the field observations and most probably reflect peak conditions for these samples, while the results obtained by conventional thermobarometry may reflect the retrograde path. For sample IS104 both, conventional thermobarometry and average PT with Thermocalc may reflect peak metamorphic conditions. Anyway, as suggested by Henry and Guidotti (2002), peak conditions in the lower sillimanite zone may have been as high as 630°C at about 3.3 kbars.

8.3. Thermobarometry derived from pseudosections

As suggested by Powell and Holland (2008) pseudosection modeling provides a powerful thermobarometric tool. Details regarding the stability field of mineral assemblages on the phase diagram were discussed in a previous section. In this section is examined the importance of the invariant points in determining PT conditions when they are well constrained by field and petrological observations. Two situations provide enough information to be sorted out by using field observations, petrological study and pseudosection modeling. These are the transition from Grt+St to Grt+St+And assemblages and from Grt+St+And to Grt+St+And+Sill assemblages.

8.3.1. The transition from Grt+St to Grt+St+And

In all samples where Grt, St and And coexist, microstructural and textural observations indicate that (i) Grt growth predated and/or was synchronous with St growth and (ii) St growth predated and/or was synchronous with And growth. The transition from Grt+St to Grt+St+And assemblages is clearly marked in the field (Fig. 3). The transition from Chl+Grt+Bt to Chl+Grt+Bt+St with the addition of staurolite can be described by the following KFMASH reactions:

$$Ms+Chl+Qtz = St+Bt+H_2O \text{ (2)},$$

if Grt was not consumed during St growth, or:

$$Ms+Chl+Grt+Qtz = St+Bt+H_2O \text{ (3)}$$

if Grt was partially consumed during St growth. Synchronous growth of Grt and St can be explained by the following reaction:

$$Chl+Ms = Mg\text{-}St+Mg\text{-richer } Bt+Mg\text{-richer } Chl+Grt+Na\text{-richer } Ms+H_2O \text{ (4)},$$

proposed by Guidotti (1974) which describes the mineralogy of Grt+St assemblages as well as the mineral chemistry. All of the above three reactions are consistent with petrological observations and probably reaction (4) was the last one to occur. On the phase diagram (Fig. 25) reactions (2) and (3) make the transition from the Chl+Grt+Bt field to the Chl+Grt+B+St field, while reaction (4) must have occurred in the Chl+Grt+Bt+St field. The transition from the staurolite field to the St+And field can be described by the following KFMASH reactions:

$$Ms+Chl+St+Qtz = And+Bt+H_2O \text{ (5)}$$

if And entered from Chl bearing assemblages or:

$$Ms+St+Qtz = And+Bt+H_2O \text{ (6)}$$

if And entered from Chl free assemblages. On the phase diagram (Fig. 25) reaction (5) implies crossing the small divariant field where Chl+Bt+Grt+St+And coexists over a very small temperature range. If andalusite was formed by reaction (6), then all chlorite must have been consumed by the reactions (3) and (4). The continuity between the inclusion trails in staurolite and andalusite and the absence of any chlorite inclusions in andalusite porphyroblasts suggest that andalusite growth started to occur as soon as reactions (3) and (4) were completed by the reaction (6). If that happened, then andalusite growth must have

occurred near the invariant point where staurolite and chlorite were set to zero modal proportions (the black dot marked IP1 in Fig. 25). The location of this invariant point in the PT space calculated with Thermocalc for all samples is shown in Table 12 and Fig. 25.

8.3.2. The transition from Grt+St+And to Grt+St+And+Sill

Another well constrained relationship in the field is the transition from Grt+St+And to Grt+St+And+Sill assemblages (Fig. 3). The appearance of sillimanite corresponds with the first evidence for garnet breaking down to biotite. The fact that in most of the samples sillimanite first appears from St+And assemblages suggests the operation of the following reactions:

And=Sill (7)

(Mg)Bt+(K,Na)Mu+Grt+(Mg)St+Qtz = Sill+(Fe)Bt+(Fe)St+(Mn,Fe)Grt+Ab+H_2O (8)

Reaction (8) was proposed by Guidotti (1974) and together with reaction (7) integrates most of the observational data in the Grt+St+And+Sill zone. This also suggests that the onset of sillimanite growth on the phase diagram in these rocks must have occurred near the invariant point where andalusite and staurolite were set to zero modal proportions (the black dot marked IP2 in Fig. 25). Table 13 and Fig. 25 show the location of this invariant point for all samples as calculated with Thermocalc.

8.4. Garnet isopleth thermo – barometry

Theoretically the PT conditions at the time of garnet growth for a specific bulk composition can be estimated by plotting the garnet core isopleths (e.g., X_{Alm}, X_{Gr}, X_{Sp}) in the PT space (Vance and Mahar; 1998; Evans, 2004; Tinkham and Ghent, 2005; Cihan et al., 2006; Sayab, 2007) for the calculated pseudosection. The method requires that garnet be compositionally zoned and the core isolated from the reacting matrix. The core of the

garnet can be analysed by EPMA analysis and garnet-core compositional isopleths can be calculated. The garnet core isopleths, when plotted on the pseudosection, should intersect at a single PT point, which is considered to be the best estimate for the onset of garnet growth.

Five samples, with different FIA trends measured in the garnet porphyroblasts, were selected to determine the PT conditions of garnet growth. From each sample, only those garnet grains that showed the minimum amount of inclusions were analyzed for both core and rim compositions (Table 6). The isopleths of the end-members almandine (X_{Alm}), grossular (X_{Gr}), and spessartine (X_{Sp}) were plotted for each sample on the pseudosection calculated from the XRF derived bulk composition. The uncertainties concerning the location of these isopleths (as calculated with the program Thermocalc) are indicated by shading. The overlap of the compositional isopleths for the garnet core (within uncertainty) for these three end-members was taken as the best approximation of core growth (Tinkham and Ghent, 2005), whereas the area defined by the intersection of all the uncertainties of isopleths was considered to represent the error ellipse within where the core growth occurred. Mineral inclusions in garnet from all samples used to plot the garnet core isopleths were checked under the microscope and with EDS in back-scatter imaging as they may indicate the mineral assemblage from which the garnets grew.

Sample IS2 contains FIA set 1 in both garnet and staurolite porphyroblasts. Garnet from this sample contain mineral inclusions consisting mainly of chlorite, ilmenite, plagioclase, muscovite, and quartz. The garnet-core isopleths were plotted using the quinivariant field Ms Pl Chl Grt. The core isopleths plotted (Fig. 26) in the quadrivariant field Ms Pl Chl Grt Bt at about 3.8 kbars and 540°C. That suggests about a 60°C

temperature overstep, while the intersection of the cores above the garnet-in line suggests a pressure increase during growth.

Sample IS77 contains FIA set 2 in garnet porphyroblasts and FIA 2 (cores) and 5 (rims) in staurolite porphyroblasts. Mineral inclusions in garnet porphyroblasts consist mainly of quartz, ilmenite, and plagioclase. The garnet-core isopleths were plotted using the quinivariant field Ms Pl Chl Grt. The core isopleths intersected (Fig. 27) in the quadrivariant field Ms Pl Chl Grt Bt at about 3.5 kbars and 540°C. That suggests about 30°C temperature overstep and growth under isobaric conditions.

Sample IS95 contains FIA set 3 in garnet porphyroblasts and FIA 3 (core), 4 (medians) and 5 (rims) in staurolite porphyroblasts. Garnets contain muscovite, plagioclase, ilmenite, and chlorite as mineral inclusions. The core isopleths were plotted for the quinivariant field Ms Pl Chl Grt and they intersected (Fig. 28) in the quadrivariant field Ms Pl Chl Grt Bt at about 3.3 kbars and 530°C. That accounts for about 50°C reaction overstep and isobaric conditions.

Sample IS74 contains FIA set 4 in garnet porphyroblasts and FIA 4 (crenulated cleavage) and 5 (crenulation cleavage) in staurolite porphyroblasts. Muscovite, plagioclase, ilmenite, and quartz were identified as mineral inclusions in garnet porphyroblasts. The quinivariant field Ms Pl Chl Grt was used to plot the core isopleths which intersected (Fig. 29) in the same field near the biotite-in line at about 4.4 kbars and 540°C. That accounts for about 25°C of reaction overstep and isobaric conditions. This sample indicates an increase in pressure of about 1.1 kbars from FIA set 3 to FIA set 4, which is unusual if we consider that the metamorphism, in the region, occurred at isobaric conditions (Henry and Guidotti, 2002). This small increase in pressure may be very significant if it is real. The

age of FIA set 4 was determined to be around 370 Ma, which coincides with the emplacement age for the Mooselookmeguntic pluton (Solar et al., 1998). It has already been suggested that the emplacement of the Mooselookmeguntic pluton was accompanied by an increase in pressure (Johnson et al., 2003). The other explanation for this increase in pressure would be that the garnet was partially homogenized under lower-sillimanite-zone conditions and/or was affected by retrogression (see the conventional thermobarometry section). It is less probable that the core of the garnet was affected by retrogression than in sample IS77. In the latter sample, where the rim was clearly affected by retrogression (Fig. 11), the core remained unaffected and there were no obvious cracks identified by backscatter imaging or thin-section study. It is possible that the composition of the core was changed by internal diffusion under sillimanite grade conditions and therefore the core equilibrium was disturbed. For example, in the case of sample IS104 there is evidence that the core chemistry was modified by internal diffusion (Figs. 11 and 12). When the core isopleths of sample IS104 for the matrix garnet were plotted with Thermocalc (Fig. 30) they gave a pressure of 5.5 kbars at 540°C. This pressure is about 1.7 kbars higher than that calculated for sample IS2 which has the same FIA, but does not contain sillimanite. Considering that the amount of sillimanite in sample IS74 is much smaller than in sample IS104, we should not exclude the possibility that a pressure of about 4.5 kbars might be the result of the Mooselookmeguntic pluton emplacement. A more detailed study is needed to confirm or reject this hypothesis.

Sample IS28A contains only garnet porphyroblasts which preserve FIA set 5 inclusion trails. Garnet porphyroblasts contain muscovite, plagioclase, biotite, ilmenite, chlorite, and quartz as mineral inclusions, which is consistent with the phase-diagram

modeling (Fig. 31). The garnet core isopleths were plotted for the quadrivariant field Ms Pl Chl Grt Bt, and they intersected in the same field at about 2.9 kbars and 543°C. This suggests a reaction overstep of about 90°C, isobaric conditions and about 1.5 kbars drop in pressure from FIA 4 to FIA 5.

9. DISCUSSION

9.1. Comparison with previous metamorphic history

The metamorphic history of the region under study and of Western Maine in general is very well documented (e.g., Guidotti, 1970, 1974, 2000; Holdway et al., 1982; Holdaway et al., 1988; DeYoreo et al., 1989; Guidotti and Johnson, 2002; Henry and Guidotti, 2002; Johnson et al., 2003; Johnson et al., 2006). Detailed structural studies have contributed to the understanding of deformation partitioning, shear zone systems, and melt generation within Central Maine Belt (e.g., Brown and Solar., 1998a, 1998b; Solar et al., 1998; Solar and Brown, 1999, 2001a, 2001b). Generally, it is accepted that at least three distinct metamorphic events affected this region, although some studies point out the possibility of at least five (M1 to M5) events (e.g., Holdaway et al., 1982; Holdaway et al., 1988). However, correlations and spatial distributions for these events are poorly constrained. For example, the region under investigation is considered to have experienced three metamorphic events – M1 to M3 (Guidotti, 2000; Henry and Guidotti, 2002; Guidotti and Johnson, 2002; Johnson et al., 2003; Johnson et al., 2006). Although Guidotti (1974, 2000) refers that at least two high-temperature events affecting the region, only two events (M2 and M3) are described. The first event, M1, produced widespread chlorite-zone metamorphism and was older than 400 Ma. The effects of this event are thought to show up in outcrops between Madison, Farmington, and Kingfield (Holdaway et al., 1988), but

are no longer preserved in the contact aureole of the Mooselookmeguntic pluton. FIA 1 garnet and staurolite porphyroblasts, which formed at about 420 Ma, must correlate with this event (Fig. 32). If that is true, then the difference in metamorphic grade, chlorite versus garnet + staurolite, must account for a few kbars of pressure increase towards the west or for a difference in the depth of the exposure surface. The second event, M2, is thought to have occurred around 400 Ma and produced And+St+Bt±Grt (e.g. Guidotti, 2000; Henry and Guidotti, 2002) as a result of a regional thermal event (e.g., Guidotti and Johnson, 2002; Johnson et al., 2006). This event may correspond with FIA 2 porphyroblasts (Fig. 32). The only difference occurs in the fact that we could not accurately separate any andalusite related to FIA 2. We do not exclude the possibility that some of the andalusite that replaced FIA 1 or FIA 2 porphyroblasts may be of this age. The third event, M3, was considered to be post-kinematic and staurolite growth occurred only in the transition zone (Guidotti and Johnson, 2002; Johnson et al., 2006). This event is characterized Sill+St+Bt (e.g., Guidotti, 2000; Henry and Guidotti, 2002) and prograde and retrograde pseudomorphs as a function of the metamorphic grade (Guidotti and Johnson, 2002) and was related to the intrusion of the Mooselookmeguntic pluton at 370 Ma. Although andalusite is present in M3 assemblages, Guidotti (1974) and Guidotti and Johnson (2002) argued that all andalusite is a remnant of the M2 event. Our data suggests that andalusite may be coeval and/or later than any of the FIAs. Therefore, andalusite growth did occur during and after M3. Figure 33a contains an example where staurolite porphyroblasts from sample IS71, which contain inclusions of monazite grains as young as 345 Ma, have been replaced by andalusite. Small grains of prismatic sillimanite (Fig. 33b)

nucleated in andalusite and in the matrix suggesting that sillimanite grade metamorphism postdate FIA 5.

We could correlate this M3 event with FIA 3 and FIA 4 (Fig. 32) since the metamorphism associated with both of these FIAs appear to be pluton emplacement related. The only way to correlate FIA 5 (360-345 Ma) metamorphism with previous studies is if we consider the M4 event described by Holdaway et al., (1982) and thought to have occurred at about 360 Ma around the Reddington, Lexington, and Skowhegan batholiths. According to Holdaway et al. (1982) the M4 aureoles around the above plutons contain staurolite, andalusite and cordierite porphyroblasts.

Further studies involving FIA measurements and monazite dating in andalusite and cordierite porphyroblasts are required to solve their relative timing. Andalusite porphyroblasts may be present with any of the five FIAs porphyroblasts, and their textural and microstructural relationships always indicate a synchronous or a later growth for andalusite. Therefore, important constraints on andalusite timing are difficult to make in the absence of FIA measurements. Cordierite usually shows later growth than andalusite but may be present with any of the five FIAs porphyroblasts. Therefore, more than one generation of cordierite may be present. The timing of some of the youngest andalusite and of the cordierite can possibly extend up to the M5 event described in Holdaway et al. (1988). This event was correlated with the emplacement of the Sebago batholith at around 325 Ma. The main effect of this event was to produce higher-pressure and -temperature assemblages than previous events towards south of the area included in this study.

9.2. PT paths in the contact aureole of the Mooselookmeguntic pluton

Assessing PT paths in low-pressure high temperature polymetamorphic terranes associated with pluton intrusions are problematic (Pattison et al., 1999). In the contact aureole of the Mooselookmeguntic pluton mineral assemblages related to the regional metamorphism were overprinted by pluton-related thermal events. The spatial and temporal extent of the pluton influence cannot be accurately estimated since there are very few data available about the garnet, andalusite, and cordierite history. Most of the previous work focused on M3 related metamorphism and therefore, on M3 staurolite history (e.g., Guidotti, 2000; Henry and Guidotti, 2002). The only mineral assemblages that can be recognized in the aureole consist of combinations of Grt+St+And+Crd+Sill. Cordierite is only sporadically present and sillimanite generally appears to be restricted to the proximity of the pluton. The sillimanite history, although very important for the PT history of the region, is difficult to integrate with time.

It has been proposed that sillimanite growth may have occurred during M2 (Guidotti, 1974, 2000; Guidotti and Johnson, 2002), but the sillimanite isograd was the result of the M3 event in response to the intrusion of the Mooselookmeguntic pluton at 370 Ma (Guidotti, 1974; Guidotti and Johnson, 2002; Johnson et al., 2006). The data herein suggests that high-grade metamorphism continued after 370 Ma until at least 345 Ma and even further to produce cordierite. Either all of the sillimanite is a metastable relict of the 370 Ma thermal event, or some is younger. The PT constraints on the mineral assemblages imposed by phase diagram modeling, average PT with Thermocalc and conventional thermobarometry cannot be extended for the entire period of metamorphism (from c. 420 to less than 345 Ma). Most probably, the PT conditions determined by thermobarometry

are strongly affected by younger events. The metastable preservation of minerals in the FIA succession (Grt+St) and the mineral assemblages in the aureole (Figs. 2 and 3) indicate an overall isobaric evolution in the St and/or St+And stability field. Garnet-core isopleths suggest that between periods of heating the rocks experienced isobaric cooling but with no more than 15°C less than the temperature required to produce staurolite, because all garnet growth occurred close to this temperature (Fig. 34a). Such a situation would be possible in the case of episodic emplacement of the pluton at similar structural levels. The end of thermal and tectonic activity must have been closely related to the cordierite history, since this is the last porphyroblastic phase in the contact aureole. The fact that cordierite porphyroblasts were also affected by prograde and retrograde pseudomorphism (Figs. 5 and 35) indicates that the timing of pseudomorphism has to be re-assessed. Although the most obvious explanation taking into consideration field relationships (Figs. 2 and 3) is to assign the timing of the pseudomorphs to the 370 Ma thermal event, the new monazite ages from FIA 5 staurolite have to be taken into consideration, as well as the cordierite history, before any significant conclusions can be reached. For example, in sample IS7B (Fig. 5) cordierite was partly replaced by chlorite indicating retrograde metamorphism, while in sample IS90, towards the pluton, cordierite was partly pseudomorphed by an aggregate of muscovite and biotite intergrowths (Fig. 35). If we consider that the latter occurs near sillimanite bearing samples, then that might be an indication of prograde break-down of cordierite. If that is true, we may consider that at least part of the sillimanite is later than 370 Ma.

Johnson et al. (2003) proposed a counterclockwise PT path (Fig. 34b) with the M3 event occurring at higher pressure than the regional M2, and followed by retrogression.

The data herein suggest rather an overall clockwise PT path (Fig. 34b) with the rock possibly maintained for a long period of time at PT conditions near the invariant point IP1 and with peak conditions near IP2 or at even higher grades followed by decompression (Fig. 36), growth of cordierite, and retrogression. The history of cordierite, andalusite, and the exact timing of pseudomorph formation have to be better documented and this requires reinterpretation of the deformation and metamorphic history in the contact aureole of the Mooselookmeguntic pluton and possibly over the entire Western Maine region.

9.3. Implications for the tectonic history of Western Maine

The high degree of preservation of a lengthy history of deformation and metamorphism in the contact aureole of the Mooselookmeguntic pluton indicates the possibility that similar histories can be deduced throughout the Northern Appalachian orogen. Five successive FIA sets indicating episodic but continuous deformation and metamorphism suggest that similar processes occurred over at least the entire region of Western Maine. Monazite dating of FIAs showed a continuous tectonic history from more than 420 Ma to 345 Ma. Similar metamorphic ages over much of the New England part of the Acadian orogeny confirm the significance of a lengthy tectono-metamorphic activity. Bell and Welch (2002), based on FIA measurements in garnet porphyroblasts from the metamorphic rocks in the Chester Dome region of Vermont, presented monazite ages in the interval 425-352 Ma. Pyle et al. (2005) reported monazite ages from southwest New Hampshire in the interval 400-352 Ma, whereas Gerbi and West (2007) described metamorphic ages from south-central Maine that ranged over a 430-350 Ma interval. Textural and microstructural evidence from garnet, staurolite, andalusite, and cordierite porphyroblasts indicate continuity from early Acadian to the Alleghanian. The preservation

of cordierite-bearing assemblages indicates termination of metamorphism through rapid cooling. The triggering of the cordierite-forming reactions on the other hand, implies that the onset of cooling took place at pressures less than 2 kbars, but at high temperature. A model is required to explain the heat source for cordierite-forming reactions. Taking into consideration that cordierite porphyroblasts were partly pseudomorphosed by chlorite, the suggestion that pseudomorphs are related to the 370 Ma thermal event associated with the emplacement of the Mooselookmeguntic pluton (Guidotti and Johnson, 2002) requires reconsideration.

The emplacement history of the Mooselookmeguntic pluton may be more complicated than that of one stage of emplacement at 370 Ma (Solar et al., 1998). The thermal effects observed in this study and the correlation of FIA 3 and FIA 4 ages with pluton ages rather suggest episodic emplacement at similar structural levels. The continuous metamorphic and deformation history supports the idea of more than one thermal pulse, with the time period between thermal pulses short enough that the rocks did not cool significantly. This would explain the continuous growth of garnet and staurolite, which requires elevated thermal regimes that are better explained by multiple intrusions emplaced at relatively close proximity over short periods of time. Such situations have been described in the Augusta area of Maine (Novak and Holdaway, 1981; Holdaway et al., 1982), the Aston region of Pyrenees (Verhoef et al., 1984), the Cima d'Asta pluton in Northern Italy (D'amico et al., 1971), and in the central Old Woman Mountains of south-eastern California (Rothstein and Hoisch, 1994). The isograd pattern (Fig. 2) and the mineral-assemblage distribution (Fig. 3) follow the pluton contour, suggesting that it was the pluton that provided the heat for metamorphism. The cordierite distribution around the

pluton is not well constrained. Therefore, no viable interpretation can be made without detailed mapping of its occurrences. Taking into consideration that in similar terranes the cordierite distribution is invariably related to the pluton proximity, we may infer that it is the same in the present case. If that is true then further research should investigate the possibility that parts of the pluton may be younger than 370 Ma. This possibility is suggested by 345 Ma monazite ages in FIA 5 porphyroblasts, and, if we consider that cordierite growth postdates FIA 5 porphyroblasts, than even younger ages should not come as a surprise. In many of the FIA 5 rocks, textural, and microtextural evidence suggest that andalusite partly replaced staurolite in the same event (Fig. 36). This implies that there was sufficient uplift between the FIA 5 metamorphism and cordierite growth to result in a change from St+And to St+And+Crd. The sporadic development of cordierite as an additional phase in rocks that show the same mineral assemblage as rocks without cordierite suggests that the temperature of the lower-pressure overprint did not exceed that of the earlier prograde sequence.

REFERENCES

Ague, J. J., 1994a. Mass transfer during Barrovian metamorphism of pelites, south-central Connecticut, I: Evidence for composition and volume change, *American Journal of Science,* **294**, 989-1057.

Ague, J. J., 1994b. Mass transfer during Barrovian metamorphism of pelites, south-central Connecticut, II: Channelized fluid flow and the growth of staurolite and kyanite, *American Journal of Science*, **194**, 1061-1134.

Bell, T. H., and Welch, P. W., 2002. Prolonged Acadian Orogenesis: Revelations from FIA controlled monazite dating of foliations in porphyroblasts and matrix. *American Journal of Science*, **302**, 549-581.

Bell, T. H., Forde, A., and Wang, J., 1995. A new indicator of movement direction during orogenesis: measurement technique and application to the Alps. *Terra Nova*, **7**, 500-508.

Bell, T. H., Hickey, K. A., and Upton, G. J. G., 1998. Distinguishing and correlating multiple phases of metamorphism across a multiply deformed region using the axes of spiral, staircase and sigmoidally curved inclusion trails in garnet. *Journal of Metamorphic Geology*, **16**, 767-794.

Bradley, D. C., Tucker, R. D., Lux, D., Harris, A. G., and McGregor, D. C., 1998. Migration of the Acadian Orogen and Foreland Basin across the Northern Appalachians. U.S. Geological Survey, Open-file report 98-770, 79 p.

Brown, M., and Solar, G. S., 1998a. Shear zone systems and melts: feedback relations and self organization in orogenic belts. *Journal of Structural Geology*, **20**, 211-227.

Brown, M., and Solar, G. S., 1998b. Granite ascent and emplacement during contractional deformation in convergent orogens. *Journal of Structural Geology*, **20**, 1365-1393.

Brown, M., and Solar, G. S., 1999. The mechanism of ascent and emplacement of granite magma during transpression: a syntectonic granite paradigm. *Tectonophysics*, **312**, 1-33.

Carlson, W. D., 1999. The case against Ostwald ripening of porphyroblasts. *The Canadian Mineralogist,* **37**, 403-413.

Cheney, J. T., and Guidotti, C. V., 1973. Paragonite contents of coexisting, but texturally different muscovites from pelitic schists of the Puzzle Mountain area, Maine. *American Mineralogist*, **58**, 1076-1079.

Chernoff, C. B., and Carlson, W. D., 1997. Disequilibrium for Ca during growth of pelitic garnet. *Journal of Metamorphic Geology*, **15**, 421-438.

Chernoff, C. B., and Carlson, W. D., 1999. Trace element zoning as a record of chemical disequilibrium during garnet growth. *Geology*, **27**, 555-558.

Cihan, M, Evins, P. M., Lisowiec, N. J., and Blake, K. L., 2006. Time constraints on deformation and metamorphism from EPMA dating of monazite in the Proterozoic Robertson River Metamorphics, NE Australia. *Precambrian Research,* **145**, 1-23.

D'Amico, C., Del Monte, M., and Gandolfi, G., 1971. Multiple intrusions in the Cima d'Asta pluton (Northern Italy). *Contributions to Mineralogy and Petrology*, **31**, 13-27.

Daniel, C. G., and Spear, F. S., 1998. Three-dimensional patterns of garnet nucleation and growth, *Geology,* **26**, 503-506.

De Yoreo, J. J., Lux, D. R., Guidotti, C. V., Decker, E. R., and Osberg, P. H., 1989. The Acadian thermal history of western Maine. *Journal of Metamorphic Geology*, **7**, 169-190.

Droop, G. T. R., and Harte, B., 1995. The effect of Mn on the phase relations of medium-grade pelites: Constraints from natural assemblages on petrogenetic grid topology. *Journal of Petrology*, **36**, 1549-1578.

Dutrow, B. L., Foster, C. T., Jr., and Henry, D. J., 1999. Tourmaline-rich pseudomorphs in sillimanite zone metapelites: demarcation of an infiltration front. *American Mineralogist*, **84**, 794-805.

Dutrow, B. L., Foster, C. T., Jr., and Whittington, J., 2008. Prograde muscovite-rich pseudomorphs as indicators of conditions during metamorphism: An example from NW Maine. *American Mineralogist*, **93**, 300-314.

Evans, T. P., 2004. A method for calculating effective bulk composition modification due to crystal fractionation in garnet-bearing schist: implications for isopleth thermobarometry. *Journal of Metamorphic Geology*, **22**, 547-557.

Foster, C. T., Jr., 1977. Mass transfer in sillimanite-bearing pelitic schists near Rangeley, Maine. *American Mineralogist*, **62**, 727-746.

Foster, C. T., Jr., 1981. A thermodynamic model of mineral segregations in lower sillimanite zone near Rangeley, Maine. *American Mineralogist*, **66**, 260-277.

Franceschelli, M., Memmi, I., and Ricci, C. A., 1982. Zoneografia metamorfica della Sardegna settentrionale. In: *Guide Geologiche Regionali, Memorie della Società Geologica Italiana*, 137-149.

Gates, A. E., and Speer, J. A., 1991. Allochemical retrograde metamorphism in shear zones: An example in metapelites, Virginia, U.S.A. *Journal of Metamorphic Geology*, **9**, 581-604.

Gerbi, C., and West, D. P., Jr., 2007. Use of U-Pb geochronology to identify successive, spatially overlapping, tectonic episodes during Silurian-Devonian orogenesis in south-central Maine, USA. *Geological Society of America Bulletin*, **119**, 1218-1231.

Guidotti, C. V., 1966. Variations of the basal spacings of muscovite in sillimanite-bearing pelitic schists of northwestern Maine. *American Mineralogist,* **51**, 1778-1786.

Guidotti, C. V., 1968. Prograde muscovite pseudomorphs after staurolite in he Rangeley-Oquossoc areas, Maine. *American Mineralogist*, **53**, 1368-1376.

Guidotti, C. V., 1970. The mineralogy and petrology of the transition from the lower to upper sillimanite zone in the Oquossoc area, Maine. *Journal of Petrology*, **11**, 277-336.

Guidotti, C. V., 1974. Transition from staurolite to sillimanite zone, Rangeley Quadrangle, Maine. *Geological Society of America Bulletin*, **85**, 475-490.

Guidotti, C. V., 1978. Compositional variation of muscovite in medium- to high-grade metapelites of northwestern Maine. *American Mineralogist*, **63**, 878-884.

Guidotti, C. V., 1989. Metamorphism in Maine: an overview: In: Studies in Maine *Geology*, **3**, 1-19.

Guidotti, C. V., 2000. The classic high-T–low-P metamorphism of west-central Maine, USA: Is it post-tectonic or syntectonic? Evidence from porphyroblast-matrix relations: Discussion. *The Canadian Mineralogist*, **38**, 1007-1026.

Guidotti, C. V., and Dyar, M. D., 1991. Ferric iron in metamorphic biotite and its petrologic and crystallographic implications. *American Mineralogist*, **76**, 161-175.

Guidotti, C. V., and Holdaway, M. J., 1993. Petrology and field relations of successive metamorphic events in pelites of west-central Maine. In: *Cheney, J.T., Hepburn, J.C. (Eds.), Field Trip Guidebook for the Northeastern United States*, **1**. Geological Society of America, L1-L26.

Guidotti, C. V., and Johnson, S. E., 2002. Pseudomorphs and associated microstructures of western Maine, USA. *Journal of Structural Geology*, **24**, 1139-1156.

Guidotti, C. V., and Sassi, F. P., 1998a. Miscellaneous isomorphous substitutions in Na-K micas: a review, with special emphasis to metamorphic micas. *Rendiconti di Scienze Fisiche, Matematiche e Naturali, Accademia Nazionale dei Lincei*, **9**, 57-78.

Guidotti, C. V., and Sassi, F. P., 1998b. Petrogenetic significance of Na-K white mica mineralogy. Recent advances for metamorphic rocks. *European Journal of Mineralogy*, **10**, 815-854.

Hayward, N., 1991. Orogenic processes, deformation and mineralization history of portions of the Appalachian orogen, USA, based on microstructural analysis. Unpublished PhD thesis, James Cook University.

Henry, D. J. and Guidotti, C. V., 2002. Ti in biotite from metapelitic rocks: temperature effects, crystallochemical controls and petrologic applications. *American Mineralogist*, **87**, 375-382.

Henry, D. J., Guidotti, C. V., and Thomson, J. A., 2005. The Ti-saturation surface for low-to-medium pressure metapelitic biotites: Implications for geothermometry and Ti-substitution mechanisms. *American Mineralogist*, **90**, 316-328.

Hirsch, D. M., Prior, D. J. and Carlson, W. D., 2003. An overgrowth model to explain multiple, dispersed high-Mn regions in the cores of garnet porphyroblasts. *American Mineralogist*, **88**, 131-141.

Holdaway, M. J., Dutrow, B. L., and Hinton, R. W., 1988. Devonian and Carboniferous metamorphism in west-central Maine: The muscovite-almandine geobarometer and the staurolite problem revised. *American Mineralogist*, **73**, 20-47.

Holdaway, M. J., Guidotti, C. V., Novak, J. M., and Henry, W. E., 1982. Polymetamorphism in medium- to high-grade pelitic metamorphic rocks, west-central Maine. *Geological Society of America Bulletin*, **93**, 572-584.

Holland, T. J. B., and Powell, R., 1998. An internally consistent thermodynamic data set for phases of petrological interest. *Journal of Metamorphic Geology*, **16**, 309-343.

Hollister, L. S., 1966. Garnet zoning, an interpretation based on the Rayleigh fractionation model. *Science*, **154**, 1647-1651.

Johnson, S. E., Dupee, M. E., and Guidotti, C. V., 2006. Porphyroblast rotation during crenulation cleavage development; an example from the aureole of the Mooselookmeguntic Pluton, Maine, U.S.A. *Journal of Metamorphic Geology*, **24**, 55-73.

Johnson, T. E., and Brown, M., 2004. Quantitative constrains on metamorphism in the Variscides of Southern Brittany – a complementary pseudosection approach. *Journal of Petrology*, **45**, 1237-1259.

Johnson, T. E., Brown, M., and Solar, G. S., 2003. Low-pressure subsolidus and suprasolidus phase equilibria in the MnNCKF-MASH system: constraints on conditions of regional metamorphism in western Maine, northern Appalachians. *American Mineralogist*, **88**, 624-638.

Loomis, T. P., 1975. Reaction zoning of garnet. *Contributions to Mineralogy and Petrology*, **52**, 285-305.

Mahar, E. M., Baker, J. M., Powell, R., Holland, T. J. B., and Howell, N., 1997. The effect of Mn on mineral stability in metapelites. *Journal of Metamorphic Geology*, **15**, 223-238.

Martínez Martínez, J. M., Soto, J. I., and Balanya, J. C., 2004. Elongated domes in extended orogens: A mode of mountain uplift in the Betics (Southeast Spain). In: *Gneiss Domes in Orogeny* (ed. Whitney, D., Teyssier, C. & Siddoway, C. S.), 391, The Geological Society of America.

Moench, R. H., and Aleinikoff, J. N., 2002. Stratigraphy, geochronology, and accretionary terrane settings of two Bronson Hill arc sequences, northern New England. *Physics and Chemistry of the Earth*, **27**, 47-95.

Moench, R. H., and Zartman, R. E., 1976. Chronology and styles of multiple deformation, plutonism, and polymetamorphism in the Merrimack synclinorium of western Maine. *Geological Society of America Memoir*, **146**, 203-238.

Novak, J. M., and Holdaway, M. J., 1981. Metamorphic petrology, mineral equilibria, and polymetamorphism in the Augusta Quadrangle, south-central Maine. *American Mineralogist*, **66**, 51-69.

Pattison, D. R. M., and Tracy, R. J., 1991. Phase equilibria and thermobarometry of metapelites. In: *Contact Metamorphism* (D.M. Kerrick, editor). Reviews in Mineralogy, **26**, 105-206, Mineralogical Society of America, Washington, D.C.

Pattison, D. R. M., Spear, F. S., and Cheney, J. T., 1999. Polymetamorphic origin of muscovite + cordierite + staurolite + biotite assemblages: implications for the metapelitic petrogenetic grid and for P-T paths. *Journal of Metamorphic Geology*, **17**, 685-703.

Pattison, D. R. M., Spear, F. S., Debuhr, C. L., Cheney, J. T., and Guidotti, C. V., 1996. Thermodynamic modeling of the reaction muscovite + cordierite → Al_2SiO_5 + biotite + quartz + H_2O: constraints from natural assemblages and implications for the metapelitic petrogenetic grid, *Contributions to Mineralogy and Petrology,* **124**, 82-89.

Powell, R., and Holland, T. J. B., 2008. On thermobarometry. *Journal of Metamorphic Geology*, **26**, 155-179.

Powell, R., and Holland, T. J. B., 1988. An internally consistent dataset with uncertainties and correlations; 3, Applications to geobarometry, worked examples and a computer program. *Journal of Metamorphic Geology*, **6**, 173-204.

Pyle, J. M., Spear, F. S., Cheney, J. T., and Layne, G., 2005. Monazite ages in the Chesham Pond Nappe, SW New Hampshire, U.S.A.: implications for assembly of central New England thrust sheets. *American Mineralogist*, **90**, 592-606.

Robinson, P., Tucker, R. D., Bradley, D. C., Berry, H. N., and Osberg, P. H., 1998. Paleozoic orogens in New England, U.S.A. *Geologiska Föreningens I Stockholm Förhandlingar*, **120**, 119-148.

Rothstein, D. A., and Hoisch, T. D., 1994. Multiple intrusions and low-pressure metamorphism in the central Old Woman Mountains, south-eastern California: constraints from thermal modelling. *Journal of Metamorphic Geology,* **12**, 723-734.

Sayab, M., 2007. Correlating multiple deformation events across the Mesoproterozoic NE Australia using foliation intersection axes (FIA) preserved within porphyroblasts. *Gondwana Research*, **13**, 331-351.

Selverstone, J., Moreani, G., and Staude, J. M., 1991. Fluid channelling during ductile shearing: transformation of granodiorite into aluminous schist in the Tauern Window, Eastern Alps, *Journal of Metamorphic Geology,* **9**, 410-431.

Skelton, A., Annersten, H., and Valley, J. W., 2002. $\delta^{18}O$ and yttrium zoning in garnet: time markers for fluid flow? *Journal of Metamorphic Geology*, **20**, 457-466.

Smith, H. A., and Barreiro, B., 1990. Monazite U-Pb dating of staurolite grade metamorphism in pelitic schists. *Contributions to Mineralogy and Petrology*, **105**, 602-615.

Solar, G. S., and Brown, M., 1999. The classic high-T – low-P metamorphism of west-central Maine, USA: Is it post-tectonic or syn-tectonic? Evidence from porphyroblast-matrix relations. *Canadian Mineralogist*, **37**, 311-333.

Solar, G. S., and Brown, M., 2001a. Deformation partitioning during transpression in response to Early Devonian oblique convergence, northern Appalachian orogen, U.S.A. *Journal of Structural Geology*, **22**, 1043-1065.

Solar, G. S., and Brown, M., 2001b. Petrogenesis of migmatites in Maine, U.S.A: possible source of peraluminous granite in plutons. *Journal of Petrology*, **42**, 789-823.

Solar, G. S., Pressley, R. A., Brown, M., and Tucker, R. D., 1998. Granite ascent in convergent orogenic belts: testing a model. *Geology*, **26**, 711-714.

Spear, F. S., and Cheney, J. T., 1989. A petrogenetic grid for pelitic schists in the system SiO_2–Al_2O_3–FeO–MgO–K_2O–H_2O. *Contributions to Mineralogy and Petrology,* **101**, 149-164.

Spear, F. S., and Kohn, M. J., 1996. Trace element zoning in garnet as a monitor of dehydration melting in pelites. *Geology,* **24**, 1099-1102.

Spear, F. S., Hickmott, D. D., and Selverstone, J., 1990. Metamorphic consequences of thrust emplacement, Fall Mountain, New Hampshire. *Geological Society of America Bulletin,* **102**, 1344-1360.

Spiess, R., Peruzzo, L., Prior, D. J., and Wheeler, J., 2001. Development of garnet porphyroblasts by multiple nucleation, coalescence and boundary misorientation driven rotations. *Journal of Metamorphic Geology,* **19**, 269-290.

Tinkham, D. K., and Ghent, E. D., 2005. Estimating P-T conditions of garnet growth with isochemical phase-diagram sections and the problem of effective bulk-composition. *The Canadian Mineralogist*, **43**, 35-50.

Tinkham, D. K., Zuluaga, C. A., and Stowell, H. H., 2001. Metapelite phase equilibria modelling in MnNCKFMASH: The effect of variable Al_2O_3 and MgO/(MgO+FeO) on mineral stability. *Geological Materials Research*, **3**, 1-35.

Tinkham, D. K., Zuluaga, C. A., and Stowell, H. H., 2003. Metapelite phase equilibria modeling in MnNCKFMASH: The effect of variable Al_2O_3 and MgO/(MgO + FeO) on mineral stability. *American Mineralogist,* **88**, 1174.

Tomascak, P. B., Brown, M., Solar, G. S., Becker, H. J., Centorbi, T. L., and Tian, J., 2005. Source contributions to Devonian granite magmatism near the Laurentian border, New Hampshire and Western Maine, U.S.A. *Lithos*, **80**, 75-99.

Tracy, R. J, 1982. Compositional zoning and inclusions in metamorphic minerals. *Reviews in Mineralogy*, **10**, 355-397.

Tracy, R. J., Robinson, P., and Thompson, A. B., 1976. Garnet composition and zoning in the determination of temperature and pressure of metamorphism: Central Massachusetts. *American Mineralogist*, **61**, 762-775.

Tuccillo, M. E., Essene, E. J., Van der Pluijm, B. A., 1990. Growth and retrograde zoning in garnets from high grade metapelites: implications for pressure-temperature paths. *Geology*, **18**, 839-842.

Vance, D., and Mahar, E., 1998. Pressure-temperature paths from P-T pseudosections and zoned garnets: potential, limitations and examples from the Zanskar Himalayas, NW India. *Contributions to Mineralogy and Petrology*, **132**, 225-245.

Verhoef, P. N. W., Visssers, R. L. M., and Zwart, H. J. 1984. A new interpretation of the structural and metamorphic history of the western Aston Massif (Central Pyrenees, France). *Geologie en Mijnbouw*, **63**, 399-410.

White, R. W, Powell, R., and Holland, T. J. B., 2001. Calculation of partial melting equilibria in the system Na_2O-CaO-K_2O-FeO-MgO-Al_2O_3-SiO_2-H_2O (NCKF-MASH). *Journal of Metamorphic Geology,* **19**, 139-153.

Whitney, D. L., Goergen, E. T., Ketcham, R. A., and Kunze, K., 2008. Formation of garnet polycrystals during metamorphic crystallization. *Journal of Metamorphic Geology*, **26**, 365-383.

Wilbur, D. E., and Ague, J. J., 2006. Chemical disequilibrium during garnet growth: Monte Carlo simulations of natural crystal morphologies. *Geology*, **34**, 689-692.

Yardley, B. W. D., 1977. An empirical study of diffusion in garnet. *American Mineralogist,* **62**, 793-800.

Zuluaga, C. A., Stowell, H. H., and Tinkham, D. K., 2005. The effect of zoned garnet on metapelite pseudosection topology and calculated metamorphic P-T paths. *American Mineralogist*, **90**, 1619-1628.

CONCLUSIONS

This study has demonstrated that by using the multidisciplinary approach of microstructural measurements, geochronology, thermobarometry and phase diagram modeling, complex tectono-metamorphic histories can be accurately revealed and described. The unique time-capsule character of porphyroblasts makes it possible to reconstruct the deformation and metamorphic history of multiply deformed metamorphic terranes in unparalleled detail. The principal conclusions of each section are summarized below:

Section A

The porphyroblast microstructures from the contact aureole of the Mooselookmeguntic pluton contain many generations of inclusion trails that reflects a succession of episodic but continuous tectono-metamorphic events. Complex microstructures such as those preserved in staurolite porphyroblasts and their timing of growth is very difficult to correlate from one sample to another and to a regional scale. Where simple inclusion trails are present, very few generations of porphyroblast growth can be resolved using the porphyroblast-matrix relationships. However, FIA measurements in both garnet and staurolite porphyroblasts reveal that at least five periods of growth of these phases occurred and that deformation and metamorphism were totally synchronous. Furthermore, FIAs allow the different generations of porphyroblast growth to be correlated across a region from one sample to another. Foliations derived from pitch measurements of inclusion trails in staurolite porphyroblasts correlate well with these

FIA sets. The dip of foliations preserved in staurolite porphyroblasts is overwhelmingly steep suggesting a compressional setting dominated the entire 425 to 345 Ma evolution of the Northern Appalachian orogen.

Section B

Monazite dating of FIAs revealed a lengthy period of tectonism that lasted from the onset of the Acadian deformation until late in the tectonic history of the Northern Appalachians. Four out of five FIA sets could be dated. These are FIA 2, 3, 4 and 5. The absolute timing of FIA 2 development was established between 415-395 Ma, for FIA 3 between 395-380 Ma, for FIA 4 between 380-360 Ma and for FIA 5 from 360 to less than 345 Ma. The age of FIA set 1 was established to be around 420 Ma based on previous geochronology in the region and on pluton crystallization ages. The time frame of FIA development correlates well with plutonic activity indicating a feed-back relationship between deformation, metamorphism and pluton emplacement. The intimate association of metamorphic grade with the pluton contours suggests that the high heat flow, plutonism and metamorphism are intimately associated. The succession of at least five lengthy periods of high grade metamorphism in the contact aureole of the Mooselookmeguntic pluton indicate that the pluton was built up in steps during many deformation events. This general association of high grade metamorphism and plutonism in Maine suggest that something other than high regional geothermal gradients was responsible for melting in the lower crust. If mylonitization at depths was associated with fluids, due to dehydration reactions and shear heating, and melting at the base of crust was responsible for magma generation then melt ascending along dilatation sites would be emplaced in the upper crust at a rate controlled by the partitioning of deformation and

the intensity of the regional stress field. Every new deformation event may have triggered melting in the lower crust. Heat may have been transferred by advection in discreet magmatic episodes that resulted in high temperature-low pressure metamorphism in the upper crust during contractional deformation.

Section C

The lengthy time of tectono-metamorphism experienced by Paleozoic Western Maine and by the Proterozoic Colorado Front Range resulted in multiple periods of staurolite growth during subsequent deformation events. Five FIA sets were measured from staurolite porphyroblasts in Western Maine and three from the Colorado Front Range. Monazite inclusions in staurolite have an absolute age of 1760±12 Ma (FIA 1), 1720.4±6.8 Ma (FIA 2), 1682±18 Ma (FIA 3) in Colorado and 408±10 Ma (FIA 2), 388±8.8 Ma (FIA 3), 372.1±5.5 Ma (FIA 4), 352.7±4.2 Ma (FIA 5) in Maine confirming the multiple periods of deformation and metamorphism indicated by the FIA succession in each region.

The metastable preservation of early staurolite porphyroblasts through successive deformation and metamorphic events highlights the importance of deformation on porphyroblast nucleation and growth. These two areas show that the reactions involved in the formation of metamorphic minerals are episodic during prograde metamorphism, starting or stopping, as a function of deformation partitioning and strain localization. Accessory minerals such as monazite can be dated and their ages can be better integrated in the deformation and metamorphic history of a region when they are well constrained by microstructural measurements.

Section D

Metamorphism in the contact aureole of the Mooselookmeguntic pluton is typical of low-pressure high-temperature terranes. The mineral associations are mainly characterized by Grt+St assemblages with sillimanite occurring at higher grades. Andalusite is present in all staurolite bearing rocks and usually has partly replaced the staurolite. Cordierite appears as an additional phase in rocks of appropriate composition. Following the growth of cordierite, retrogression into chlorite field occurred. Normally the mineral chemistry changes gradually with increasing metamorphic grade suggesting an approach towards equilibrium. Garnet porphyroblasts from staurolite bearing assemblages have a normal high Mn core growth zoning pattern while in the sillimanite zone most of the garnet appears to have been homogenized. Calcium zoning in garnet indicates that metamorphic fluids have affected the garnet rim composition even though no evidence for this was found in the matrix.

Phase diagram modeling in the NCMnKFMASH system of the mineral assemblages from the contact aureole of the Mooselookmeguntic pluton, using the computer software Thermocalc, is in good agreement with petrological observations and provides realistic results. The stability field of the cordierite bearing assemblages was not accurately predictable and further work is required to resolve this facet of the metamorphism. Changes in bulk composition reflect in the pseudosection topology mainly on garnet stability with minor influence on the staurolite stability field. The garnet-in line shifts to lower temperature with increasing bulk MnO. Higher bulk Al_2O_3 increases the staurolite stability to lower temperature and decreases biotite stability.

Conventional thermobarometry gives close results, but with higher uncertainties, to the average PT mode of Thermocalc for prograde assemblages. However, it appears to be much more sensitive to compositional changes due to retrogression. The peak conditions were determined to be around 4 kbars and 600°C. Pseudosections used with detailed petrological observations provide much better constraints on PT conditions during metamorphism.

Core isopleth thermobarometry revealed that all garnet forming reactions were temperature overstepped and took place near the staurolite-in reaction. The PT conditions in the contact aureole must have been close to the St+And stability field for more than 60 Ma as suggested by the FIAs, monazite ages, mineral assemblages and thermobarometry. The overall PT path in the contact aureole of the Mooselookmeguntic pluton was clockwise with decompression occurring in the last stages of tectonism.

Recommendations for further investigations

FIAs have been used to distinguish a succession of five periods of staurolite and garnet growth in the contact aureole of the Mooselookmeguntic pluton. The consistent succession of FIAs from sample to sample is considered to reflect periods of time over which the relative plate motion was constantly directed before shifting to another trend. FIA measurements could also be attempted using andalusite and cordierite porphyroblasts. Monazite dating of FIAs obtained from cordierite and andalusite porphyroblasts would allow one to accurately asses the absolute timing of growth of these phases. This would allow the complete characterization of the tectonic evolution in the contact aureole of the Mooselookmeguntic pluton and in Western Maine. FIA measurements in porphyroblasts

from the contact aureole of other plutons from Maine would permit regional correlations to be made and the nature of regional tectonism to be better understood. Crystallization ages for the Mooselookmeguntic pluton are available only for the southern lobe of the pluton. Further geochronology for the middle and the northern part of the pluton may reveal a much longer history of pluton build-up.

- SECTION A -

PARTITIONING OF DEFORMATION IN THE CONTACT AUREOLE OF THE MOOSELOOKMEGUNTIC PLUTON (WESTERN MAINE, USA) AND ITS EFFECT ON PORPHYROBLAST GROWTH AND INCLUSION TRAIL/MATRIX RELATIONSHIPS

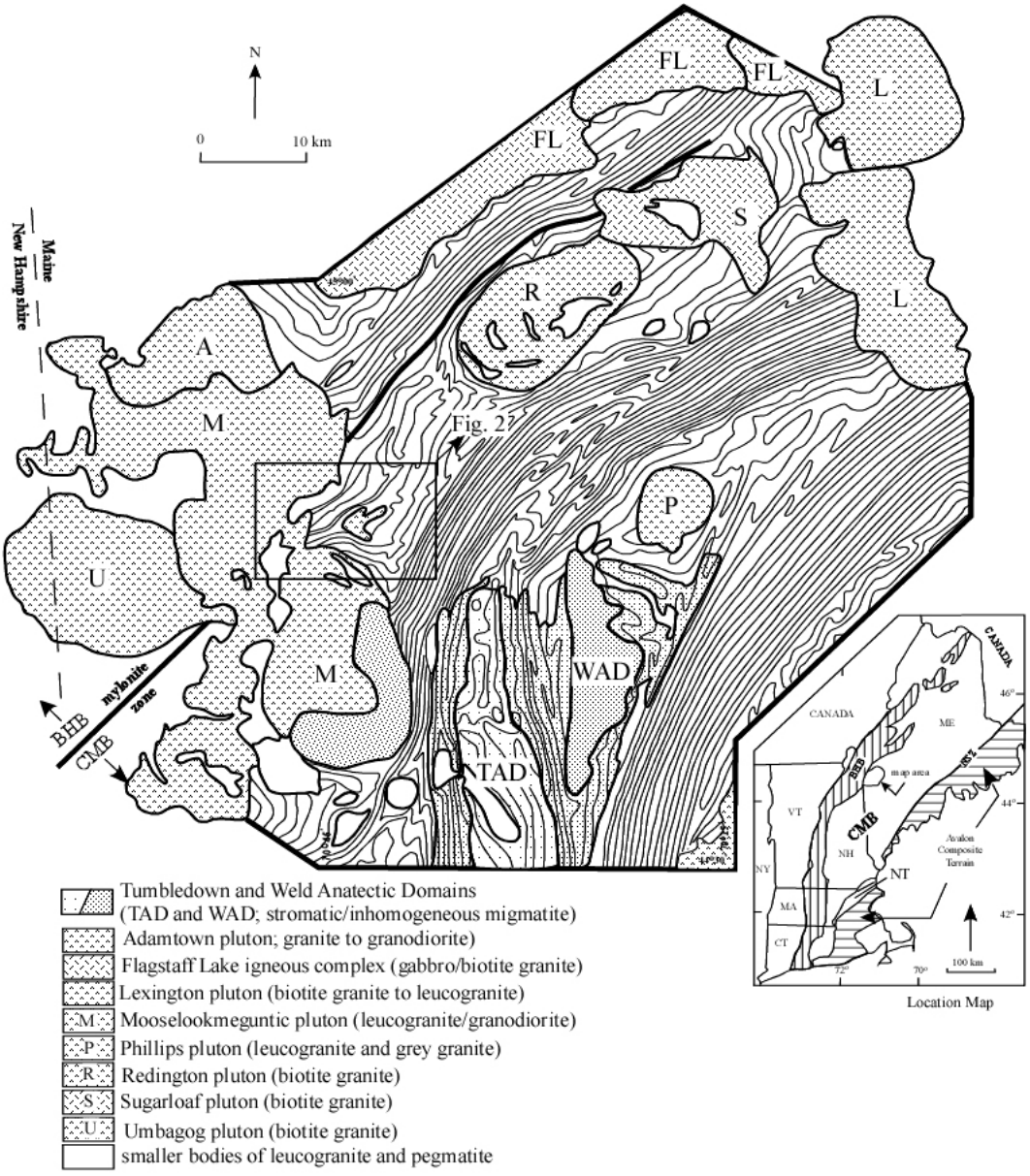

Figure 1. Location map of the area in west central Maine showing the major structural features. Solid lines represent strike of foliation form lines. Foliation dips generally SE. Closely-spaced lines — steeply dipping; widely-spaced lines — moderately dipping. BHB - Bronson Hill Belt. CMB - Central Maine Belt. CT - Connecticut. MA - Massachusetts. ME - Maine. NH - New Hampshire. NY - New York. VT - Vermont. NSZ - Norumbega Shear Zone System. NT - Nashoba Terrane. (after Brown and Solar, 1998)

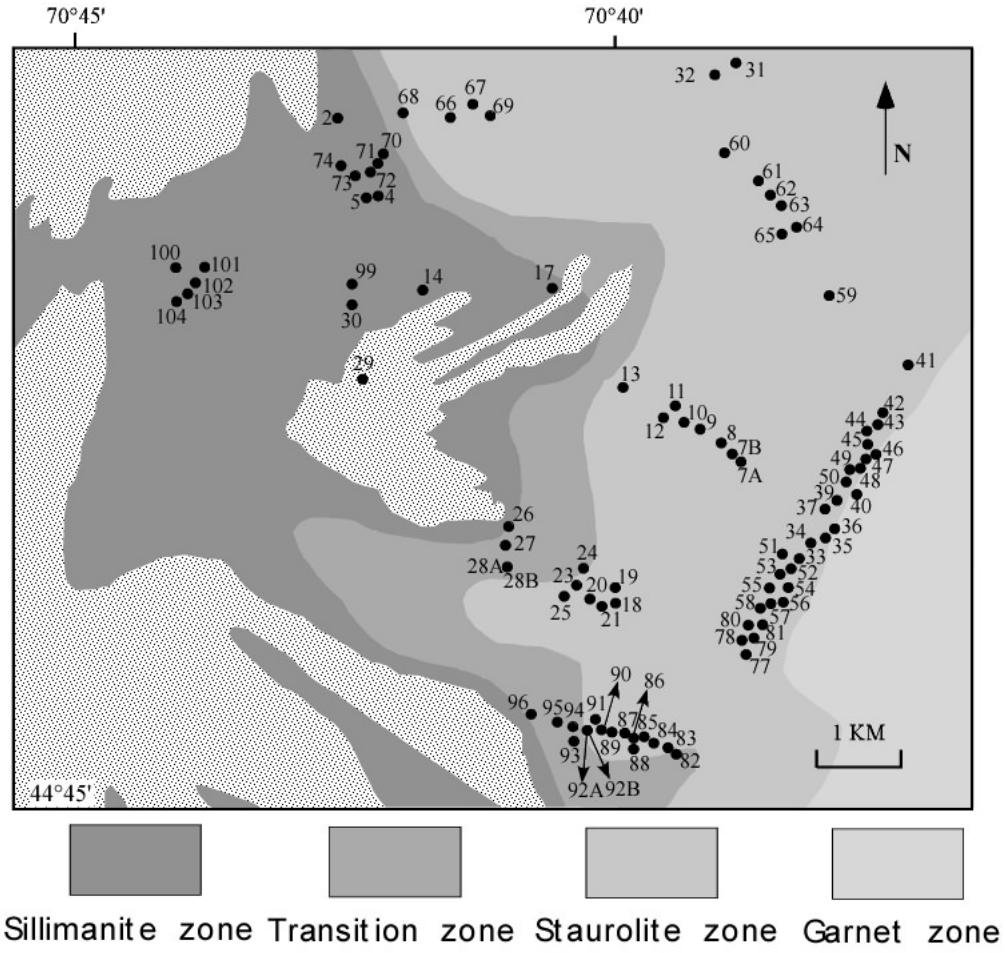

Figure 2. Simplified geological map of the study area showing the sample location. Isograds after Guidotti and Johnson (2002).

Sample no.	Grt	St	And	Sill	Crd	Retro-grade pseudo-morphs	Pro-grade pseudo-morphs	Observations
IS2	x	x	x				x	Grt→St→And
IS4	x	x	x	x			x	Grt→St→And
IS5	x	x	x				x	Grt→St→And
IS7a	x	x			x	x		Grt→St→Crd
IS7b	x	x			x	x		Grt→St→Crd
IS8	x	x						Grt→St
IS9	x	x						Grt→St
IS10	x	x						Grt→St
IS11	x	x						Grt→St
IS12	x	x	x					Grt→St→And
IS13	x							
IS14	x	x	x	x				Grt→St→And,Sill
IS17	x	x	x	x			x	Grt→St→And,Sill
IS18	x	x						Grt→St
IS19	x	x						Grt→St
IS20	x	x						Grt→St
IS21	x	x						Grt→St
IS23	x	x						Grt→St
IS24	x	x	x					Grt→St→And
IS25	x	x						Grt→St
IS26	x						x	
IS27	x	x		x			x	Grt→St,Sill
IS28a	x			x			x	
IS28b	x	x		x			x	Grt→St
IS29	x			x				
IS30	x	x		x				Grt→St
IS31	x	x				x		Grt→St
IS32	x	x				x		Grt→St
IS33	x	x				x		Grt→St
IS34	x	x				x		Grt→St
IS35	x	x				x		Grt→St
IS36	x	x				x		Grt→St
IS37	x	x				x		Grt→St
IS39	x	x				x		Grt→St
IS40	x	x				x		Grt→St
IS41	x	x				x		Grt→St
IS42	x	x				x		Grt→St
IS43	x	x				x		Grt→St
IS44	x	x				x		Grt→St
IS45	x	x				x		Grt→St
IS46	x	x				x		Grt→St
IS47	x	x				x		Grt→St
IS48	x	x				x		Grt→St
IS49	x	x				x		Grt→St
IS50	x	x				x		Grt→St
IS51	x	x				x		Grt→St
IS52	x	x				x		Grt→St
IS53	x	x				x		Grt→St
IS54	x	x				x		Grt→St
IS55	x	x				x		Grt→St
IS56	x	x				x		Grt→St
IS57	x	x				x		Grt→St
IS58	x	x				x		Grt→St
IS59	x	x				x		Grt→St
IS60	x					x		
IS61	x					x		

Sample no.	Grt	St	And	Sill	Crd	Retro-grade pseudo-morphs	Pro-grade pseudo-morphs	Observations
IS62	x	x				x		Grt→St
IS63	x					x		
IS64	x	x				x		Grt→St
IS65	x	x				x		Grt→St
IS66	x	x	x				x	Grt→St→And
IS67	x	x	x				x	Grt→St→And
IS68	x	x	x				x	Grt→St→And
IS69	x						x	
IS70	x	x					x	Grt→St
IS71	x	x	x				x	Grt→St→And
IS72	x	x						Grt→St
IS73	x	x	x	x			x	Grt→St→And,Sill
IS74	x	x	x	x			x	Grt→St→And,Sill
IS77	x	x				x		Grt→St
IS78	x	x				x		Grt→St
IS79	x	x				x		Grt→St
IS80	x	x				x		Grt→St
IS81	x	x				x		Grt→St
IS82	x	x						Grt→St
IS83	x	x	x		x			Grt→St→And→Crd
IS84		x	x		x			St→And,Crd
IS85	x	x	x					Grt→St→And
IS86		x			x			St→Crd
IS87		x						
IS88		x						
IS89	x	x						Grt→St
IS90	x	x			x			Grt→St→Crd
IS91		x	x		x			St→And→Crd
IS92a	x	x						Grt→St
IS92b		x			x			St→Crd
IS93	x	x			x			Grt→St→Crd
IS94	x	x		x				Grt→St
IS95	x	x		x				Grt→St
IS96	x							
IS99	x							
IS100	x	x	x	x			x	Grt→St→And,Sill
IS101	x	x		x			x	Grt→St→Sill
IS102	x	x	x	x			x	Grt→St→And,Sill
IS103	x	x	x	x			x	Grt→St→And,Sill
IS104	x	x	x	x			x	Grt→St→And,Sill

Table 1. Mineral assemblages contained in every sample and their relative succession in the paragenesis. Arrows indicate the crystallization order.

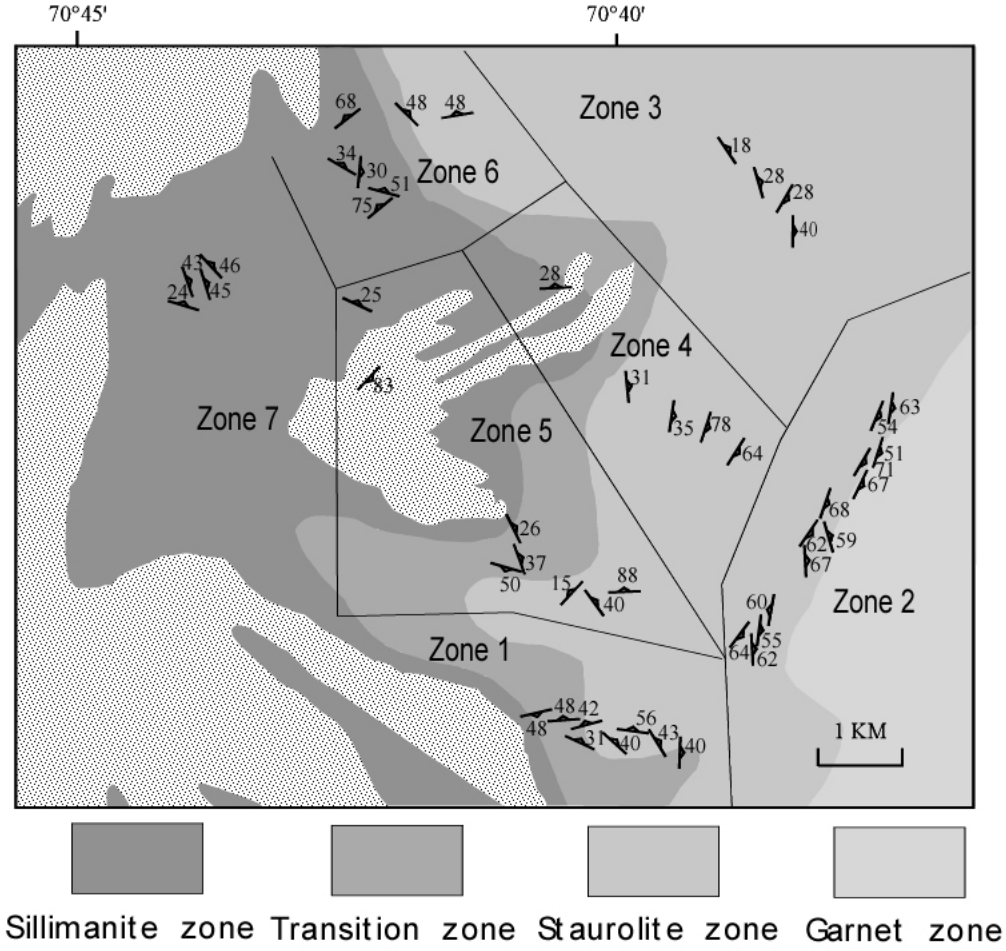

Figure 3. Geological map of the area showing the strike and dip of foliations. Isograds after Guidotti and Johnson (2002).

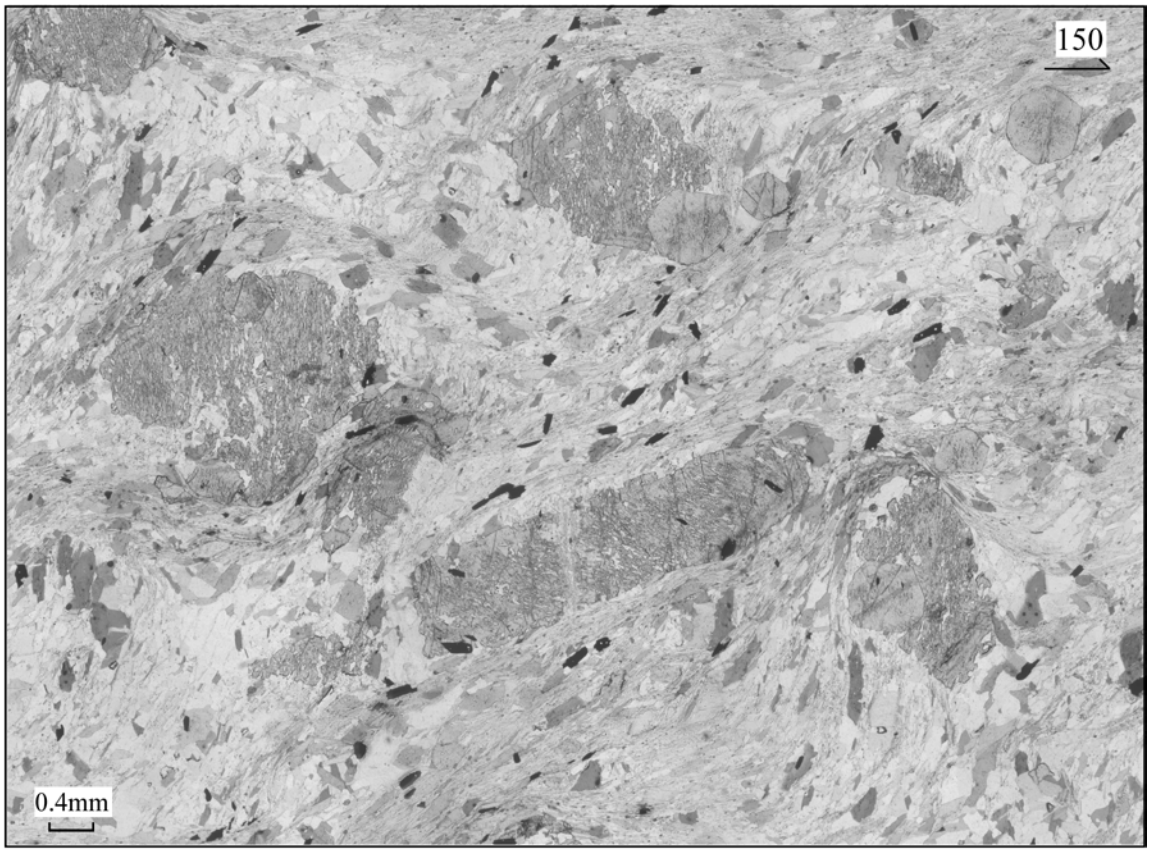
150
0.4mm

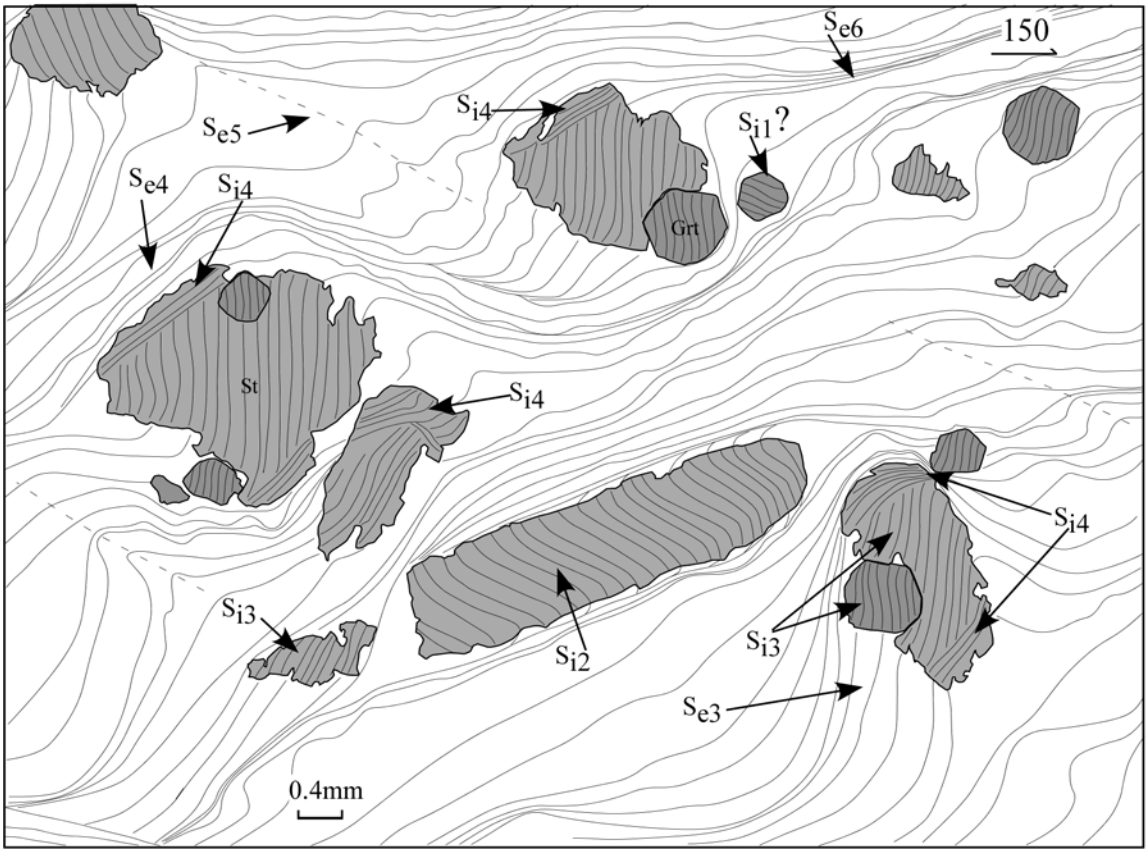
Se6
150
Se5
Si4
Si1?
Se4
Si4
Grt
St
Si4
Si4
Si3
Si2
Si3
Se3
0.4mm

Figure 4. Photomicrograph showing the relationship between the inclusion trails preserved in garnet and staurolite porphyroblasts and the matrix foliation. Most garnet and staurolite porphyroblasts overgrew a sub-vertical foliation (S_{i3}) that is preserved only as inclusion trails. This type of porphyroblast is present all over Zone 1. Many of the staurolite porphyroblasts show growth rims (S_{i4}). These growth rims occur only on S_{i3} staurolites. Staurolite porphyroblasts that overgrew a foliation similar to S_{i4} rims are common in the matrix. A few samples contain garnet and staurolite porphyroblasts that overgrew a sub-horizontal foliation (S_{i1} respectively S_{i2}).

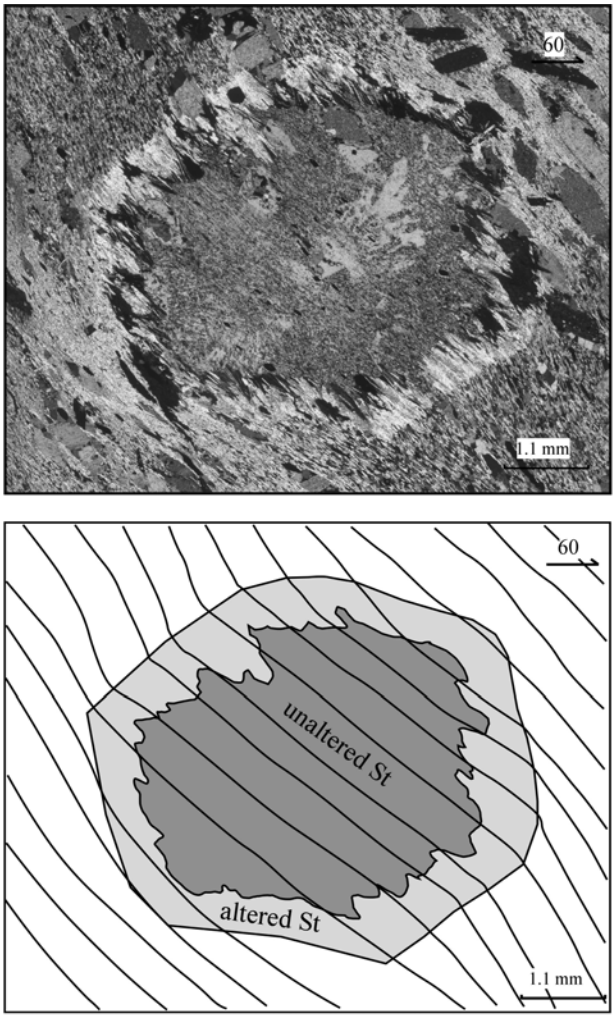

Figure 5. Incipiently-pseudomorphosed staurolite porphyroblast (plus line diagram). Mica and chlorite grains that have replaced the staurolite rim have (001) aligned with the matrix foliation. The matrix foliation is deflected against porphyroblast margins, and the trails that radiate from the staurolite curve into the matrix.

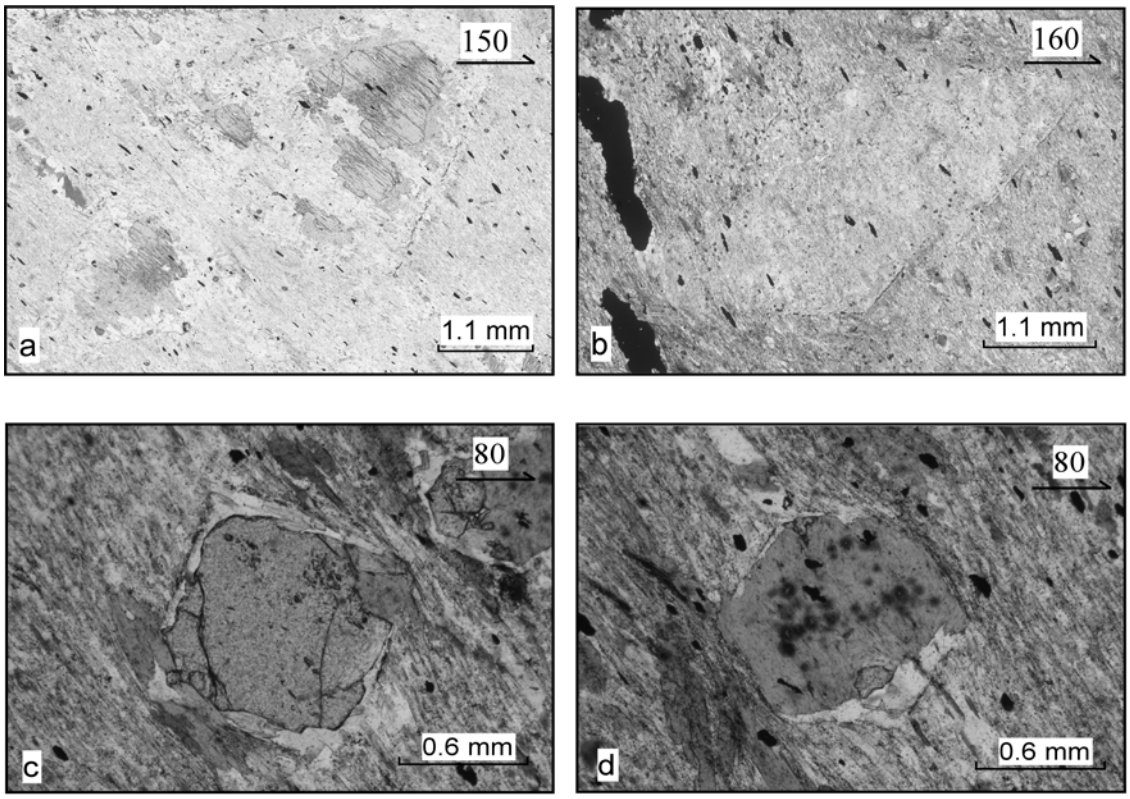

Figure 5. Partially- and completely- pseudomorphosed porphyroblasts. Partial (a and c) and complete (b and d) pseudomorphs of staurolite and garnet. Garnet is commonly replaced by chlorite, staurolite by white micas. Notice that all the grains in staurolite pseudomorphs are aligned with the matrix foliation.

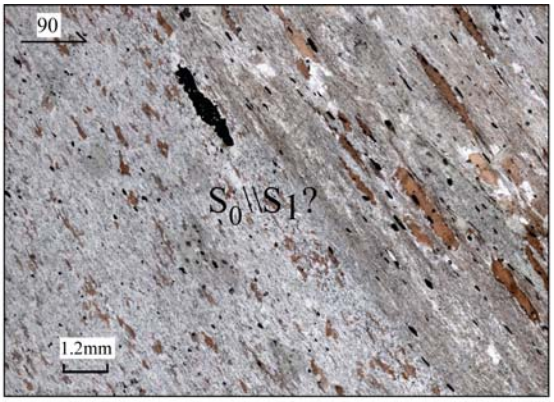

Figure 7. Photomicrograph showing schistosity parallel to layering from Zone 2.

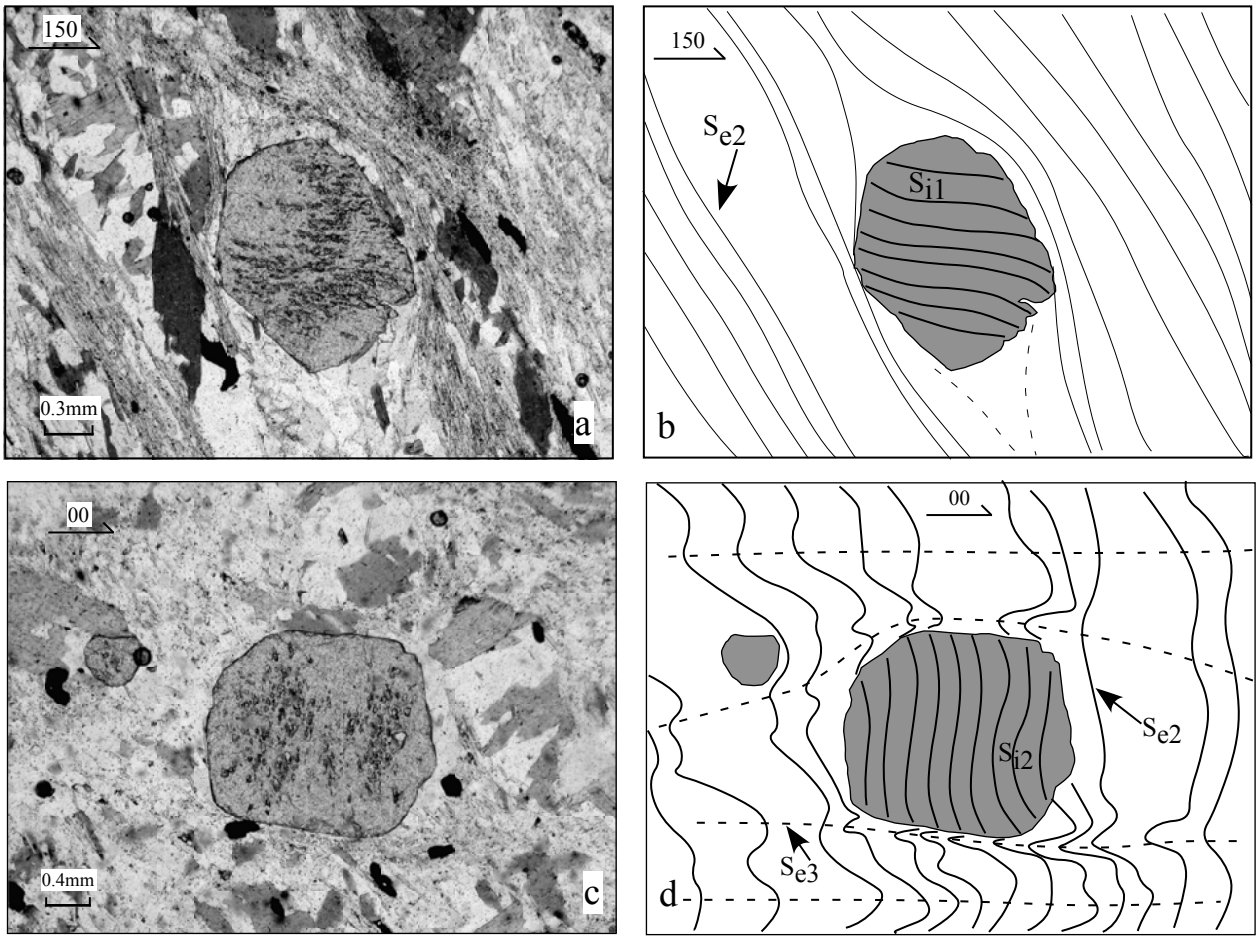

Figure 8. Photomicrographs and line diagrams showing the relationship between garnet porphyroblasts inclusion trails and the matrix foliation in Zone 2. All garnet porphyroblasts that overgrew a sub-horizontal fabric (S_{i1}) are truncated by the matrix foliation. Garnet porphyroblasts that overgrew a sub-vertical fabric (S_{i2}) may appear continuous and/or truncated by the matrix foliation.

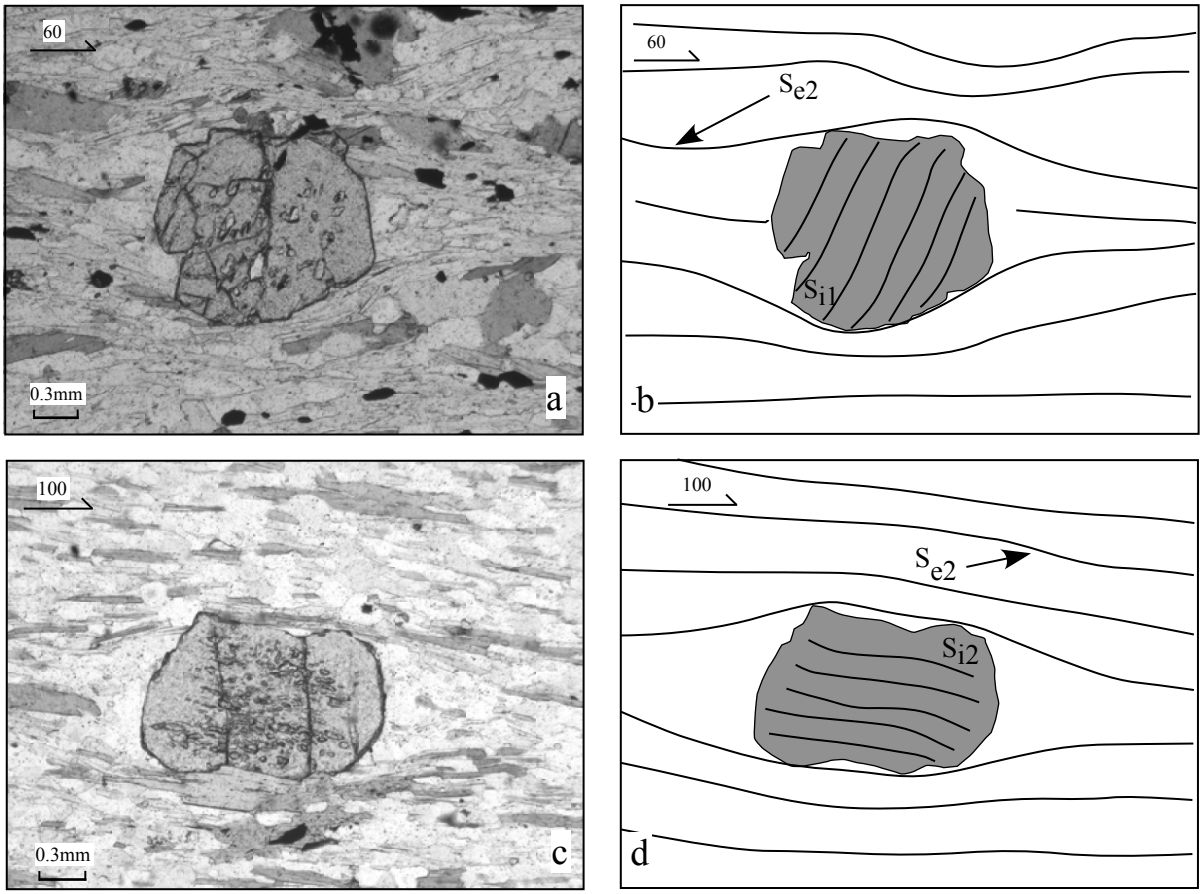

Figure 9. Photomicrographs and line diagrams showing the relationship between garnet porphyroblasts and the matrix in Zone 3. All porphyroblasts that overgrew a sub-vertical fabric (S_{i1}) appear truncated by the matrix foliation S_{e2}. Garnet porphyroblasts contain a sub-horizontal fabric (S_{i2}) that is sub-parallel to the external matrix foliation S_{e2}. Note in Fig. 9c that the inclusion trails in garnet appear continuous with the matrix but only in the strain shadow.

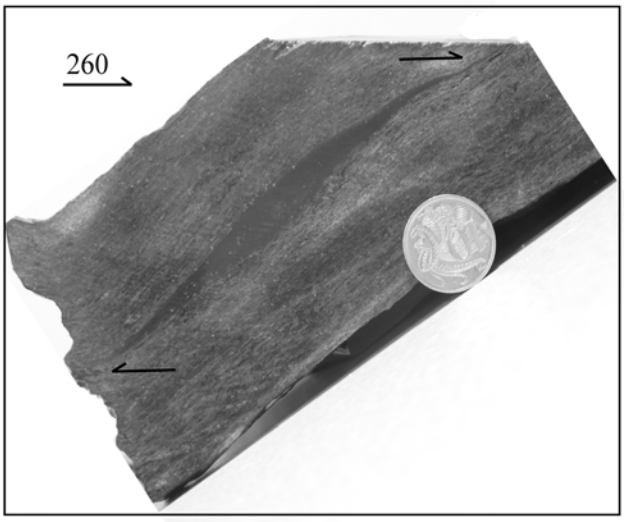

Figure 10. Graphite rich quartz lenses in a sample from Zone 4. These lenses lie in the foliation plane and preserve a top- to- the-west shear sense that is identical to the differentiation asymmetry into crenulation cleavages (Bell et al., 2003). They are common in Zone 4 but none was found in other zones.

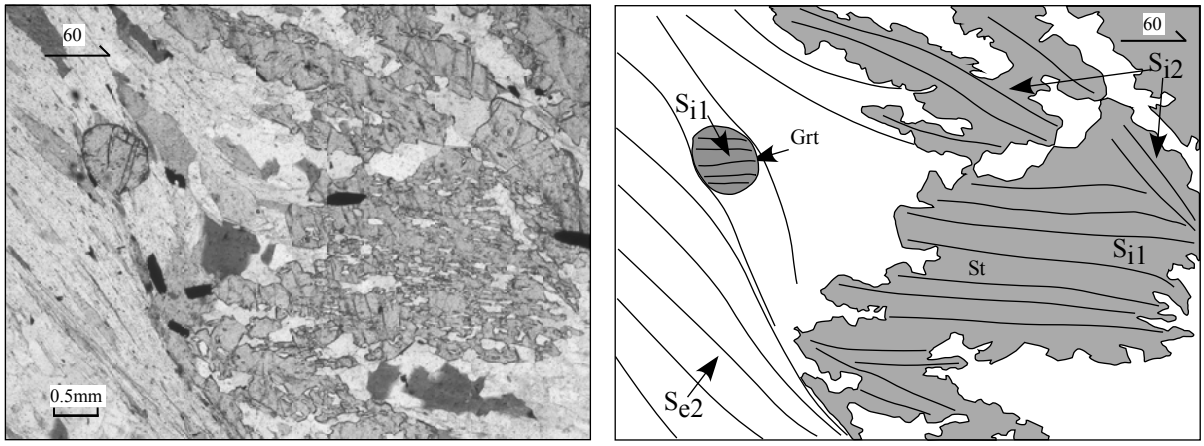

Figure 11. Photomicrograph and line diagram showing a staurolite porphyroblast from Zone 4 that preserves a core to rim relationship. The core of the staurolite overgrew a similar sub-horizontal foliation (S_{i1}) with that preserved in the garnet porphyroblast. A second generation of staurolite growth occurred over a sub-vertical foliation (S_{i2}) that dominates the matrix. Most staurolite porphyroblasts from this zone preserve this foliation.

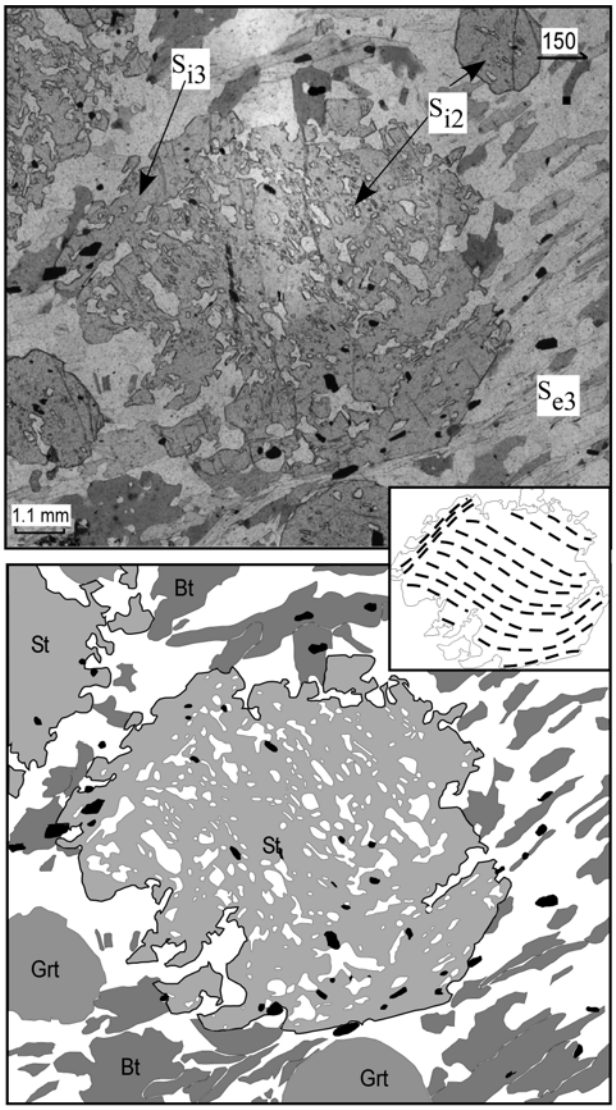

Figure 12. Photomicrograph and line diagram of garnet and staurolite porphyroblasts from Zone 4. Staurolite cores and garnet porphyroblasts overgrew a sub-vertical foliation (S_{i2}) in the crenulations hinges of a differentiated crenulation cleavage (S_{e3}). Locally, staurolite rim growth occurred over the differentiated cleavage. This differentiated cleavage (S_{e3}) is not present in all samples from Zone 4 but the crenulated cleavage S_{e2} is. The rim inclusion trails are almost orthogonal to the core foliation and seem to be continuous with the matrix.

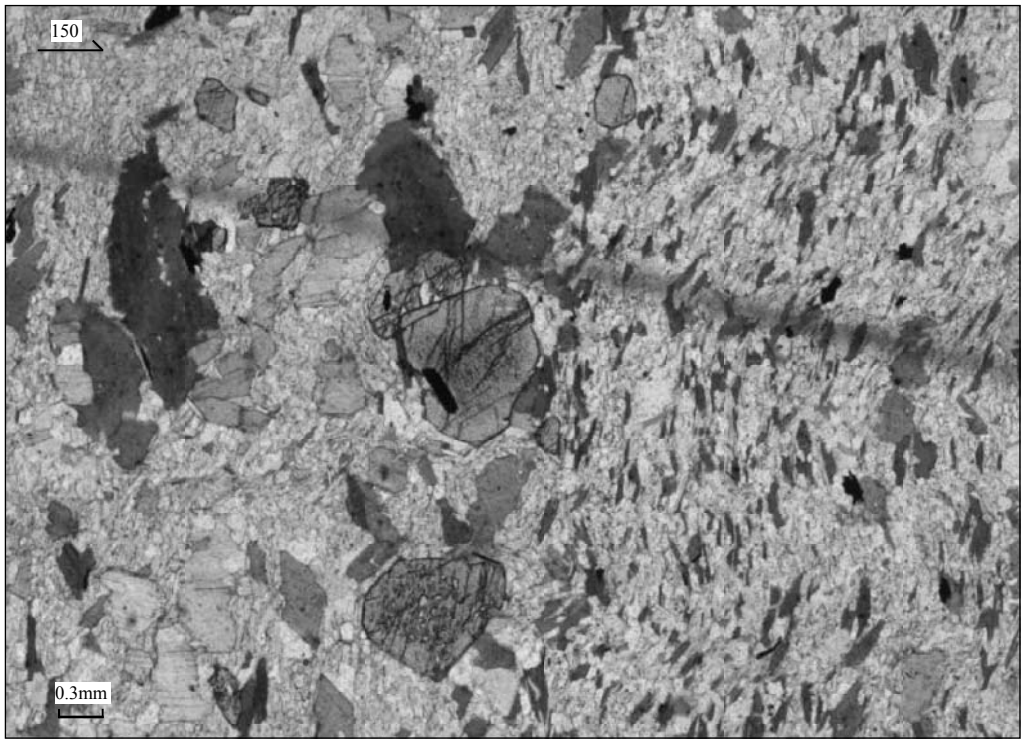
150
0.3mm

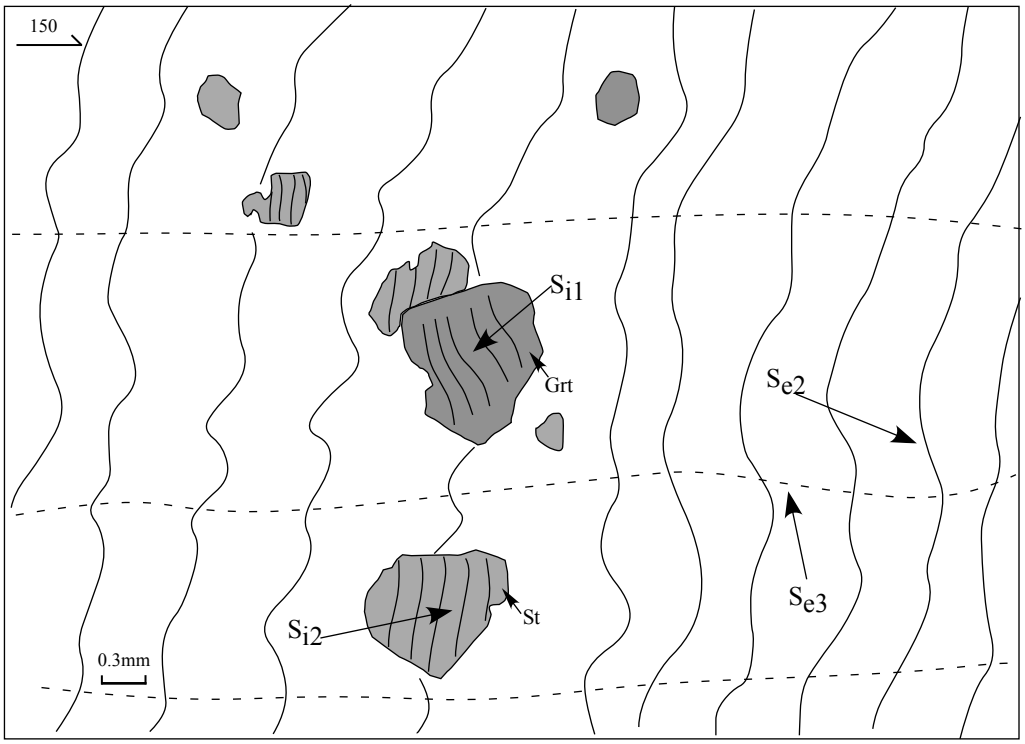
150
Si1
Grt
Se2
Se3
Si2
St
0.3mm

Figure 13. Photomicrograph and line diagram of a thin section from Zone 5. Garnet and staurolite porphyroblasts overgrew a sub-vertical cleavage that appears to be continuous with the matrix. The opposite asymmetry preserved by inclusion trails in garnet (clockwise) and in staurolite (anti-clockwise) indicate that these phases grew at different times, during different deformation events. Note the schistosity-parallel layering that is crenulated by a sub-horizontal axial-planar crenulation cleavage.

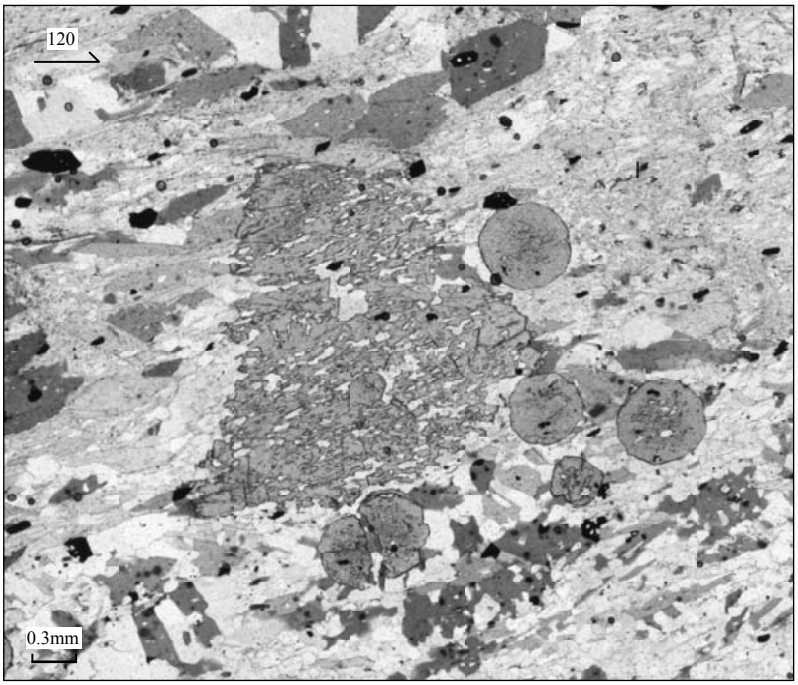
120
0.3mm

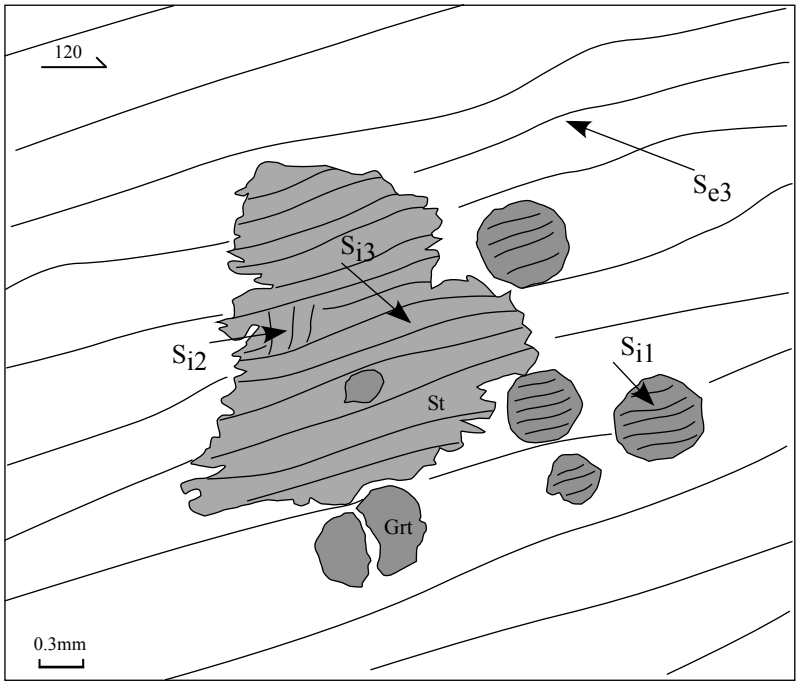
120
S_{e3}
S_{i3}
S_{i2}
S_{i1}
St
Grt
0.3mm

Figure 14. Photomicrograph and line diagram showing garnet and staurolite porphyroblasts that overgrew a shallow-dipping foliation. Both garnet and staurolite porphyroblasts preserve similar inclusion trails but with different asymmetries, suggesting growth at different times. Some quartz inclusions in staurolite porphyroblasts show a sub-vertical orientation (S_{i2}) that is possibly a remnant of a previous crenulation cleavage.

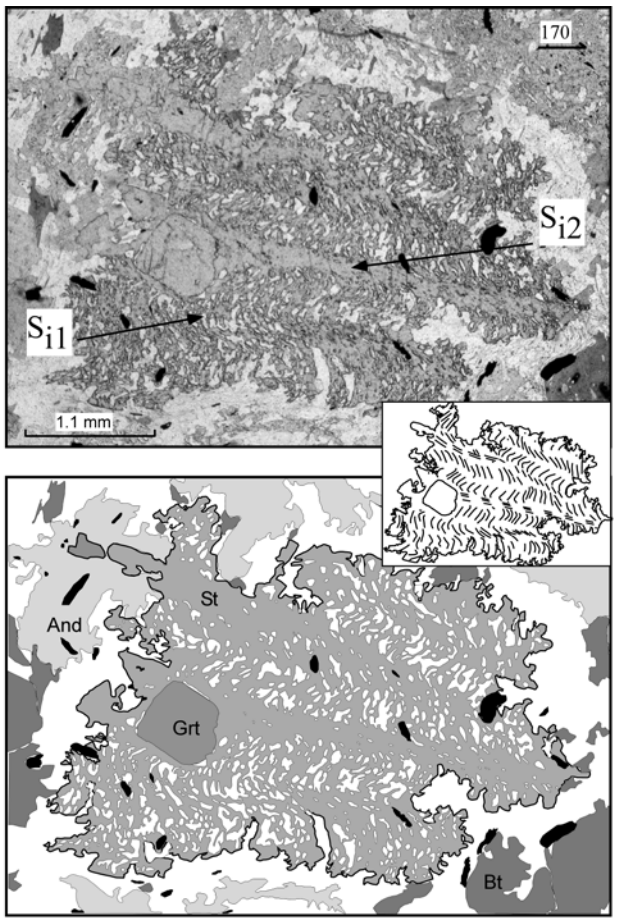

Figure 15. Staurolite porphyroblast and line diagram from Zone 6 that preserves a differentiated crenulation cleavage (stage 4) as inclusion trails. Poikilitic andalusite has partially replaced the staurolite porphyroblasts. The original sub-vertical fabric is crenulated by a sub-horizontal crenulation cleavage.

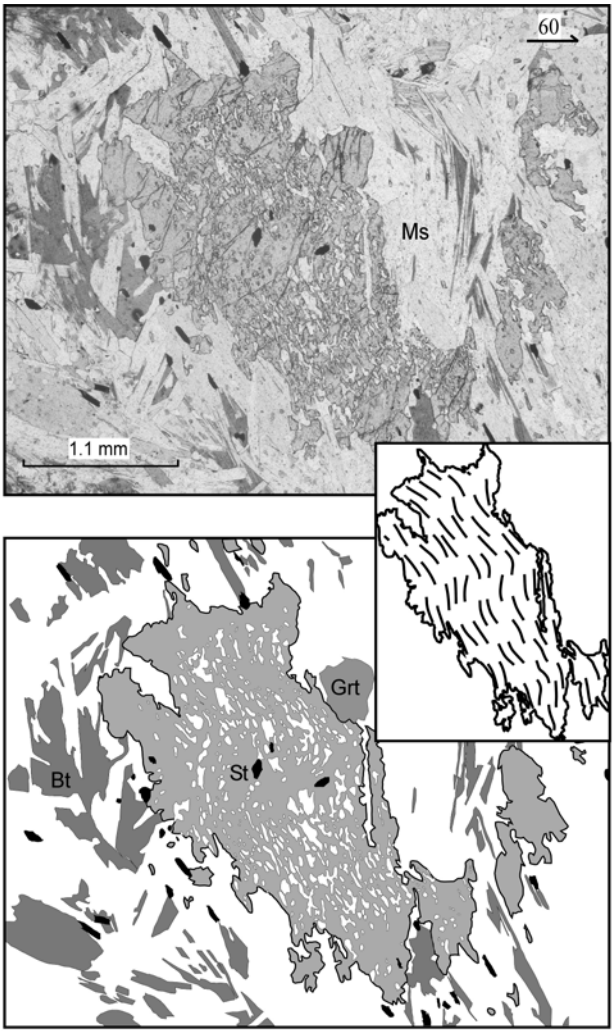

Figure 16. Incipient crenulation cleavage (stage 2) in a staurolite porphyroblast from Zone 7. The staurolite has been prograde-pseudomorphosed by large Ms+Bt.

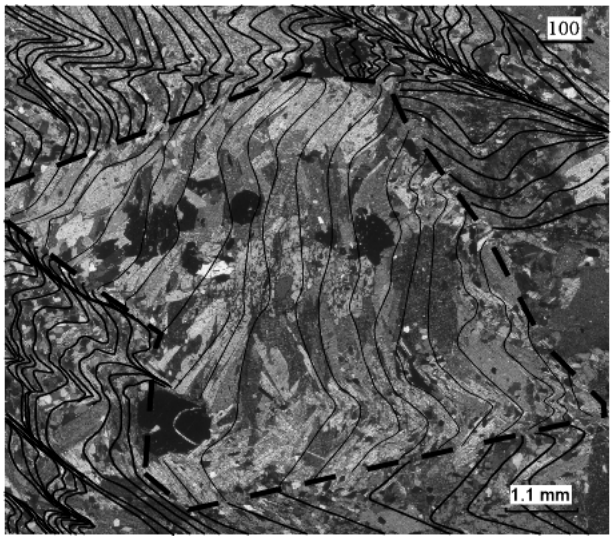

Figure 17. Deformed staurolite pseudomorph from Zone 7. Coarse Ms+Bt has locally replaced the staurolite. The mica blades have a sub-vertical orientation that was later slightly crenulated by a sub-horizontal event. The foliation in the matrix shows a differentiated crenulation cleavage.

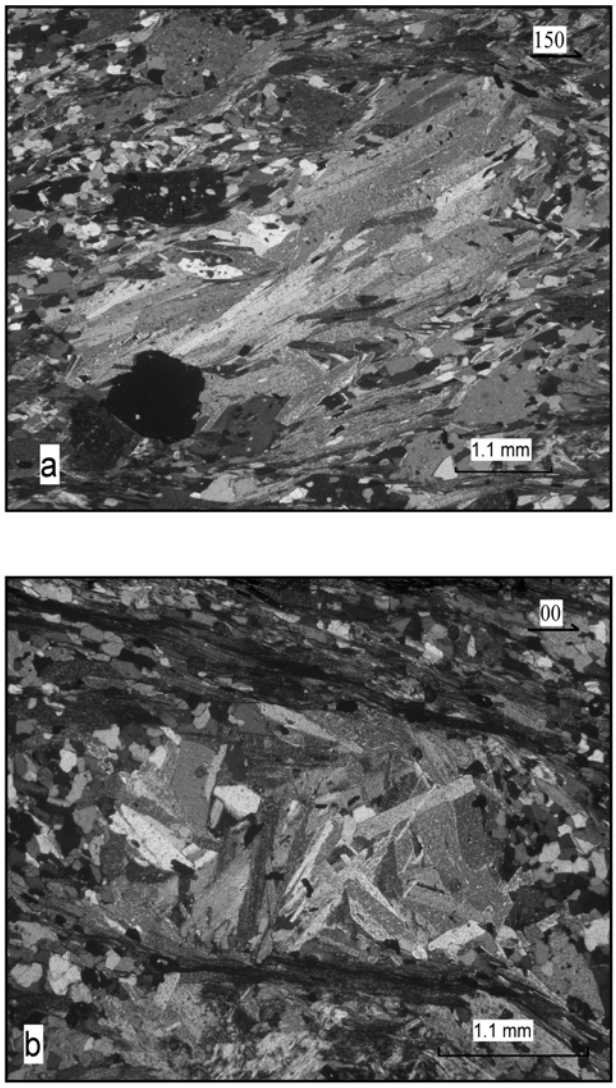

Figure 18. Deformed (a) and undeformed (b) staurolite pseudomorphs from zone 7. The preferential alignment of Ms blades in deformed pseudomorphs contrasts with the randomly-oriented Ms blades in undeformed ones.

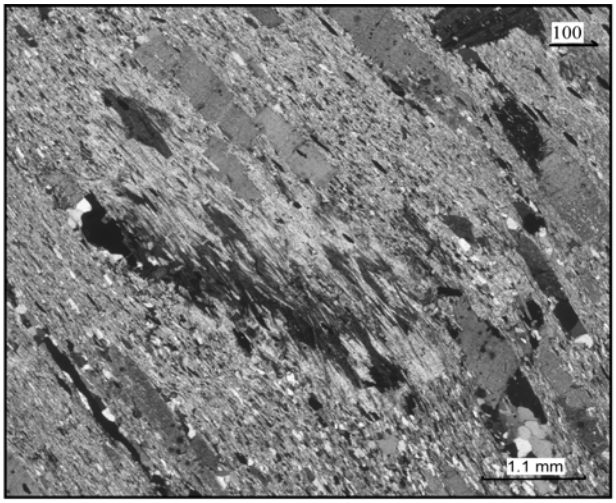

Figure 19. Deformed retrograde pseudomorph from Zone 2. All Ms+Bt+Chl grains are aligned parallel to the matrix. In deformed retrograde pseudomorphs the grain size is larger than in undeformed ones.

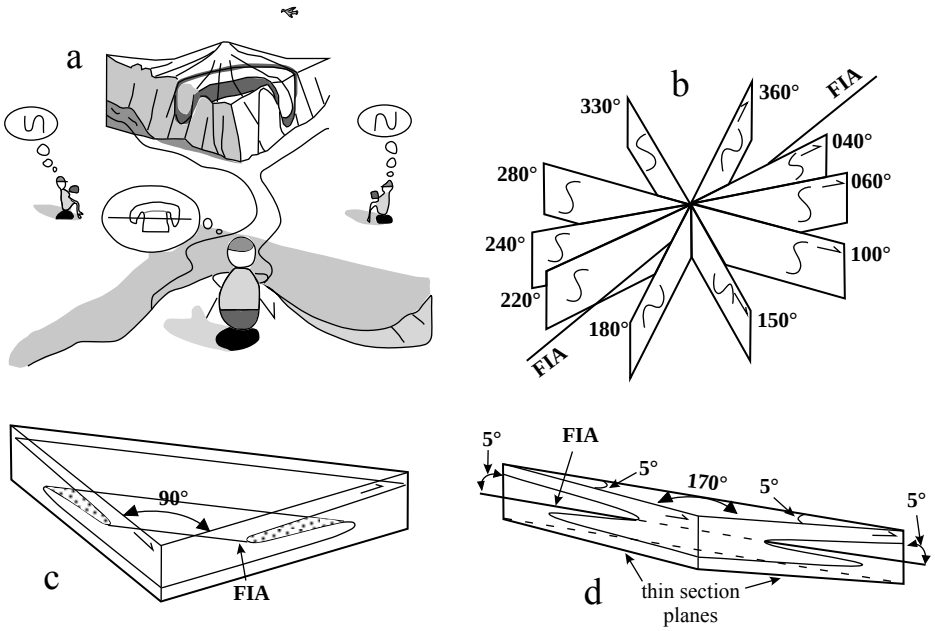

Figure 20. Sketch illustrating the principle behind FIA measurement (after Bell et al., 2004). a) The geologists to either side see the opposite asymmetry for same fold in a cliff face. They have no idea of its trend in 3-D. The geologist in the centre sees the fold on both cliff faces and knows it must trend from one to the other. b) Shows the asymmetry on a series of differently-striking vertical sections. The asymmetry flips across the compass when viewed in the same direction. (c) Shows asymmetry of a sigmoid axis in two sections cut 90° apart. (d) Shows the sigmoid axis of (c) in two sections cut 10° apart lying on either side of the axis. The switch in asymmetry between them defines the location of the axis within a 10° range.

Sample	FIA 1		FIA 2		FIA 3		FIA 4		FIA 5	
no.	St	Grt	St	Grt	St	Grt	St	Grt	St	Grt
IS2		125					75			
IS4	125	125	165r							
IS5	125c	120			95r					
IS7a	125	115								
IS7b									15	40
IS8									45	45
IS9b		120					65			
IS10		115							30	
IS11		120							35	
IS12				145					35	
IS13		125								
IS14		120							40	
IS17	125	125					75			
IS18			165	165						
IS19				165	95					
IS20			165	165						
IS21			175	175						
IS23					95	95				
IS24								75	45	
IS25		120							45	
IS26								75		
IS27							75	75		
IS28a										35
IS28b		130							25	
IS29		115								
IS30	120	115								
IS33								65		
IS34								85		
IS35		125								
IS36								75		
IS37								65		
IS42	115	125								
IS43	110	125								
IS45								75		
IS46				175						
IS47	115	125								
IS49	110	125								
IS50				175						
IS52	110	125								
IS53								75		
IS54	115	115								
IS55			175	175						
IS56			175c	175					45r	
IS57	120	110								
IS59				165						
IS60								75		
IS61								75		
IS62				160						
IS63				160						
IS64				170						
IS65								75		
IS66	125	125								
IS67								65	40	
IS68	125	115								
IS69								65		

Sample	FIA 1		FIA 2		FIA 3		FIA 4		FIA 5	
no.	St	Grt	St	Grt	St	Grt	St	Grt	St	Grt
IS70										25
IS71									40	45
IS72				175			65			
IS73			165p	165					45	
IS74							75p	75	40	
IS77			170c	170					45r	
IS78									55	
IS79	110									
IS81										45
IS82							65			
IS83	120	110								
IS84	125									
IS85							65c	65	35r	
IS86	115c						75r			
IS87	115									
IS88					100c				45r	
IS89	115	115								
IS90	130c	120	165r							
IS91					100c		85m		45r	
IS92a			170							
IS92b	125									
IS93			165	165						
IS94					90c	100	65m		25r	
IS95					95c	95	65m		35r	
IS96								65		
IS99								70		
IS101				155						
IS102									45	45
IS103	120	125								
IS104	115	120								

Table 2. A list of FIA measurements for garnet and staurolite porphyroblasts. c – core-inclusion trails; m –median-inclusion trails; r – rim-inclusion trails; p – pre-FIA.

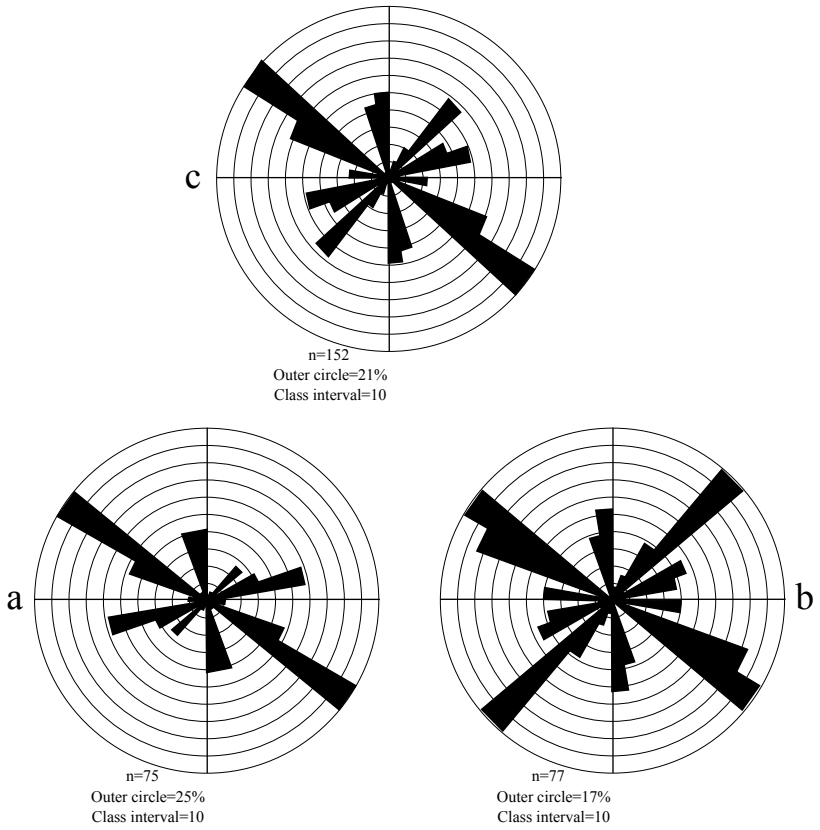

Figure 21. Equal-area rose diagrams of the FIAs in garnet (a), staurolite (b), and combined (c) garnet and staurolite porphyroblasts.

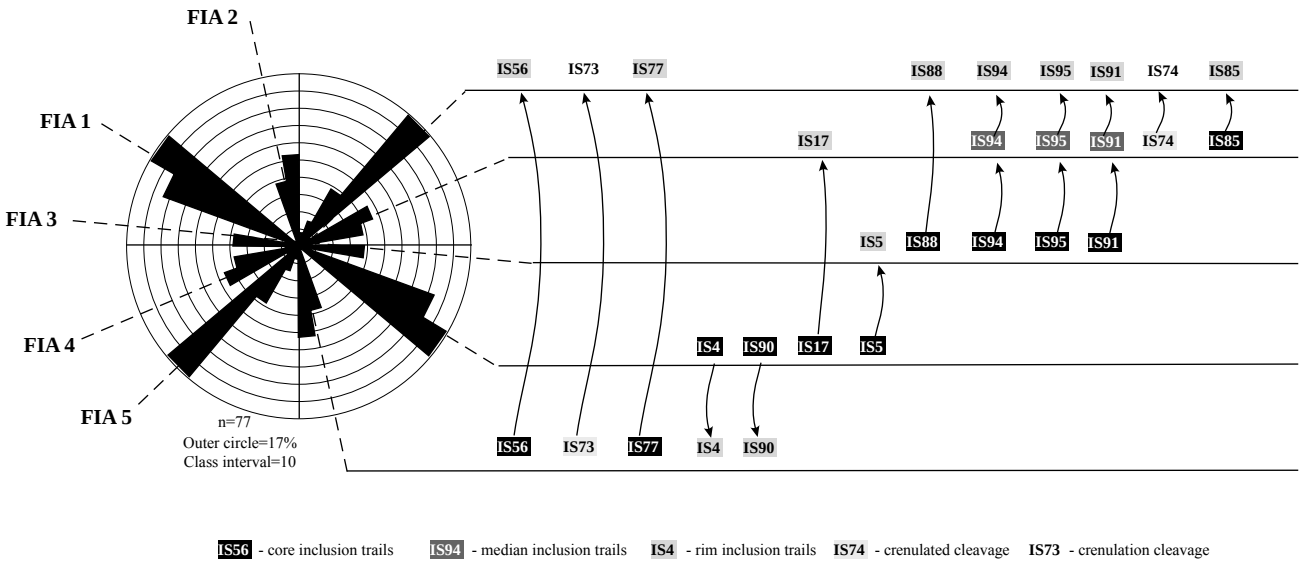

Figure 22. Equal-area rose diagrams of the FIAs in staurolite porphyroblasts illustrating how the relative FIA succession was established. Arrows show core- to- rim changes. A consistent succession is revealed by total combinations of changes.

Sample no.	FIA 1		FIA 2		FIA 3		FIA 4		FIA 5	
	Grt	St	Grt	St	Grt	St	Grt	St	Grt	St
IS2	125							75		
IS4	125	125c		165r						
IS5	120	125c				95r				
IS7a	115	125								
IS9b	120							65		
IS10	115									30
IS11	120									35
IS14	120									40
IS17	125	125						75r		
IS25	120									45
IS28b	130									25
IS30	115	120								
IS42	125	115								
IS43	125	110								
IS47	125	115								
IS49	125	110								
IS52	125	110								
IS54	115	115								
IS57	110	120								
IS66	125	125								
IS68	115	125								
IS83	110	120								
IS89	115	115								
IS90	120	130c		165r						
IS103	125	120								
IS104	120	115								
IS12			145							35
IS18			165	165						
IS19			165			95				
IS20			165	165						
IS21			175	175						
IS55			175	175						
IS56			175	175c						45r
IS72			175					65		
IS73			165	165p						45
IS77			170	170c						45
IS93			165	165						
IS23					95	95				
IS94					100	90c		65m		25r
IS95					95	95c		65m		35r
IS24							75			45
IS27							75	75		
IS67							65			40
IS74							75	75p		40
IS85							65	65c		35r
IS7b									40	15
IS8									45	45
IS71									45	40
IS102									45	45

Table 3. FIA measurements for garnet and staurolite porphyroblasts, for only those samples where garnet porphyroblasts were included in staurolite. A clear succession from FIA 1 to FIA 5 can be established in this way.

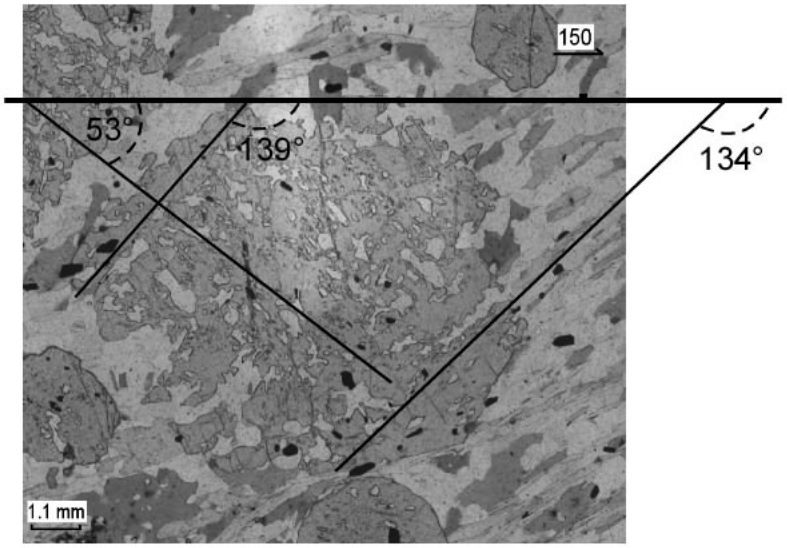

Figure 23. Inclusion-trail pitches were measured from the horizontal plane in all staurolite porphyroblasts for each sample, around the compass, for both core- and rim-inclusion trails.

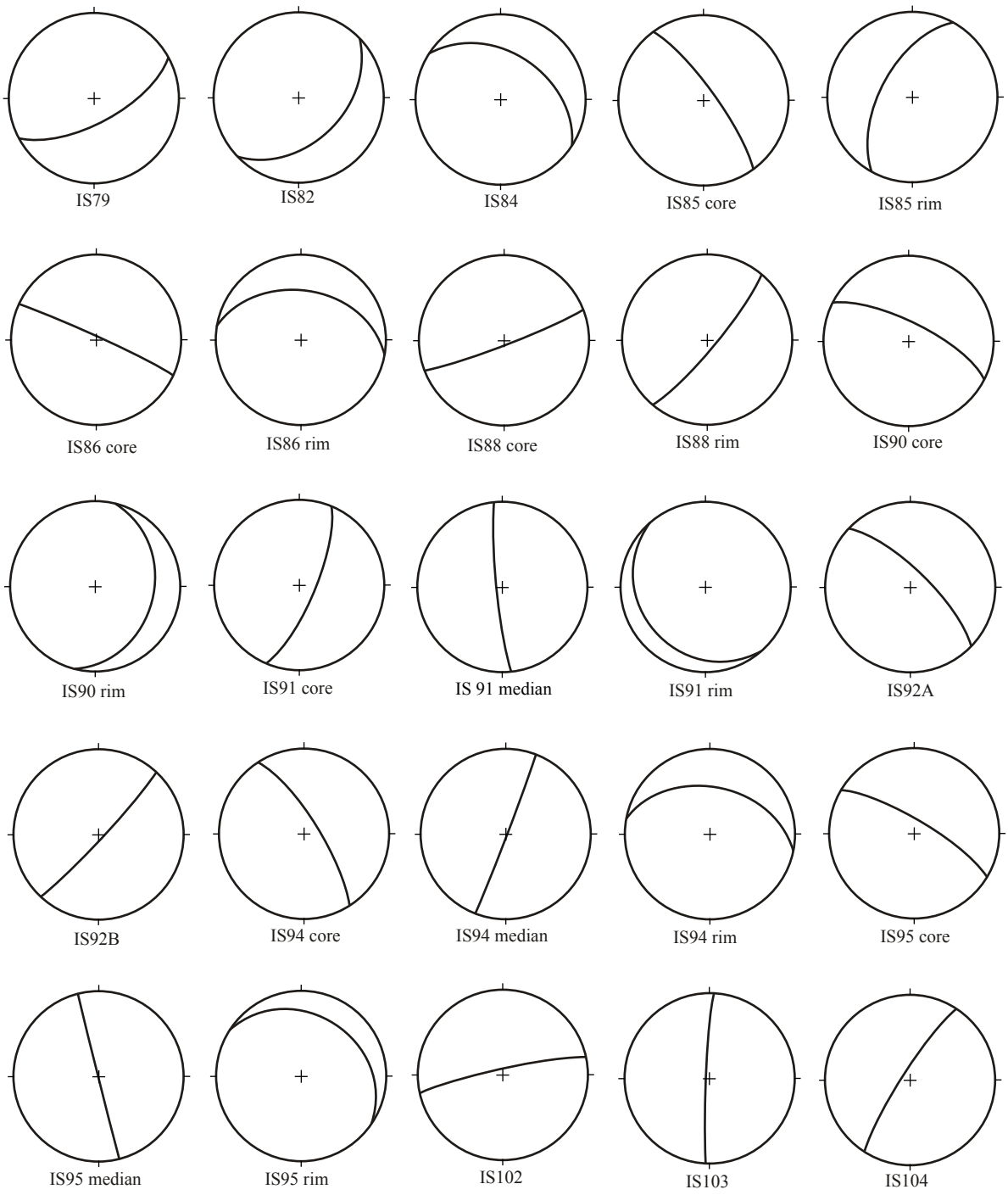

Figure 24 (continued). Inclusion-trail foliations measured from staurolite porphyroblasts plotted on stereonets.

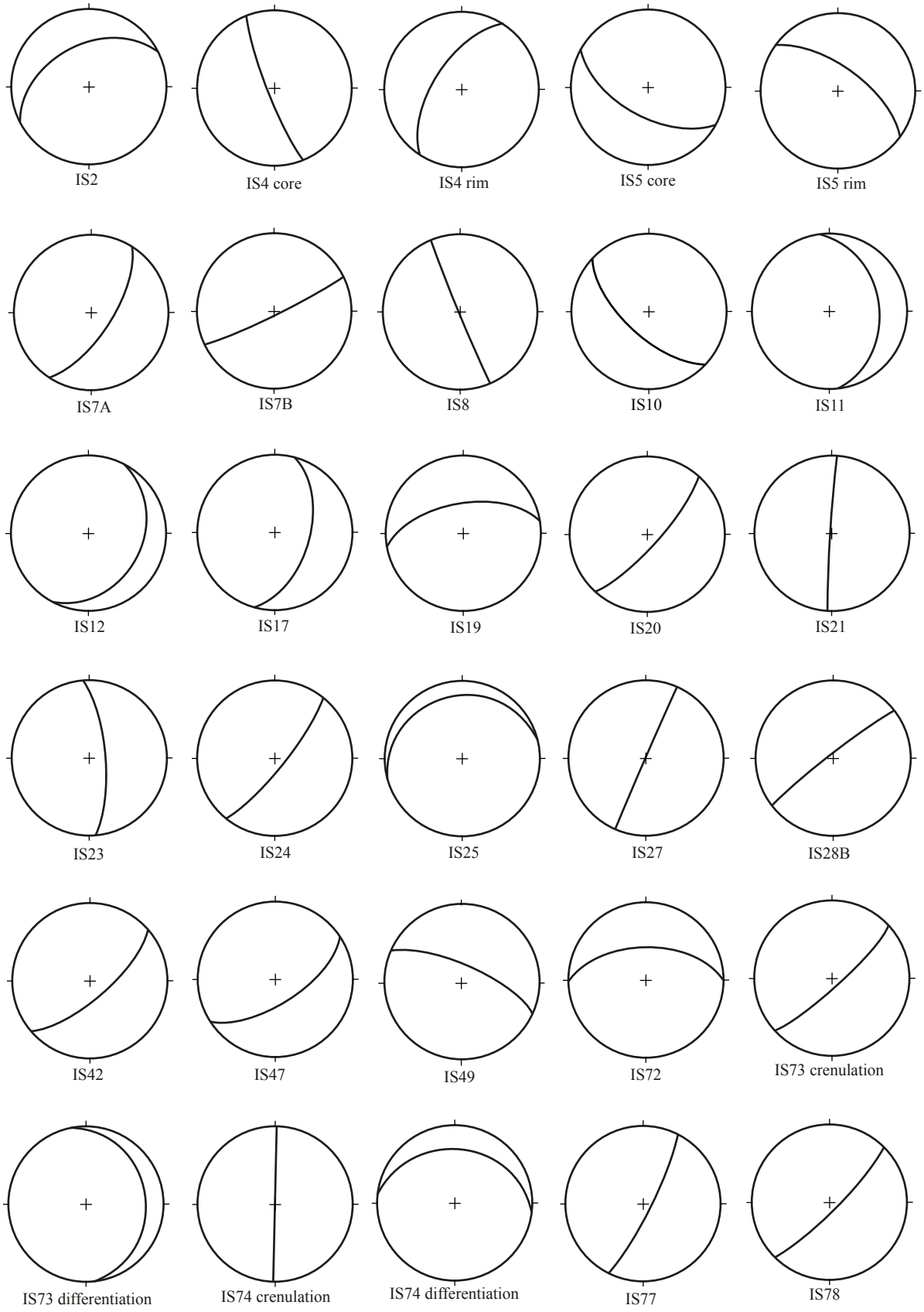

Figure 24.

continues on the next page ⟶

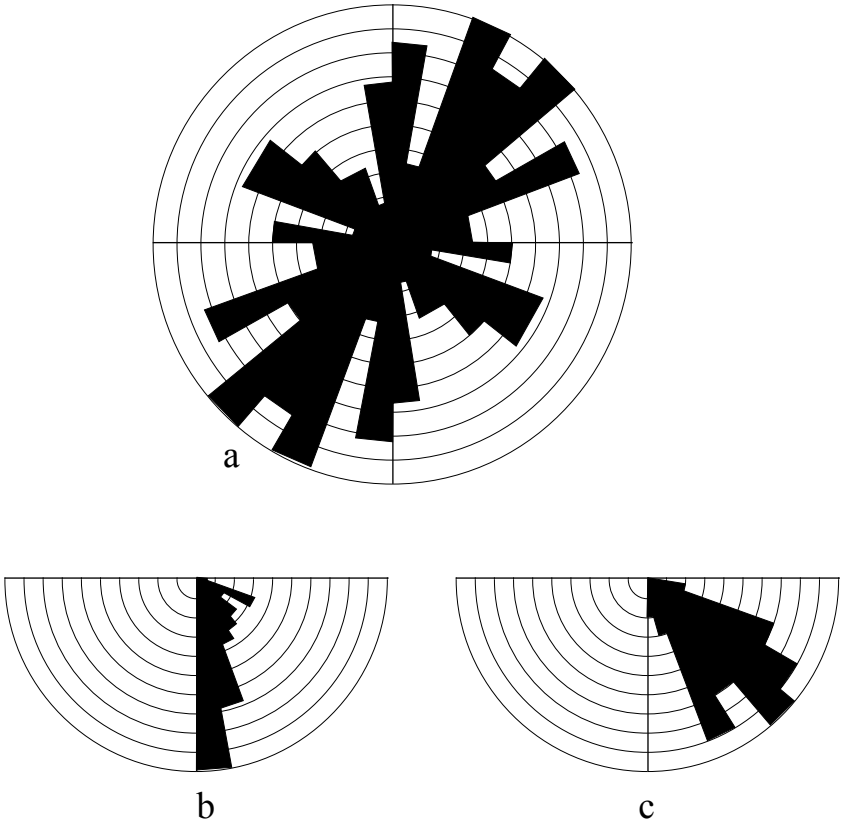

Figure 25. Equal-area rose diagram showing the trends (a) and the dips (b) of the foliations measured from staurolite porphyroblasts and the dips of the matrix foliation (c).

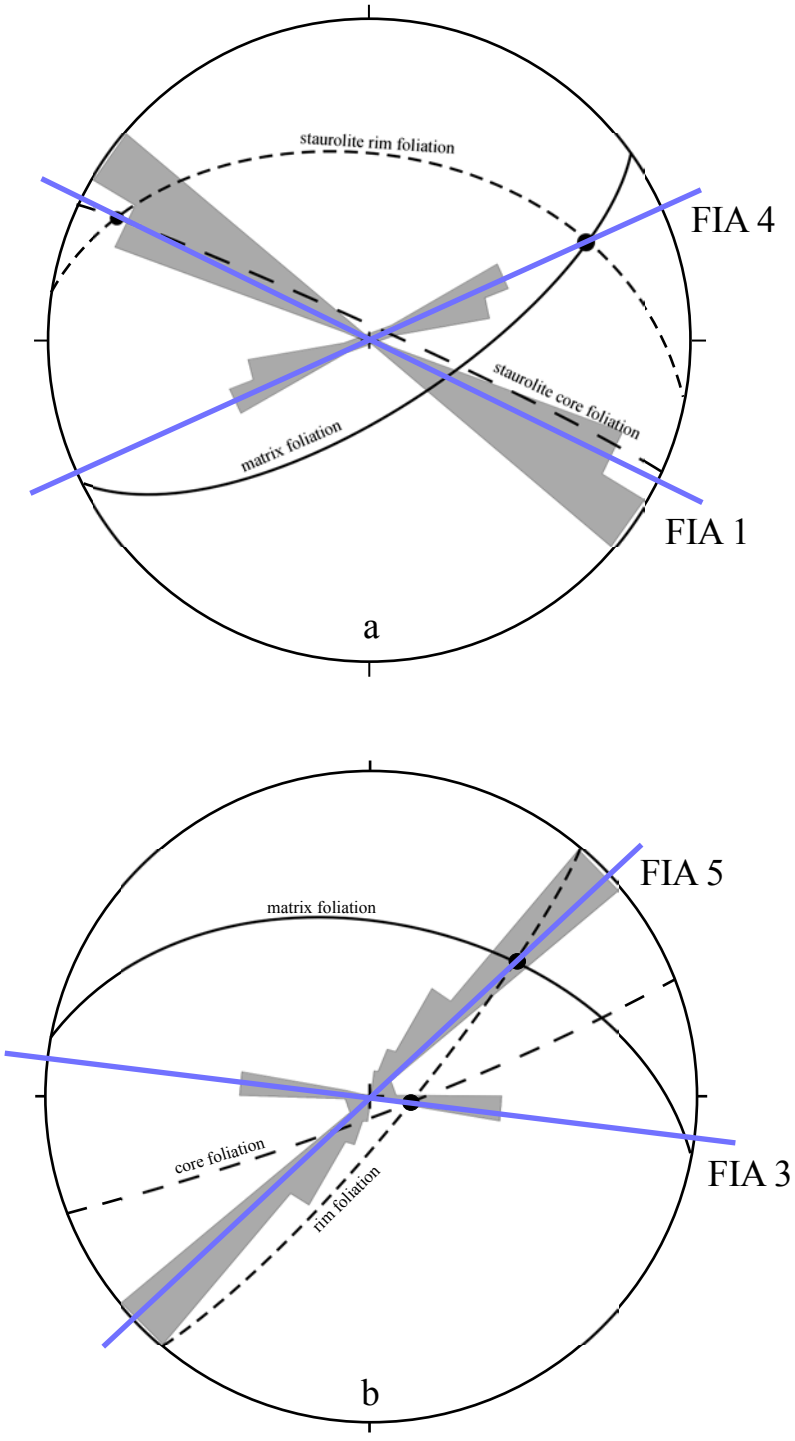

Figure 26. Stereonet projections showing the relationships between FIAs, foliations measured from staurolite porphyroblasts, and the matrix foliaton from sample IS86 (a) and IS88 (b). Shaded areas represent FIA trends measured by asymmetry method. Blue lines represent the trend of the intersection axes between two different foliations.

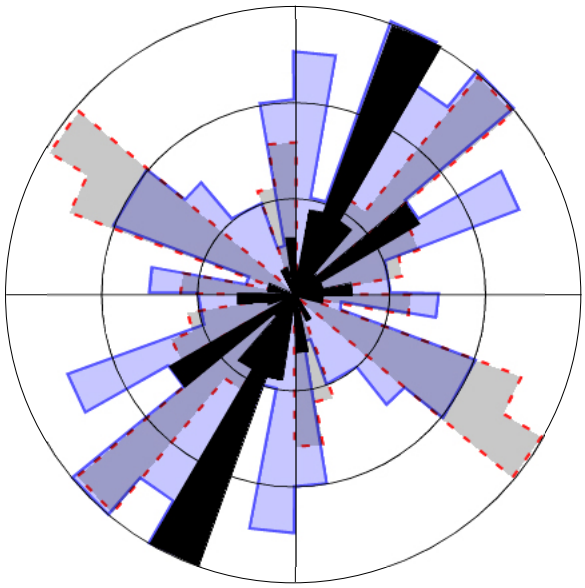

Figure 27. Rose diagram showing how pitch measurements ofJohnson et al. (2006) (black peaks) correlate with FIAs (red dashed lines grey shading) and foliations measured from staurolite porphyroblasts (blue peaks).

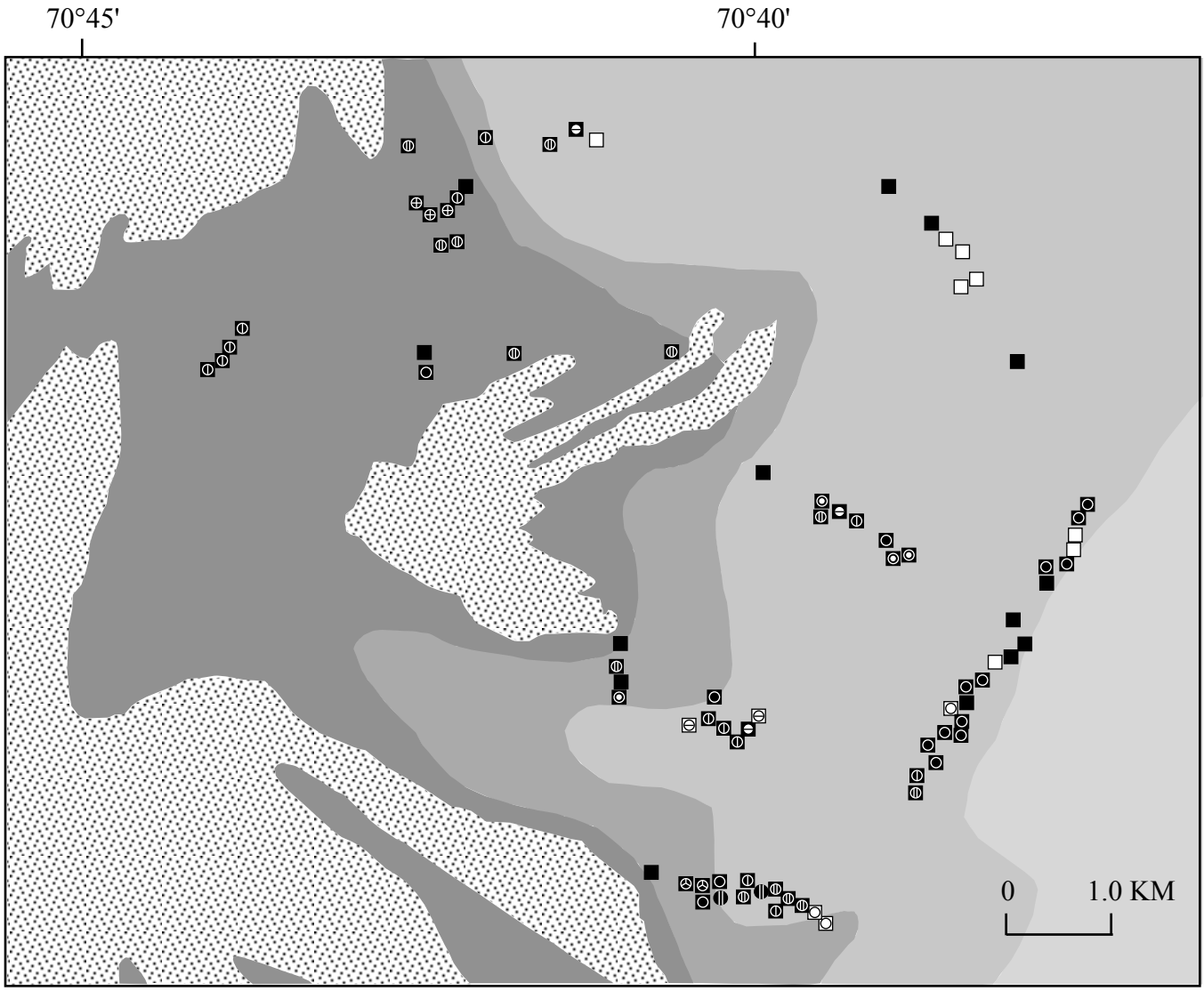

Sillimanite zone Transition zone Staurolite zone Garnet zone

- □ Grt - continous
- ■ Grt - truncated
- ◐ St - truncated, 2 generations of growth
- ◙ Grt, St - truncated
- ◘ Grt - truncated; St - slightly crenulated, appears continous
- ⊜ Grt - appears continous; St - slightly crenulated, appears continous
- ◍ Grt - truncated; St - crenulated, truncated
- ⊕ Grt - truncated; St - differentiated crenulations, truncated
- ⊙ Grt - appears continuous; St - sigmoidal, appears continuous
- ◉ Grt - truncated; St - sigmoidal, truncated
- ◍ Grt - truncated; St - 2 generations of growth, truncated
- ✇ Grt - truncated; St - 3 generations of growth, truncated

Figure 28. Simplified geological map of the study area showing some of the porphyroblast-matrix relationships for most of the samples.

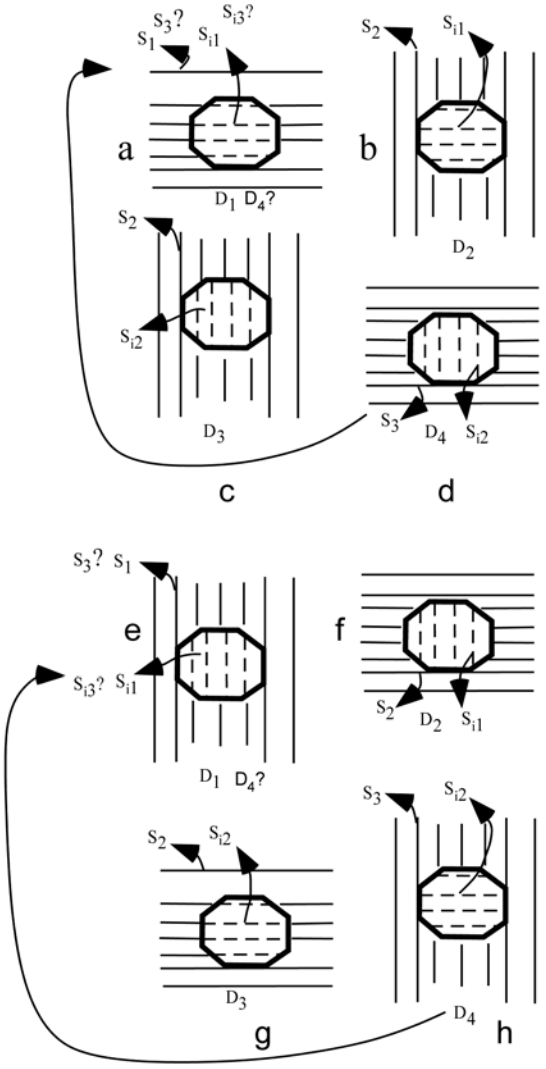

Figure 29. Schematic representation of the transition from a sub-horizontal fabric (a) to a sub-vertical fabric (b) and back to sub-horizontal (d) which is similar or identical to (a). Schematic representation of the same cycle but starting with a sub-vertical fabric (e). Crenulation events can locally erase any trace of previous foliations, and the inclusion trails in porphyroblasts can appear to be continuous with a different foliation than the one contemporaneous with the porphyroblast growth

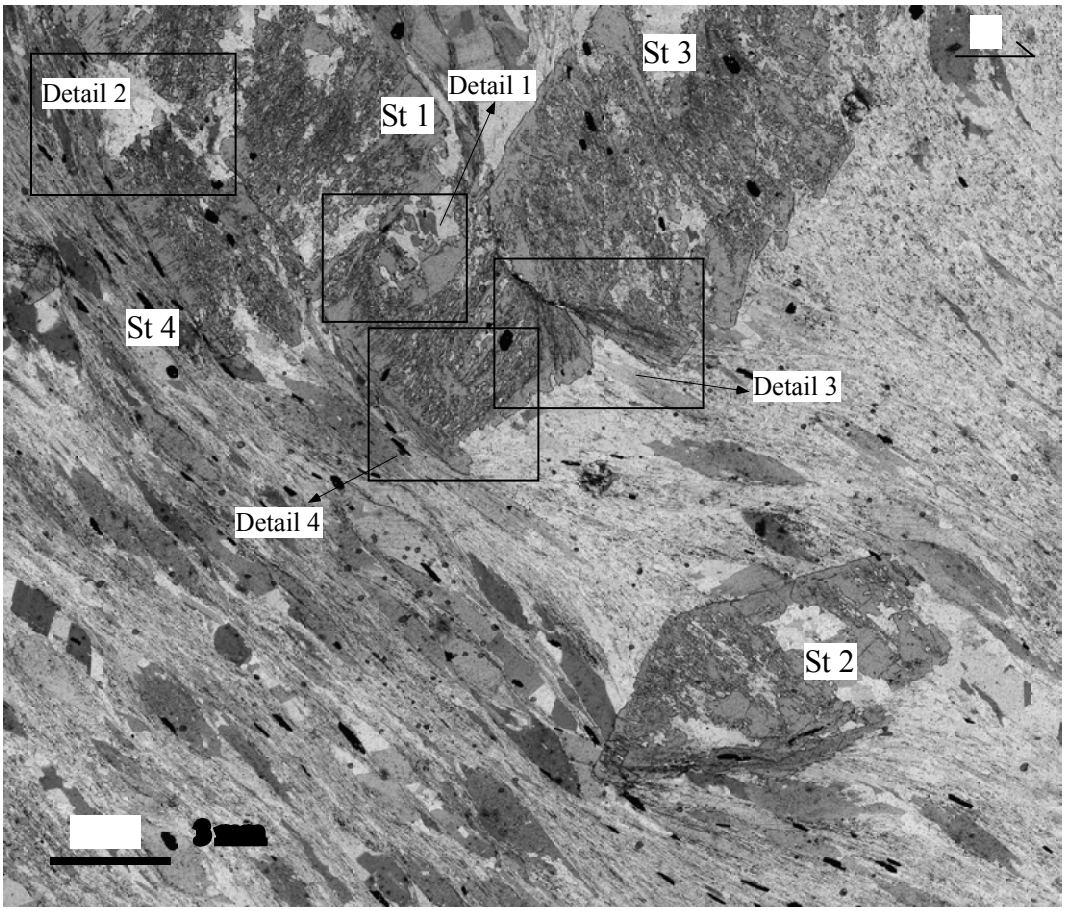
Detail 2
Detail 1
St 3
St 1
St 4
Detail 3
Detail 4
St 2

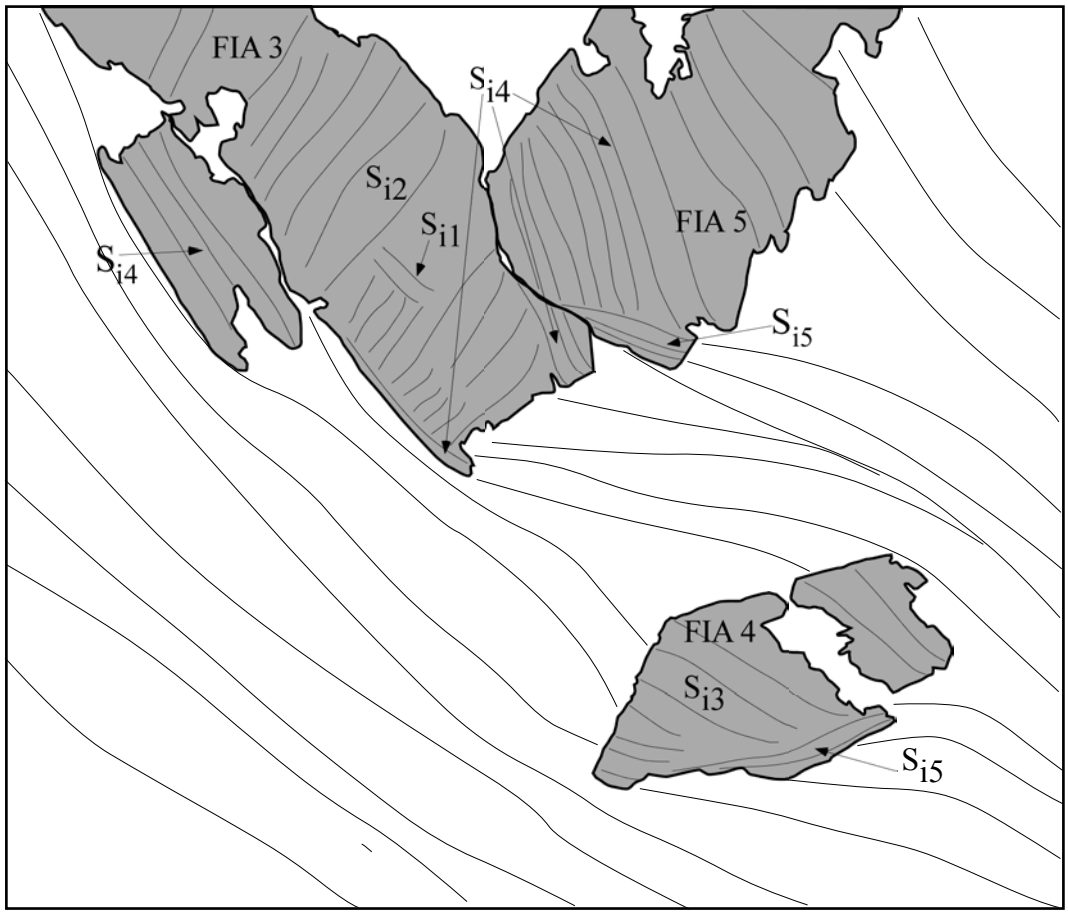
FIA 3
S_{i4}
S_{i2}
S_{i1}
FIA 5
S_{i4}
S_{i5}
FIA 4
S_{i3}
S_{i5}

Figure 30. Photomicrograph from sample IS91 showing different generations of inclusion trails preserved in staurolite porphyroblasts. See text for description.

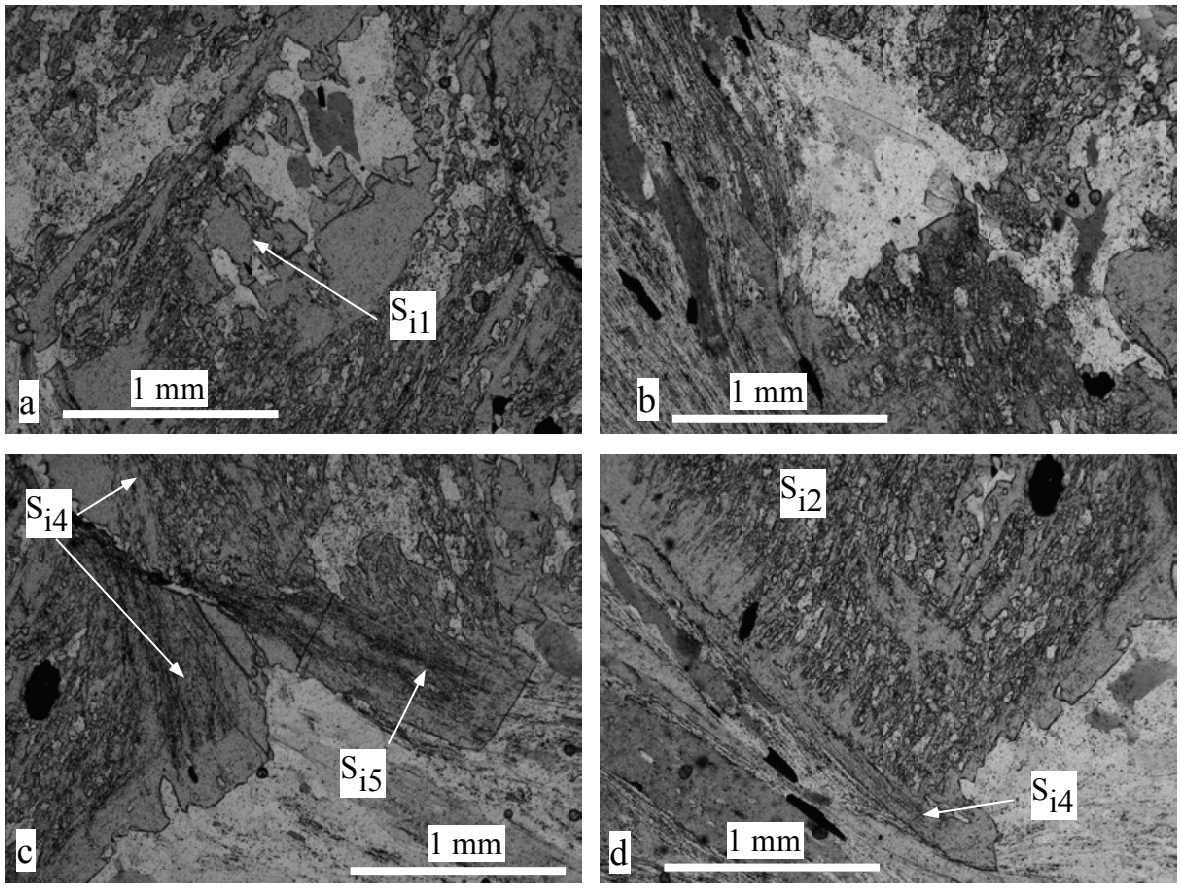

Figure 31. Photomicrographs showing details of the microstructures presented in Fig. 30. See text for description.

- SECTION B -

70 MILLION YEARS OF TECTONO-METAMORPHISM REVEALED BY STAUROLITE GROWTH ADJACENT TO THE MOOSELOOKMEGUNTIC PLUTON

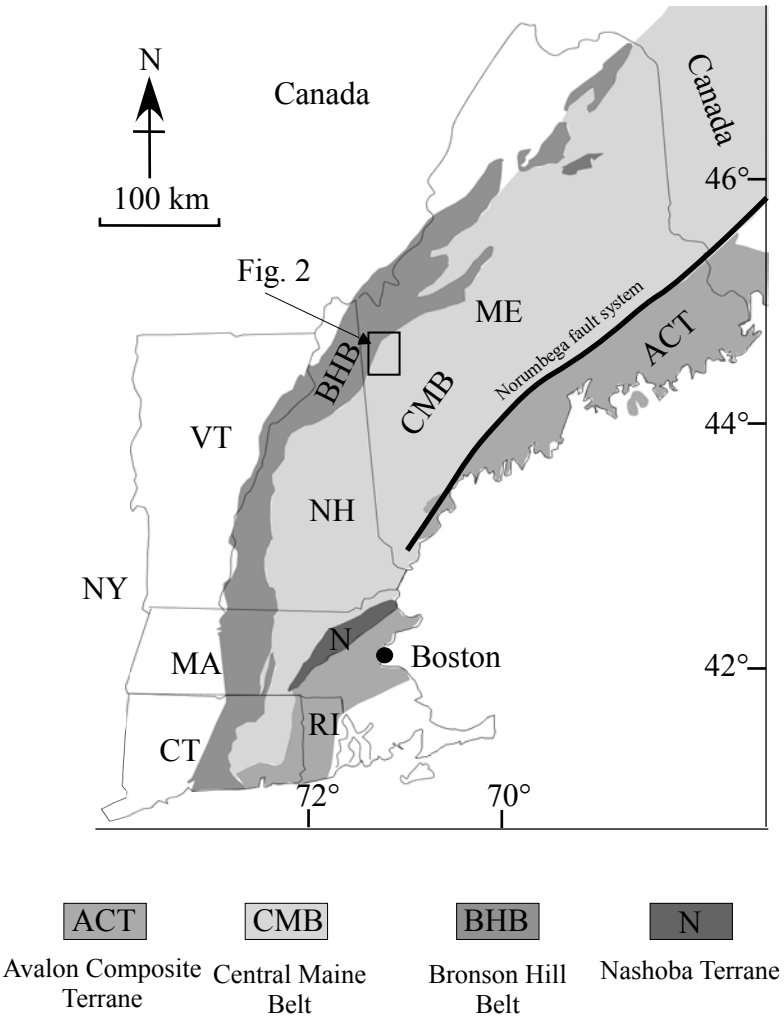

Figure 1. Simplified map of New England showing the major structural units.

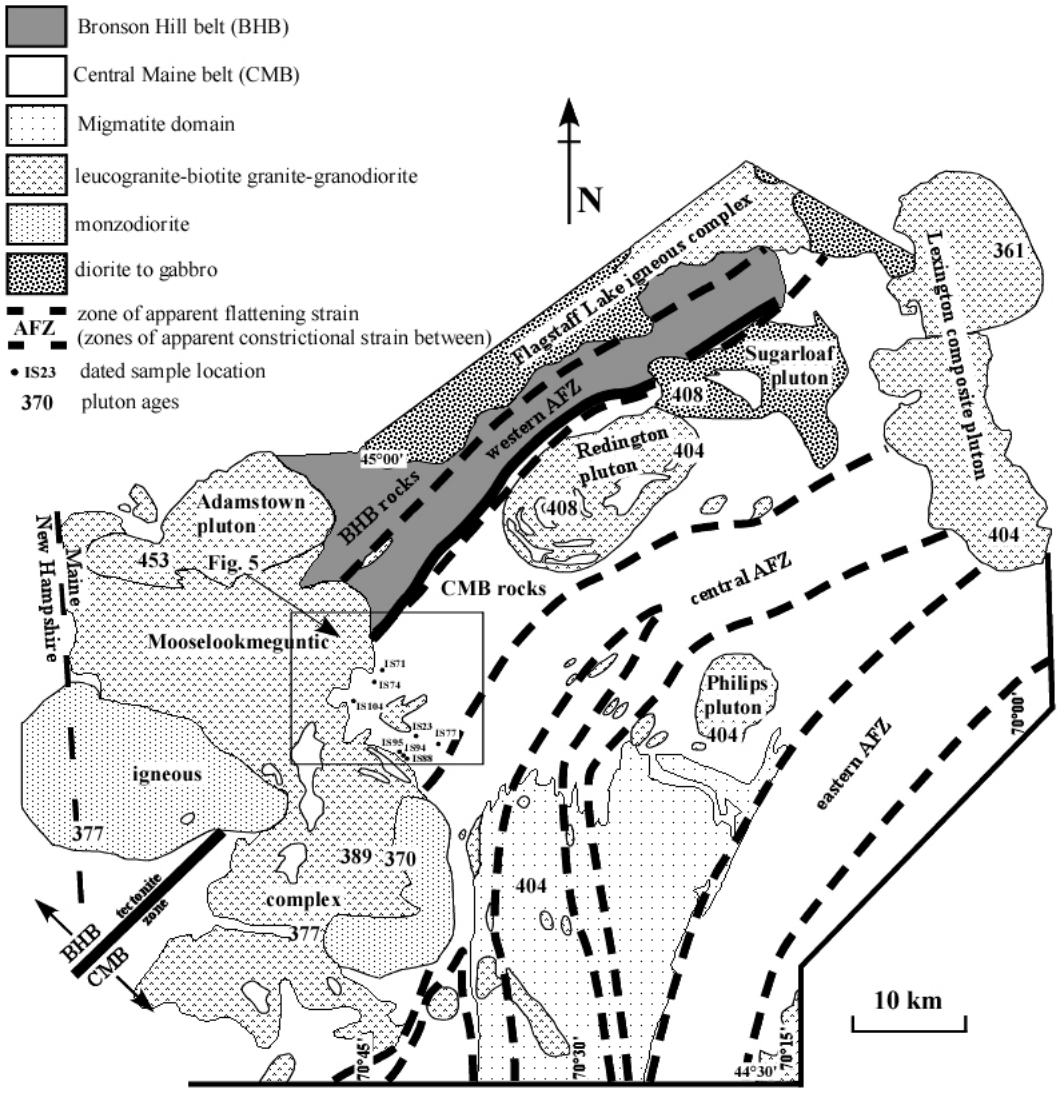

Figure 2. Simplified geological map of west-central Maine showing the major structural features. Modified after Tomascak et al. (2005).

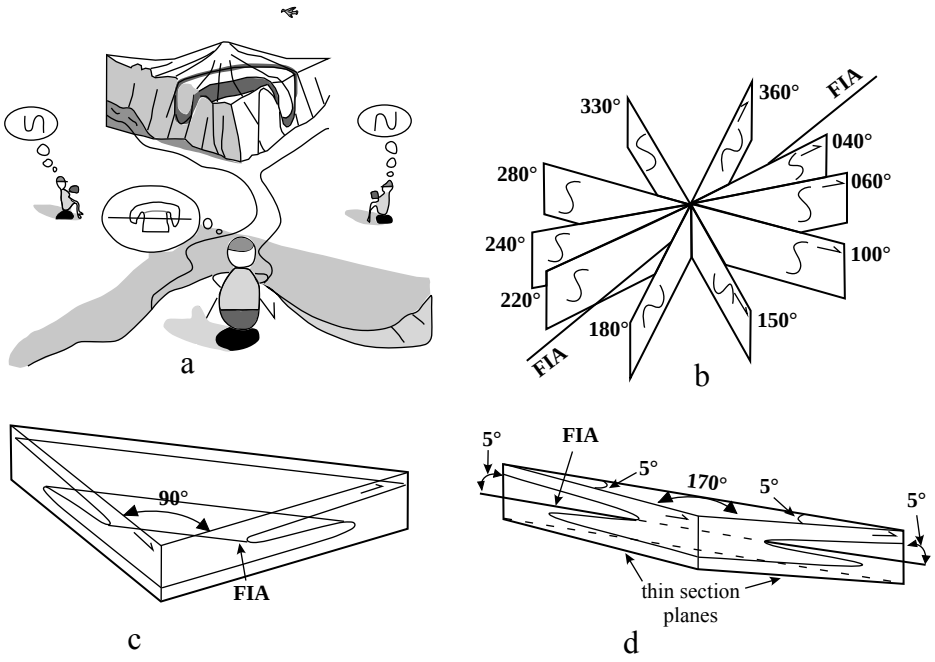

Figure 3. Sketch illustrating the principle behind FIA measurement (after Bell et al., 2004). a) The geologists to either side see the opposite asymmetry for same fold in a cliff face. They have no idea of its trend in 3-D. The geologist in the centre sees the fold on both cliff faces and knows it must trend from one to the other. b) Shows the asymmetry on a series of differently-striking vertical sections. The asymmetry flips across the compass when viewed in the same direction. (c) Shows asymmetry of a sigmoid axis in two sections cut 90° apart. (d) Shows the sigmoid axis of (c) in two sections cut 10° apart lying on either side of the axis. The switch in asymmetry between them defines the location of the axis within a 10° range.

Sample	FIA 1		FIA 2		FIA 3		FIA 4		FIA 5	
no.	St	Grt	St	Grt	St	Grt	St	Grt	St	Grt
IS2		125					75			
IS4	125	125	165r							
IS5	125c	120			95r					
IS7a	125	115								
IS7b									15	40
IS8									45	45
IS9b		120					65			
IS10		115							30	
IS11		120							35	
IS12				145					35	
IS13		125								
IS14		120							40	
IS17	125	125					75			
IS18			165	165						
IS19				165	95					
IS20			165	165						
IS21			175	175						
IS23					95	95				
IS24								75	45	
IS25		120							45	
IS26								75		
IS27							75	75		
IS28a										35
IS28b		130							25	
IS29		115								
IS30	120	115								
IS33								65		
IS34								85		
IS35		125								
IS36								75		
IS37								65		
IS42	115	125								
IS43	110	125								
IS45								75		
IS46				175						
IS47	115	125								
IS49	110	125								
IS50				175						
IS52	110	125								
IS53								75		
IS54	115	115								
IS55			175	175						
IS56			175c	175					45r	
IS57	120	110								
IS59				165						
IS60								75		
IS61								75		
IS62				160						
IS63				160						
IS64				170						
IS65								75		
IS66	125	125								
IS67								65	40	
IS68	125	115								
IS69								65		

Sample	FIA 1		FIA 2		FIA 3		FIA 4		FIA 5	
no.	St	Grt	St	Grt	St	Grt	St	Grt	St	Grt
IS70										25
IS71									40	45
IS72				175			65			
IS73			165p	165					45	
IS74							75p	75	40	
IS77			170c	170					45r	
IS78									55	
IS79	110									
IS81										45
IS82							65			
IS83	120	110								
IS84	125									
IS85							65c	65	35r	
IS86	115c						75r			
IS87	115									
IS88					100c				45r	
IS89	115	115								
IS90	130c	120	165r							
IS91					100c		85m		45r	
IS92a			170							
IS92b	125									
IS93			165	165						
IS94					90c	100	65m		25r	
IS95					95c	95	65m		35r	
IS96								65		
IS99								70		
IS101				155						
IS102									45	45
IS103	120	125								
IS104	115	120								

Table 2. A list of FIA measurements for garnet and staurolite porphyroblasts. c – core-inclusion trails; m –median-inclusion trails; r – rim-inclusion trails; p – pre-FIA.

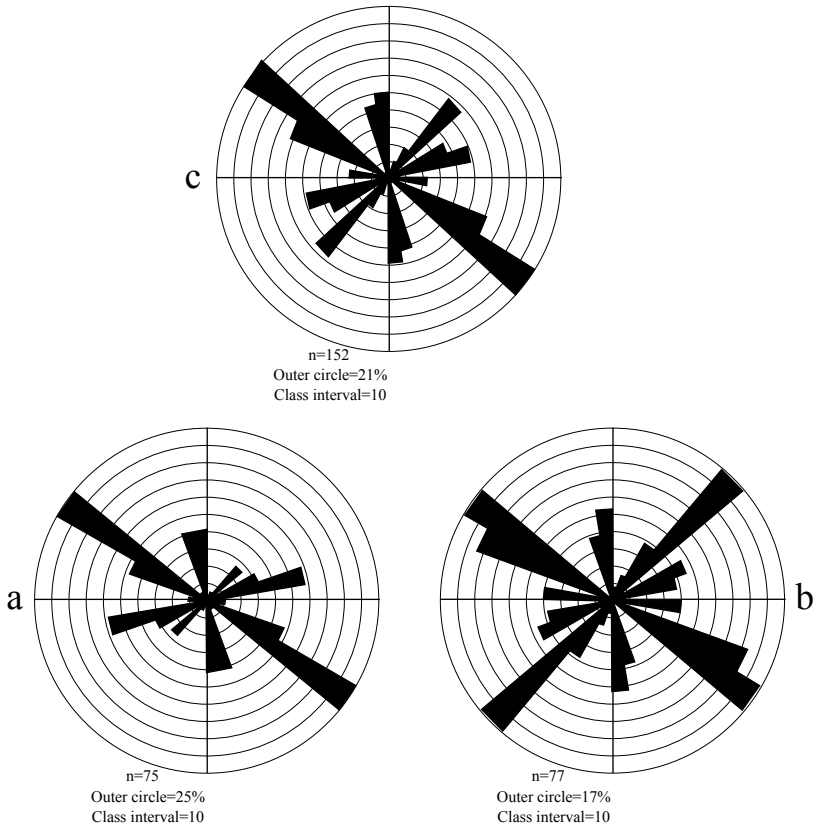

Figure 4. Equal-area rose diagrams of the FIAs in garnet (a), staurolite (b), and combined (c) garnet and staurolite porphyroblasts.

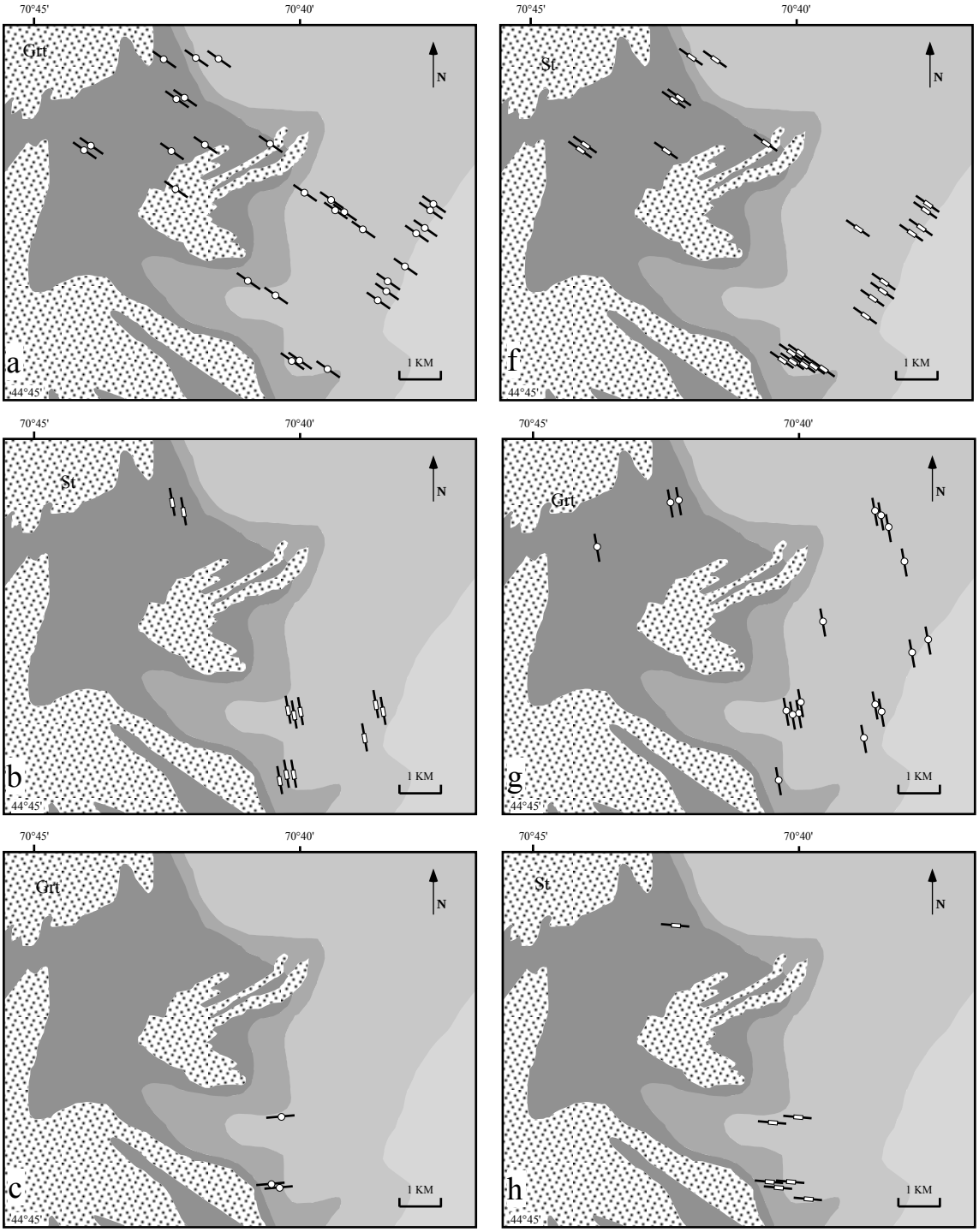

continues on the next page ⟶

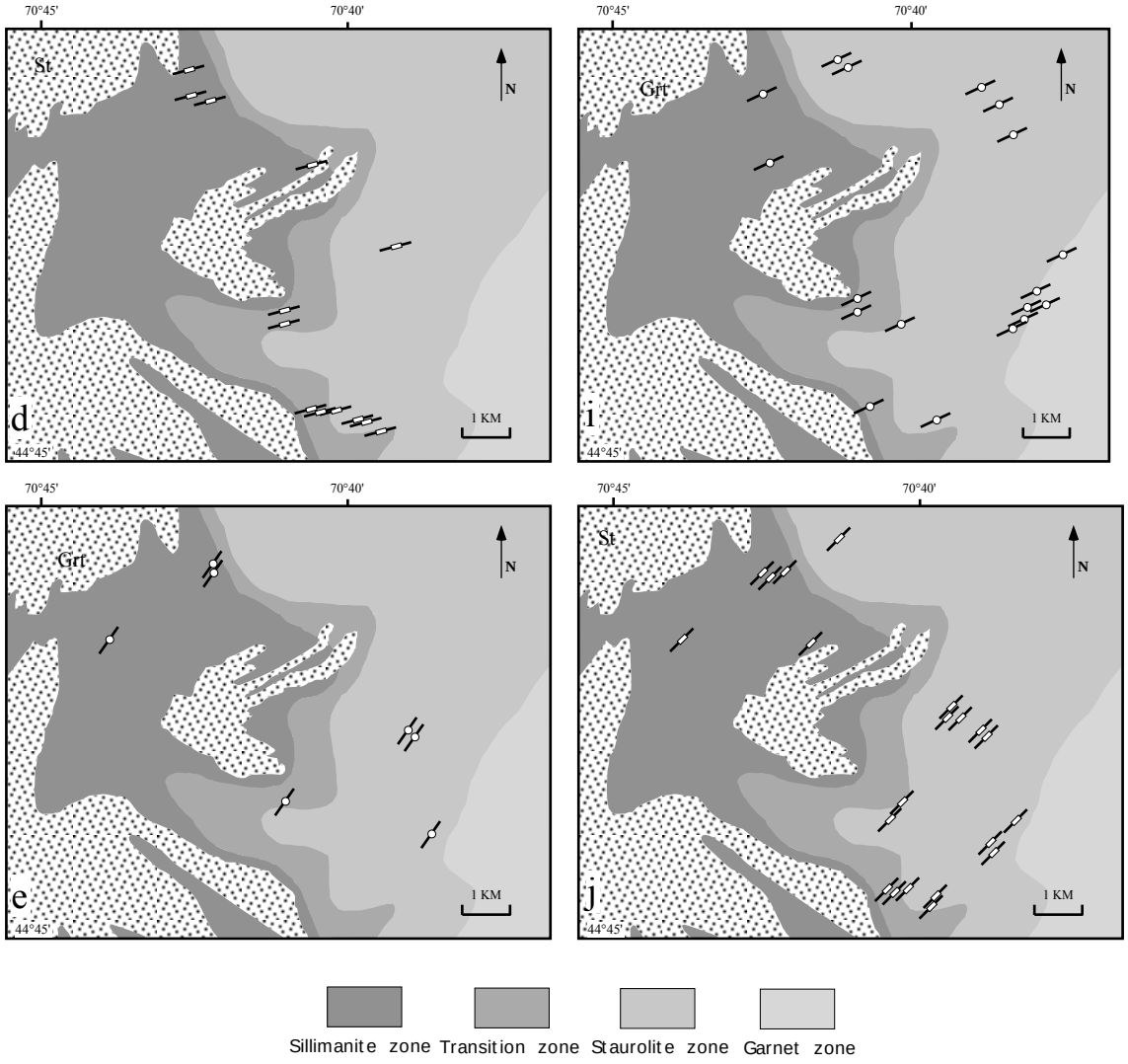

Figure 5. Simplified geological map of the study area showing the distribution of FIA trends based on sample location.

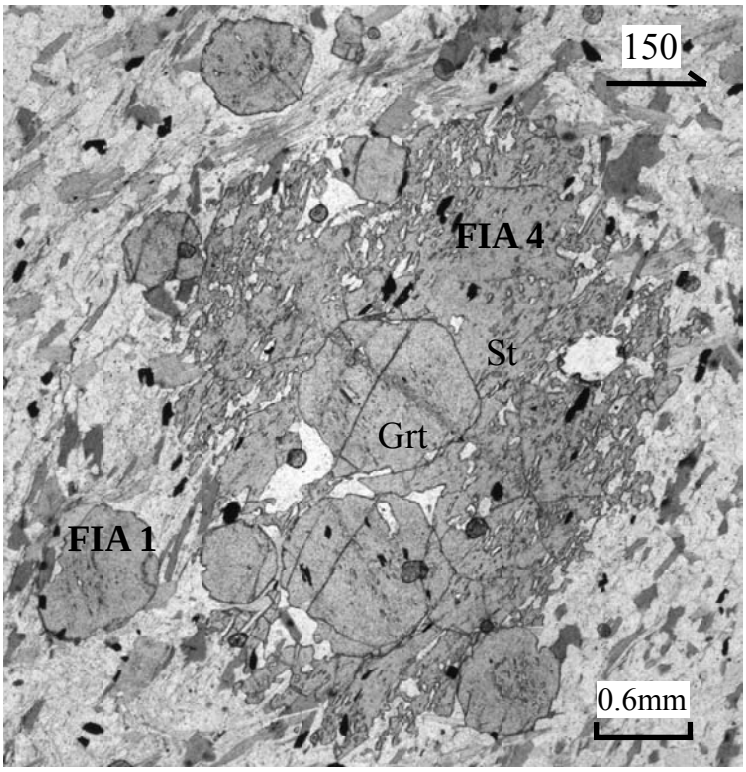

Figure 6. Photomicrograph showing the relationship between garnet and staurolite porphyroblast from sample IS2. Inclusion trails in garnet porphyroblasts contain FIA 1and are truncated by the inclusion trails in the staurolite porphyroblast that contains FIA 4.

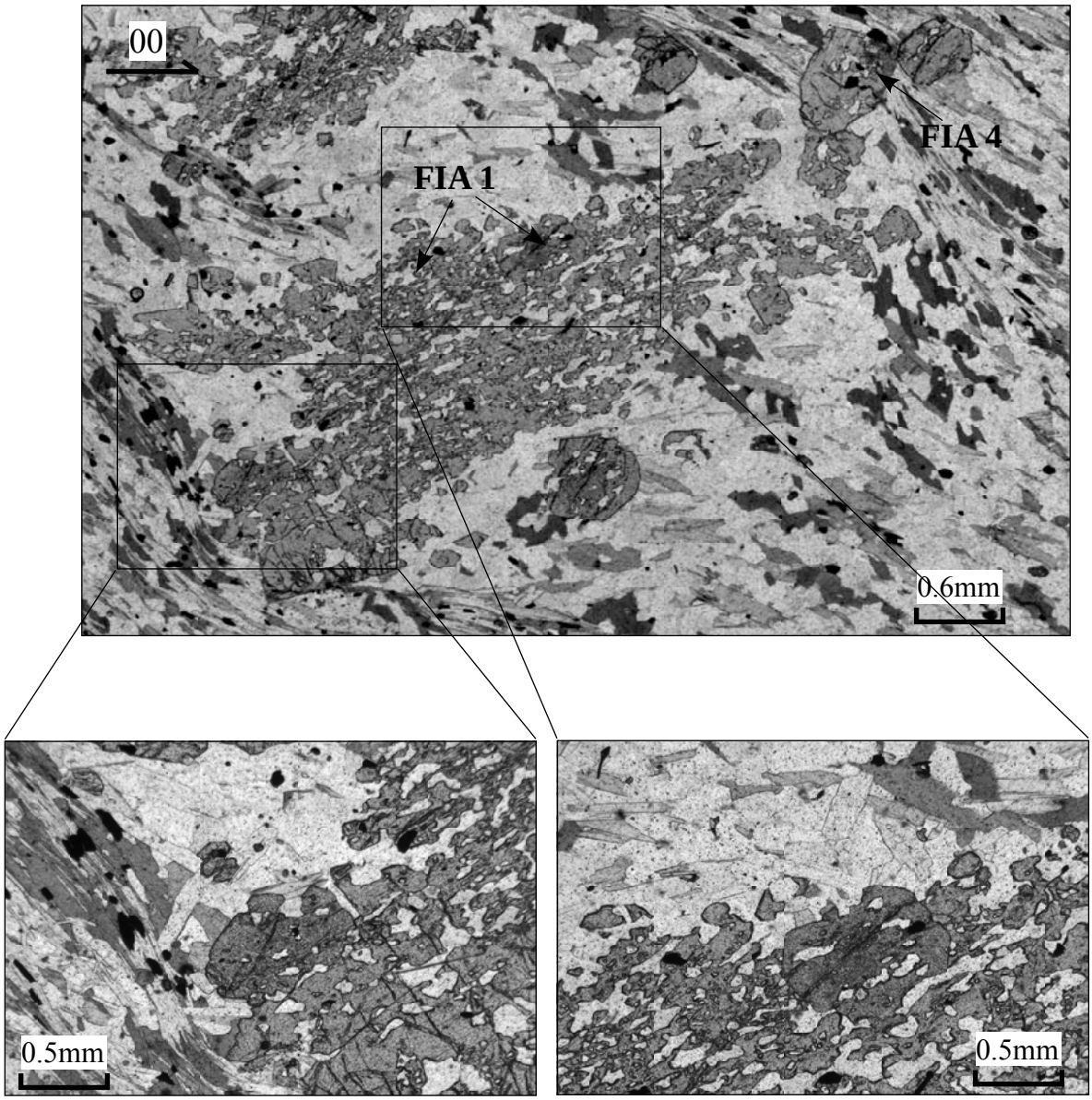

Figure 7. Photomicrograph showing the relationship between garnet and staurolite porphyroblasts from sample IS17. The inclusion trails in garnet are similar and continuous with the inclusion trails from the staurolite core. They both contain FIA1. Staurolite porphyroblasts from this sample usually have a rim growth that contains FIA 4.

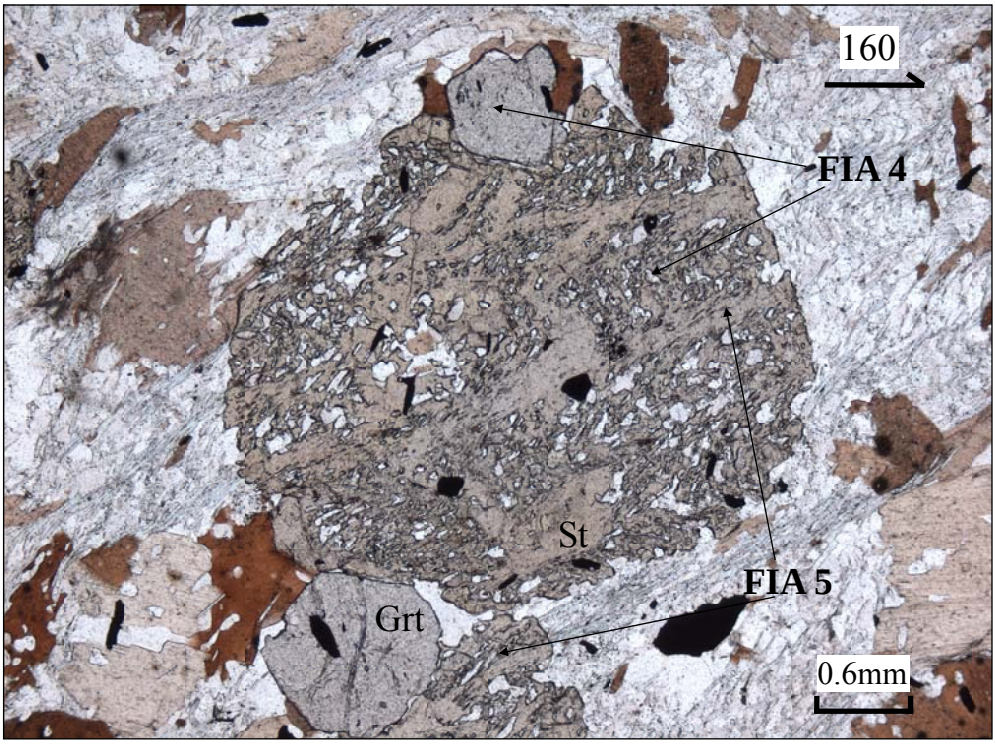

Figure 8. Photomicrograph showing the relationship between staurolite and garnet porphyroblasts from sample IS74. Garnet porphyroblasts grew in the hinge of a crenulation during FIA 4, which was overprinted by staurolite growth during FIA 5.

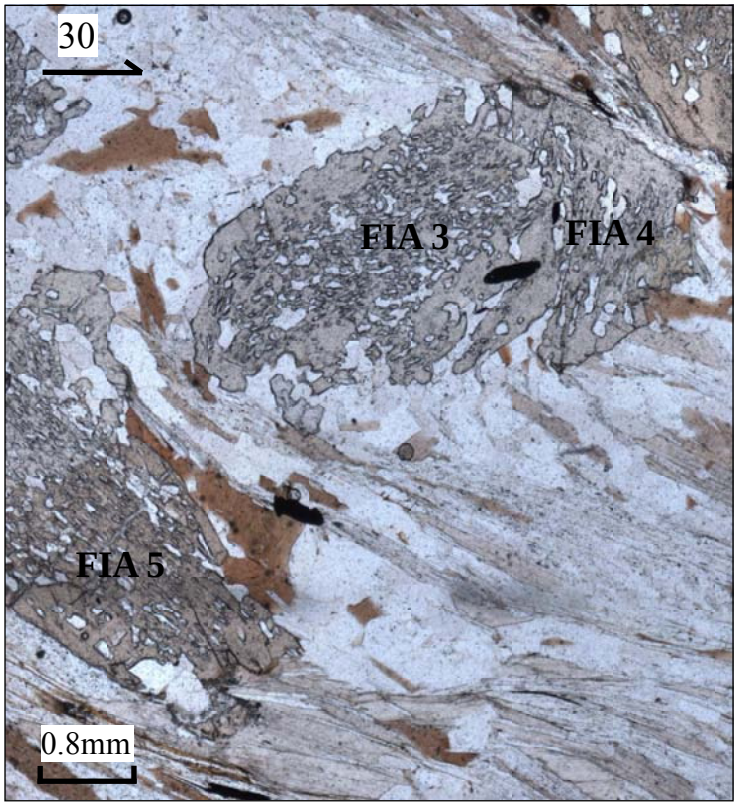

Figure 9. Photomicrograph from sample IS94 showing three generations of staurolite growth which correspond to FIAs 3, 4 and 5. In most cases FIA 5 staurolite overgrew the rim of FIA 4 staurolite, but it is not uncommon to find FIA 5 staurolite overgrowing the latest matrix foliation.

Sample no.	FIA 1		FIA 2		FIA 3		FIA 4		FIA 5	
	Grt	St	Grt	St	Grt	St	Grt	St	Grt	St
IS2	125							75		
IS4	125	125c		165r						
IS5	120	125c				95r				
IS7a	115	125								
IS9b	120							65		
IS10	115									30
IS11	120									35
IS14	120									40
IS17	125	125						75r		
IS25	120									45
IS28b	130									25
IS30	115	120								
IS42	125	115								
IS43	125	110								
IS47	125	115								
IS49	125	110								
IS52	125	110								
IS54	115	115								
IS57	110	120								
IS66	125	125								
IS68	115	125								
IS83	110	120								
IS89	115	115								
IS90	120	130c		165r						
IS103	125	120								
IS104	120	115								
IS12			145							35
IS18			165	165						
IS19			165			95				
IS20			165	165						
IS21			175	175						
IS55			175	175						
IS56			175	175c						45r
IS72			175					65		
IS73			165	165p						45
IS77			170	170c						45
IS93			165	165						
IS23					95	95				
IS94					100	90c		65m		25r
IS95					95	95c		65m		35r
IS24							75			45
IS27							75	75		
IS67							65			40
IS74							75	75p		40
IS85							65	65c		35r
IS7b									40	15
IS8									45	45
IS71									45	40
IS102									45	45

Table 3. FIA measurements for garnet and staurolite porphyroblasts, for only those samples where garnet porphyroblasts were included in staurolite. A clear succession from FIA 1 to FIA 5 can be established in this way.

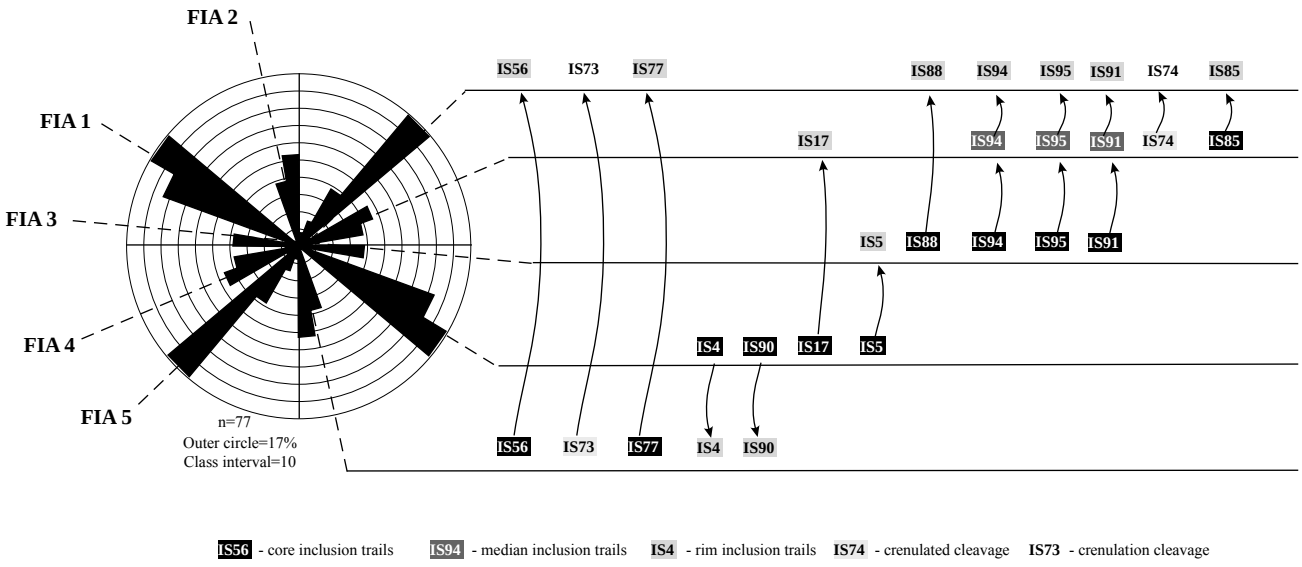

Figure 10. Equal-area rose diagrams of the FIAs in staurolite porphyroblasts illustrating how the relative FIA succession was established. Arrows show core-to-rim changes. A consistent succession is revealed by total combinations of changes.

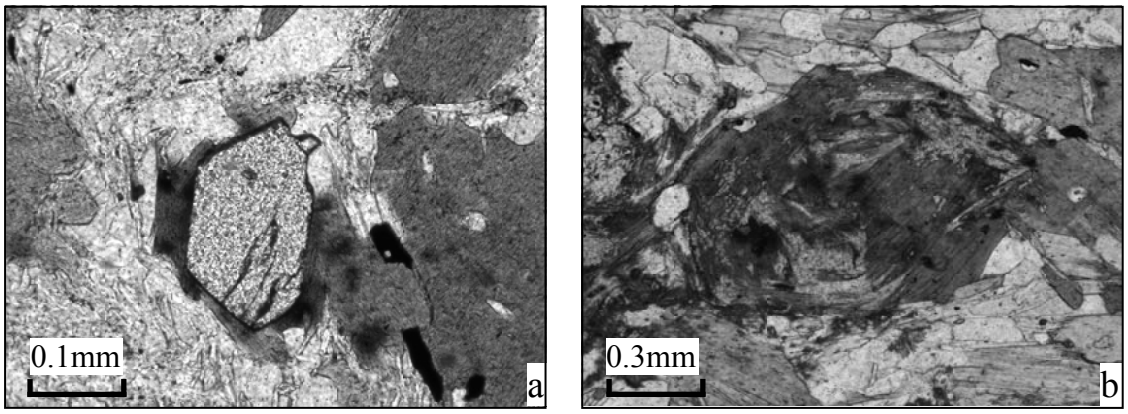

Figure 11. Photomicrographs showing a partially-dissolved garnet that has been replaced by biotite in sample IS71 (a) and a garnet that has been completely replaced by biotite and sillimanite from sample IS104 (b).

Element	X-ray	Crystal	Peak time (secs)	Background time (secs)	Background --/+ (mm)	Standard
P	Kά	TAP-1	20	10	3/4	[3]$CePO_4$
Pb	Mά	PETJ-2*	180	90	4/6	[1]$PbSiO_3$
La	Lά	LIFH-3*	10	5	1/4	[3]$DyPO_4$
U	Mβ	PETJ-4	180	90	3.5/2.5	[1]U
Th	Mά	PETJ-5	90	45	2.5/3	[2]ThO_2
Y	Lά	TAP-1	60	30	1.25/2	[3]YPO_4
Ce	Lά	LIFH-3*	10	5	1/1	[3]$GdPO_4$
Ca	Kά	PETJ-5	20	10	1.6/1.6	[1]$CaSiO_3$
Si	Kά	TAP-1	20	10	5/3	[1]$PbSiO_3$
Pr	Lβ	LIFH-3*	20	10	1/1	[3]$SmPO_4$
S	Kά	PETJ-5*	30	15	6/4	[1]$BaSO_4$
Nd	Lβ	LIFH-3*	10	5	1/1	[3]$NdPO_4$
Sm	Lβ	LIFH-3*	40	20	1/1	[3]$PrPO_4$
Gd	Lβ	LIFH-3*	40	20	3.2/3.2	[3]$CePO_4$
Dy	Lβ	LIFH-3*	40	20	1.6/1.6	[3]$LaPO_4$

[1] – Astimex, [2] – Taylor, [3] – Pb-free synthetic from Pyle (Rensselaer Polytechnic Institute, USA)
** - sealed Xe detectors*

Table 3. Analytical setup for monazite analyses.

No.	PbO	UO_2	ThO_2	Y_2O_3	Age (Ma)	Error (2σ)	Comments
1	0.107	0.429	4.700	1.430	**414**	**43**	is23-m-1-1
2	0.065	0.251	3.040	1.320	**395**	**64**	is23-m-2-1
3	0.073	0.356	3.320	1.420	**384**	**56**	is23-m-3-1
4	0.084	0.407	3.960	1.350	**373**	**48**	is23-m-4-1
5	0.078	0.410	3.350	1.410	**394**	**54**	is23-m-5-1
6	0.084	0.329	4.440	1.410	**362**	**45**	is23-st1-1
7	0.127	0.433	5.820	1.350	**415**	**38**	is23-st1-2
8	0.062	0.355	2.020	1.540	**463**	**77**	is23-st1-3
9	0.133	0.436	6.320	1.440	**404**	**35**	is23-st2-1

No.	PbO	UO_2	ThO_2	Y_2O_3	Age (Ma)	Error (2σ)	Comments
10	0.073	0.357	3.840	1.320	**343**	**51**	is71-m-1-1
11	0.119	1.121	3.040	2.020	**365**	**40**	is71-m-2-1
12	0.093	0.895	2.920	1.800	**322**	**44**	is71-m-2-2
13	0.103	0.933	3.110	1.860	**339**	**42**	is71-m-2-3
14	0.093	0.772	2.730	1.920	**356**	**49**	is71-m-2-4
15	0.094	0.843	2.990	1.560	**337**	**45**	is71-m-2-5
16	0.093	0.345	4.500	1.310	**389**	**47**	is71-m-3-1
17	0.143	0.383	8.330	1.320	**352**	**29**	is71-m-4-1
18	0.148	0.400	7.960	1.420	**377**	**30**	is71-m-4-2
19	0.143	0.378	7.470	1.500	**388**	**32**	is71-m-4-3
20	0.162	0.352	9.240	1.300	**368**	**27**	is71-m-4-4
21	0.155	0.330	8.540	1.268	**382**	**30**	is71-m-4-5
22	0.071	0.350	3.920	1.370	**334**	**49**	is71-m-5-3
23	0.080	0.342	3.760	1.400	**388**	**53**	is71-m-6-1
24	0.053	0.266	2.820	1.205	**339**	**66**	is71-m-7-1
25	0.063	0.408	2.930	1.370	**349**	**58**	is71-m-8-1
26	0.071	0.411	3.230	1.340	**366**	**57**	is71-m-8-2
27	0.063	0.288	3.400	1.270	**345**	**58**	is71-m-9-1
28	0.063	0.252	3.770	1.196	**324**	**54**	is71-m-9-2
29	0.086	0.362	4.120	1.350	**385**	**50**	is71-m-9-3
30	0.064	0.304	3.560	1.244	**333**	**54**	is71-m-9-4
31	0.064	0.264	2.780	1.230	**414**	**71**	is71-m-9-5
32	0.053	0.271	2.710	1.246	**349**	**68**	is71-m-9-6
33	0.071	0.264	3.670	1.168	**372**	**56**	is71-m-10-1
34	0.123	0.304	6.960	1.340	**365**	**34**	is71-m-10-2
35	0.070	0.387	3.520	1.410	**346**	**52**	is71-m-11-1
36	0.114	0.323	6.340	1.320	**366**	**37**	is71-st1-1
37	0.078	0.424	3.850	1.560	**353**	**49**	is71-st1-2
38	0.047	0.382	2.070	1.430	**333**	**71**	is71-st1-3
39	0.087	0.501	4.630	1.620	**329**	**40**	is71-st1-4
40	0.078	0.300	4.150	1.310	**360**	**50**	is71-st1-5
41	0.062	0.290	3.140	1.270	**365**	**35**	is71-st2-1
42	0.089	0.308	4.540	1.266	**295**	**59**	is71-st2-2
43	0.100	0.363	5.430	1.223	**321**	**46**	is71-st2-3
44	0.085	0.321	3.810	1.290	**357**	**36**	is71-st2-4
45	0.077	0.405	3.470	1.300	**355**	**54**	is71-st2-5
46	0.124	0.328	5.870	1.390	**319**	**53**	is71-st2-6
47	0.148	0.379	6.830	1.430	**369**	**39**	is71-st2-7
48	0.062	0.383	2.570	1.320	**383**	**35**	is71-st2-8
49	0.113	0.294	5.310	1.247	**318**	**64**	is71-st2-9
50	0.085	0.292	3.910	1.234	**373**	**44**	is71-st2-10
51	0.137	0.370	5.620	1.460	**353**	**54**	is71-st2-11
52	0.091	0.437	3.240	1.550	**379**	**65**	is71-st3-1
53	0.094	0.502	3.130	1.480	**396**	**56**	is71-st3-2
54	0.111	0.495	4.850	1.350	**405**	**56**	is71-st3-3
55	0.099	0.499	3.830	1.490	**353**	**41**	is71-st3-4
56	0.085	0.472	3.620	1.500	**368**	**48**	is71-st4-1
57	0.073	0.403	3.240	1.400	**329**	**48**	is71-st4-2
58	0.079	0.411	3.500	1.460	**318**	**54**	is71-st4-3
59	0.071	0.411	3.590	1.460	**324**	**50**	is71-st4-4
60	0.099	0.438	4.430	1.430	**347**	**55**	is71-st4-5
61	0.099	0.423	3.730	1.570	**397**	**46**	is71-st4-6
62	0.076	0.460	2.590	1.450	**392**	**51**	is71-st5-1
63	0.083	0.422	2.890	1.480	**372**	**62**	is71-st5-2
64	0.069	0.441	2.550	1.440	**390**	**60**	is71-st5-3
65	0.071	0.488	2.780	1.460	**339**	**61**	is71-st5-4
66	0.061	0.426	1.820	1.370	**322**	**57**	is71-st5-5
67	0.068	0.450	2.040	1.350	**341**	**57**	is71-st5-6
68	0.082	0.431	3.560	1.330	**389**	**72**	is71-st5-7
69	0.102	0.450	4.840	1.280	**334**	**52**	is71-st5-8
70	0.113	0.423	5.820	1.280	**331**	**41**	is71-st5-9
71	0.094	0.368	4.000	1.251	**322**	**36**	is71-st5-10
72	0.094	0.394	4.500	1.264	**369**	**51**	is71-st5-11
73	0.111	0.343	5.260	1.241	**328**	**45**	is71-st5-12
74	0.131	0.519	6.620	1.470	**359**	**42**	is71-st5-13
75	0.121	0.615	5.330	1.620	**322**	**32**	is71-st5-14
76	0.097	0.669	3.700	1.600	**339**	**36**	is71-st5-15
77	0.146	0.578	6.550	1.540	**335**	**44**	is71-st5-16
78	0.135	0.417	6.940	1.360	**360**	**33**	is71-st5-17
79	0.104	0.377	4.960	1.390	**336**	**33**	is71-st5-18
80	0.101	0.344	4.850	1.320	**341**	**43**	is71-st5-19
81	0.140	0.517	6.610	1.490	**343**	**44**	is71-st5-20
82	0.124	0.617	4.660	1.630	**350**	**33**	is71-st5-21
83	0.109	0.706	4.190	1.600	**384**	**40**	is71-st5-22
84	0.059	0.353	2.640	1.320	**342**	**40**	is71-st5-23
85	0.084	0.345	4.050	1.300	**297**	**63**	is71-st5-24
86	0.090	0.304	4.730	1.215	**327**	**49**	is71-st5-25
87	0.080	0.340	3.790	1.268	**316**	**44**	is71-st5-26
88	0.126	0.370	6.550	1.340	**329**	**52**	is71-st5-27
89	0.127	0.377	6.430	1.204	**335**	**35**	is71-st5-28
90	0.080	0.401	3.110	1.390	**344**	**35**	is71-st5-29
91	0.066	0.368	2.910	1.350	**365**	**57**	is71-st5-30
92	0.108	0.407	4.520	1.400	**315**	**59**	is71-st5-31
93	0.085	0.431	3.180	1.430	**379**	**46**	is71-st5-32
94	0.091	0.447	4.050	1.410	**376**	**56**	is71-st5-33
95	0.100	0.430	4.010	1.310	**335**	**47**	is71-st5-34
96	0.074	0.422	3.520	1.270	**379**	**49**	is71-st5-35
97	0.077	0.434	3.150	1.340	**365**	**63**	is71-st5-36
98	0.073	0.429	2.640	1.370	**340**	**55**	is71-st5-37
99	0.053	0.445	2.180	1.350	**359**	**63**	is71-st5-38
100	0.077	0.451	2.860	1.360	**351**	**84**	is71-st6-1
101	0.090	0.504	2.950	1.460	**359**	**59**	is71-st6-2
102	0.092	0.546	2.880	1.590	**402**	**57**	is71-st6-3
103	0.065	0.452	2.700	1.410	**400**	**56**	is71-st6-4
104	0.073	0.484	2.860	1.470	**306**	**58**	is71-st6-5
105	0.086	0.519	3.200	1.540	**325**	**56**	is71-st6-6
106	0.098	0.526	3.880	1.078	**354**	**53**	is71-st6-7
107	0.135	0.356	7.030	1.192	**368**	**48**	is71-st6-8
108	0.108	0.266	5.650	1.153	**343**	**33**	is71-st6-9
109	0.159	0.419	8.070	1.360	**339**	**40**	is71-st6-10

No.	PbO	UO_2	ThO_2	Y_2O_3	Age (Ma)	Error (2σ)	Comments
110	0.169	0.434	8.080	1.400	**352**	**30**	is71-st6-11
111	0.129	0.383	5.980	1.350	**372**	**30**	is71-st6-12
112	0.100	0.440	4.550	1.310	**371**	**38**	is71-st6-13

No.	PbO	UO_2	ThO_2	Y_2O_3	Age (Ma)	Error (2σ)	Comments
113	0.053	0.350	2.190	1.480	**373**	**73**	is74-m-1-1
114	0.067	0.467	2.580	1.720	**385**	**61**	is74-m-1-2
115	0.050	0.352	2.170	1.420	**355**	**72**	is74-m-1-3
116	0.065	0.378	3.000	1.450	**365**	**59**	is74-m-1-4
117	0.048	0.349	2.420	1.430	**322**	**67**	is74-m-1-5
118	0.054	0.360	2.200	1.340	**380**	**73**	is74-m-1-6
119	0.070	0.339	2.800	1.330	**424**	**67**	is74-m-1-7
120	0.063	0.400	3.220	1.253	**331**	**55**	is74-m-1-8
121	0.093	0.593	4.270	1.510	**353**	**42**	is74-m-1-9
122	0.070	0.487	3.210	1.610	**347**	**52**	is74-m-1-10
123	0.044	0.353	2.060	1.410	**324**	**72**	is74-m-1-11
124	0.076	0.402	3.230	1.310	**395**	**57**	is74-m-1-12
125	0.046	0.426	1.850	1.580	**337**	**73**	is74-m-2-1
126	0.077	0.440	3.970	1.420	**339**	**48**	is74-m-2-2
127	0.058	0.348	2.530	1.400	**376**	**67**	is74-m-3-1
128	0.089	0.505	3.810	1.700	**386**	**48**	is74-m-3-2
129	0.059	0.390	2.890	1.620	**335**	**59**	is74-m-3-3
130	0.086	0.732	2.710	1.840	**397**	**51**	is74-m-4-1
131	0.059	0.444	2.630	1.420	**344**	**60**	is74-m-5-1
132	0.072	0.396	3.340	1.650	**365**	**54**	is74-m-6-1
133	0.071	0.418	3.710	1.370	**331**	**49**	is74-m-6-2
134	0.080	0.394	3.590	1.162	**388**	**54**	is74-m-6-3
135	0.070	0.409	3.210	1.254	**363**	**56**	is74-m-6-4
136	0.092	0.525	4.420	1.300	**355**	**43**	is74-m-6-5
137	0.127	0.459	6.750	0.956	**364**	**34**	is74-m-6-6
138	0.108	0.908	4.170	1.610	**359**	**38**	is74-m-6-7
139	0.044	0.307	2.210	1.219	**322**	**75**	is74-m-7-1
140	0.069	0.430	3.720	1.350	**320**	**49**	is74-m-7-2
141	0.070	0.483	3.120	1.500	**352**	**53**	is74-m-8-1
142	0.124	0.980	4.450	1.650	**384**	**36**	is74-m-8-2
143	0.068	0.426	2.900	1.350	**376**	**60**	is74-m-8-3
144	0.156	0.836	7.330	2.190	**366**	**28**	is74-st1-1
145	0.089	0.424	4.720	1.650	**346**	**43**	is74-st1-2
146	0.069	0.374	3.160	1.530	**372**	**58**	is74-st2-1
147	0.076	0.428	3.470	1.630	**368**	**52**	is74-st3-1
148	0.175	0.638	8.790	1.830	**381**	**27**	is74-st4-1
149	0.110	0.426	5.030	1.470	**405**	**42**	is74-st5-1
150	0.087	0.378	4.210	1.610	**378**	**48**	is74-st5-2
151	0.141	0.471	7.590	1.600	**365**	**30**	is74-st5-3
152	0.055	0.337	2.830	1.310	**332**	**62**	is74-st6-1

No.	PbO	UO_2	ThO_2	Y_2O_3	Age (Ma)	Error (2σ)	Comments
153	0.105	0.486	3.930	1.280	**447**	**50**	is77-m-1-1
154	0.110	0.271	5.460	1.450	**410**	**43**	is77-m-2-1
155	0.168	0.324	9.110	1.380	**390**	**29**	is77-m-3-1
156	0.202	0.304	10.590	1.530	**412**	**26**	is77-m-4-1
157	0.250	0.336	13.130	1.350	**414**	**22**	is77-m-5-1
158	0.100	0.293	5.190	1.410	**384**	**43**	is77-st1-1
159	0.089	0.270	4.130	1.450	**419**	**52**	is77-st2-1
160	0.100	0.265	4.830	1.470	**414**	**47**	is77-st2-2
161	0.179	0.284	9.280	1.390	**413**	**29**	is77-st3-1
162	0.184	0.344	9.080	1.460	**425**	**29**	is77-st4-1
163	0.088	0.278	4.070	1.370	**415**	**54**	is77-st5-1
164	0.133	0.267	7.140	1.420	**393**	**35**	is77-st5-2
165	0.225	0.321	11.750	1.222	**415**	**24**	is77-st5-3
166	0.145	0.340	7.410	1.129	**401**	**33**	is77-st5-4
167	0.092	0.287	4.960	1.310	**368**	**45**	is77-st6-1
168	0.196	0.360	10.160	1.500	**408**	**26**	is77-st7-1
169	0.038	0.116	1.720	1.350	**425**	**114**	is77-st8-1

No.	PbO	UO_2	ThO_2	Y_2O_3	Age (Ma)	Error (2σ)	Comments
170	0.191	0.437	10.860	1.400	**367**	**23**	is88-m-1-1
171	0.098	0.382	4.590	1.270	**396**	**45**	is88-m-2-1
172	0.104	0.737	4.530	1.340	**355**	**38**	is88-m-3-1
173	0.255	0.515	14.340	1.460	**376**	**19**	is88-m-3-2
174	0.051	0.372	1.990	1.216	**375**	**74**	is88-m-4-1
175	0.134	0.400	6.950	1.310	**384**	**33**	is88-m-4-2
176	0.056	0.370	1.940	1.270	**419**	**79**	is88-m-5-1
177	0.150	0.476	8.410	1.400	**355**	**27**	is88-m-6-1
178	0.159	0.491	8.650	1.380	**367**	**27**	is88-m-6-2
179	0.143	0.378	7.480	1.320	**389**	**32**	is88-st1-1
180	0.175	0.446	9.250	1.320	**386**	**26**	is88-st1-2
181	0.175	0.463	9.460	1.320	**377**	**26**	is88-st2-1
182	0.156	0.438	8.400	1.320	**374**	**28**	is88-st2-2
183	0.136	0.437	6.700	1.310	**394**	**34**	is88-st2-3
184	0.117	0.422	5.820	1.300	**382**	**37**	is88-st3-1
185	0.197	0.459	10.430	1.290	**390**	**24**	is88-st4-1
186	0.173	0.418	8.870	1.390	**400**	**28**	is88-st4-2
187	0.122	0.384	6.520	1.290	**370**	**34**	is88-st4-3

No.	PbO	UO_2	ThO_2	Y_2O_3	Age (Ma)	Error (2σ)	Comments
188	0.087	0.682	2.990	1.440	**392**	**49**	is94-m-1-1
189	0.082	0.604	3.200	1.248	**374**	**50**	is94-m-1-2
190	0.089	0.542	3.650	0.947	**389**	**48**	is94-m-1-3
191	0.105	0.512	4.960	0.532	**374**	**41**	is94-m-1-4
192	0.098	0.493	4.970	0.406	**351**	**41**	is94-m-1-5
193	0.120	0.559	5.770	0.466	**374**	**36**	is94-m-1-6
194	0.077	0.398	3.930	0.575	**350**	**49**	is94-m-1-7
195	0.068	0.348	3.440	0.492	**354**	**56**	is94-m-1-8
196	0.088	0.457	4.200	0.633	**364**	**47**	is94-m-1-9
197	0.093	0.448	4.350	0.516	**376**	**46**	is94-m-1-10
198	0.073	0.361	3.120	0.639	**404**	**62**	is94-m-1-11
199	0.096	0.432	4.180	0.392	**403**	**48**	is94-m-1-12
200	0.109	0.500	4.860	0.454	**397**	**42**	is94-m-1-13
201	0.090	0.393	4.410	0.559	**372**	**48**	is94-m-1-14
202	0.085	0.508	4.540	0.501	**324**	**42**	is94-m-1-15
203	0.076	0.445	3.610	0.617	**355**	**51**	is94-m-1-16
204	0.065	0.390	2.690	0.751	**385**	**64**	is94-m-1-17
205	0.061	0.377	2.560	0.745	**379**	**67**	is94-m-1-18
206	0.059	0.345	2.610	0.702	**372**	**67**	is94-m-1-19
207	0.065	0.338	3.460	0.465	**339**	**56**	is94-m-1-20
208	0.064	0.353	3.200	0.373	**346**	**60**	is94-m-1-21
209	0.082	0.375	3.880	0.244	**379**	**52**	is94-m-1-22
210	0.062	0.332	2.410	0.645	**419**	**74**	is94-m-1-23

No.	PbO	UO_2	ThO_2	Y_2O_3	Age (Ma)	Error (2σ)	Comments
211	0.074	0.393	3.680	0.382	**353**	**53**	is94-m-1-24
212	0.082	0.380	4.270	0.310	**353**	**48**	is94-m-1-25
213	0.083	0.423	4.030	0.251	**363**	**49**	is94-m-1-26
214	0.080	0.410	3.370	0.666	**399**	**56**	is94-m-1-27
215	0.082	0.445	4.130	0.414	**347**	**48**	is94-m-1-28
216	0.106	0.542	5.190	0.475	**359**	**39**	is94-m-1-29
217	0.124	0.571	6.160	0.420	**366**	**35**	is94-m-1-30
218	0.086	0.386	4.040	0.377	**381**	**51**	is94-m-1-31
219	0.090	0.487	4.130	0.333	**374**	**47**	is94-m-1-32
220	0.104	0.584	4.650	0.847	**373**	**41**	is94-m-2-1
221	0.053	0.359	2.650	0.616	**329**	**65**	is94-m-2-2
222	0.066	0.435	2.840	0.781	**364**	**60**	is94-m-2-3
223	0.065	0.489	2.880	0.904	**345**	**56**	is94-m-2-4
224	0.063	0.444	3.190	0.784	**320**	**54**	is94-m-2-5
225	0.073	0.408	3.260	0.692	**376**	**56**	is94-m-2-6
226	0.062	0.377	3.090	1.034	**338**	**57**	is94-m-2-7
227	0.129	0.433	6.420	0.334	**387**	**36**	is94-m-2-8
228	0.098	0.432	5.190	0.432	**350**	**40**	is94-m-2-9
229	0.095	0.509	4.880	0.588	**344**	**40**	is94-m-2-10
230	0.080	0.423	3.810	0.492	**365**	**51**	is94-m-2-11
231	0.087	0.442	3.730	0.755	**396**	**51**	is94-m-2-12
232	0.113	0.523	5.030	0.669	**395**	**41**	is94-m-2-13
233	0.100	0.534	5.370	0.525	**334**	**37**	is94-m-2-14
234	0.120	0.528	5.220	0.447	**407**	**40**	is94-m-2-15
235	0.108	0.612	5.140	0.667	**358**	**38**	is94-m-2-16
236	0.108	0.563	5.020	0.627	**372**	**40**	is94-m-2-17
237	0.115	0.577	5.280	0.692	**378**	**38**	is94-m-2-18
238	0.117	0.526	5.350	0.420	**391**	**39**	is94-m-2-19
239	0.096	0.516	4.810	0.485	**348**	**41**	is94-m-2-20
240	0.112	0.507	5.330	0.514	**380**	**39**	is94-m-2-21
241	0.084	0.389	4.070	0.325	**370**	**51**	is94-m-2-22
242	0.110	0.583	5.280	0.436	**363**	**38**	is94-m-2-23
243	0.117	0.544	5.460	0.432	**383**	**38**	is94-m-2-24
244	0.132	0.594	6.250	0.369	**380**	**34**	is94-m-2-25
245	0.125	0.448	6.040	0.338	**394**	**37**	is94-m-2-26
246	0.154	0.420	8.090	0.062	**385**	**30**	is94-m-3-1
247	0.164	0.450	8.610	0.086	**385**	**28**	is94-m-3-2
248	0.101	0.437	4.880	0.105	**378**	**43**	is94-m-3-3
249	0.092	0.415	4.690	0.131	**359**	**45**	is94-m-3-4
250	0.106	0.397	5.300	0.101	**379**	**42**	is94-m-3-5
251	0.130	0.412	6.300	0.095	**401**	**37**	is94-m-3-6
252	0.084	0.380	4.140	0.115	**371**	**50**	is94-m-3-7
253	0.185	0.441	9.410	0.065	**402**	**27**	is94-m-3-8
254	0.058	0.365	2.510	0.808	**372**	**68**	is94-st1-1
255	0.072	0.426	3.340	0.767	**359**	**55**	is94-st1-2
256	0.082	0.429	3.740	0.647	**378**	**51**	is94-st1-3
257	0.129	0.585	6.160	0.428	**378**	**35**	is94-st1-4
258	0.089	0.429	4.320	0.502	**369**	**48**	is94-st1-5
259	0.104	0.513	5.120	0.635	**361**	**41**	is94-st1-6
260	0.067	0.377	2.980	0.797	**375**	**63**	is94-st1-7
261	0.071	0.389	3.580	0.751	**344**	**54**	is94-st2-1
262	0.089	0.366	4.160	0.735	**392**	**51**	is94-st2-2
263	0.073	0.322	3.690	0.744	**362**	**56**	is94-st2-3
264	0.092	0.330	4.290	0.756	**406**	**51**	is94-st2-4
265	0.055	0.183	2.660	0.928	**396**	**79**	is94-st2-5
266	0.032	0.094	1.990	0.982	**325**	**99**	is94-st2-6
267	0.051	0.165	3.080	0.970	**334**	**67**	is94-st3-1
268	0.065	0.242	3.380	1.170	**367**	**61**	is94-st3-2
269	0.060	0.284	2.990	1.040	**365**	**66**	is94-st3-3
270	0.052	0.231	2.470	1.123	**381**	**78**	is94-st3-4
271	0.032	0.145	1.680	0.853	**354**	**109**	is94-st3-5
272	0.044	0.175	2.240	0.874	**373**	**87**	is94-st3-6
273	0.054	0.122	2.570	1.320	**427**	**83**	is94-st3-7
274	0.068	0.354	2.860	0.770	**401**	**67**	is94-st3-8
275	0.108	0.507	4.730	0.932	**401**	**43**	is94-st3-9
276	0.068	0.331	3.040	0.816	**391**	**65**	is94-st3-10
277	0.086	0.340	4.640	0.597	**355**	**47**	is94-st3-11
278	0.078	0.303	4.220	0.530	**352**	**52**	is94-st3-12
279	0.084	0.303	4.210	0.438	**379**	**53**	is94-st3-13
280	0.116	0.346	5.680	0.353	**402**	**42**	is94-st3-14
281	0.138	0.514	6.920	0.681	**378**	**34**	is94-st3-15
282	0.091	0.366	4.760	0.582	**360**	**46**	is94-st3-16
283	0.085	0.371	4.150	0.864	**375**	**50**	is94-st3-17
284	0.083	0.356	3.660	0.795	**406**	**56**	is94-st3-18
285	0.105	0.387	5.540	0.371	**364**	**41**	is94-st4-1
286	0.083	0.310	3.850	0.577	**401**	**56**	is94-st4-2
287	0.047	0.232	2.540	1.072	**336**	**74**	is94-st4-3
288	0.033	0.103	1.980	0.914	**338**	**101**	is94-st4-4
289	0.074	0.419	3.990	1.470	**329**	**47**	is94-st4-5
290	0.055	0.213	2.660	1.100	**387**	**75**	is94-st4-6
291	0.054	0.293	2.690	0.850	**348**	**70**	is94-st4-7
292	0.071	0.367	3.000	0.837	**399**	**63**	is94-st4-8

No.	PbO	UO_2	ThO_2	Y_2O_3	Age (Ma)	Error (2σ)	Comments
293	0.060	0.759	0.505	1.920	**385**	**81**	is95-st1-1
294	0.066	0.808	0.739	1.740	**391**	**73**	is95-st1-2
295	0.071	0.461	1.870	1.221	**434**	**78**	is95-st2-1
296	0.155	0.819	6.700	0.726	**358**	**31**	is95-st2-2
297	0.125	0.788	4.790	0.988	**362**	**38**	is95-st2-3
298	0.084	0.380	3.440	1.240	**367**	**56**	is95-st2-4
299	0.115	0.558	4.400	1.460	**382**	**44**	is95-st2-5
300	0.115	0.536	4.970	1.500	**352**	**40**	is95-st2-6
301	0.105	0.431	4.120	1.360	**391**	**48**	is95-st2-7
302	0.083	0.758	1.500	1.790	**421**	**65**	is95-st3-1
303	0.083	0.684	2.250	1.660	**375**	**58**	is95-st3-2
304	0.066	0.792	0.940	1.590	**375**	**71**	is95-st3-3
305	0.081	0.520	3.010	1.244	**352**	**55**	is95-st8-3-1
306	0.165	0.586	7.410	0.546	**384**	**32**	is95-st8-3-2
307	0.060	0.540	1.740	1.420	**338**	**72**	is95-st8-3-3
308	0.082	0.501	3.030	1.029	**364**	**58**	is95-st8-3-4
309	0.073	0.409	2.310	1.174	**409**	**73**	is95-st8-3-5
310	0.062	0.464	1.630	1.400	**393**	**81**	is95-st8-3-6
311	0.074	0.492	2.340	1.189	**386**	**67**	is95-st8-3-7
312	0.073	0.579	2.060	1.400	**374**	**66**	is95-st8-3-8
313	0.126	0.755	5.060	0.724	**361**	**38**	is95-st5-1
314	0.166	0.692	7.950	0.400	**353**	**29**	is95-st5-2
315	0.223	0.576	11.33	0.161	**369**	**24**	is95-st6-1
316	0.201	0.708	8.920	0.261	**394**	**27**	is95-st6-2
317	0.075	0.513	2.950	0.712	**345**	**59**	is95-st6-3
318	0.073	0.461	2.350	0.859	**401**	**70**	is95-st6-4
319	0.073	0.628	2.540	0.817	**333**	**59**	is95-st6-5

No.	PbO	UO_2	ThO_2	Y_2O_3	Age (Ma)	Error (2σ)	Comments
320	0.148	0.781	6.320	0.425	**364**	**33**	is95-st6-6
321	0.059	0.267	2.560	1.249	**356**	**46**	is95-st7-1
322	0.071	0.341	2.520	1.320	**389**	**72**	is95-st7-2
323	0.074	0.351	3.110	1.164	**351**	**62**	is95-st7-3
324	0.071	0.378	2.740	1.420	**355**	**64**	is95-st7-4
325	0.067	0.409	2.400	1.330	**359**	**67**	is95-st7-5
326	0.121	0.478	4.900	1.440	**390**	**42**	is95-st8-1-1
327	0.274	0.588	14.77	0.336	**356**	**19**	is95-st8-1-2
328	0.156	0.487	8.330	0.920	**332**	**28**	is95-st8-1-3
329	0.095	0.426	4.570	1.270	**324**	**43**	is95-st8-1-4
330	0.247	0.530	13.28	0.330	**356**	**21**	is95-st8-1-5
331	0.121	0.463	5.730	1.280	**347**	**37**	is95-st8-1-6
332	0.079	0.533	3.060	0.971	**343**	**55**	is95-st8-1-7
333	0.154	0.679	6.950	1.310	**355**	**31**	is95-st8-1-8
334	0.188	0.521	9.410	0.670	**364**	**26**	is95-st8-1-9
335	0.147	0.556	7.240	0.412	**351**	**32**	is95-st8-1-10
336	0.097	0.560	3.610	1.280	**368**	**49**	is95-st8-2-1
337	0.080	0.399	3.380	1.133	**349**	**55**	is95-st8-2-2
338	0.159	0.697	7.400	0.585	**355**	**30**	is95-st8-2-3
339	0.113	0.552	4.620	0.763	**376**	**43**	is95-st8-2-4
340	0.069	0.465	2.000	1.022	**405**	**75**	is95-st8-2-5
341	0.058	0.464	1.680	1.077	**372**	**78**	is95-st8-2-6
342	0.110	0.761	3.960	1.032	**364**	**43**	is95-st8-2-7
343	0.051	0.359	1.640	1.154	**354**	**87**	is95-st8-2-8
344	0.069	0.501	2.330	1.038	**358**	**65**	is95-st8-2-9
345	0.094	0.599	3.340	1.078	**370**	**51**	is95-st8-2-10
346	0.066	0.327	2.600	1.057	**366**	**70**	is95-st8-2-11
347	0.083	0.381	3.270	1.095	**381**	**58**	is95-st8-2-12
348	0.069	0.531	2.490	1.209	**329**	**59**	is95-st8-2-13

No.	PbO	UO_2	ThO_2	Y_2O_3	Age (Ma)	Error (2σ)	Comments
349	0.144	0.859	6.530	0.373	**365**	**32**	is104-m-1-1
350	0.083	0.768	3.540	0.601	**326**	**45**	is104-m-2-1
351	0.151	0.847	6.500	0.585	**384**	**32**	is104-m-3-1
352	0.080	0.612	3.530	1.330	**342**	**47**	is104-m-4-1
353	0.095	0.693	3.720	1.510	**375**	**44**	is104-m-5-1
354	0.097	1.199	2.250	0.963	**374**	**45**	is104-m-6-1
355	0.106	0.546	4.570	0.566	**395**	**44**	is104-m-7-1
356	0.091	0.969	2.220	1.219	**399**	**51**	is104-m-8-1
357	0.076	0.727	2.730	0.646	**354**	**53**	is104-m-9-1
358	0.075	0.565	3.530	0.360	**329**	**51**	is104-m-10-1
359	0.070	0.541	3.150	0.388	**339**	**55**	is104-m-10-2
360	0.119	1.191	3.960	1.053	**358**	**36**	is104-m-11-1
361	0.122	1.094	3.640	1.009	**399**	**40**	is104-m-11-2
362	0.075	1.058	1.980	1.330	**328**	**47**	is104-m-12-1
363	0.092	0.978	2.350	1.076	**392**	**49**	is104-m-12-2
364	0.049	0.395	2.350	0.587	**317**	**70**	is104-m-13-1
365	0.111	0.612	4.960	0.334	**376**	**41**	is104-m-14-1
366	0.087	0.515	4.340	0.276	**340**	**46**	is104-m-14-2
367	0.079	0.559	3.920	0.483	**326**	**47**	is104-m-15-1
368	0.058	0.463	2.910	0.476	**313**	**59**	is104-m-16-1
369	0.084	0.475	3.580	0.514	**388**	**53**	is104-m-16-2
370	0.113	0.601	5.640	0.512	**352**	**37**	is104-m-17-1
371	0.085	0.534	4.220	0.469	**337**	**46**	is104-m-17-2
372	0.103	0.514	5.030	0.527	**365**	**41**	is104-m-17-3
373	0.086	0.562	3.900	0.545	**354**	**48**	is104-m-17-4
374	0.097	0.672	3.710	1.550	**389**	**46**	is104-m-17-5
375	0.066	0.416	2.860	0.583	**369**	**63**	is104-m-17-6
376	0.079	0.595	3.770	1.015	**329**	**46**	is104-m-17-7
377	0.090	0.630	3.760	1.214	**367**	**46**	is104-m-17-8
378	0.128	0.647	6.010	0.529	**372**	**36**	is104-m-17-9
379	0.075	0.477	3.550	0.511	**347**	**53**	is104-m-17-10
380	0.118	0.638	5.470	0.529	**369**	**38**	is104-m-18-1
381	0.166	0.923	7.630	0.484	**368**	**28**	is104-m-18-2
382	0.202	0.939	9.500	0.256	**380**	**25**	is104-m-19-1
383	0.157	0.632	8.130	0.291	**364**	**29**	is104-m-20-1

Table 4. Monazite chemistry and calculated ages for every analytical spot.

Sample no.	Grain no.	Grain location	FIA	Yttrium statistics							Age (Ma)	
				Mean (%)	Std. error	Median	Mode	Stdev	Variance	Count	Grain	Location
IS23	is23-stx	core	3	1.435	0.040	1.425	N/A	0.079	0.006	4	403±22	403±22
IS71	is71-st1	core	5	1.448	0.062	1.430	N/A	0.140	0.019	5	350±20	350,6±5.2
	is71-st2			1.312	0.024	1.290	N/A	0.080	0.006	11	354±13	
	is71-st3			1.468	0.042	1.485	N/A	0.084	0.007	4	378±26	
	is71-st4			1.470	0.024	1.460	1.460	0.059	0.004	6	349±20	
	is71-st5			1.381	0.018	1.355	1.350	0.113	0.013	38	345,1±7.3	
	is71-st6			1.359	0.041	1.360	1.360	0.149	0.022	13	357±12	
IS74	is74-stx	crenulated cleavege	4	1.647	0.083	1.610	N/A	0.248	0.061	9	371±13	371±13
IS77	is77-st5	core	2	1.285	0.067	1.296	N/A	0.134	0.018	4	407±16	408±10
	is77-stx			1.418	0.023	1.430	N/A	0.065	0.004	8	408±13	
IS88	is88-stx	core	3	1.318	0.010	1.320	1.320	0.030	0.001	9	385±9.7	385±9.7
IS94	is94-st1	median	4	0.655	0.056	0.647	N/A	0.148	0.022	7	371±18	375.9±9.6
	is94-st2			0.816	0.045	0.754	N/A	0.109	0.012	6	376±24	
	is94-st3			0.817	0.061	0.835	N/A	0.258	0.067	18	378±13	
	is94-st4	rim	5	0.899	0.118	0.882	N/A	0.335	0.112	8	363±21	363±21
IS95	is95-st2	median	4	1.214	0.104	1.240	N/A	0.275	0.076	7	369±16	370.2±8
	is95-st8-3			1.175	0.102	1.216	1.400	0.289	0.083	8	376±20	
	is95-st6			0.539	0.121	0.568	N/A	0.298	0.089	6	373±14	
	is95-st7			1.296	0.043	1.320	N/A	0.096	0.009	5	360±27	
	is95-stx			1.403	0.224	1.660	N/A	0.591	0.350	7	368±18	
	is95-st8-1	rim	5	0.894	0.137	0.945	N/A	0.432	0.187	10	353.2±9.1	356.1±7.7
	is95-st8-2			1.040	0.051	1.077	N/A	0.182	0.033	13	363±14	

Table 5. Monazite grain ages, their microstructural location, and yttrium statistics for every grain analyzed from staurolite porphyroblasts.

Sample no.	Grain no.	Grain location	Yttrium statistics							Age (Ma)
			Mean (%)	Std. error	Median	Mode	Stdev	Variance	Count	
IS23	is23-m-x	N/A	1.386	0.022	1.410	N/A	0.048	0.002	5	393±23
IS71	is71-m-2	Crenulation cleavage	1.832	0.077	1.860	N/A	0.172	0.030	5	344±20
	is71-m-4	Crenulated cleavage	1.362	0.043	1.320	N/A	0.096	0.009	5	372±13
	is71-m-9	Crenulation cleavage	1.256	0.021	1.245	N/A	0.052	0.003	6	356±24
	is71-m-x	N/A	1.323	0.025	1.340	1.370	0.079	0.006	10	360±16
IS74	is74-m-1	Crenulation cleavage	1.439	0.038	1.425	N/A	0.131	0.017	12	361±17
	is74-m-6	Crenulated cleavage	1.329	0.092	1.300	N/A	0.244	0.060	7	360±17
	is74-m-x	N/A	1.504	0.051	1.460	1.420	0.177	0.031	12	360±15
IS77	is77-m-x	N/A	1.398	0.043	1.380	N/A	0.096	0.009	5	410±13
IS88	is88-m-x	N/A	1.338	0.026	1.340	1.400	0.079	0.006	9	371±10
IS94	is94-m-1	Crenulation cleavage	0.562	0.046	0.496	N/A	0.259	0.067	32	369.2±8.6
	is94-m-2	Crenulated cleavage	0.585	0.037	0.556	N/A	0.190	0.036	26	369.9±8.3
	is94-m-3	Crenulated cleavage	0.095	0.008	0.098	N/A	0.024	0.001	8	386±12
IS104	is104-m-17	Crenulation cleavage	0.745	0.120	0.537	N/A	0.378	0.143	10	358±14
	is104-m-x	N/A	0.690	0.075	0.566	1.330	0.377	0.142	25	365.1±8.1

Table 6. Monazite grain ages, their microstructural location, and yttrium statistics for every grain analyzed from the matrix.

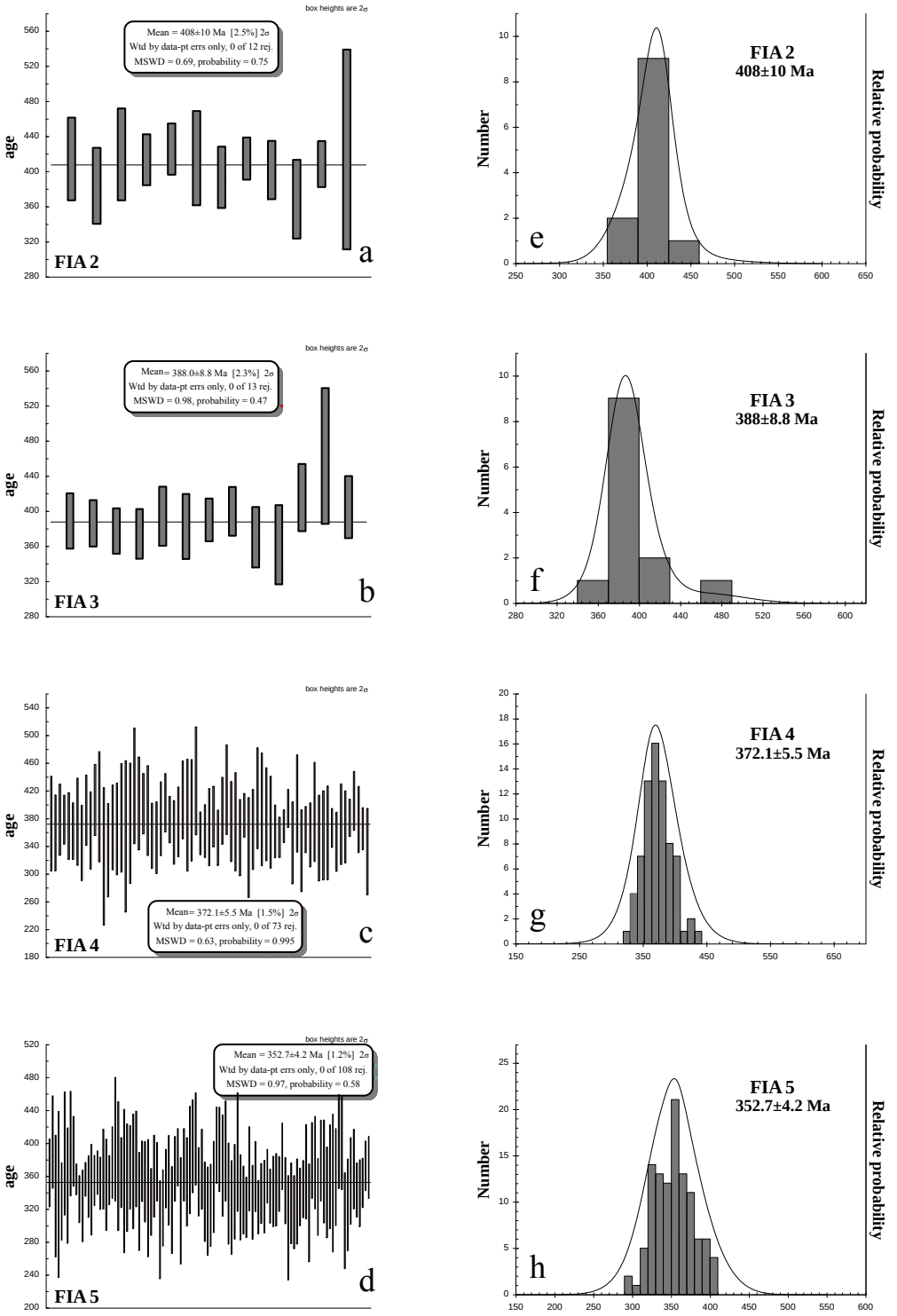

Figure 12. Probability diagrams and monazite ages for FIA set 2 (a and e), for FIA set 3 (b and f), for FIA set 4 (c and g), and for FIA set 5 (d and h).

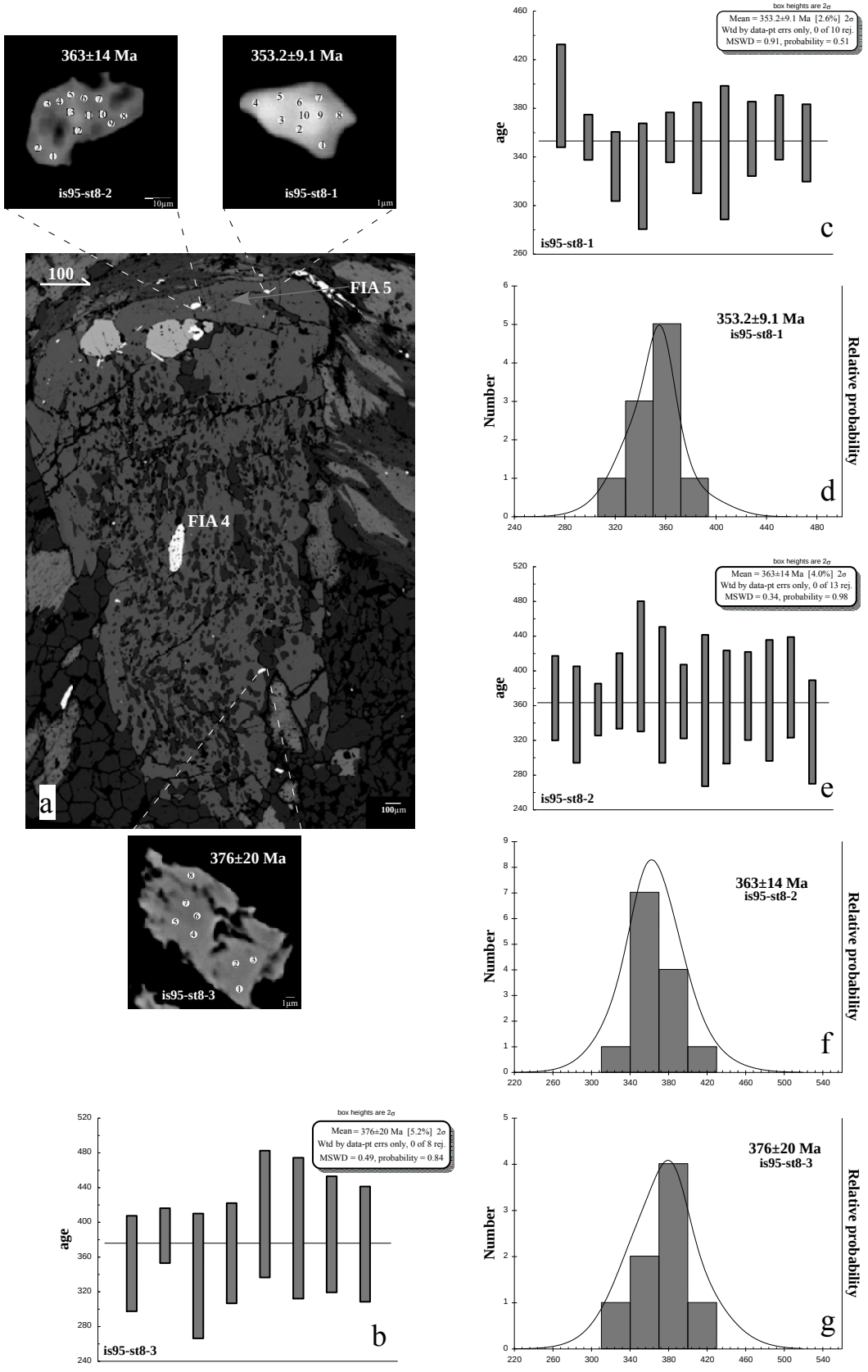

Figure 13. Back-scattered electron image (a) of a staurolite porphyroblast from sample IS95 which has a core containing FIA 4 and a rim overgrowth containing FIA5. The monazite grain from the core (b and g) is older than the monazite grains located in the rim (c, d, e, and f).

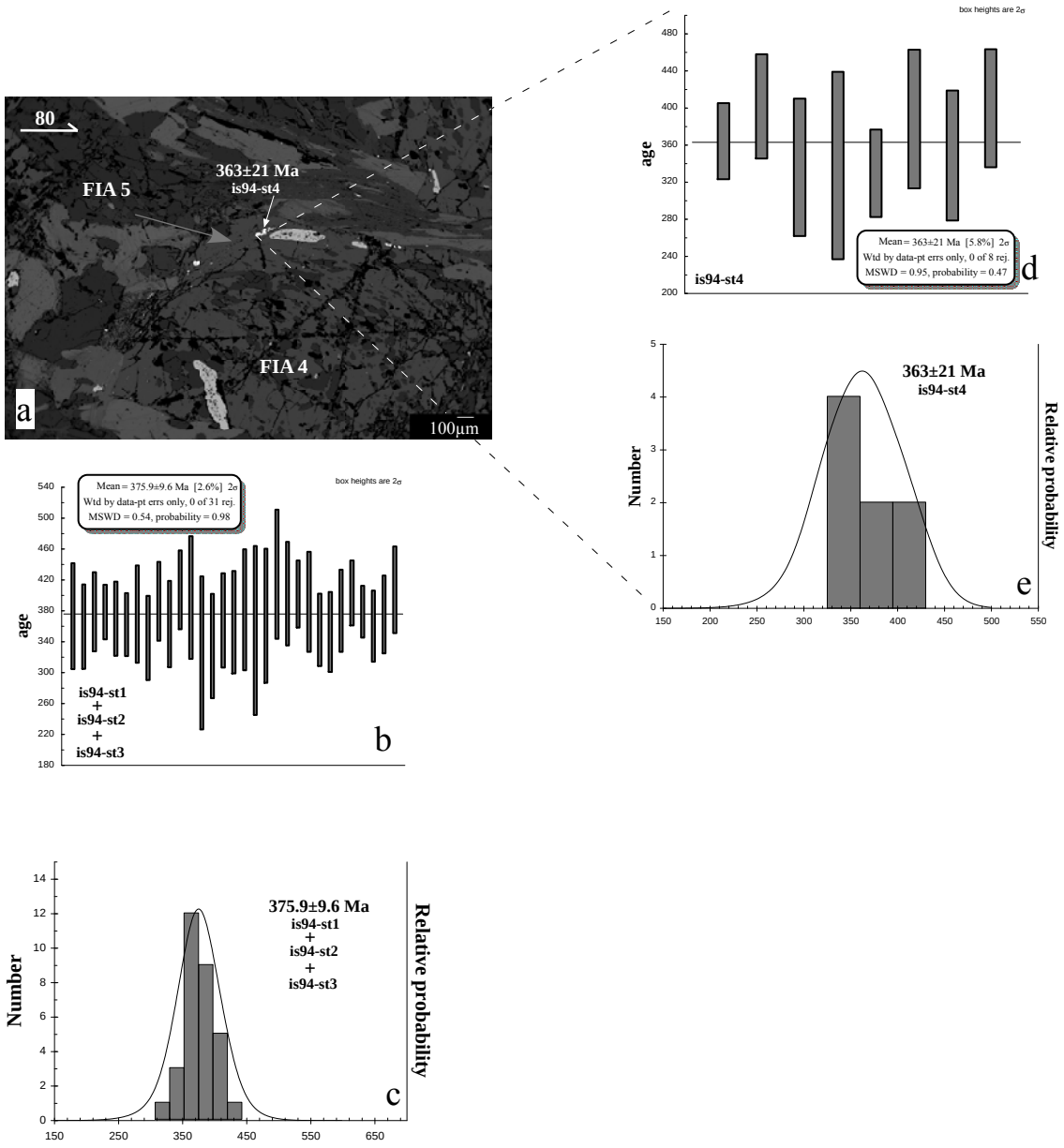

Figure 14. Back-scattered electron image (a) showing the location of the monazite grain is94-st4 from sample IS94 in the rim of a FIA 4 staurolite. The rim inclusion trails contain FIA 5. The age of the monazite grain (d and e) located in the FIA 5 rim is younger than the age of the monazite grains located in FIA 4 staurolites (b and c).

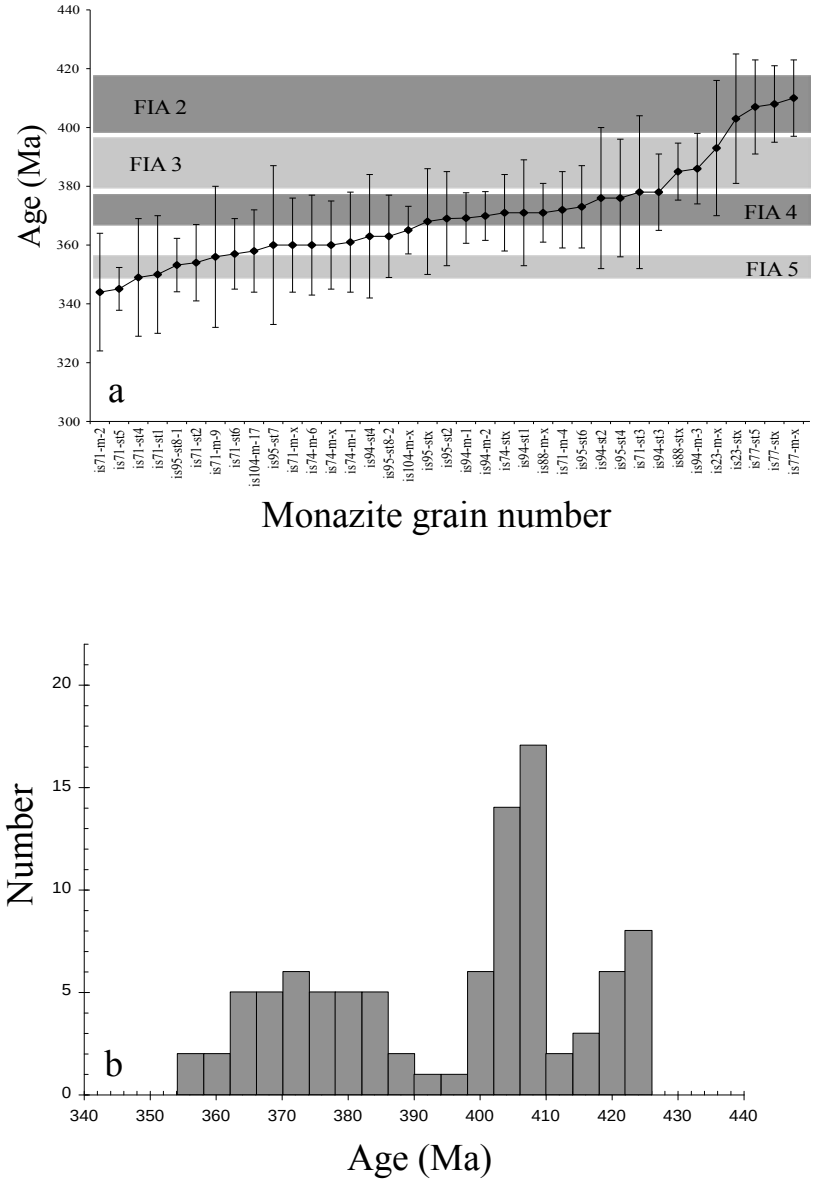

Figure 15. (a) Diagram showing the calculated ages and their errors for every monazite grain included in this study. (b) diagram showing the distribution of the crystallization ages for the plutons located in Maine and adjacent areas.

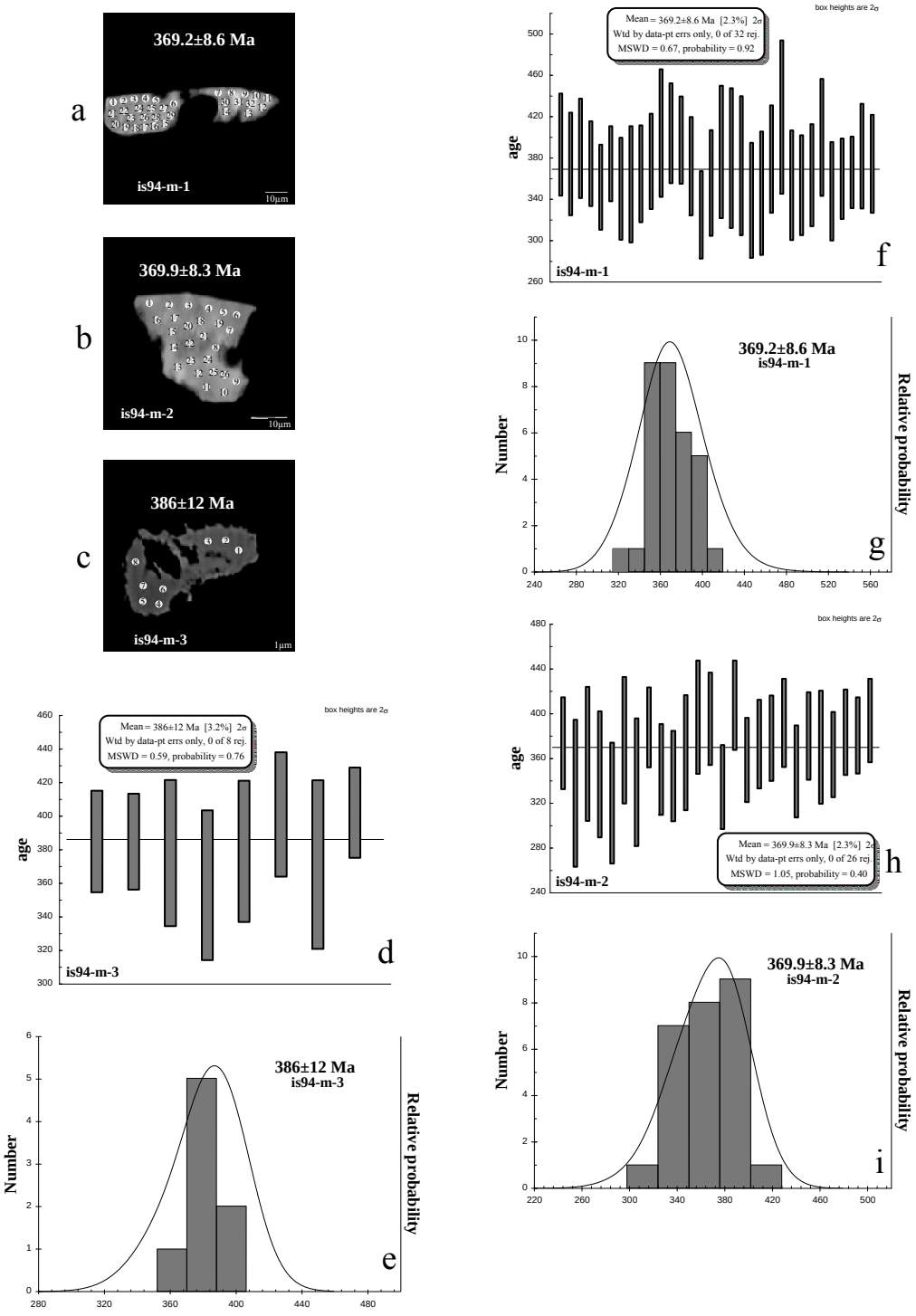

Figure 16. Back-scattered electron images of some of the matrix monazites and their apparent ages.

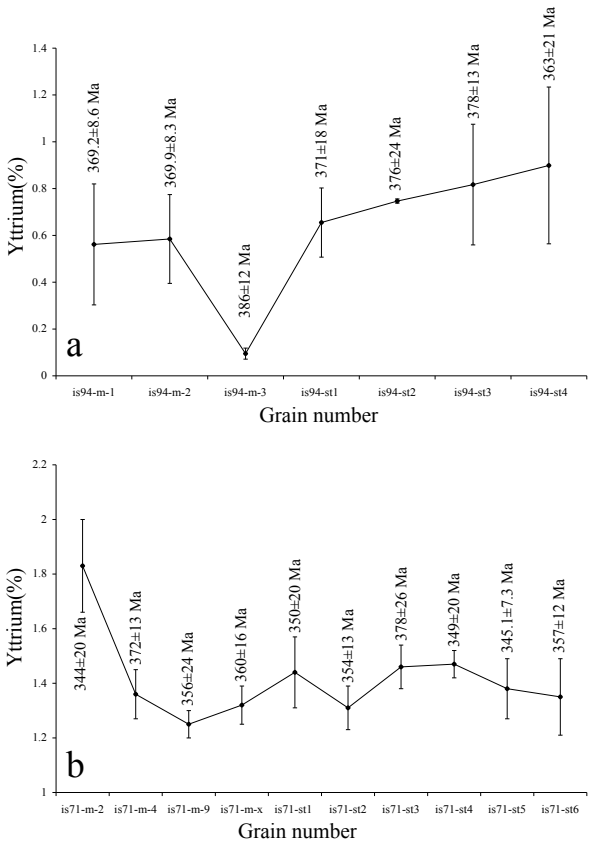

Figure 17. Diagrams showing the relationship between the yttrium content and the monazite grain ages from sample IS94 (a) and IS71 (b).

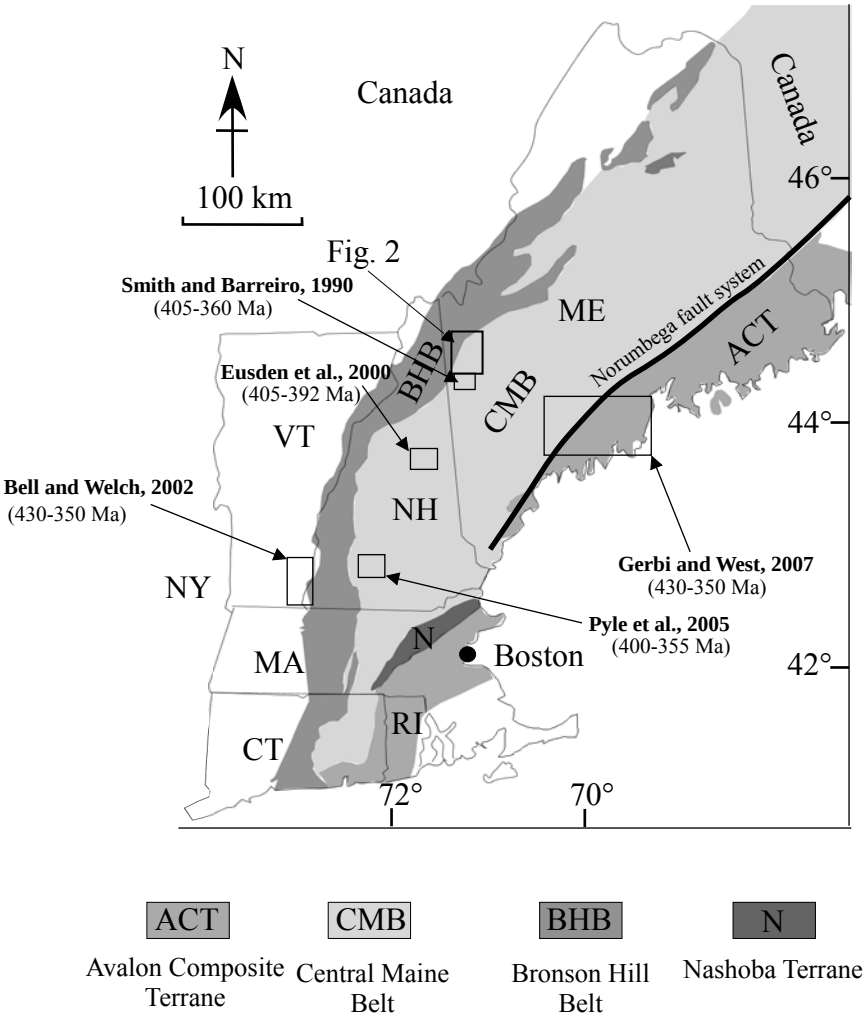

Figure 18. Simplified geological map of the New England showing the location of dated samples and the spread in monazite ages cited in this study.

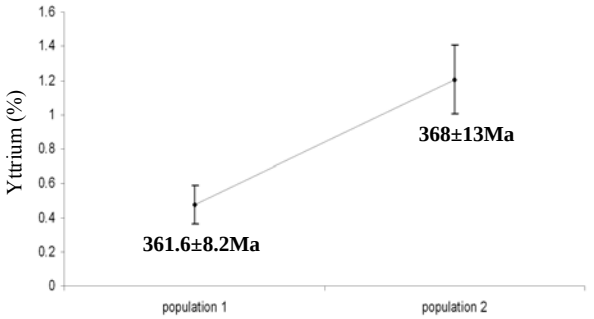

No.	average	standard error	median	mode	standard deviation	variance	count	Age (Ma)
population 1	0.48	0.02	0.51	N/A	0.11	0.01	24.00	361.6±8.2
population 2	1.21	0.06	1.21	1.33	0.20	0.04	11.00	368±13

Figure 19. Diagram showing the realationship between the yttrium content and monazite ages for sample IS104.

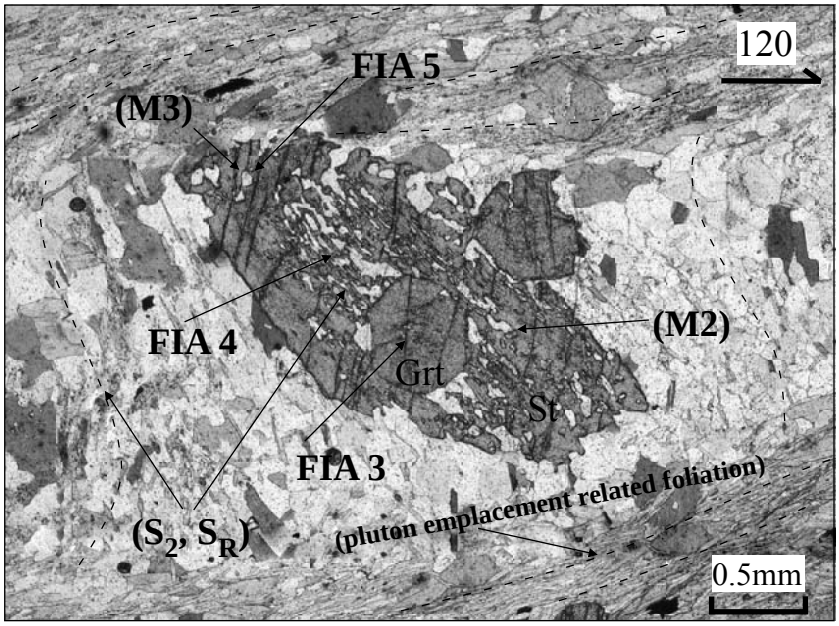

Figure 20. Photomicrograph showing typical microstructural relationships between garnet, staurolite and, matrix from the contact aureole of the Mooselookmeguntic pluton. Note that the inclusion trails in the garnet porphyroblast are restricted to the core of the garnet, and they are oblique to the inclusion trails from the staurolite core. This suggests that the garnet growth occurred in an earlier event compared to that in the core of the staurolite. See text for more details.

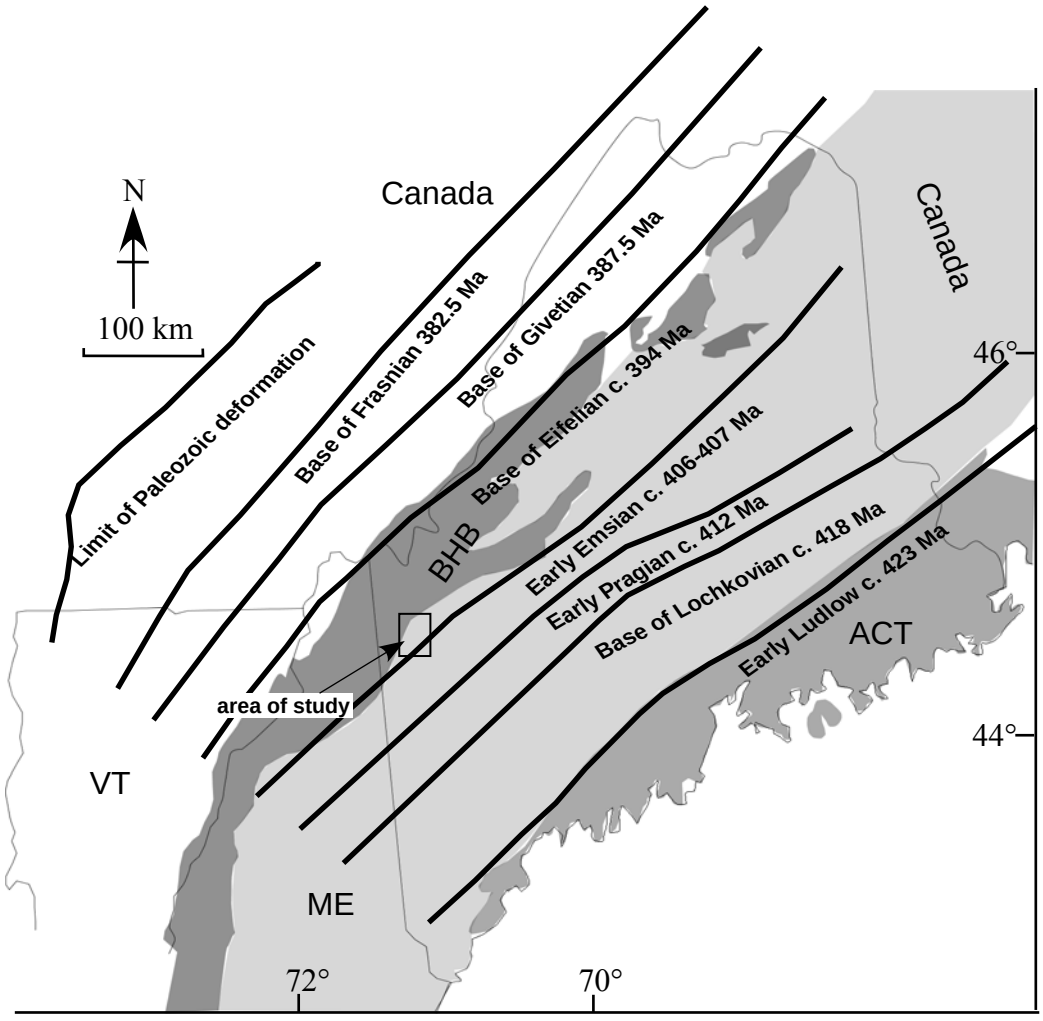

Figure 21. Simplified geological map of Maine and adjacent areas showing location of the orogenic front after Bradley et al., (1998) and location of the study area.

– SECTION C –

THE PROBLEM, SIGNIFICANCE, AND METAMORPHIC IMPLICATIONS OF 60 MILLION YEARS OF POLYPHASE STAUROLITE GROWTH

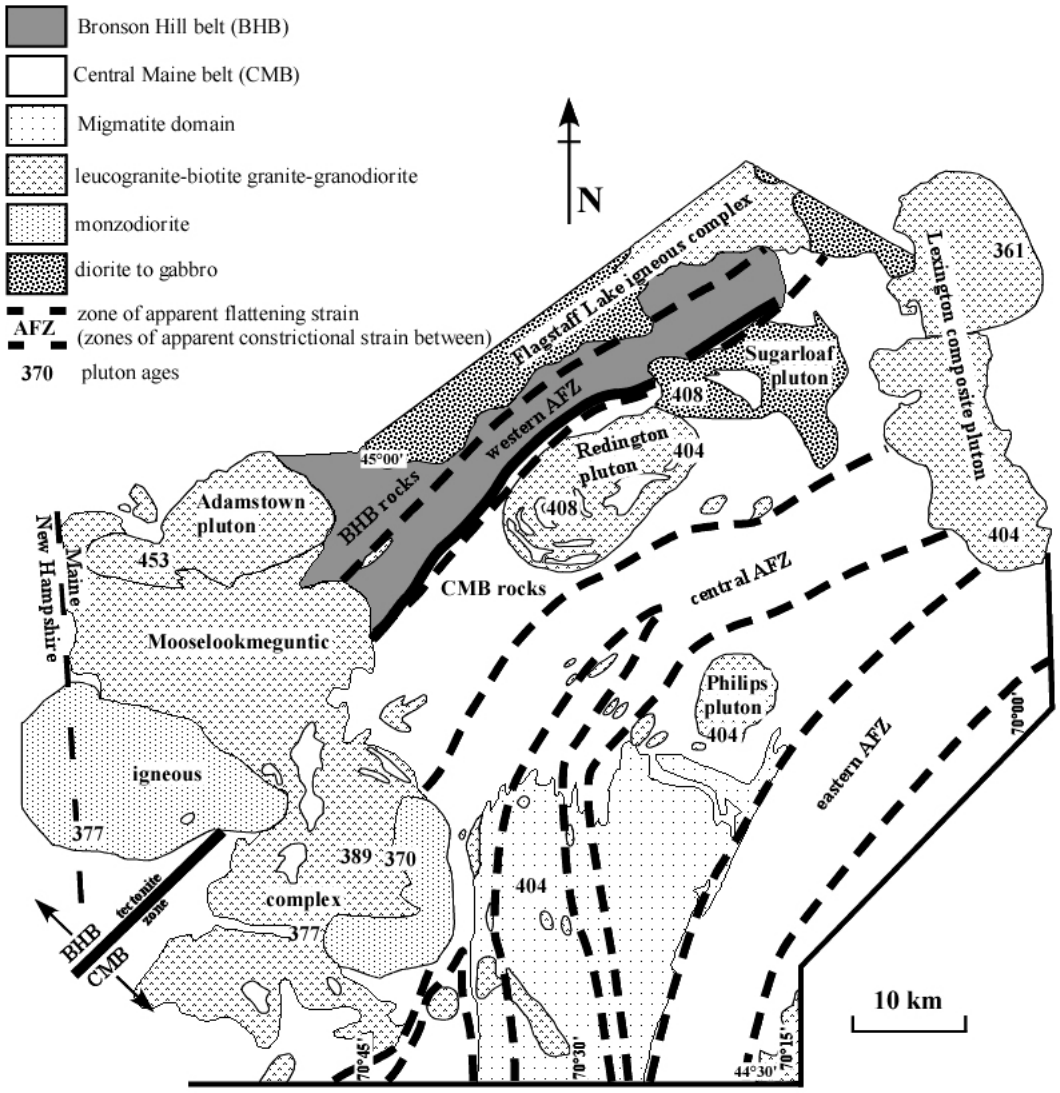

Figure 1. Simplified geological map of the west central Maine showing the major structural features, pluton intrusions, and their crystalization ages. Modified after Tomascak et al. (2005).

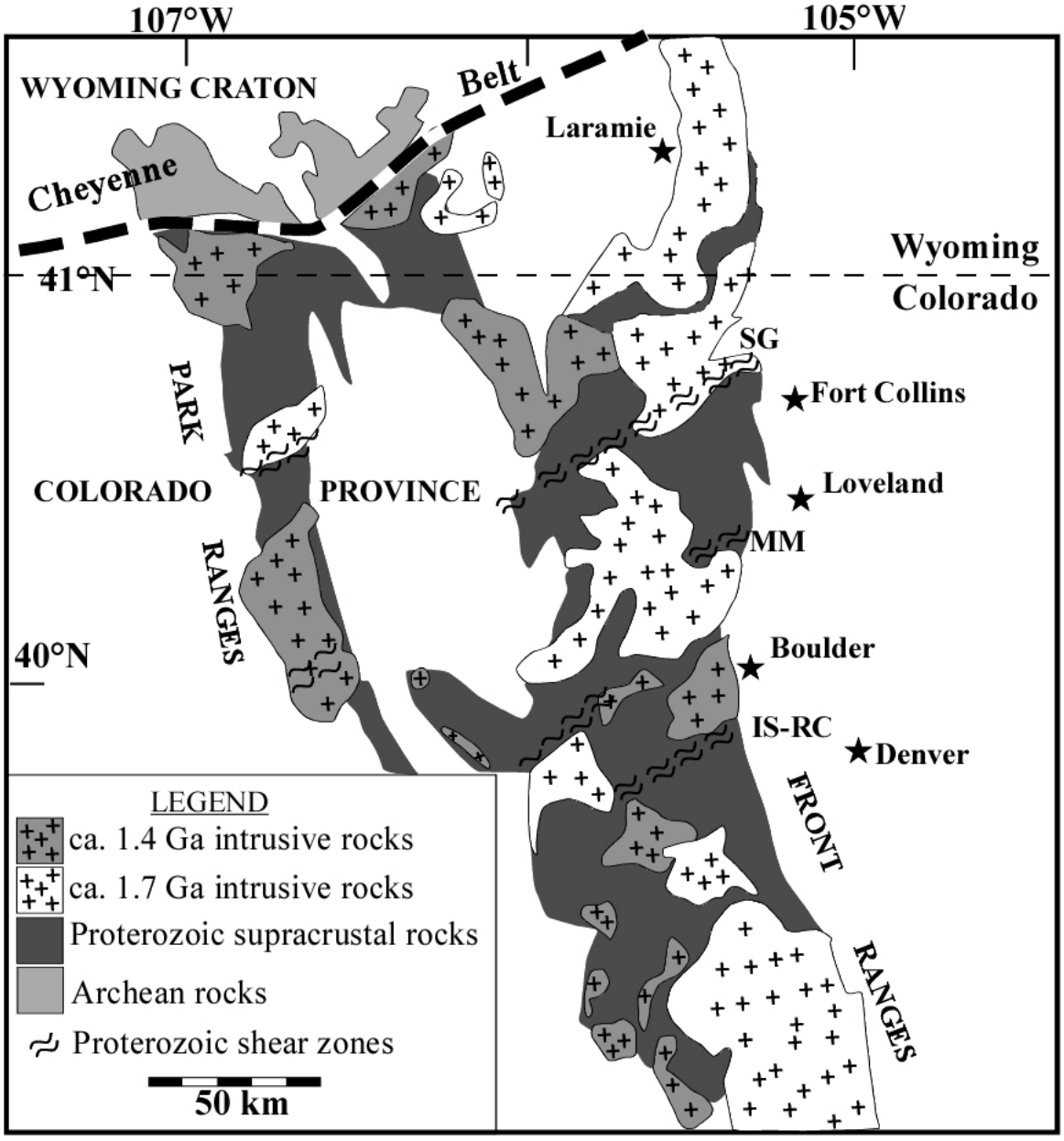

Figure 2. Simplified geological map showing the juxtaposition of the Proterozoic Colorado province rocks against the Archean Wyoming craton along the Cheyenne belt suture and the distribution of Proterozoic suprcrustal rocks, intrusions, and shear zones (after Selverstone et al., 1997). SG - Skin Gulch shear zone, MM - Moose Mountain shear zone, IS-RC - Idaho Springs-Ralston Creek shear zone.

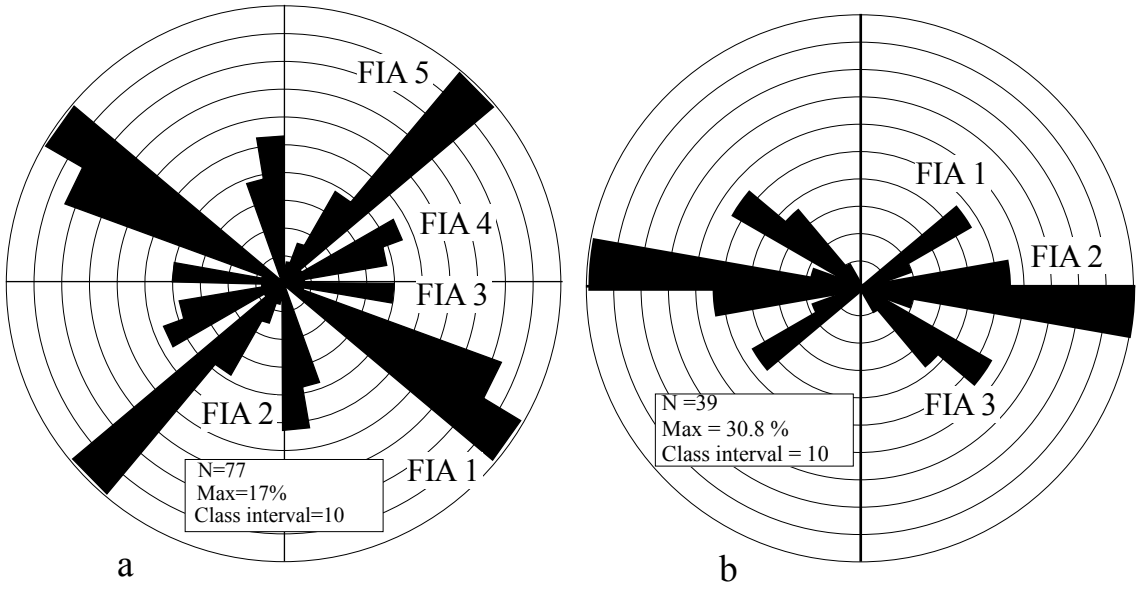

Figure 3. Equal-area rose diagrams showing the trends of FIAs measured in staurolite porphyroblasts from Western Maine (a) and Colorado Front Range (b).

FIA 1

No.	PbO (%)	UO_2 (%)	ThO_2 (%)	Y_2O_3 (%)	Age (Ma)	Error (2σ)	Comment
1	0.501	0.455	4.910	1.470	**1735**	**68**	C75 St M1 1
2	0.423	0.369	4.190	1.420	**1739**	**77**	C75 St M1 2
3	0.378	0.394	3.490	1.540	**1746**	**85**	C75 St M1 3
4	0.344	0.369	3.180	1.490	**1732**	**90**	C75 St M1 4
5	0.351	0.383	3.140	1.520	**1759**	**90**	C75 St M1 5
6	0.342	0.371	3.100	1.510	**1749**	**91**	C75 St M1 6
7	0.323	0.283	3.070	1.430	**1786**	**100**	C75 St M1 7
8	0.348	0.334	3.070	1.470	**1836**	**97**	C75 St M1 8
9	0.326	0.328	3.060	1.460	**1742**	**95**	C75 St M1 9
10	0.318	0.326	3.020	1.480	**1724**	**95**	C75 St M1 10
11	0.313	0.289	3.010	1.410	**1751**	**100**	C75 St M1 11
12	0.328	0.330	2.970	1.460	**1783**	**98**	C75 St M1 12
13	0.310	0.286	2.970	1.410	**1758**	**101**	C75 St M1 13
14	0.300	0.312	2.840	1.420	**1717**	**100**	C75 St M1 14
15	0.298	0.296	2.700	1.400	**1788**	**106**	C75 St M1 15
16	0.288	0.292	2.450	1.440	**1852**	**113**	C75 St M1 16
17	0.265	0.251	2.380	1.400	**1823**	**120**	C75 St M1 17
18	0.244	0.254	2.230	1.370	**1759**	**123**	C75 St M1 18
19	0.442	0.366	4.330	1.380	**1773**	**78**	C75 St M 2 1
20	0.390	0.463	3.380	1.158	**1748**	**83**	C75 St M 2 2
21	0.338	0.288	3.380	1.280	**1738**	**94**	C75 St M 2 3
22	0.312	0.310	2.920	1.340	**1753**	**102**	C75 St M 2 4
23	0.337	0.431	2.880	1.059	**1723**	**92**	C75 St M 2 5
24	0.315	0.360	2.800	1.197	**1744**	**99**	C75 St M 2 6
25	0.302	0.293	2.750	1.269	**1795**	**107**	C75 St M 2 7
26	0.266	0.243	2.390	1.122	**1839**	**124**	C75 St M 2 8
27	0.249	0.296	2.090	0.948	**1786**	**125**	C75 St M 2 9
28	0.442	0.386	4.310	1.360	**1759**	**77**	C84 St M3 1
29	0.434	0.404	4.200	1.360	**1742**	**77**	C84 St M3 2
30	0.396	0.457	3.520	1.650	**1738**	**82**	C84 St M3 3
31	0.398	0.513	3.430	1.600	**1711**	**79**	C84 St M3 4
32	0.352	0.361	3.240	1.360	**1758**	**92**	C84 St M3 5
33	0.377	0.468	3.020	1.610	**1809**	**88**	C84 St M3 6
34	0.339	0.435	2.740	1.570	**1780**	**95**	C84 St M3 7
35	0.305	0.335	2.720	1.520	**1758**	**102**	C84 St M3 8
36	0.288	0.309	2.560	1.320	**1777**	**109**	C84 St M3 9
37	0.281	0.284	2.560	1.290	**1773**	**111**	C84 St M3 10
38	0.268	0.289	2.310	1.320	**1804**	**118**	C84 St M3 11
39	0.251	0.311	2.100	1.300	**1764**	**121**	C84 St M3 12
40	0.258	0.331	2.090	1.340	**1776**	**118**	C84 St M3 13
41	0.239	0.297	2.020	1.340	**1749**	**124**	C84 St M3 14
42	0.237	0.284	2.010	1.340	**1765**	**127**	C84 St M3 15
43	0.241	0.311	1.960	1.310	**1772**	**125**	C84 St M3 16

No.	PbO (%)	UO_2 (%)	ThO_2 (%)	Y_2O_3 (%)	Age (Ma)	Error (2σ)	Comment
44	0.231	0.309	1.880	1.340	**1749**	**128**	C84 St M3 17
45	0.417	0.566	3.240	1.620	**1784**	**80**	C84 St3 M4 1
46	0.301	0.382	2.560	1.390	**1734**	**101**	C84 St3 M4 2
47	0.288	0.377	2.520	1.360	**1688**	**101**	C84 St3 M4 3
48	0.283	0.330	2.470	1.340	**1752**	**108**	C84 St3 M4 4
49	0.272	0.312	2.380	1.430	**1758**	**113**	C84 St3 M4 5
50	0.264	0.297	2.200	1.300	**1820**	**121**	C84 St3 M4 6
51	0.246	0.223	2.140	1.250	**1885**	**135**	C84 St3 M4 7
52	0.515	0.320	5.650	0.988	**1722**	**67**	65A St M5 1
53	0.442	0.366	4.330	1.380	**1773**	**78**	65A St M5 2
54	0.390	0.463	3.380	1.158	**1748**	**83**	65A St M5 3
55	0.338	0.288	3.380	1.280	**1738**	**94**	65A St M5 4
56	0.312	0.310	2.920	1.340	**1753**	**102**	65A St M5 7
57	0.337	0.431	2.880	1.059	**1723**	**92**	65A St M5 8
58	0.315	0.360	2.800	1.197	**1744**	**99**	65A St M5 9
59	0.302	0.293	2.750	1.269	**1795**	**107**	65A St M5 10
60	0.266	0.243	2.390	1.122	**1839**	**124**	65A St M5 11
61	0.249	0.296	2.090	0.948	**1786**	**125**	65A St M5 12

FIA 2

No.	PbO (%)	UO_2 (%)	ThO_2 (%)	Y_2O_3 (%)	Age (Ma)	Error (2σ)	Comment
62	0.479	0.394	5.030	0.246	**1690**	**69**	C43 10 St M6 1
63	0.586	0.845	4.710	0.612	**1715**	**58**	C43 10 St M6 2
64	0.592	0.808	4.630	1.630	**1774**	**61**	C43 10 St M6 3
65	0.569	0.814	4.580	0.732	**1719**	**60**	C43 10 St M6 4
66	0.563	0.803	4.520	0.654	**1722**	**61**	C43 10 St M6 5
67	0.462	0.549	4.120	1.880	**1718**	**70**	C43 10 St M6 6
68	0.466	0.597	4.080	1.870	**1698**	**69**	C43 10 St M6 7
69	0.464	0.575	4.070	2.080	**1714**	**71**	C43 10 St M6 8
70	0.461	0.588	3.860	0.890	**1749**	**73**	C43 10 St M6 9
71	0.392	0.487	3.420	1.980	**1720**	**80**	C43 10 St M6 10
72	0.349	0.387	3.110	1.800	**1756**	**91**	C43 10 St M6 11
73	0.334	0.432	2.880	1.790	**1711**	**90**	C43 10 St M6 12
74	0.272	0.325	2.440	0.748	**1711**	**110**	C43 10 St M6 13
75	0.268	0.418	1.970	1.670	**1742**	**110**	C43 10 St M6 14
76	0.534	0.349	5.810	0.806	**1718**	**65**	65A St M7 1
77	0.554	0.397	5.660	1.188	**1771**	**66**	65A St M7 2
78	0.501	0.360	5.640	0.974	**1647**	**65**	65A St M7 3
79	0.506	0.363	5.430	0.844	**1709**	**67**	65A St M7 4
80	0.480	0.398	5.110	0.786	**1670**	**68**	65A St M7 5
81	0.477	0.367	5.040	0.711	**1706**	**70**	65A St M7 6
82	0.465	0.351	4.960	0.864	**1702**	**72**	65A St M7 7
83	0.446	0.352	4.680	0.762	**1705**	**74**	65A St M7 8
84	0.398	0.355	4.100	0.687	**1684**	**80**	65A St M7 9
85	0.404	0.348	4.040	0.618	**1732**	**82**	65A St M7 10
86	0.406	0.355	4.030	0.628	**1738**	**81**	65A St M7 11
87	0.384	0.361	3.760	0.567	**1722**	**84**	65A St M7 12
88	0.373	0.378	3.540	0.614	**1727**	**87**	65A St M7 13
89	0.376	0.372	3.530	0.600	**1753**	**87**	65A St M7 14
90	0.368	0.358	3.520	0.751	**1735**	**87**	65A St M7 15
91	0.274	0.275	2.630	0.760	**1719**	**110**	65A St M7 16
92	0.248	0.281	2.280	0.564	**1713**	**119**	65A St M7 17
93	0.753	0.360	8.970	0.554	**1673**	**49**	65A St M8 1
94	0.788	0.449	8.970	0.533	**1695**	**48**	65A St M8 2
95	0.739	0.350	8.660	0.598	**1697**	**51**	65A St M8 3
96	0.756	0.457	8.330	0.675	**1724**	**50**	65A St M8 4
97	0.687	0.485	7.290	0.912	**1728**	**54**	65A St M8 5
98	0.671	0.365	7.270	0.868	**1774**	**57**	65A St M8 6
99	0.632	0.362	7.240	0.778	**1686**	**56**	65A St M8 7
100	0.685	0.502	7.100	0.992	**1746**	**55**	65A St M8 8
101	0.684	0.489	7.070	1.127	**1757**	**56**	65A St M8 9
102	0.621	0.385	6.820	1.066	**1722**	**58**	65A St M8 10
103	0.596	0.354	6.620	1.032	**1717**	**60**	65A St M8 11
104	0.614	0.487	6.550	1.218	**1683**	**57**	65A St M8 12

No.	PbO (%)	UO_2 (%)	ThO_2 (%)	Y_2O_3 (%)	Age (Ma)	Error (2σ)	Comment
105	0.586	0.346	6.490	1.014	**1722**	**61**	65A St M8 13
106	0.571	0.495	5.740	1.330	**1725**	**62**	65A St M8 14
107	0.460	0.364	4.820	1.159	**1709**	**72**	65A St M8 15
108	0.451	0.365	4.730	1.151	**1700**	**72**	65A St M8 16
109	0.425	0.339	4.390	1.153	**1722**	**78**	65A St M8 17
110	0.762	0.370	8.770	0.522	**1717**	**50**	65A St M9 1
111	0.705	0.408	7.830	0.580	**1725**	**53**	65A St M9 2
112	0.636	0.450	6.800	1.052	**1719**	**57**	65A St M9 3
113	0.525	0.321	5.660	0.860	**1749**	**67**	65A St M9 4
114	0.503	0.328	5.510	0.933	**1710**	**68**	65A St M9 5
115	0.500	0.338	5.440	1.121	**1711**	**68**	65A St M9 6
116	0.471	0.368	5.020	1.106	**1689**	**70**	65A St M9 7
117	0.370	0.336	3.700	1.370	**1714**	**85**	65A St M9 8
118	0.340	0.299	3.450	1.155	**1709**	**92**	65A St M9 9
119	0.342	0.415	2.860	0.995	**1777**	**94**	65A St M9 10
120	0.304	0.319	2.850	1.132	**1725**	**101**	65A St M9 11
121	0.527	0.642	4.610	1.800	**1727**	**64**	C108 St M10 1
122	0.426	0.429	4.100	1.640	**1714**	**76**	C108 St M10 2
123	0.425	0.448	3.900	1.660	**1749**	**77**	C108 St M10 3
124	0.406	0.481	3.620	1.650	**1721**	**78**	C108 St M10 4
125	0.371	0.371	3.530	1.560	**1732**	**85**	C108 St M10 5
126	0.402	0.544	3.420	1.740	**1697**	**77**	C108 St M10 6
127	0.307	0.289	2.950	1.400	**1745**	**100**	C108 St M10 7
128	0.346	0.499	2.840	1.710	**1694**	**87**	C108 St M10 8
129	0.278	0.277	2.660	1.450	**1723**	**108**	C108 St M10 9
130	0.307	0.387	2.530	1.550	**1771**	**101**	C108 St M10 10
131	0.278	0.383	2.260	1.530	**1731**	**106**	C108 St M10 11
132	0.277	0.400	2.150	1.600	**1749**	**106**	C108 St M10 12
133	0.245	0.350	2.060	1.580	**1678**	**114**	C108 St M10 13
134	0.232	0.346	1.930	1.540	**1663**	**118**	C108 St M10 14
135	0.464	0.517	4.200	1.800	**1737**	**71**	C108 St M11 1
136	0.468	0.598	4.110	1.890	**1696**	**68**	C108 St M11 2
137	0.487	0.632	4.100	1.850	**1732**	**67**	C108 St M11 3
138	0.447	0.515	4.090	1.690	**1706**	**72**	C108 St M11 4
139	0.452	0.532	3.970	1.740	**1740**	**73**	C108 St M11 5
140	0.438	0.546	3.690	1.740	**1753**	**74**	C108 St M11 6
141	0.411	0.487	3.660	1.720	**1721**	**77**	C108 St M11 7
142	0.443	0.614	3.660	1.860	**1711**	**71**	C108 St M11 8
143	0.370	0.371	3.610	1.550	**1701**	**83**	C108 St M11 9
144	0.400	0.501	3.320	1.720	**1764**	**81**	C108 St M11 10
145	0.357	0.404	3.310	1.580	**1704**	**86**	C108 St M11 11
146	0.369	0.442	3.250	1.700	**1730**	**84**	C108 St M11 12
147	0.366	0.438	3.250	1.730	**1722**	**84**	C108 St M11 13
148	0.355	0.420	3.200	1.600	**1710**	**87**	C108 St M11 14
149	0.320	0.344	3.100	1.410	**1679**	**93**	C108 St M11 15

No.	PbO (%)	UO_2 (%)	ThO_2 (%)	Y_2O_3 (%)	Age (Ma)	Error (2σ)	Comment
150	0.321	0.352	2.990	1.490	**1710**	**94**	C108 St M11 16
151	0.327	0.374	2.930	1.550	**1733**	**94**	C108 St M11 17
152	0.333	0.403	2.920	1.560	**1726**	**92**	C108 St M11 18
153	0.281	0.265	2.660	1.430	**1761**	**110**	C108 St M11 19
154	0.261	0.266	2.540	1.360	**1695**	**111**	C108 St M11 20
155	0.273	0.370	2.350	1.560	**1683**	**104**	C108 St M11 21
156	0.250	0.323	2.180	1.430	**1700**	**114**	C108 St M11 22
157	0.255	0.364	2.090	1.510	**1701**	**112**	C108 St M11 23
158	0.544	0.626	4.830	1.820	**1741**	**63**	C75 St M12 1
159	0.520	0.597	4.520	1.830	**1765**	**66**	C75 St M12 2
160	0.485	0.566	4.370	1.790	**1716**	**68**	C75 St M12 3
161	0.488	0.571	4.330	1.770	**1732**	**68**	C75 St M12 4
162	0.422	0.452	3.840	1.590	**1750**	**77**	C75 St M12 5
163	0.360	0.369	3.350	1.420	**1747**	**88**	C75 St M12 6
164	0.345	0.397	3.120	1.530	**1721**	**89**	C75 St M12 7
165	0.312	0.357	2.840	1.490	**1718**	**96**	C75 St M12 8
166	0.409	0.349	4.010	1.490	**1763**	**81**	C75 St M13 1
167	0.409	0.404	3.910	1.550	**1730**	**79**	C75 St M13 2
168	0.375	0.356	3.740	1.560	**1698**	**83**	C75 St M13 3
169	0.397	0.441	3.670	1.520	**1715**	**79**	C75 St M13 4
170	0.364	0.366	3.470	1.540	**1725**	**86**	C75 St M13 5
171	0.324	0.329	3.210	1.530	**1678**	**92**	C75 St M13 6
172	0.331	0.297	3.190	1.430	**1760**	**95**	C75 St M13 7
173	0.320	0.287	3.070	1.390	**1768**	**99**	C75 St M13 8
174	0.596	0.790	5.010	2.250	**1721**	**58**	C117B St M14 1
175	0.359	0.490	2.970	1.630	**1721**	**87**	C117B St M14 2
176	0.318	0.388	2.850	1.690	**1699**	**95**	C117B St M14 3
177	0.294	0.357	2.410	1.520	**1794**	**108**	C117B St M14 4
178	0.266	0.349	2.230	1.650	**1728**	**112**	C117B St M14 5
179	0.245	0.352	1.970	1.670	**1715**	**120**	C117B St M14 6

FIA 3

No.	PbO (%)	UO_2 (%)	ThO_2 (%)	Y_2O_3 (%)	Age (Ma)	Error (2σ)	Comment
180	0.466	0.465	4.530	1.640	**1706**	**71**	C83 St M15 1
181	0.479	0.530	4.470	1.690	**1706**	**70**	C83 St M15 2
182	0.422	0.511	3.890	1.650	**1678**	**75**	C83 St M15 3
183	0.391	0.412	3.770	1.590	**1692**	**81**	C83 St M15 4
184	0.405	0.483	3.680	1.690	**1698**	**79**	C83 St M15 5
185	0.361	0.379	3.630	1.530	**1648**	**84**	C83 St M15 6
186	0.369	0.432	3.450	1.620	**1679**	**83**	C83 St M15 7
187	0.234	0.241	2.470	1.310	**1600**	**117**	C83 St M15 8
188	0.261	0.334	2.410	1.460	**1644**	**109**	C83 St M15 9
189	0.217	0.259	2.020	1.360	**1673**	**130**	C83 St M15 10
190	0.462	0.356	4.880	1.450	**1707**	**72**	C84 St16 1
191	0.393	0.378	3.930	1.440	**1690**	**80**	C84 St16 2
192	0.361	0.341	3.600	1.520	**1701**	**86**	C84 St16 3
193	0.299	0.291	3.120	1.410	**1636**	**96**	C84 St16 4
194	0.308	0.318	3.040	1.350	**1673**	**97**	C84 St16 5
195	0.242	0.256	2.420	1.340	**1654**	**116**	C84 St16 6
196	0.462	0.356	4.880	1.450	**1707**	**72**	C84 St16 7
197	0.393	0.378	3.930	1.440	**1690**	**80**	C84 St16 8
198	0.361	0.341	3.600	1.520	**1701**	**86**	C84 St16 9
199	0.299	0.291	3.120	1.410	**1636**	**96**	C84 St16 10
200	0.308	0.318	3.040	1.350	**1673**	**97**	C84 St16 11
201	0.242	0.256	2.420	1.340	**1654**	**116**	C84 St16 12

Table 1. Electron microprobe analysis and calculated ages for every analytical spot from monazite grains included in staurolite porphyroblasts from Colorado Front Range.

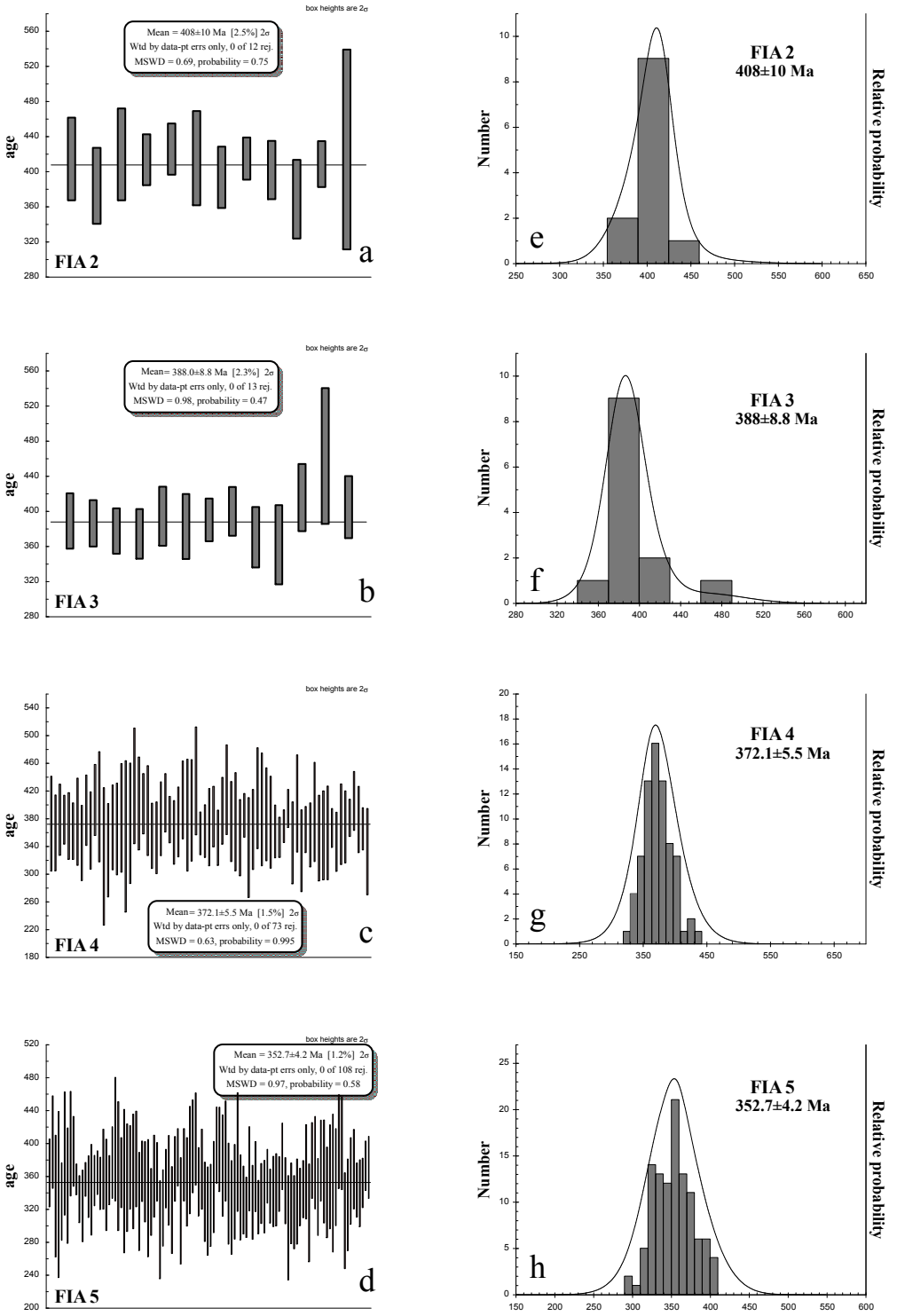

Figure 4. Probability diagrams and monazite ages for FIA set 2 (a and e), FIA set 3 (b and f), FIA set 4 (c and g) and for FIA set 5 (d and h)determined from the monazite inclusions in staurolite porphyroblasts from west-central Maine.

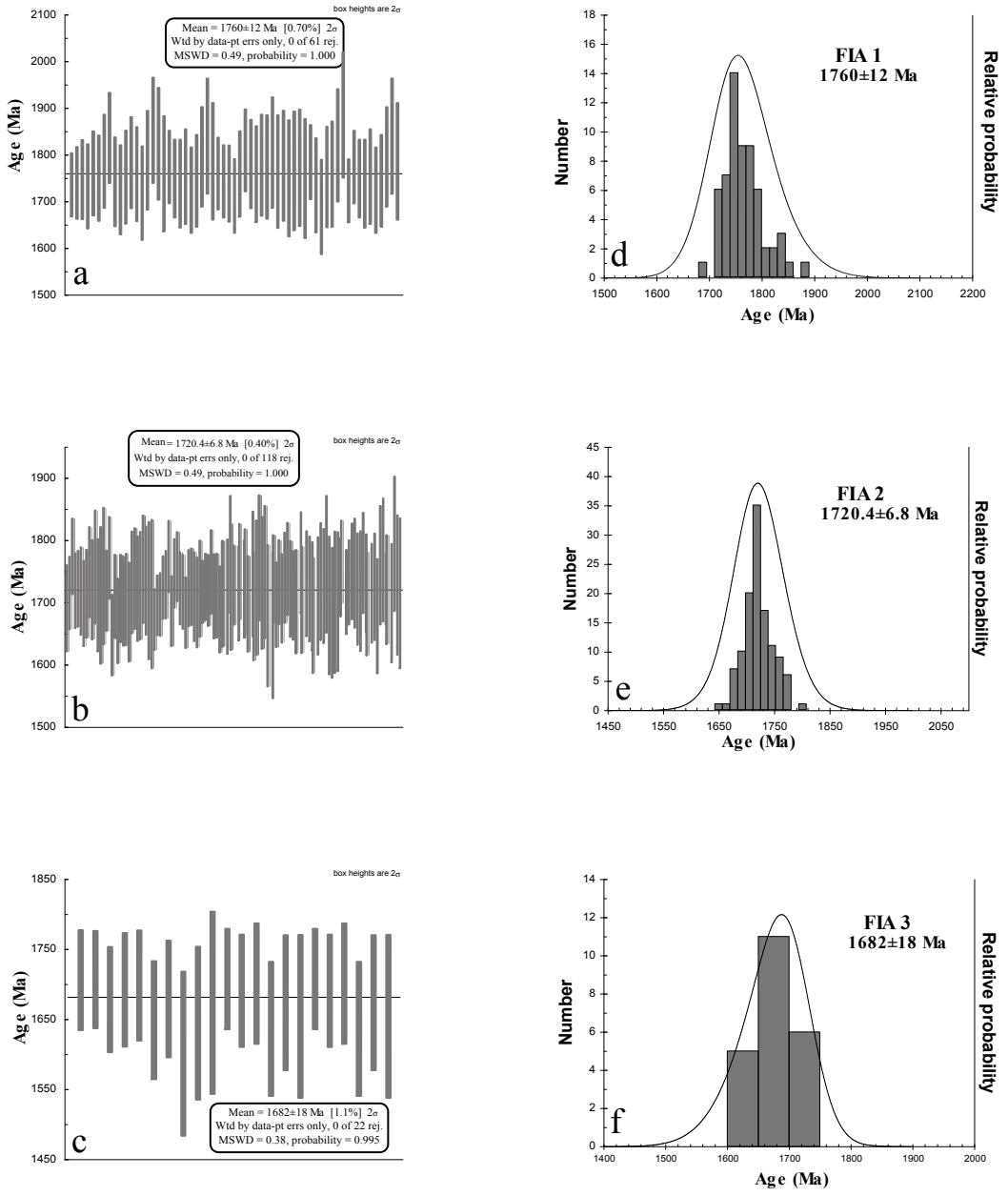

Figure 5. Probability diagrams and monazite ages for FIA set 1 (a and d), FIA set 2 (b and e) and for FIA set 3 (c and f) determined from the monazite inclusions in staurolite porphyroblasts from Colorado Front Range.

Sample no.	C65A	C68B	C75	C77	C78B	C80	C108	Average
SiO_2	63.07	64.39	63.48	64.20	63.43	64.30	66.25	64.16
TiO_2	0.75	0.66	0.81	0.81	0.67	0.75	0.81	0.75
Al_2O_3	19.46	17.70	18.24	18.33	17.28	18.82	16.84	18.10
Fe_2O_3T	7.42	7.15	8.23	7.90	8.89	7.21	7.40	7.74
MnO	0.08	0.06	0.08	0.10	0.12	0.06	0.08	0.08
MgO	1.40	1.94	1.89	2.11	2.21	1.85	1.82	1.89
CaO	0.41	0.30	0.84	0.69	0.66	0.33	0.66	0.56
Na_2O	0.81	0.88	1.29	0.86	1.11	0.78	0.92	0.95
K_2O	4.62	4.64	3.79	3.40	3.88	4.14	3.57	4.01
P_2O_5	0.11	0.10	0.13	0.14	0.06	0.11	0.13	0.11
l.o.i.	2.34	2.29	1.69	1.93	1.97	2.18	1.72	2.02
Total	100.47	100.11	100.47	100.47	100.28	100.53	100.20	100.36

Table 2. XRF bulk-compositions for samples collected from Colorado Front Range.

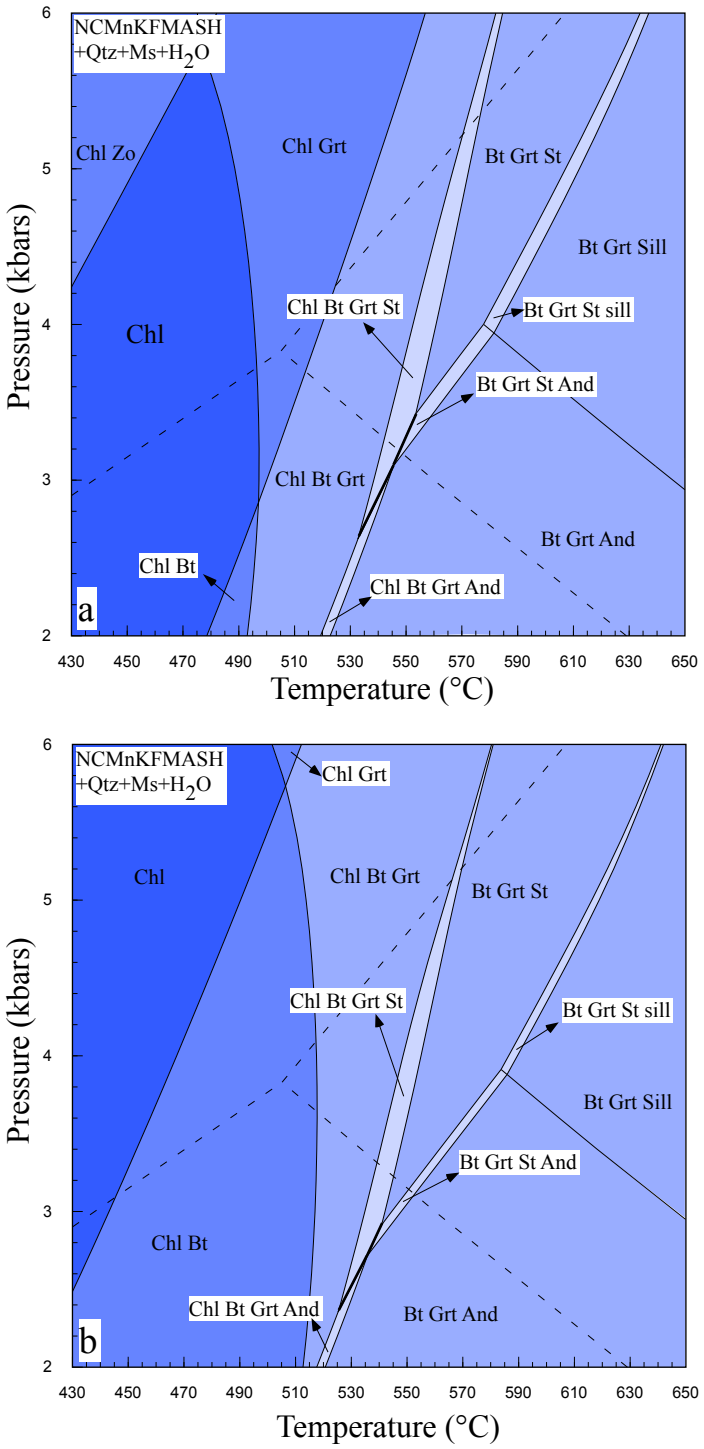

Figure 6. P-T pseudosection modelled in the NCMnKFMASH system for the avergae composition of the pelites from west-central Maine (a) and from Colorado Front Range (b). All assemblages contain plagioclase.

– SECTION D –

P-T-d-t EVOLUTION IN THE CONTACT AUREOLE OF THE MOOSELOOKMEGUNTIC PLUTON: PROGRESSIVE PLUTON CONSTRUCTION OVER 70 MILLION YEARS

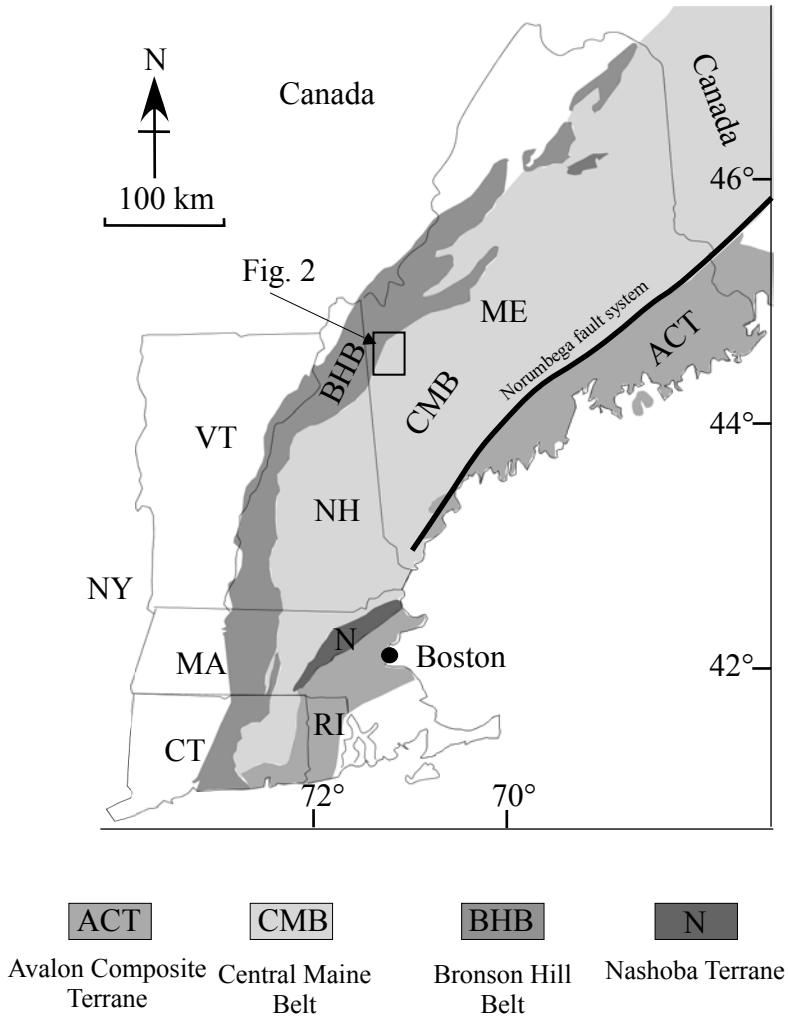

Figure 1. Simplified map of New England showing the major tectonic units.

Sample no.	Grt	St	And	Sill	Crd	Retro-grade pseudo-morphs	Pro-grade pseudo-morphs	Observations
IS2	x	x	x				x	Grt→St→And
IS4	x	x	x	x			x	Grt→St→And
IS5	x	x	x				x	Grt→St→And
IS7a	x	x			x	x		Grt→St→Crd
IS7b	x	x			x	x		Grt→St→Crd
IS8	x	x						Grt→St
IS9	x	x						Grt→St
IS10	x	x						Grt→St
IS11	x	x						Grt→St
IS12	x	x	x					Grt→St→And
IS13	x							
IS14	x	x	x	x				Grt→St→And,Sill
IS17	x	x	x	x			x	Grt→St→And,Sill
IS18	x	x						Grt→St
IS19	x	x						Grt→St
IS20	x	x						Grt→St
IS21	x	x						Grt→St
IS23	x	x						Grt→St
IS24	x	x	x					Grt→St→And
IS25	x	x						Grt→St
IS26	x						x	
IS27	x	x		x			x	Grt→St,Sill
IS28a	x			x			x	
IS28b	x	x		x			x	Grt→St
IS29	x			x				
IS30	x	x		x				Grt→St
IS31	x	x				x		Grt→St
IS32	x	x				x		Grt→St
IS33	x	x				x		Grt→St
IS34	x	x				x		Grt→St
IS35	x	x				x		Grt→St
IS36	x	x				x		Grt→St
IS37	x	x				x		Grt→St
IS39	x	x				x		Grt→St
IS40	x	x				x		Grt→St
IS41	x	x				x		Grt→St
IS42	x	x				x		Grt→St
IS43	x	x				x		Grt→St
IS44	x	x				x		Grt→St
IS45	x	x				x		Grt→St
IS46	x	x				x		Grt→St
IS47	x	x				x		Grt→St
IS48	x	x				x		Grt→St
IS49	x	x				x		Grt→St
IS50	x	x				x		Grt→St
IS51	x	x				x		Grt→St
IS52	x	x				x		Grt→St
IS53	x	x				x		Grt→St
IS54	x	x				x		Grt→St
IS55	x	x				x		Grt→St
IS56	x	x				x		Grt→St
IS57	x	x				x		Grt→St
IS58	x	x				x		Grt→St
IS59	x	x				x		Grt→St
IS60	x					x		
IS61	x					x		

Sample no.	Grt	St	And	Sill	Crd	Retro-grade pseudo-morphs	Pro-grade pseudo-morphs	Observations
IS62	x	x				x		Grt→St
IS63	x					x		
IS64	x	x				x		Grt→St
IS65	x	x				x		Grt→St
IS66	x	x	x				x	Grt→St→And
IS67	x	x	x				x	Grt→St→And
IS68	x	x	x				x	Grt→St→And
IS69	x						x	
IS70	x	x					x	Grt→St
IS71	x	x	x				x	Grt→St→And
IS72	x	x						Grt→St
IS73	x	x	x	x			x	Grt→St→And,Sill
IS74	x	x	x	x			x	Grt→St→And,Sill
IS77	x	x				x		Grt→St
IS78	x	x				x		Grt→St
IS79	x	x				x		Grt→St
IS80	x	x				x		Grt→St
IS81	x	x				x		Grt→St
IS82	x	x						Grt→St
IS83	x	x	x		x			Grt→St→And→Crd
IS84		x	x		x			St→And,Crd
IS85	x	x	x					Grt→St→And
IS86		x			x			St→Crd
IS87		x						
IS88		x						
IS89	x	x						Grt→St
IS90	x	x			x			Grt→St→Crd
IS91		x	x		x			St→And→Crd
IS92a	x	x						Grt→St
IS92b		x			x			St→Crd
IS93	x	x			x			Grt→St→Crd
IS94	x	x		x				Grt→St
IS95	x	x		x				Grt→St
IS96	x							
IS99	x							
IS100	x	x	x	x			x	Grt→St→And,Sill
IS101	x	x		x			x	Grt→St→Sill
IS102	x	x	x	x			x	Grt→St→And,Sill
IS103	x	x	x	x			x	Grt→St→And,Sill
IS104	x	x	x	x			x	Grt→St→And,Sill

Table 1. Mineral assemblages contained in every sample and their relative succession in the paragenesis. Arrows indicate the crystallization order.

Sample	FIA 1		FIA 2		FIA 3		FIA 4		FIA 5	
no.	St	Grt	St	Grt	St	Grt	St	Grt	St	Grt
IS2		125					75			
IS4	125	125	165r							
IS5	125c	120			95r					
IS7a	125	115								
IS7b									15	40
IS8									45	45
IS9b		120					65			
IS10		115							30	
IS11		120							35	
IS12				145					35	
IS13		125								
IS14		120							40	
IS17	125	125					75			
IS18			165	165						
IS19				165	95					
IS20			165	165						
IS21			175	175						
IS23					95	95				
IS24								75	45	
IS25		120							45	
IS26								75		
IS27							75	75		
IS28a										35
IS28b		130							25	
IS29		115								
IS30	120	115								
IS33								65		
IS34								85		
IS35		125								
IS36								75		
IS37								65		
IS42	115	125								
IS43	110	125								
IS45								75		
IS46				175						
IS47	115	125								
IS49	110	125								
IS50				175						
IS52	110	125								
IS53								75		
IS54	115	115								
IS55			175	175						
IS56			175c	175					45r	
IS57	120	110								
IS59				165						
IS60								75		
IS61								75		
IS62				160						
IS63				160						
IS64				170						
IS65								75		
IS66	125	125								
IS67								65	40	
IS68	125	115								
IS69								65		

Sample	FIA 1		FIA 2		FIA 3		FIA 4		FIA 5	
no.	St	Grt	St	Grt	St	Grt	St	Grt	St	Grt
IS70										25
IS71									40	45
IS72				175			65			
IS73			165p	165					45	
IS74							75p	75	40	
IS77			170c	170					45r	
IS78									55	
IS79	110									
IS81										45
IS82							65			
IS83	120	110								
IS84	125									
IS85							65c	65	35r	
IS86	115c						75r			
IS87	115									
IS88					100c				45r	
IS89	115	115								
IS90	130c	120	165r							
IS91					100c		85m		45r	
IS92a			170							
IS92b	125									
IS93			165	165						
IS94					90c	100	65m		25r	
IS95					95c	95	65m		35r	
IS96								65		
IS99								70		
IS101				155						
IS102									45	45
IS103	120	125								
IS104	115	120								

Table 2. A list of FIA measurements for garnet and staurolite porphyroblasts. c – core-inclusion trails; m –median-inclusion trails; r – rim-inclusion trails; p – pre-FIA.

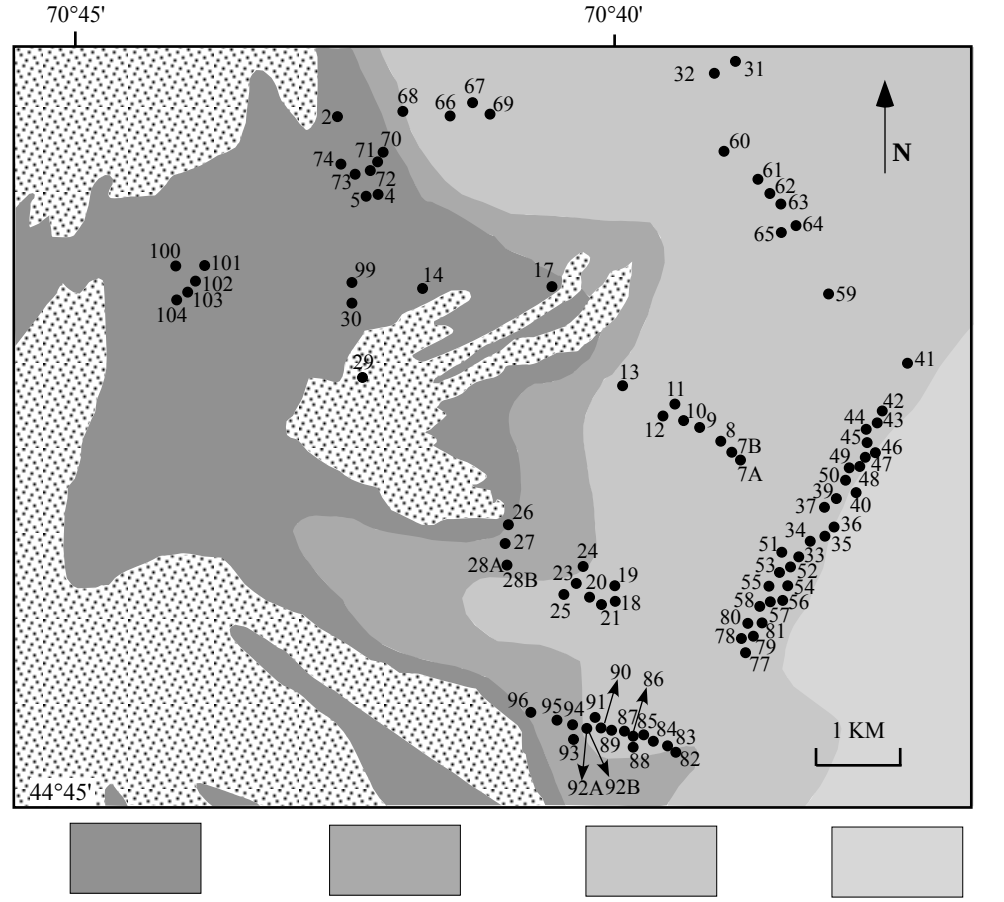

Figure 2. Simplified geological map of the study area showing sample locations. Isograds after Guidotti and Johnson (2002).

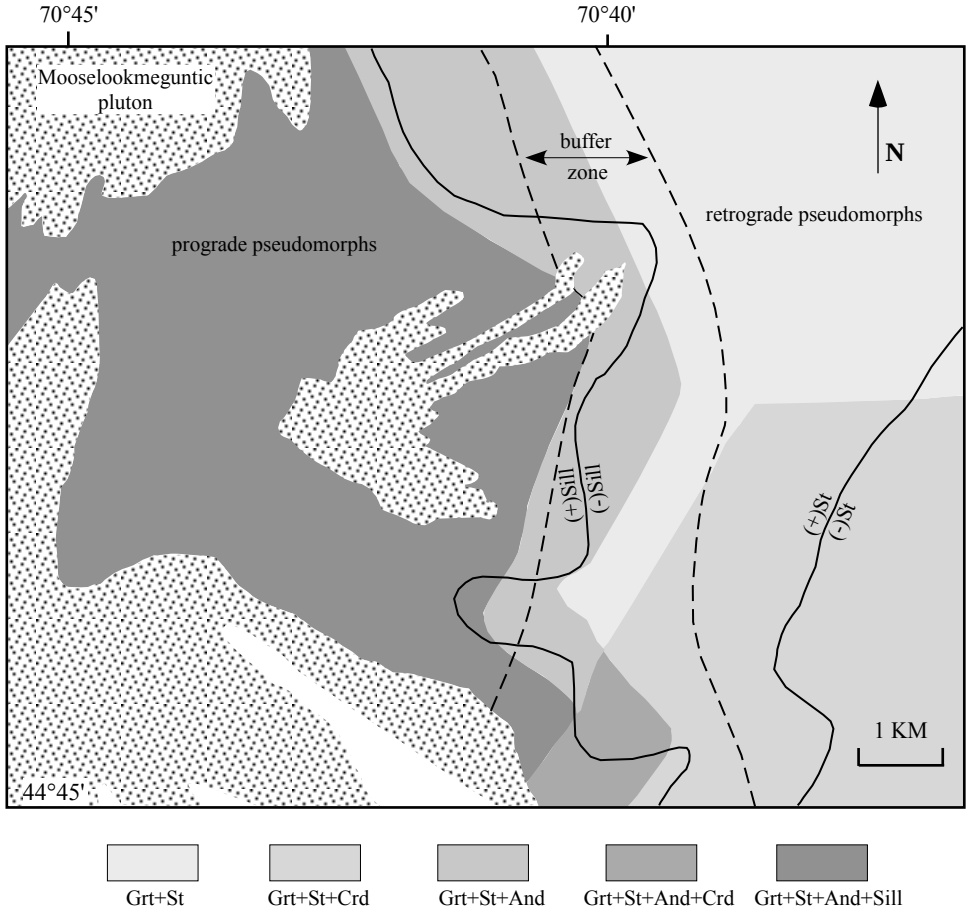

Figure 3. Simplified map of the study area showing the distribution of the mineral assemblages discussed in this paper. Dashed lines mark the boundaries between prograde and retrograde pseudomorphs. Between the dashed lines, there is an intervening zone, marked as buffer zone, where no pseudomorphs were found.

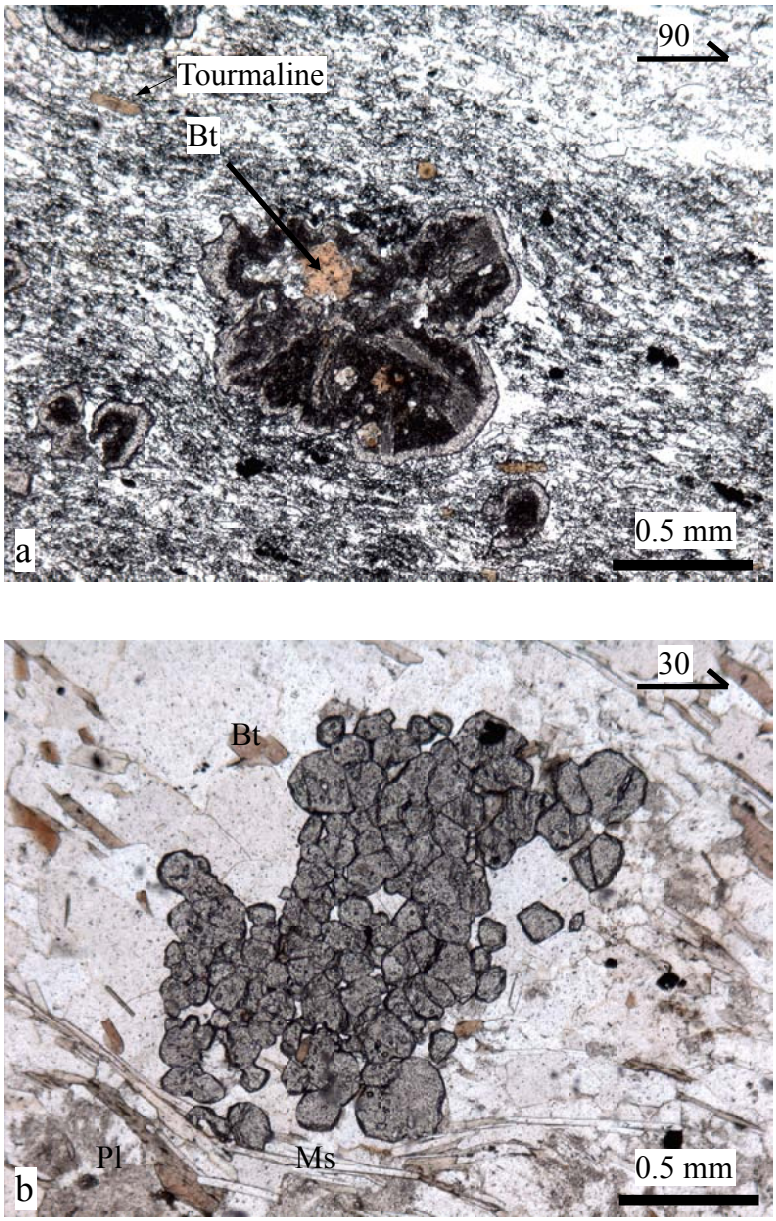

Figure 4. Garnet porphyroblast textures showing textural zoning and clustering. a) Garnet porphyroblast from sample IS 12 showing textural zoning. This garnet porphyroblast grew in a graphite-rich quartz layer. The shape of multiple grains that coalesce together can be recognized. The textural zoning is marked by zones rich in graphite inclusions. Other minerals present in this picture are tourmaline, biotite, and apatite. Note that the weak foliation present in the matrix wraps around the garnet porphyroblasts, indicating syn-kinematic growth. b) Garnet cluster from sample IS 99. Note that individual garnet grains are larger along the margin of the porphyroblasts and smaller within the centre. Such textures may indicate garnet growth by multiple nucleation and coalescence. Other minerals present in this picture are biotite, muscovite, and plagioclase. Note that the weak cleavage defined by muscovite wraps around the garnet cluster, indicating that garnet nucleation took place during deformation in zones of low strain. Plane polarized light.

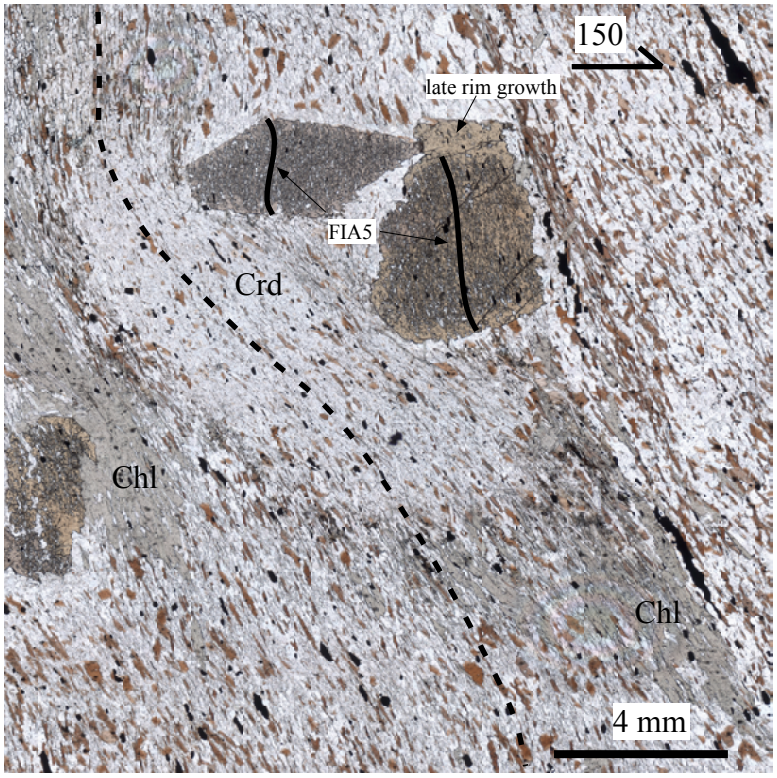

Figure 5. Photomicrograph from sample IS7B showing the relationship between staurolite and cordierite porphyroblasts. Staurolite porphyroblasts have sigmoidal inclusion trails and grew during FIA5. Note that the larger staurolite porphyroblast on the right has late rim growth which is almost inclusion-free. Such rims were interpreted previously as the result of M3 metamorphism at 370 Ma (see Johnson et al., 2006). Monazite dating of FIA 5 porphyroblasts revealed that staurolite growth during this FIA event ceased at c. 345 Ma. That would make the inclusion-free rim even younger. The cordierite porphyroblasts grew even later over the cleavage that wraps around the staurolite porphyroblasts. The sigmoidal inclusion trails in cordierite indicate syn-kinematic growth for this phase as well. Note that both staurolite and cordierite porphyroblasts were partly replaced by chlorite. Plane polarized light.

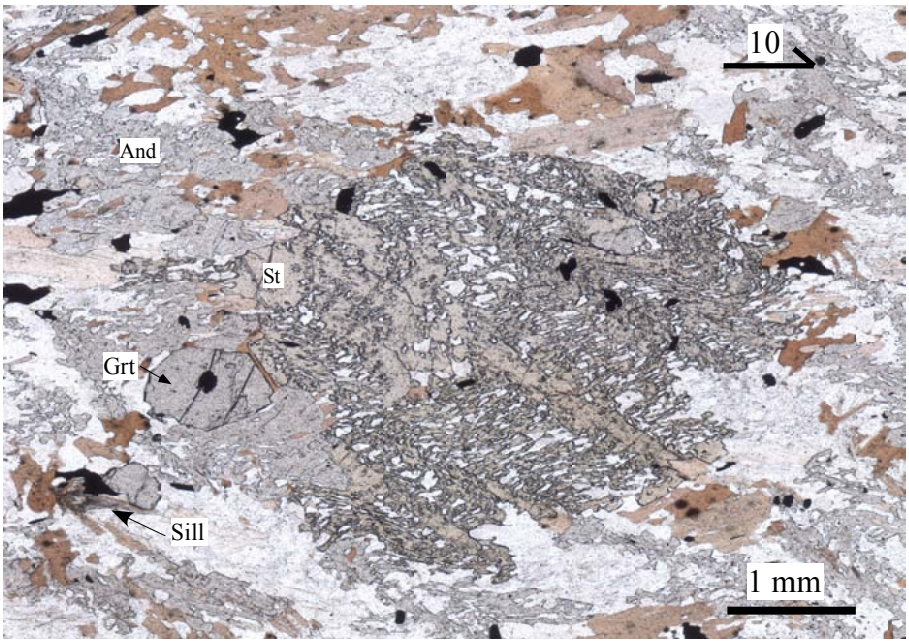

Figure 6. Photomicrograph from sample IS73 showing typical textural and microstructural features from this part of the study area. Samples IS71, IS72, and IS74 show similar features. Staurolite porphyroblasts overgrew a differentiated crenulation cleavage and were partly replaced by poikilitic andalusite that overgrows the entire matrix. Some sillimanite that nucleated inside biotite is present in the matrix. Plane polarized light.

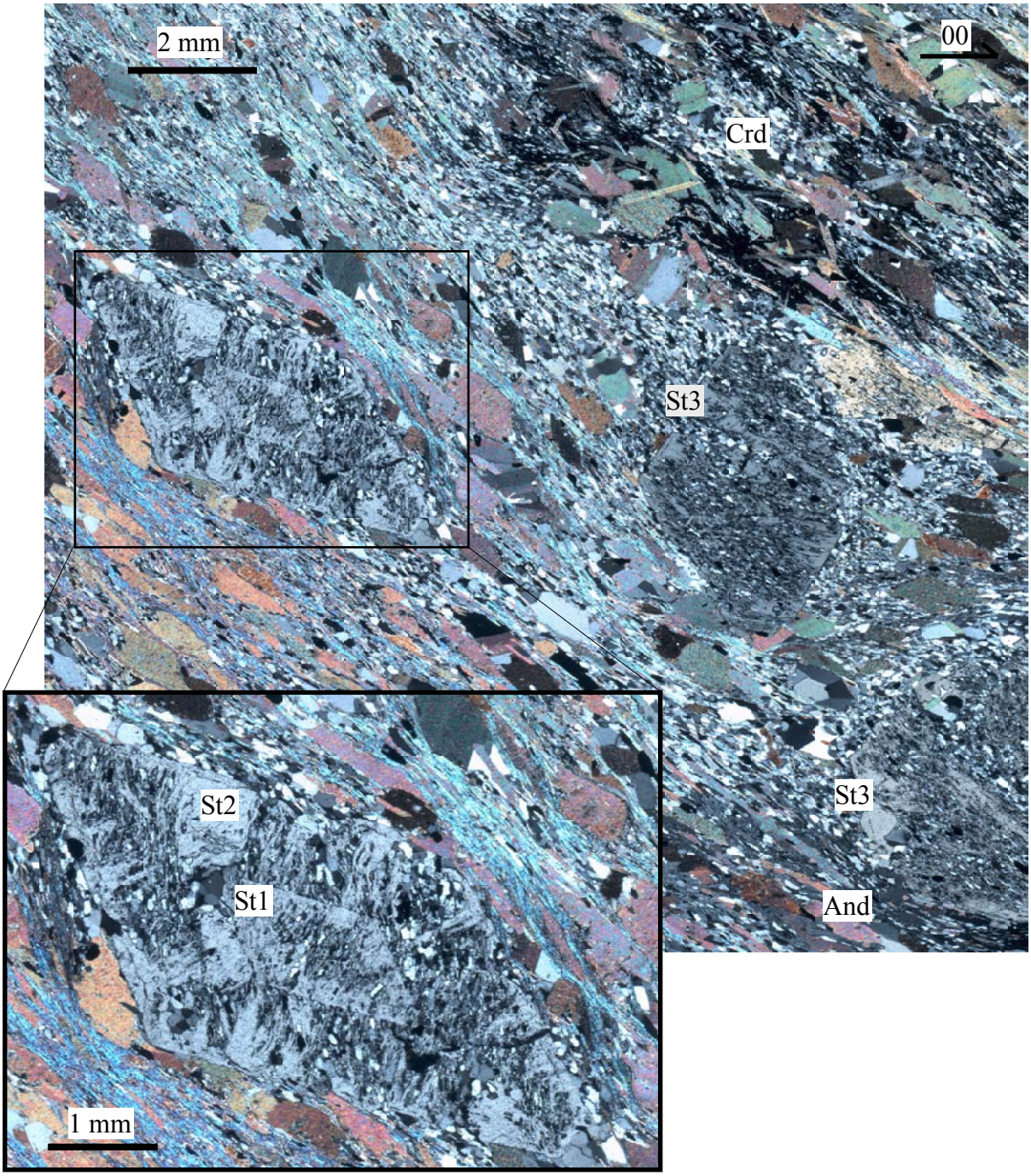

Figure 7. Photomicrograph from sample IS91 showing the textural and microstructural relationships between staurolite, andalusite, and cordierite porphyroblasts. Three generations of staurolite are present in this sample (marked with St1, St2, and St 3 in picture) that correspond with FIA set 3 (St1), FIA set 4 (St2), and FIA set 5 (St3). Note that FIA 3 (St1) staurolite has an inclusion-rich core surrounded by an inclusion-poor rim. The inclusion trails in FIA 4 (St2) staurolite are truncated by the matrix whereas FIA 5 (St3) staurolite inclusion trails appear to be continuous with the matrix. In the bottom-right corner the foliation that wraps around the FIA 5 staurolite is overgrown by andalusite (first-order interference colors). The cordierite porphyroblast (top-right dark color because is at extinction) overgrew the matrix and was partly replaced by coarse biotite and muscovite. Crossed polarized light.

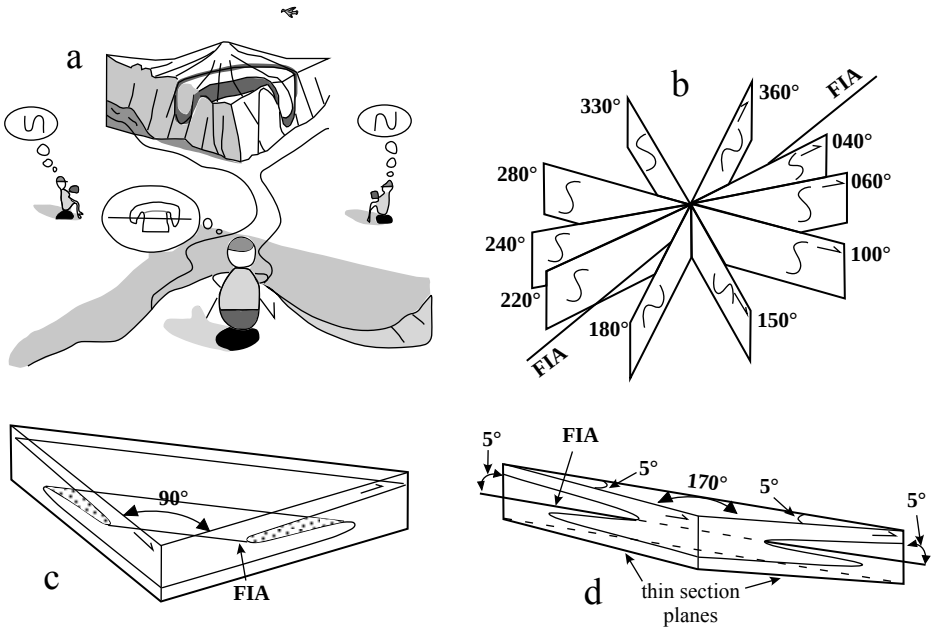

Figure 8. Sketch illustrating the principle behind FIA measurement (after Bell et al., 2004). a) The geologists to either side see the opposite asymmetry for same fold in a cliff face. They have no idea of its trend in 3-D. The geologist in the centre sees the fold on both cliff faces and knows it must trend from one to the other. b) Shows the asymmetry on a series of differently-striking vertical sections. The asymmetry flips across the compass when viewed in the same direction. (c) Shows asymmetry of a sigmoid axis in two sections cut 90° apart. (d) Shows the sigmoid axis of (c) in two sections cut 10° apart lying on either side of the axis. The switch in asymmetry between them defines the location of the axis within a 10° range.

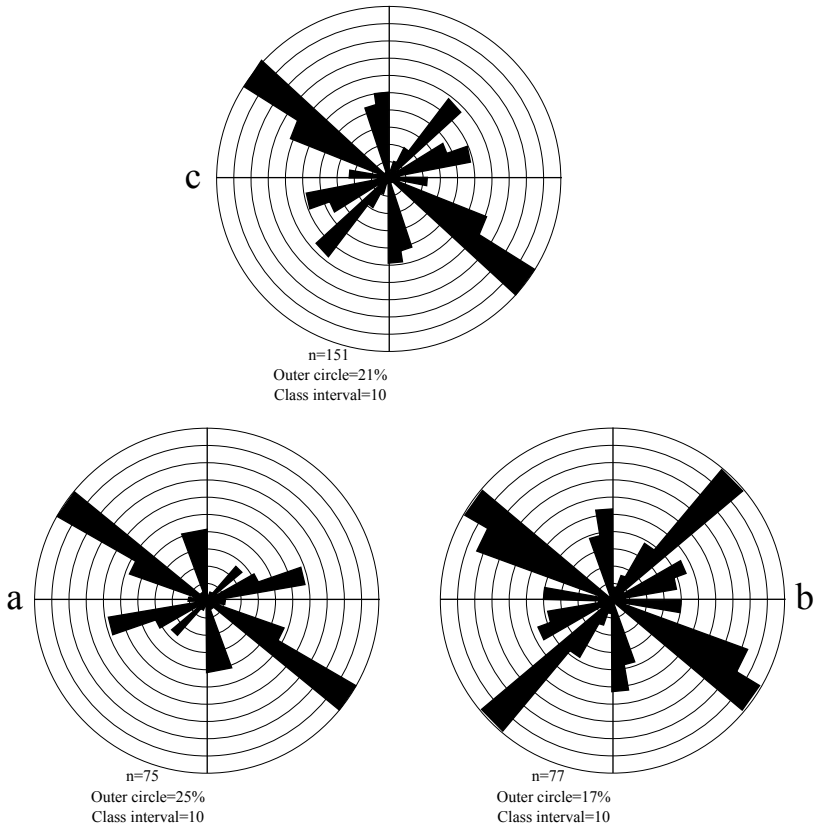

Figure 9. Equal-area rose diagrams of the FIAs in garnet (a), staurolite (b), and combined (c) garnet and staurolite porphyroblasts.

Sample no.	FIA 1		FIA 2		FIA 3		FIA 4		FIA 5	
	Grt	St	Grt	St	Grt	St	Grt	St	Grt	St
IS2	125							75		
IS4	125	125c		165r						
IS5	120	125c				95r				
IS7a	115	125								
IS9b	120							65		
IS10	115									30
IS11	120									35
IS14	120									40
IS17	125	125						75r		
IS25	120									45
IS28b	130									25
IS30	115	120								
IS42	125	115								
IS43	125	110								
IS47	125	115								
IS49	125	110								
IS52	125	110								
IS54	115	115								
IS57	110	120								
IS66	125	125								
IS68	115	125								
IS83	110	120								
IS89	115	115								
IS90	120	130c		165r						
IS103	125	120								
IS104	120	115								
IS12			145							35
IS18			165	165						
IS19			165			95				
IS20			165	165						
IS21			175	175						
IS55			175	175						
IS56			175	175c						45r
IS72			175					65		
IS73			165	165p						45
IS77			170	170c						45
IS93			165	165						
IS23					95	95				
IS94					100	90c		65m		25r
IS95					95	95c		65m		35r
IS24							75			45
IS27							75	75		
IS67							65			40
IS74							75	75p		40
IS85							65	65c		35r
IS7b									40	15
IS8									45	45
IS71									45	40
IS102									45	45

Table 3. FIA measurements for garnet and staurolite porphyroblasts, for only those samples where garnet porphyroblasts were included in staurolite. A clear succession from FIA 1 to FIA 5 can be established in this way.

	IS77	IS74	IS2	IS104a	IS104b
SiO_2	46.89	47.10	46.88	46.55	46.43
TiO_2	0.24	0.35	0.38	0.55	0.52
Al_2O_3	37.68	37.84	37.69	37.40	37.58
FeO	0.64	0.64	0.76	0.80	0.79
MnO	0.00	0.00	0.01	0.00	0.01
MgO	0.32	0.43	0.41	0.42	0.43
CaO	0.02	0.00	0.00	0.01	0.00
Na_2O	1.21	1.11	0.98	0.77	1.04
K2O	6.90	8.23	8.08	7.67	8.12
Cl	0.04	0.00	0.00	0.04	0.00
Total	93.94	95.70	95.20	94.21	94.92
Si	6.163	6.126	6.124	6.132	6.095
Al(IV)	1.837	1.874	1.876	1.868	1.905
Σ(IV)	8.000	8.000	8.000	8.000	8.000
Al(VI)	4.002	3.928	3.928	3.941	3.911
Ti	0.024	0.034	0.038	0.054	0.052
Fe	0.070	0.070	0.083	0.088	0.087
Mn	0.000	0.000	0.010	0.000	0.001
Mg	0.063	0.083	0.080	0.083	0.084
Σ(VI)	4.158	4.115	4.139	4.166	4.133
Ca	0.002	0.000	0.000	0.001	0.000
Na	0.309	0.280	0.249	0.196	0.264
K	1.158	1.365	1.347	1.289	1.360
Cl	0.010	0.000	0.001	0.010	0.001
Σ(XII)	1.480	1.646	1.597	1.496	1.625
Total	13.628	13.762	13.735	13.652	13.758
Ti-Ms	0.012	0.017	0.019	0.027	0.026
phl-ann	0.079	0.058	0.069	0.083	0.067
pg	0.155	0.140	0.124	0.098	0.132
ms	0.754	0.785	0.788	0.792	0.776
Fe/Mg	1.116	0.839	1.035	1.065	1.037
Na/(Na+K)	0.211	0.170	0.156	0.132	0.162
X_{Fe}	0.527	0.455	0.479	0.515	0.507
X_{Mg}	0.472	0.543	0.462	0.483	0.489

a – muscovite grain from a staurolite pseudomorph
b – matrix muscovite

Table 4. Electron microprobe analyses of muscovite grains. Each analysis represents the average of seven analytical spots. Ti-Ms = Ti-muscovite; phl-ann=phlogopite-annite; pg=paragonite;
ms=muscovite.

	IS77	IS74	IS2	IS104a	IS104b
SiO_2	36.38	35.24	35.59	35.25	34.99
TiO_2	1.20	1.52	1.59	1.41	1.27
Al_2O_3	19.81	19.59	20.03	19.79	19.69
FeO	18.64	19.90	20.21	21.72	22.56
MnO	0.08	0.07	0.06	0.11	0.12
MgO	10.53	9.21	8.81	8.05	8.07
CaO	0.01	0.02	0.00	0.01	0.00
Na_2O	0.32	0.34	0.24	0.28	0.24
K_2O	8.25	8.68	8.60	8.51	8.14
Cl	0.01	0.01	0.00	0.01	0.01
Total	95.23	94.58	95.13	95.13	95.09
Si	5.462	5.396	5.407	5.401	5.378
Al(IV)	2.538	2.604	2.593	2.599	2.622
Σ(IV)	8.000	8.000	8.000	8.000	8.000
Al(VI)	0.969	0.932	0.995	0.976	0.945
Ti	0.135	0.175	0.182	0.163	0.147
Fe	2.340	2.548	2.569	2.783	2.900
Mn	0.010	0.009	0.008	0.015	0.015
Mg	2.356	2.102	1.995	1.838	1.849
Σ(VI)	5.811	5.767	5.748	5.775	5.857
Ca	0.001	0.003	0.000	0.001	0.001
Na	0.093	0.102	0.071	0.083	0.072
K	1.581	1.680	1.667	1.663	1.596
Cl	0.003	0.003	0.001	0.003	0.003
Σ(XII)	1.678	1.788	1.739	1.750	1.672
Total	15.486	15.551	15.486	15.522	15.525
Ti-Bt	0.068	0.088	0.091	0.081	0.073
tlc-mi	0.163	0.108	0.131	0.126	0.166
ms	0.027	0.029	0.035	0.031	-
eas-sid	0.431	0.409	0.427	0.425	0.476
won	0.047	0.051	0.036	0.042	0.036
phl-ann	0.266	0.316	0.280	0.294	0.249
Fe/Mg	0.993	1.212	1.288	1.514	1.568
X_{Fe}	0.497	0.547	0.562	0.600	0.609
X_{Mg}	0.501	0.451	0.436	0.397	0.388

a – biotite grain from a staurolite pseudomorph
b – matrix biotite in contact with garnet

Table 5. Electron microprobe analyses of biotite grains. Each analysis represents the average of seven analytical spots. Ti-Bt=Ti-biotite; tlc-mi=talc-minnesotaite; ms=muscovite; eas-sid=eastonite-siderophyllite; won=wonesite; phl-ann=phlogopite-annite.

	IS2		IS28A		IS74		IS77		IS95		IS104	
	core	rim	core	rim	core	rim	core	rim	core	rim	core	rim
SiO_2	37.62	37.59	37.36	37.13	37.33	37.75	37.36	37.47	37.23	37.27	37.46	37.56
TiO_2	0.05	0.00	0.01	0.00	0.01	0.02	0.04	0.00	0.05	0.02	0.01	0.01
Al_2O_3	21.33	21.38	21.32	21.30	21.43	21.30	21.33	21.30	21.21	21.36	21.35	21.42
FeO	33.80	36.45	31.18	34.01	32.93	34.54	32.41	33.80	30.02	32.85	32.82	33.96
MnO	4.18	3.39	6.87	4.21	4.21	4.47	5.52	4.89	7.28	5.09	5.35	4.84
MgO	2.28	1.75	2.62	2.57	2.48	2.17	2.75	2.58	2.23	2.42	2.06	2.34
CaO	2.37	1.30	1.43	0.84	2.12	1.71	1.15	0.93	2.37	1.75	1.29	0.96
Total	101.32	101.87	100.79	100.07	100.51	101.96	100.56	100.97	100.39	100.75	100.34	101.09
Si	2.995	3.000	2.994	2.997	2.994	3.002	2.997	3.001	2.995	2.989	3.015	3.004
Al	2.001	2.011	2.013	2.026	2.026	1.996	2.016	2.010	2.011	2.019	2.025	2.019
Ti	0.003	0.000	0.001	0.000	0.001	0.001	0.002	0.000	0.003	0.001	0.001	0.001
Fe	2.250	2.433	2.090	2.296	2.209	2.296	2.174	2.263	2.020	2.204	2.209	2.272
Mn	0.282	0.229	0.466	0.288	0.286	0.301	0.375	0.332	0.496	0.346	0.365	0.328
Mg	0.270	0.208	0.313	0.309	0.296	0.257	0.329	0.308	0.268	0.289	0.247	0.279
Ca	0.202	0.111	0.123	0.073	0.182	0.146	0.099	0.080	0.204	0.151	0.111	0.082
Total	8.002	7.994	7.999	7.989	7.993	7.999	7.993	7.994	7.997	7.999	7.972	7.985
Almandine	0.749	0.816	0.698	0.774	0.743	0.765	0.730	0.759	0.676	0.737	0.754	0.767
Grossular	0.067	0.037	0.041	0.025	0.061	0.049	0.033	0.027	0.068	0.050	0.038	0.028
Pyrope	0.090	0.070	0.105	0.104	0.100	0.086	0.110	0.103	0.090	0.097	0.084	0.094
Spessartine	0.094	0.077	0.156	0.097	0.096	0.100	0.126	0.111	0.166	0.116	0.124	0.111
Fe/(Fe+Mg)	0.893	0.921	0.870	0.881	0.882	0.899	0.869	0.880	0.883	0.884	0.900	0.891
Mg/(Mg+Fe)	0.107	0.079	0.130	0.119	0.118	0.101	0.131	0.120	0.117	0.116	0.100	0.109
X_{Fe}	0.803	0.848	0.728	0.794	0.792	0.805	0.755	0.780	0.726	0.776	0.783	0.789
X_{Mg}	0.096	0.073	0.109	0.107	0.106	0.090	0.114	0.106	0.096	0.102	0.087	0.097

Table 6. Electron microprobe analysis of garnet cores and rims. Each analysis represents the average of eight analytical spots for the garnet core and five analytical spots for the garnet rim.

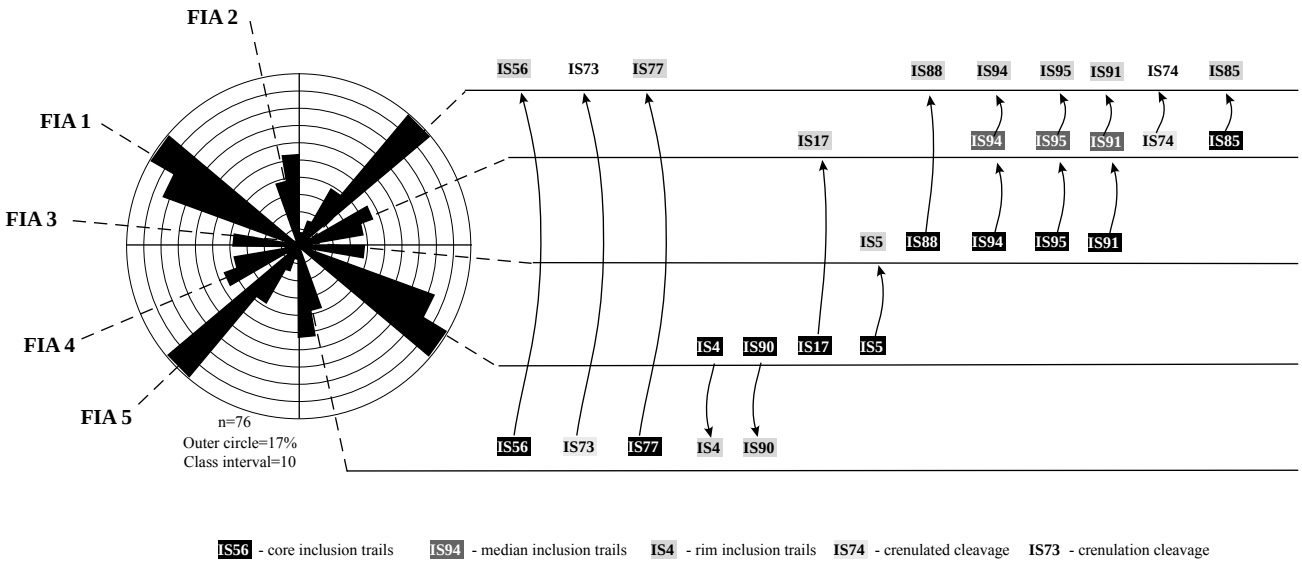

Figure 10. Equal-area rose diagrams of the FIAs in staurolite porphyroblast illustrating how the relative FIA succession was established. Arrows show core to rim changes. A consistent succession is revealed by total combinations of changes.

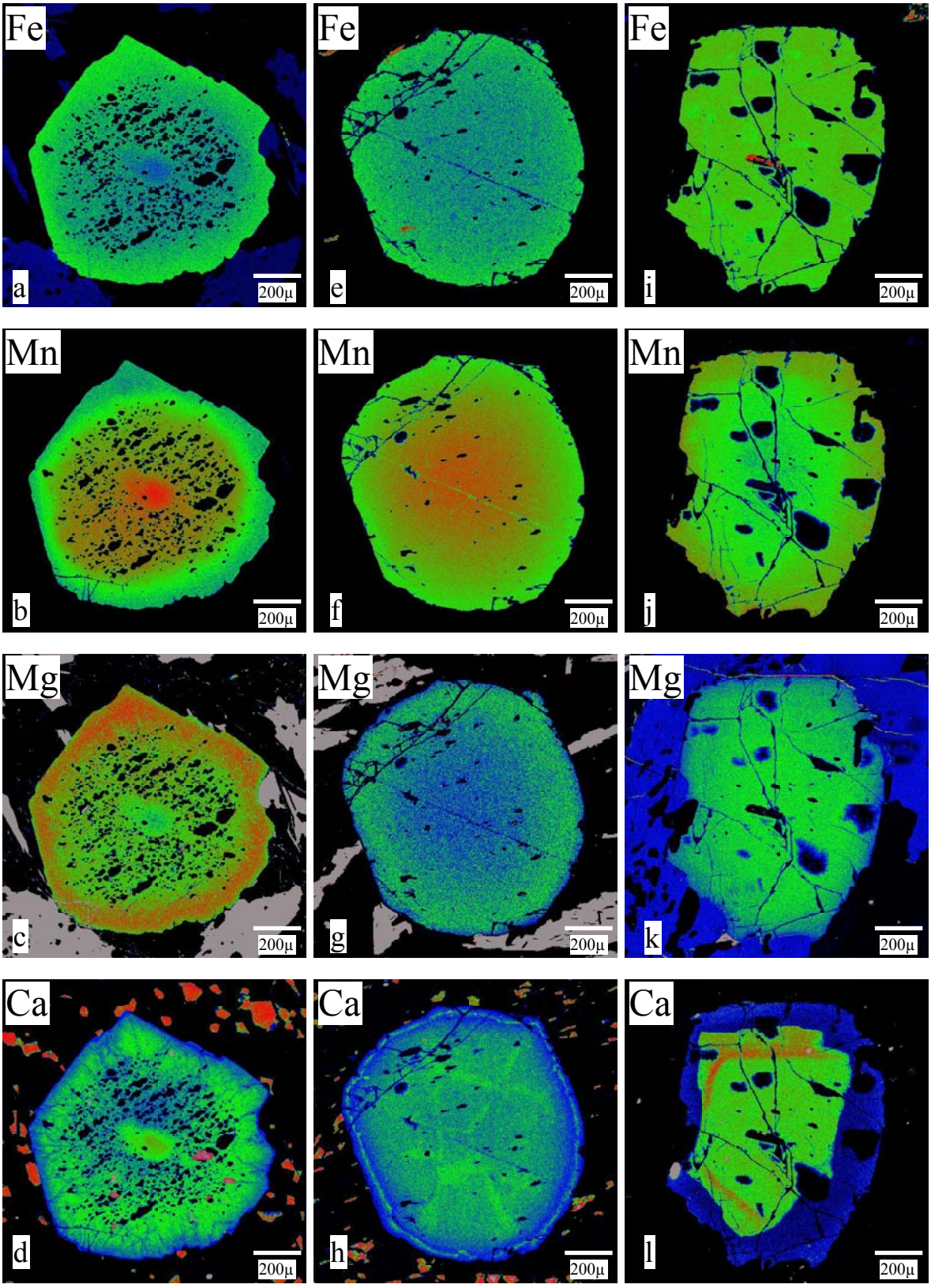
Fe
a
200µ
Fe
e
200µ
Fe
i
200µ
Mn
b
200µ
Mn
f
200µ
Mn
j
200µ
Mg
c
200µ
Mg
g
200µ
Mg
k
200µ
Ca
d
200µ
Ca
h
200µ
Ca
l
200µ

Figure 11. WDS X-ray intensity maps of a garnet in sample IS28A (a, b, c and d), sample IS77 (e, f, g and h) and in sample IS104 (i, j, k and l).

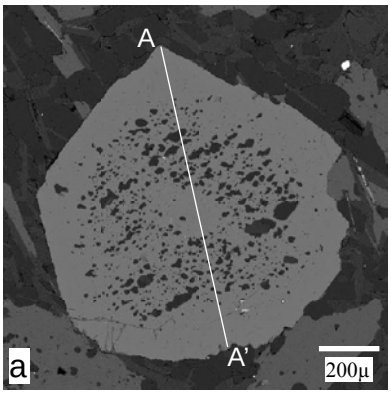
A
A'
a
200µ

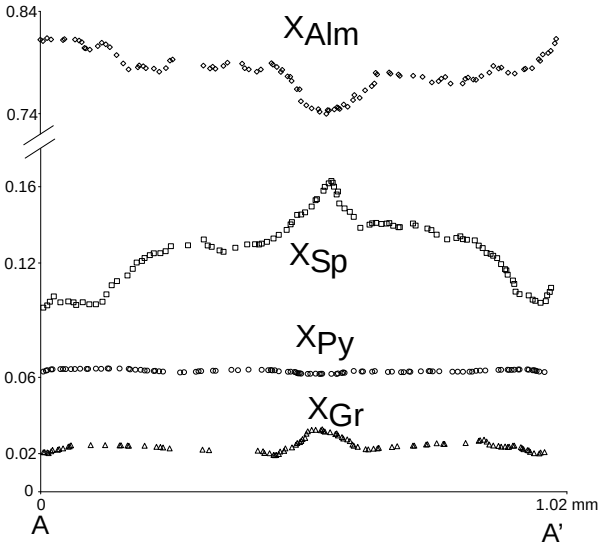
0.84
0.74
0.16
0.12
0.06
0.02
0
XAlm
XSp
XPy
XGr
0
1.02 mm
A
A'

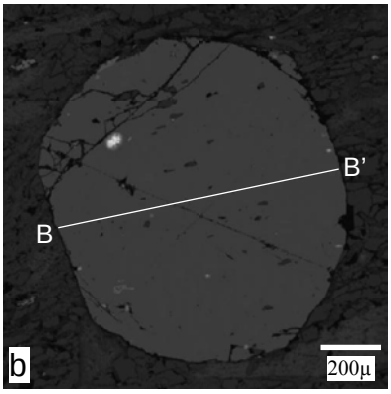
B'
B
b
200µ

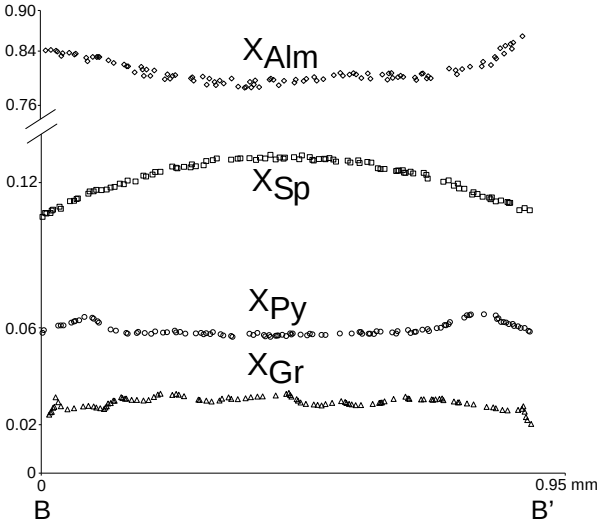
0.90
0.84
0.76
0.12
0.06
0.02
0
XAlm
XSp
XPy
XGr
0
0.95 mm
B
B'

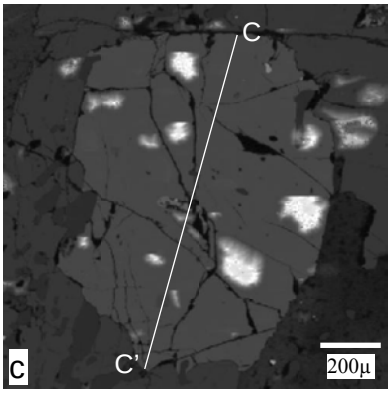
C
C'
c
200µ

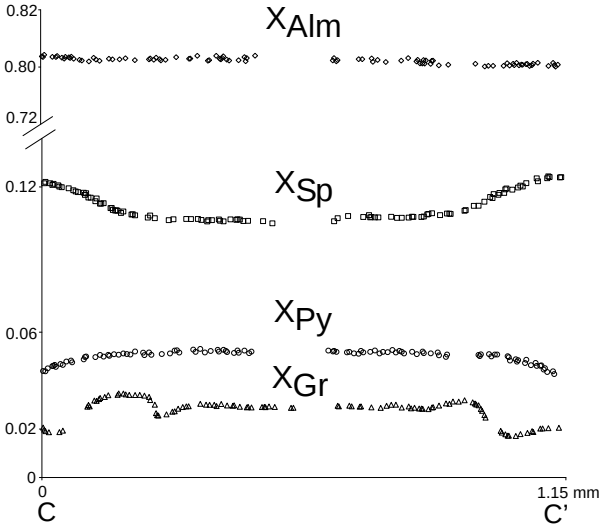
0.82
0.80
0.72
0.12
0.06
0.02
0
XAlm
XSp
XPy
XGr
0
1.15 mm
C
C'

Figure 12. Back-scattered electron images and line profile of garnet porphyroblasts from sample IS28A (a), IS77 (b) and IS104 (c).

	IS77	IS74	IS2	IS104a	IS104b
SiO_2	27.73	27.63	27.07	26.60	26.51
TiO_2	0.40	0.42	0.47	0.36	0.30
Al_2O_3	53.52	54.27	54.94	54.92	55.46
FeO	13.75	14.59	13.74	13.49	13.47
MnO	0.24	0.23	0.10	0.29	0.31
MgO	1.87	1.59	1.52	1.15	1.18
CaO	0.00	0.01	0.01	0.01	0.00
Na_2O	0.01	0.01	0.00	0.00	0.00
K_2O	0.00	0.00	0.00	0.01	0.00
Total	97.52	98.77	97.86	96.83	97.25
Si	7.722	7.625	7.508	7.455	7.398
Al(IV)	0.278	0.375	0.492	0.545	0.602
Σ(IV)	8.000	8.000	8.000	8.000	8.000
Al(VI)	17.289	17.285	17.474	17.603	17.644
Ti	0.083	0.088	0.098	0.076	0.064
Mg	0.628	0.627	0.428	0.321	0.293
Σ(VI)	18.000	18.000	18.000	18.000	18.000
Fe	3.202	3.368	3.187	3.162	3.143
Mn	0.058	0.054	0.024	0.069	0.073
Mg	0.150	0.029	0.196	0.161	0.198
Ca	0.000	0.002	0.001	0.002	0.001
Na	0.003	0.007	0.001	0.000	0.000
K	0.001	0.001	0.001	0.003	0.000
Σ(IV)	3.413	3.460	3.412	3.397	3.415
Total	29.413	29.460	29.412	29.397	29.415
Fe/Mg	4.117	5.136	5.106	6.562	6.411
X_{Fe}	0.793	0.826	0.831	0.852	0.848
X_{Mg}	0.193	0.161	0.163	0.130	0.132

a – staurolite relict from a pseudomorph
b – matrix staurolite

Table 7. Electron microprobe analysis of staurolite. Each analysis represents the average of five analytical spots.

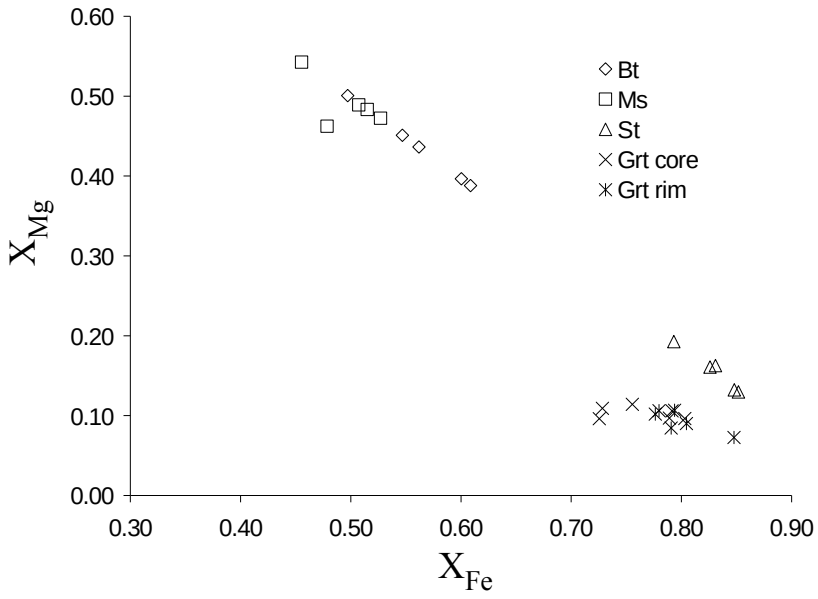

Figure 13. X_{Mg} - X_{Fe} plot for the muscovite, biotite, staurolite and garnet core and rim compositions. X_{Mg}=Mg/(Mg+Fe+Mn) and X_{Fe}=Fe/(Fe+Mg+Mn).

	IS74-core	IS74-rim	IS104a	IS104b-core	IS104b-rim
SiO_2	64.34	63.89	63.55	63.61	63.40
TiO_2	0.00	0.03	0.07	0.09	0.08
Al_2O_3	23.25	23.40	22.71	22.64	22.88
FeO	0.00	0.00	0.23	0.22	0.24
MnO	0.01	0.01	0.01	0.01	0.01
CaO	3.71	4.08	3.70	3.61	3.94
Na_2O	8.05	7.98	8.72	8.70	8.81
K_2O	0.05	0.04	0.05	0.05	0.04
Total	99.41	99.43	99.03	98.92	99.42
Si	2.834	2.818	2.824	2.828	2.812
Ti	0.000	0.001	0.002	0.003	0.003
Al	1.207	1.217	1.190	1.187	1.196
Fe	0.000	0.000	0.009	0.008	0.009
Mn	0.001	0.000	0.000	0.000	0.000
Ca	0.175	0.193	0.176	0.172	0.187
Na	0.688	0.683	0.752	0.750	0.758
K	0.003	0.003	0.003	0.003	0.003
Total	4.907	4.915	4.956	4.952	4.968
Ab	0.795	0.777	0.808	0.811	0.799
An	0.202	0.220	0.189	0.186	0.198
Or	0.003	0.003	0.003	0.003	0.003

a – plagioclase grain from a staurolite pseudomorph
b – matrix plagioclase

Table 8. Electron microprobe analysis of plagioclase.

Sample no.	IS2	IS12	IS14	IS23	IS28A	IS28B	IS71	IS74	IS77	IS93	IS94	IS95	IS102	IS104	IS-X
SiO_2	62.14	61.46	63.47	59.01	64.13	60.86	64.94	60.51	60.37	66.52	60.93	60.37	65.71	59.40	62.58
TiO_2	0.95	0.96	0.97	0.88	0.84	0.90	0.84	0.98	1.08	0.82	1.00	0.99	0.86	0.95	0.92
Al_2O_3	19.23	19.61	17.31	19.60	16.43	18.25	18.56	20.16	18.61	15.72	19.16	19.46	17.27	20.70	18.33
Fe_2O_3T	7.85	8.10	7.35	8.14	7.40	8.42	6.45	8.44	9.55	6.69	8.26	8.26	6.90	8.33	7.76
MnO	0.15	0.18	0.10	0.15	0.23	0.33	0.05	0.08	0.12	0.09	0.22	0.19	0.07	0.10	0.15
MgO	2.17	2.16	2.54	2.87	2.48	2.71	2.15	2.40	3.01	2.37	2.64	2.58	2.03	2.33	2.44
CaO	0.50	0.48	0.93	0.89	0.59	0.96	0.48	0.68	0.47	1.05	0.50	0.32	0.35	0.47	0.61
Na_2O	0.60	0.59	1.35	2.26	0.74	1.40	0.73	1.09	1.11	2.39	0.48	0.38	0.60	2.30	1.02
K_2O	4.00	3.94	3.41	3.68	4.24	3.60	3.06	3.53	3.16	2.55	4.13	4.46	3.49	3.53	3.62
P_2O_5	0.11	0.09	0.10	0.08	0.10	0.11	0.10	0.14	0.14	0.09	0.13	0.12	0.07	0.10	0.10
l.o.i.	1.66	1.56	1.54	1.63	2.03	1.67	1.67	1.63	1.63	1.20	2.04	2.02	1.82	1.51	1.71
Total	99.33	99.09	99.05	99.19	99.21	99.19	99.02	99.62	99.23	99.46	99.48	99.12	99.14	99.72	99.23

Table 9. XRF analysis of major elements from samples collected from the contact aureole of the Mooselookmeguntic pluton. IS-X represents the average composition determined as described in text.

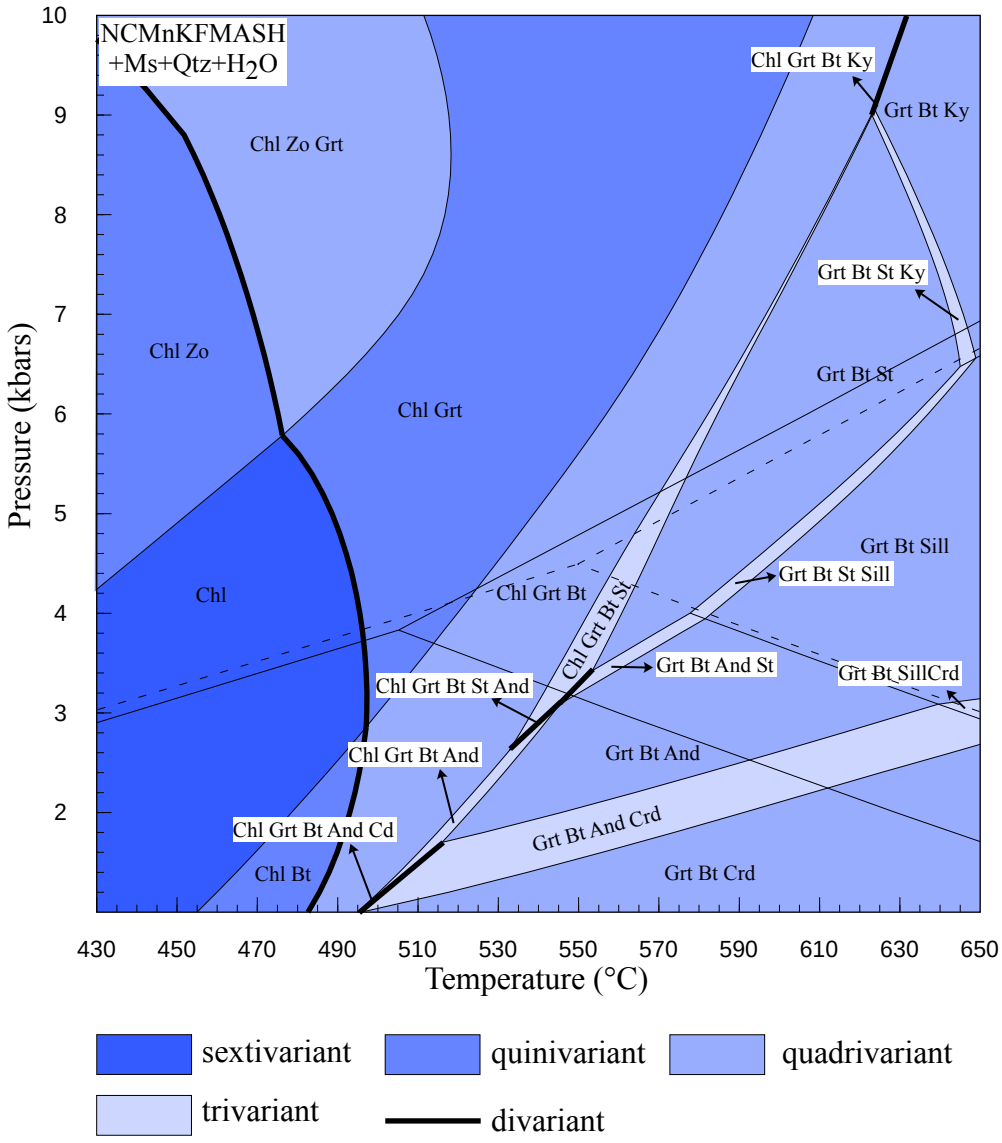

Figure 14. PT pseudosection illustrating mineral stability field calculated with the average composition determined as described in text. All assemblages contain plagioclase

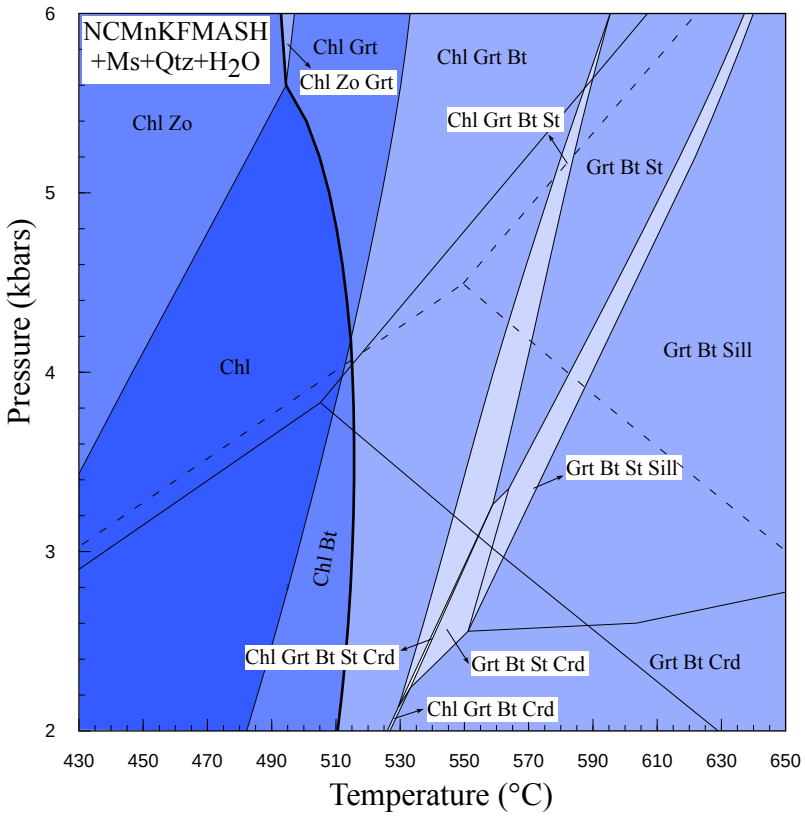

Figure 15. PT pseudosection for sample IS77 showing the stability fields for St+Crd assemblages. All assemblages contain plagioclase.

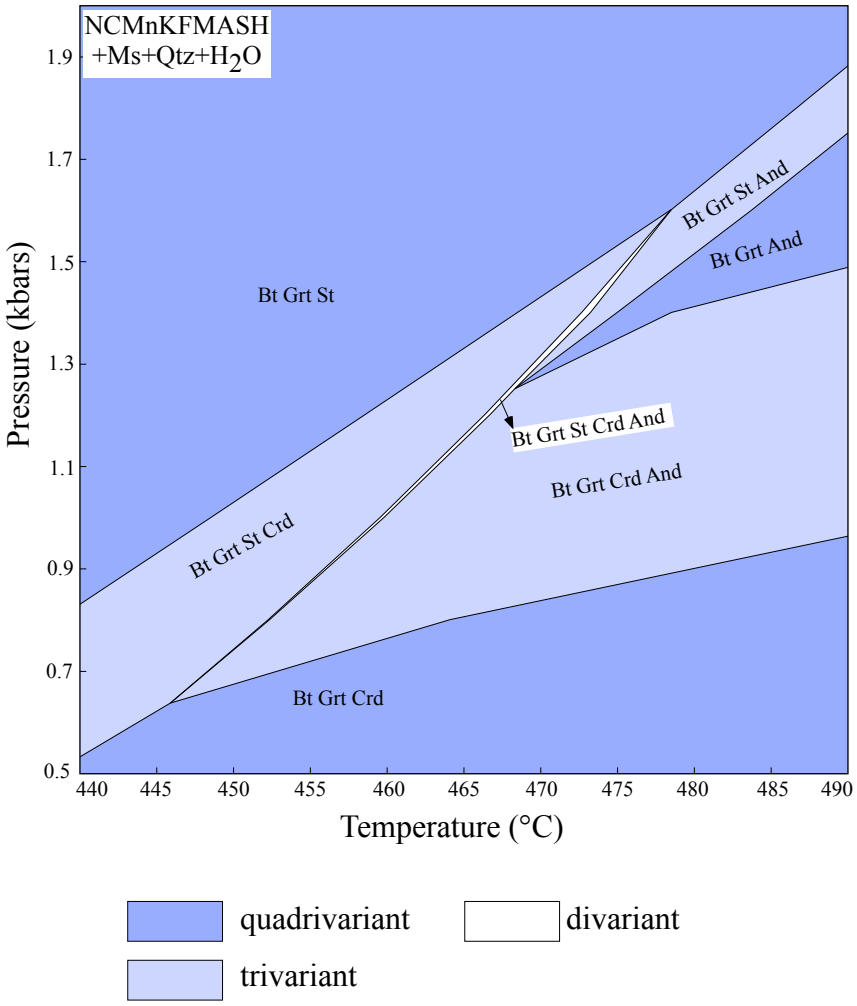

Figure 16. PT pseudosection showing the stability field calculated with Thermocalc for the assemblage Bt+Grt+St+And+Crd. All assemblages contain plagioclase.

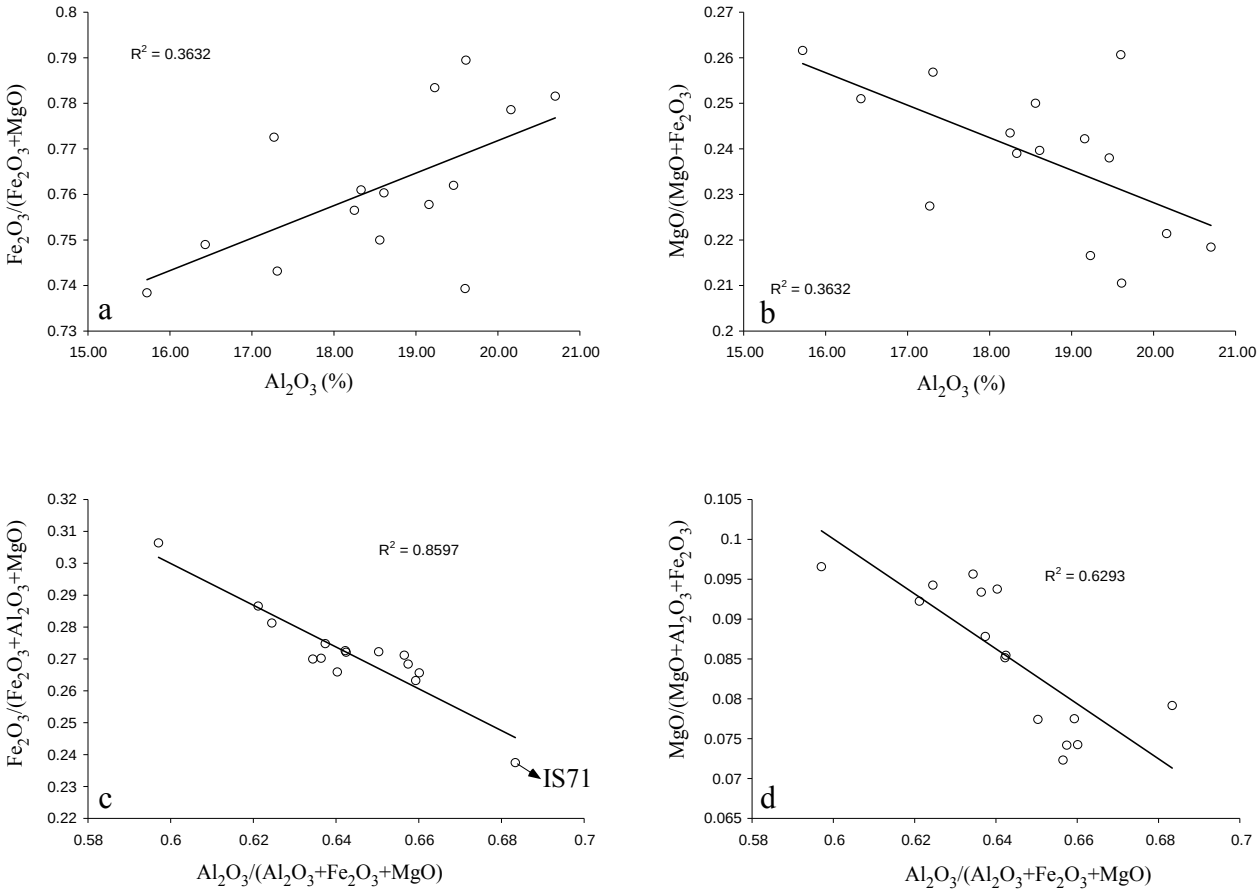

Figure 17. Series of plots showing the relationship between the bulk rock Al_2O_3 and the Fe_2O_3 (as Fe total) and MgO.

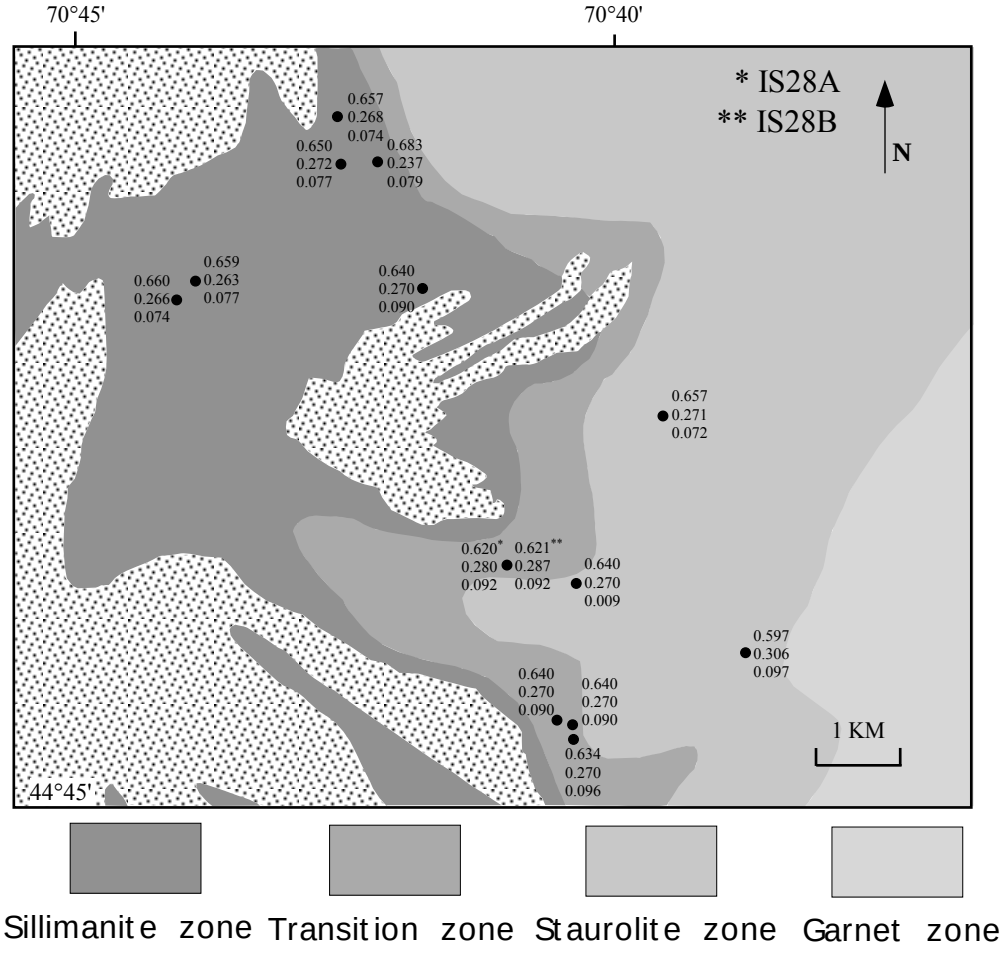

Figure 18. Simplified geological map showing how $Al_2O_3/(Al_2O_3+ Fe_2O_3+MgO)$ (top value), $Fe_2O_3/(Al_2O_3+ Fe_2O_3+MgO)$ (middle value) and $MgO/(Al_2O_3+ Fe_2O_3+MgO)$ (bottom value) varies in the field.

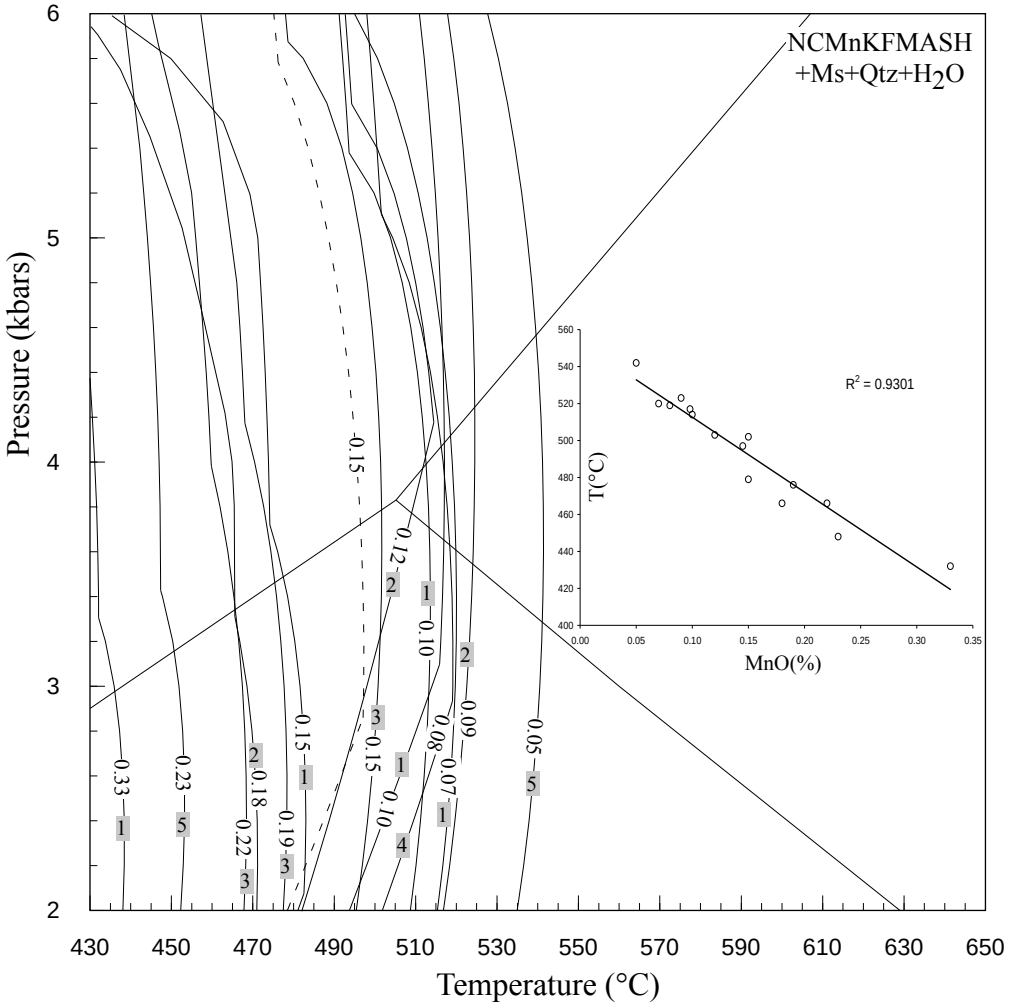

Figure 19. PT pseudosection showing how the location of garnet-in line changes with bulk MnO. At 3.3 kbars the garnet-in line (inset) is strictly dependent on the bulk MnO. Dashed line represents the average composition. Values for MnO as in Table 9. Shaded numbers (1 to 5) represent the FIA set for that specific sample.

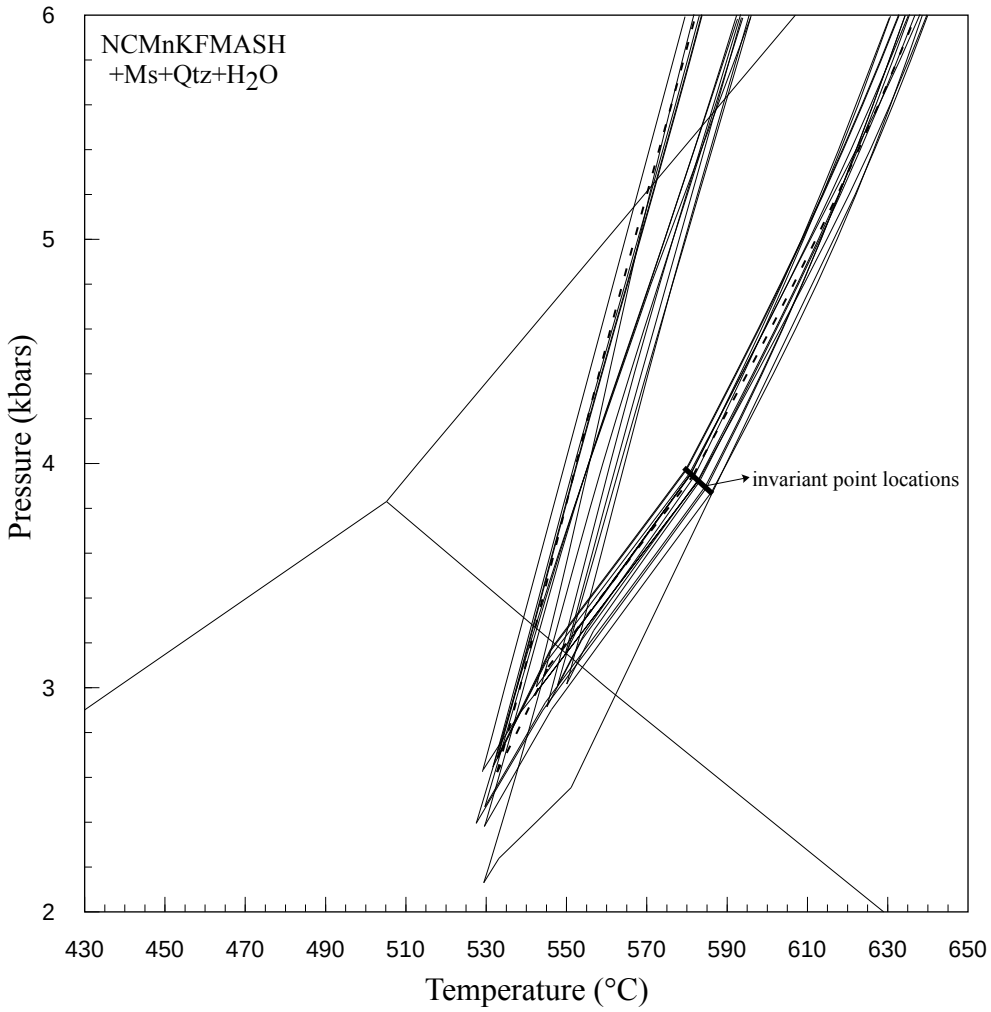

Figure 20. PT pseudosection showing the stability field for staurolite calculated for all samples. Dashed line represents the average composition. The invariant point location shows the location of the invariant point IP2 (see text for details).

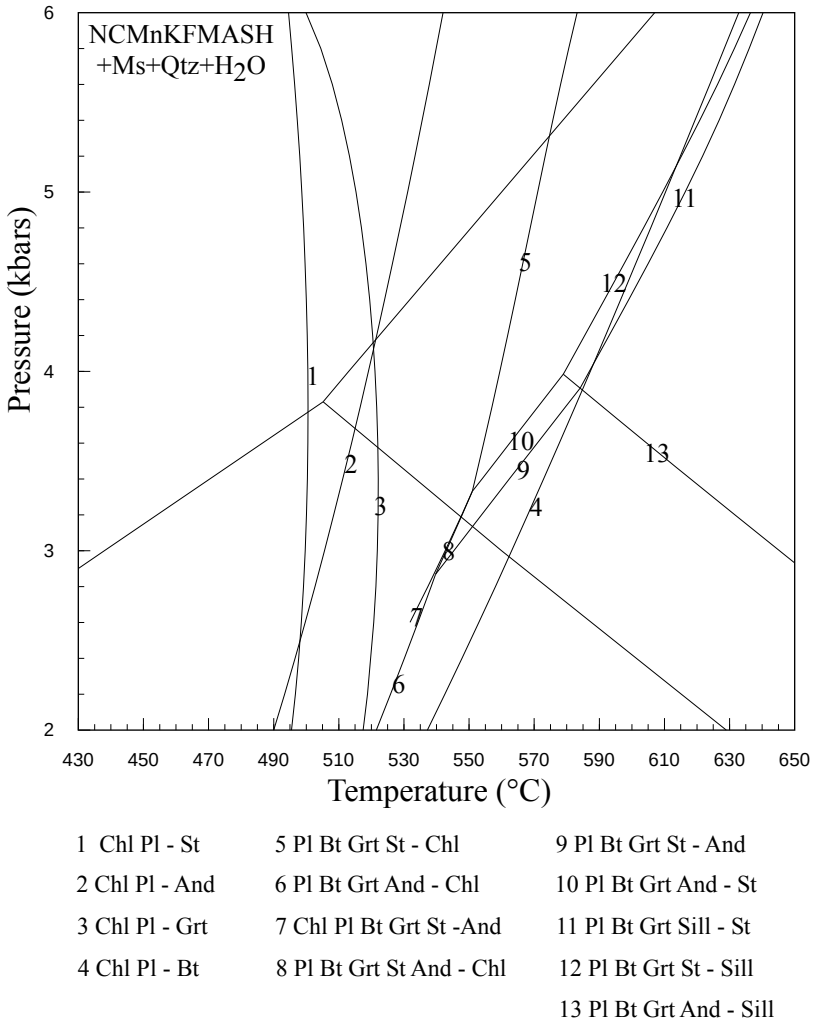

1 Chl Pl - St	5 Pl Bt Grt St - Chl	9 Pl Bt Grt St - And
2 Chl Pl - And	6 Pl Bt Grt And - Chl	10 Pl Bt Grt And - St
3 Chl Pl - Grt	7 Chl Pl Bt Grt St -And	11 Pl Bt Grt Sill - St
4 Chl Pl - Bt	8 Pl Bt Grt St And - Chl	12 Pl Bt Grt St - Sill
		13 Pl Bt Grt And - Sill

Figure 21. Pt pseudosection calculated for sample IS71 showing how the staurolite stability was shift to lower temperature by higher bulk Al2O3.

	avP	sd	avT	sd	cor	fit
lsq	4	0.3	589	12	0.2	1.64

	P	sd(P)	T	sd(T)	cor	fit	e	hat
py	3.96	0.28	590	11	0.202	1.59	-1.09	0.01
gr	3.93	0.27	590	11	0.196	1.52	1.64	0.02
alm	3.99	0.28	586	12	0.127	1.59	0.87	0.13
phl	3.95	0.28	589	12	0.2	1.63	-0.47	0
ann	3.93	0.28	590	11	0.178	1.61	-0.83	0.05
east	3.95	0.28	589	11	0.199	1.6	-0.91	0.01
mu	3.94	0.28	590	11	0.191	1.6	0.61	0.01
pa	3.99	0.29	587	13	0.035	1.62	-0.57	0.35
an	3.94	0.28	589	11	0.198	1.58	-0.78	0
ab	3.97	0.29	588	12	0.122	1.63	0.29	0.09
mst	3.89	0.22	591	9	0.187	1.26	2.67	0.03
fst	3.99	0.29	587	13	0.061	1.62	-0.5	0.21
sill	3.96	0.29	589	12	0.2	1.64	0	0
and	3.96	0.29	589	12	0.2	1.64	0	0
q	3.96	0.29	589	12	0.2	1.64	0	0
H_2O	3.96	0.29	589	12	0.2	1.64	0	0

Independent set of reactions:
and = sill
gr + 2sill + q = 3an
75an + 6mst = 8py + 25gr + 96sill + 12H_2O
75an + 6fst = 25gr + 8alm + 96sill + 12H_2O
7phl + 12sill = 5py + 3east + 4mu
ann + 2sill + q = alm + mu
3east + 6q = py + phl + 2mu
13phl + 12pa + 60sill = 5py + 13mu + 12ab + 6mst

Table 10. Average PT results calculated with the computer software Thermocalc for sample IS74. End-members abbreviations as in Thermocalc.

	avP	sd	avT	sd	cor	fit
lsq	3.9	0.2	592	10	0.193	1.34

	P	sd(P)	T	sd(T)	cor	fit	e*	hat
py	3.88	0.23	593	10	0.194	1.33	-0.37	0.01
gr	3.88	0.23	593	10	0.19	1.33	0.26	0.01
alm	3.89	0.23	592	10	0.12	1.33	0.28	0.13
mu	3.86	0.22	593	9	0.183	1.27	0.65	0.01
pa	3.94	0.23	588	10	0.027	1.25	-1.01	0.35
phl	3.87	0.23	592	9	0.193	1.3	-0.72	0
ann	3.86	0.23	593	9	0.169	1.29	-0.84	0.05
east	3.87	0.23	593	9	0.192	1.29	-0.88	0
an	3.88	0.23	592	10	0.191	1.33	-0.11	0
ab	3.91	0.23	590	10	0.115	1.3	0.5	0.09
mst	3.83	0.18	594	7	0.181	0.93	2.42	0.03
fst	3.88	0.24	593	11	0.049	1.33	0.11	0.21
sill	3.88	0.23	592	10	0.193	1.34	0	0
and	3.88	0.23	592	10	0.193	1.34	0	0
q	3.88	0.23	592	10	0.193	1.34	0	0
H_2O	3.88	0.23	592	10	0.193	1.34	0	0

Independent set of reactions
and = sill
gr + 2sill + q = 3an
7phl + 12sill = 5py + 4mu + 3east
3east + 6q = py + 2mu + phl
17py + 25mu + 6mst = 25phl + 96sill + $12H_2O$
ann + 2sill + q = alm + mu
25py + 25mu + 6fst = 8alm + 25phl + 96sill + $12H_2O$
12pa + 13phl + 60sill = 5py + 13mu + 12ab + 6mst

Table 11. Average PT results calculated with the computer software Thermocalc for sample IS104. End-members abbreviations as in Thermocalc

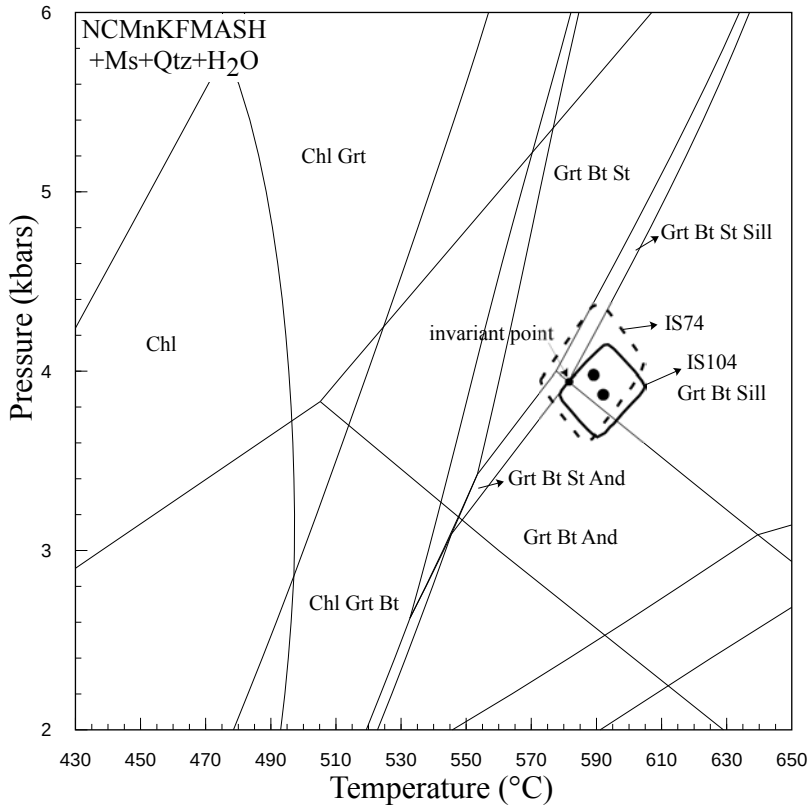

Figure 22. PT pseudosection for the average composition showing where the average PT results for sample IS74 and IS104 plot on the phase diagram.

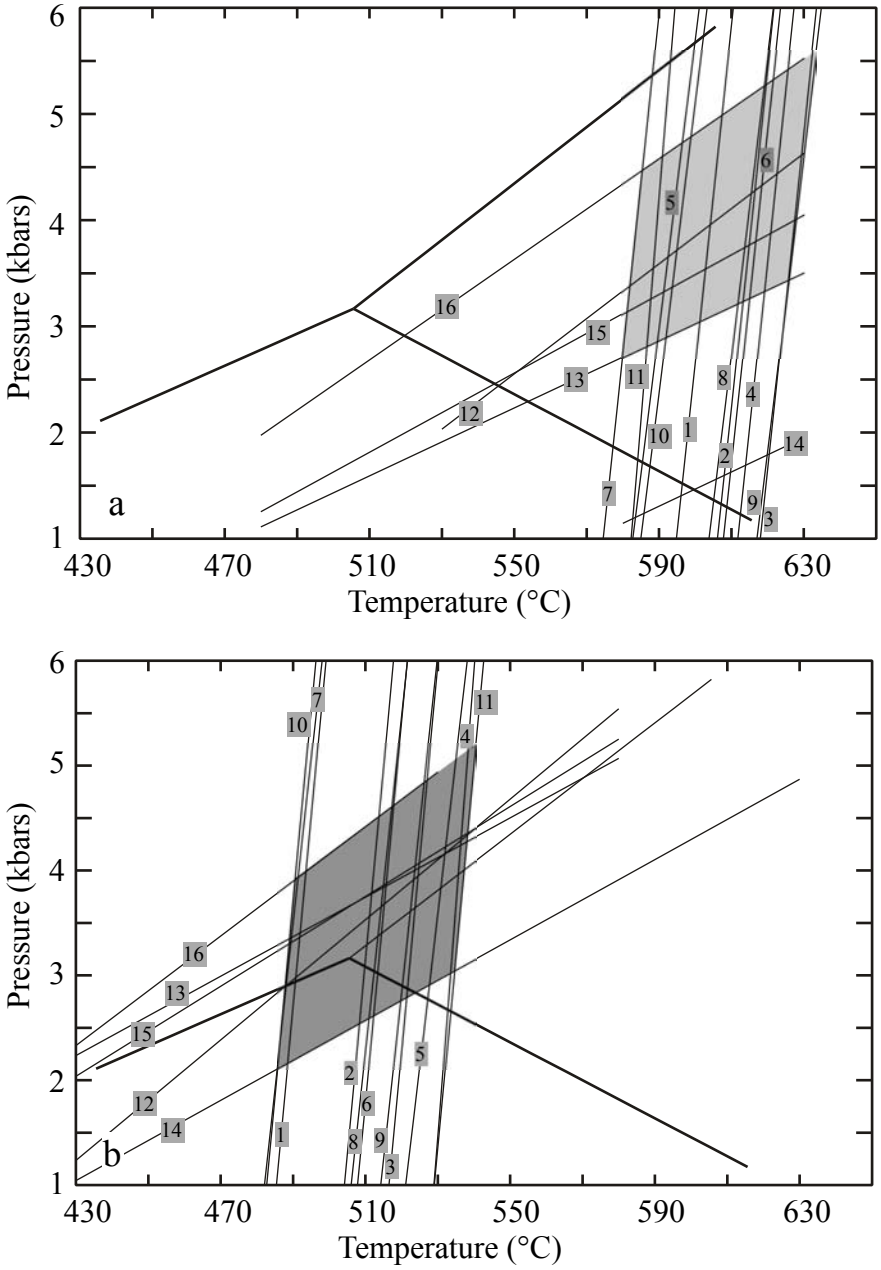

Figure 23. P-T estimates using different calibrations for conventional geothermobarometers for sample IS104 (a) and for sample IS74 (b). The calculations were carried out with the computer software GTB v.2.1 of Spear and Kohn, (http://ees2.geo.rpi.edu/MetaPetaRen/Software/GTB_Prog/GTB.html). 1-11 garnet-biotite geothermometer: 1 - Ferry and Spear (1978); 2 - Hodges and Spear (1982); 3 - Ganguly and Saxena (1984; symmetric model); 4 - Ganguly and Saxena (1984; asymmetric model); 5 - Perchuk and Lavrent'eva (1984); 6 and 7 - Indares and Martingnole (1985); 8 - Ferry and Spear (1990); 9 - Patino Douce (1993); 10- Gesman et al., (1997); 11 - Kleemann and Reinhardt (1994). 12 - 16 GASP barometer: 12 - Newton and Haselton (1981); 13 - Hodges and Spear (1982); 14 - Ganguly and Saxena (1984); 15 - Hodges and Crowley (1985); 16 - Koziol (1989).

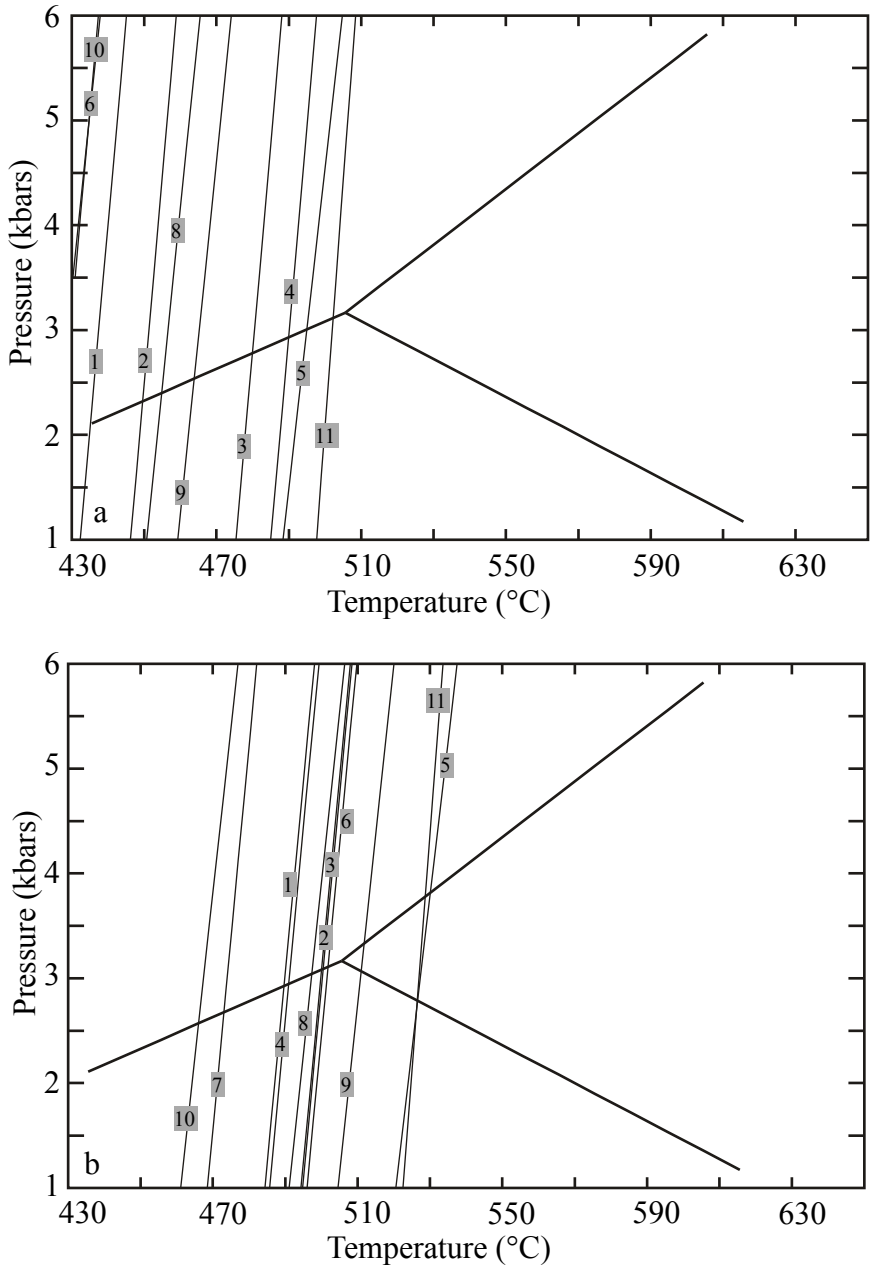

Figure 24. T estimates for sample IS2 (a) and IS77 (b) using different calibrations for conventional garnet-biotite geothermometer. The calculations were carried out with the computer software GTB v.2.1 of Spear and Kohn, (http://ees2.geo.rpi.edu/MetaPetaRen/Software/GTB_Prog/GTB.html). Calibration numbers are similar with those in Fig. 23.

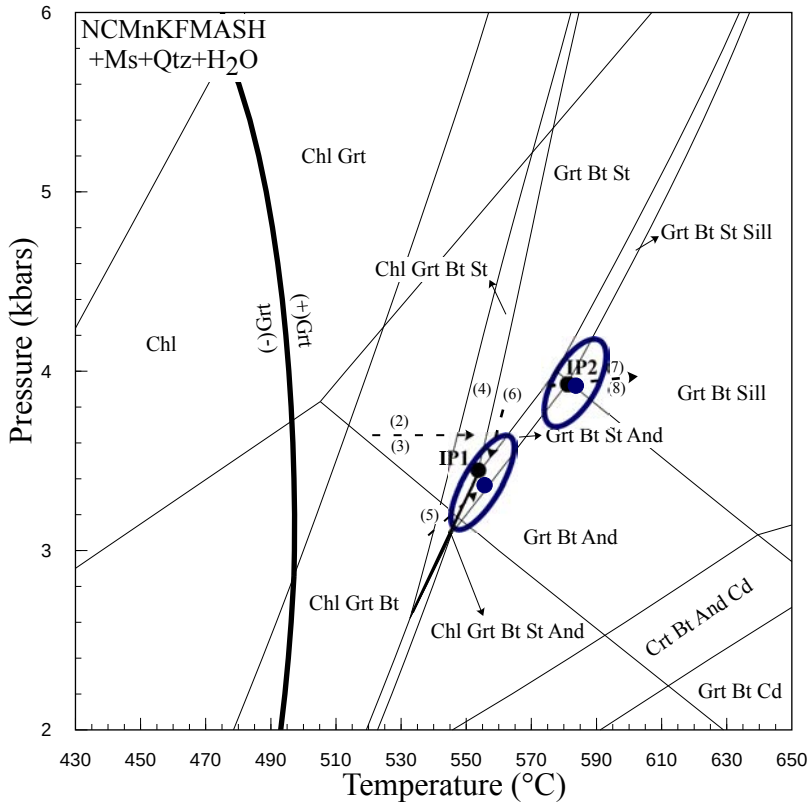

Figure 25. PT pseudosection for the average composition showing the location of the invariant points IP1 and IP2. The invariant points and their uncertainties (dark blue dots and the error ellipsoid) were plotted as the average of all the invariant points calculated for each sample with Thermocalc.

Sample no.	Pressure	sd (P)	Temperature	sd (T)	correl
IS2	3.24	0.2	551.78	7	0.773
IS12	3.23	0.2	551.63	7	0.778
IS14	3.47	0.2	559.68	7	0.786
IS23	3.49	0.2	562.4	7	0.816
IS28A	3.38	0.2	555.86	7	0.788
IS28B	3.48	0.2	560.1	7	0.817
IS71	3.42	0.2	553.2	7	0.754
IS74	3.28	0.2	555.22	7	0.783
IS94	3.51	0.2	554.19	7	0.742
IS95	3.44	0.2	552.41	7	0.738
IS102	3.34	0.2	551.15	7	0.734
IS104	3.22	0.2	550.39	7	0.761
IS-X	3.42	0.2	553.43	7	0.742

Table 12. PT results calculated with Thermocalc for the invariant point IP1. See text for details.

Sample no.	Pressure	sd (P)	Temperature	sd (T)	correl
IS2	3.9	0.2	584.61	7	0.573
IS12	3.89	0.2	584.85	6	0.581
IS14	3.92	0.2	582.84	7	0.579
IS28A	3.954	0.2	580.93	6	0.586
IS28B	3.94	0.2	581.82	6	0.618
IS23	3.92	0.2	583.26	6	0.605
IS71	3.93	0.2	582.65	7	0.551
IS74	3.87	0.2	586.25	7	0.568
IS94	3.97	0.2	579.81	7	0.54
IS95	3.96	0.2	580.64	7	0.532
IS102	3.92	0.2	583.06	7	0.513
IS104	3.9	0.2	584.65	7	0.525
IS-X	3.94	0.2	581.5	7	0.53

Table 13. PT results calculated with Thermocalc for the invariant point IP2. See text for details.

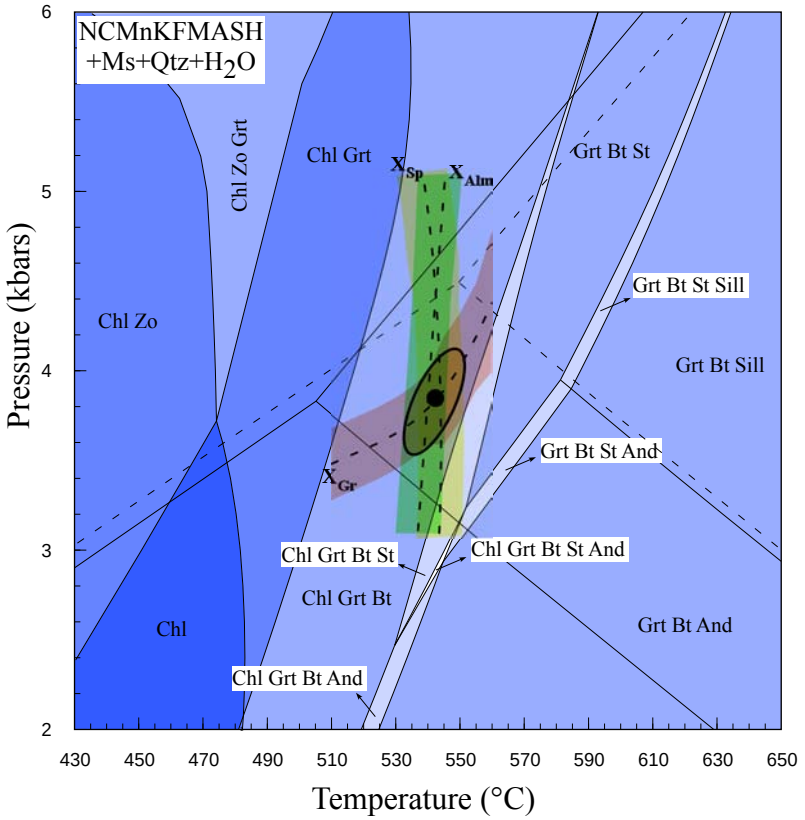

Figure 26. PT pseudosection and garnet-core isopleths for sample IS2 (FIA1).

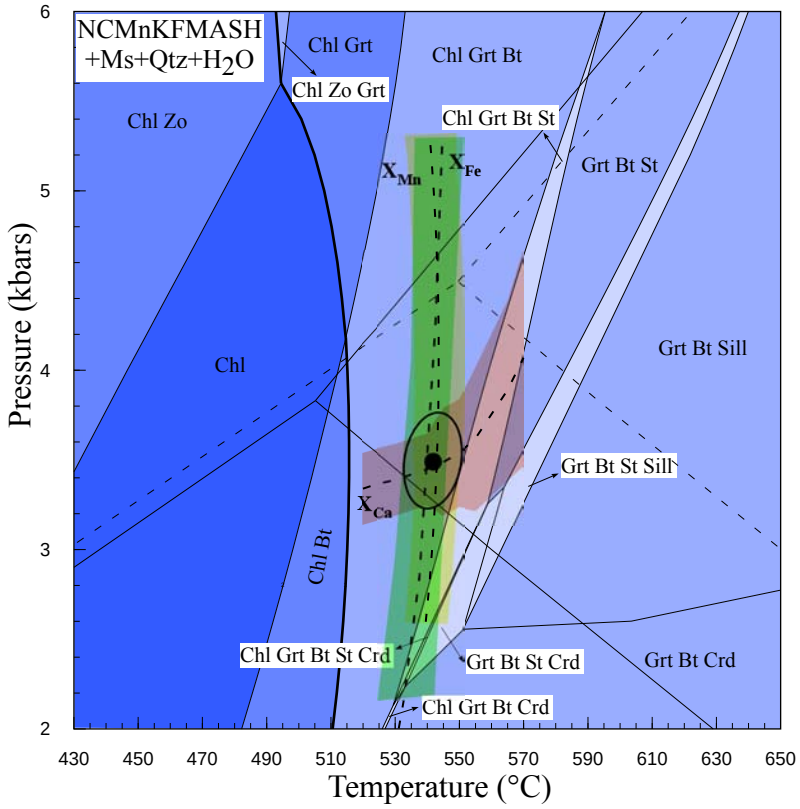

Figure 27. PT pseudosection and garnet-core isopleths for sample IS77 (FIA2).

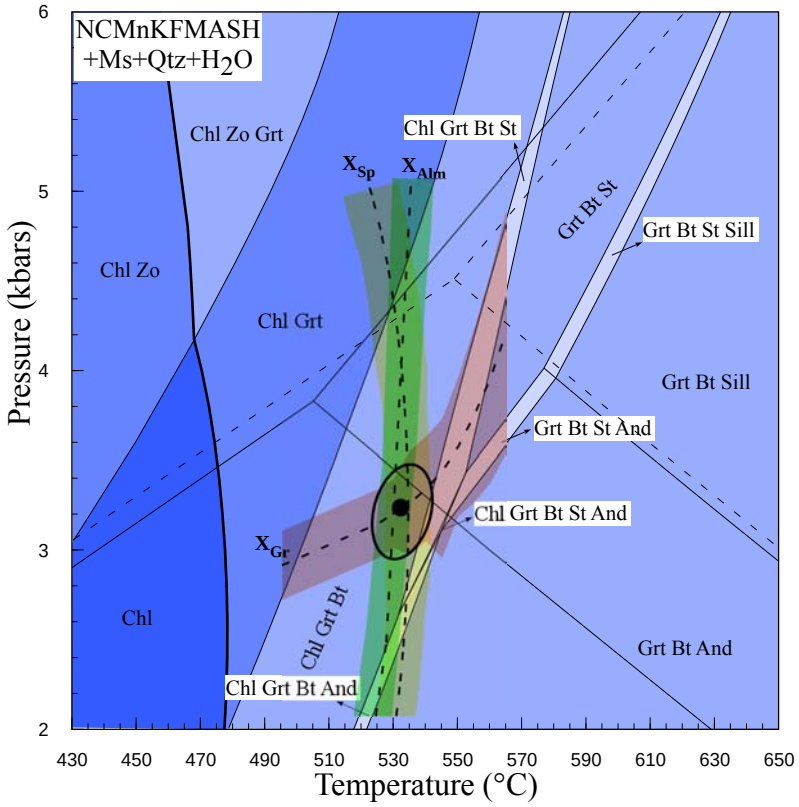

Figure 28. PT pseudosection and garnet-core isopleths for sample IS95 (FIA3).

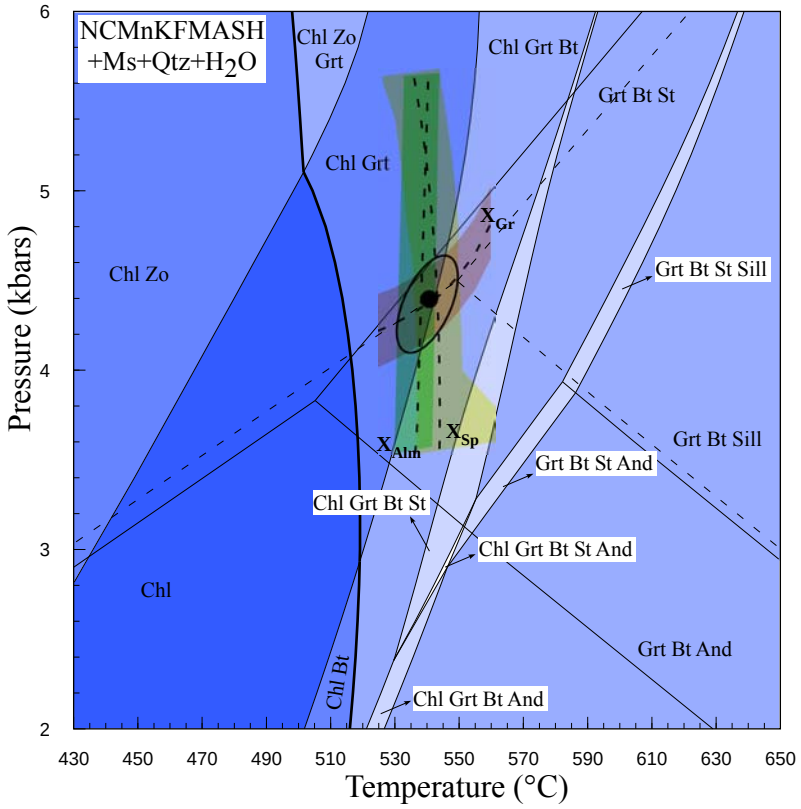

Figure 29. PT pseudosection and garnet-core isopleths for sample IS74 (FIA4).

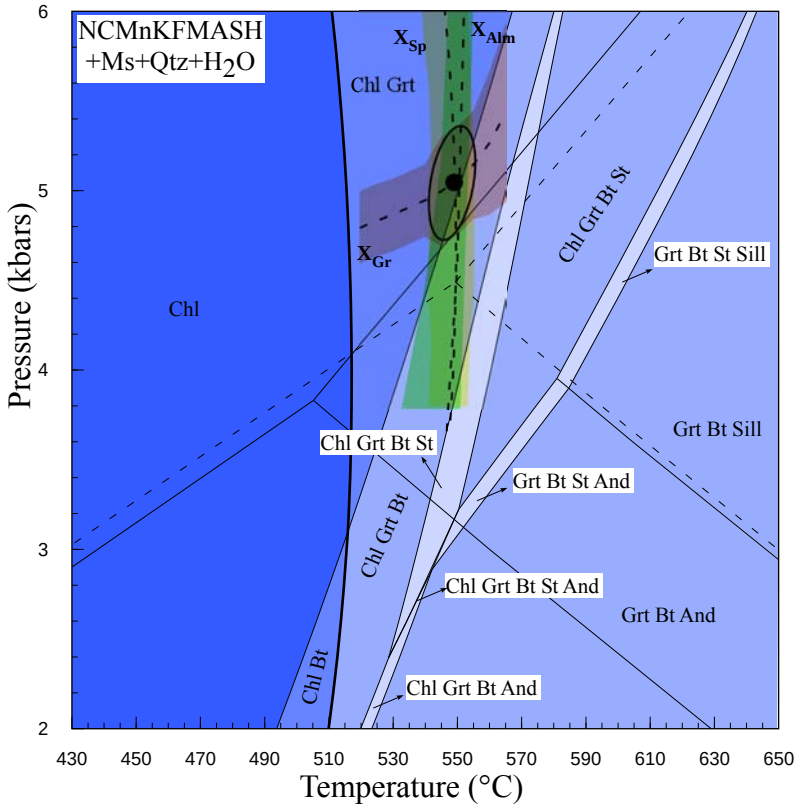

Figure 30. PT pseudosection and garnet-core isopleths for sample IS104 (FIA1).

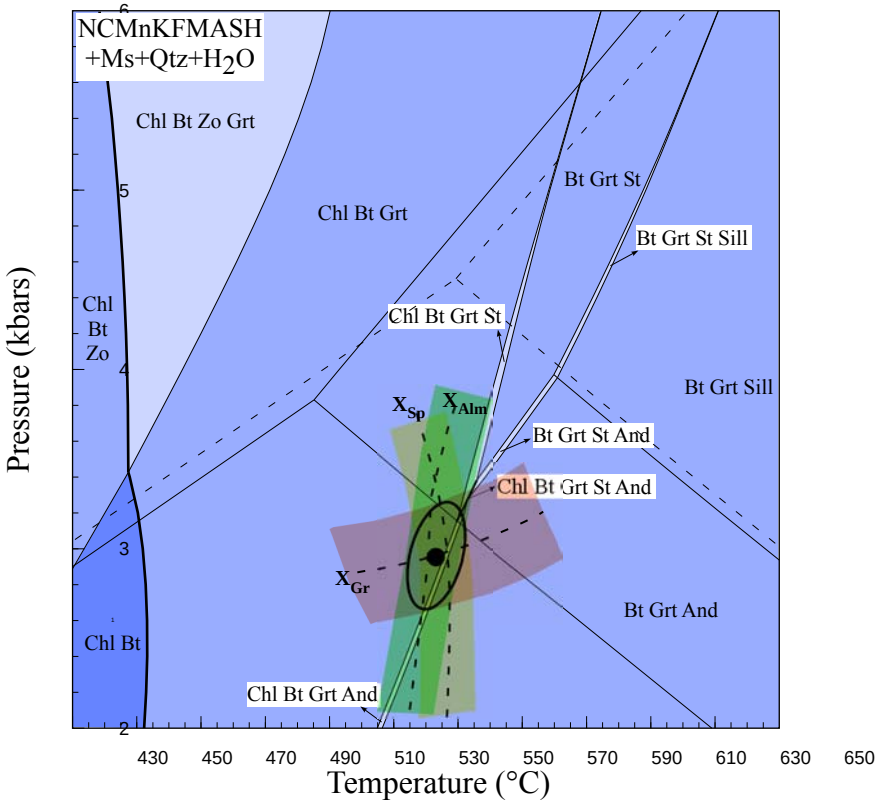

Figure 31. PT pseudosection and garnet-core isopleths for sample IS28A (FIA5).

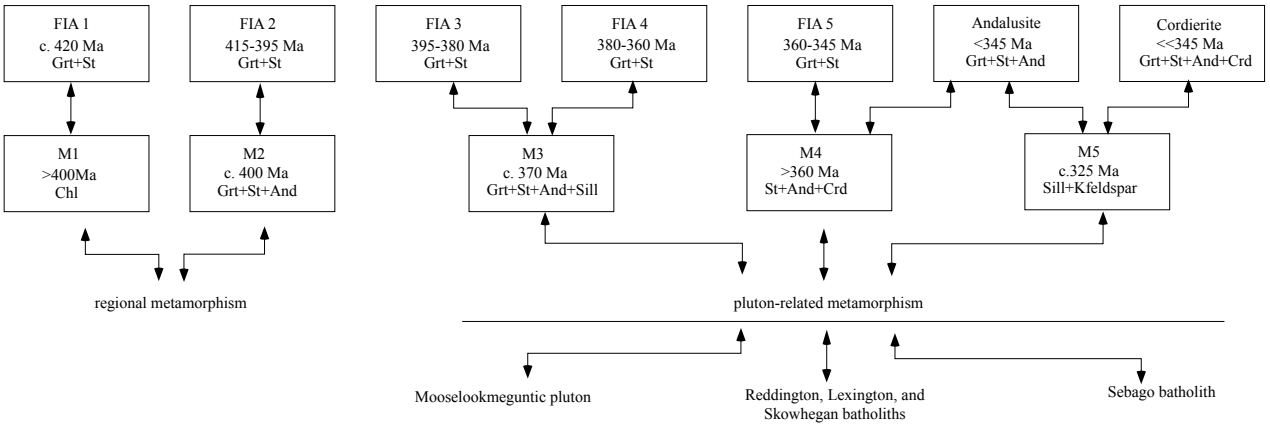

Figure 32. Schematic representation showing the possible correlation between FIA data and previous metamorphic history in the region. See text for details.

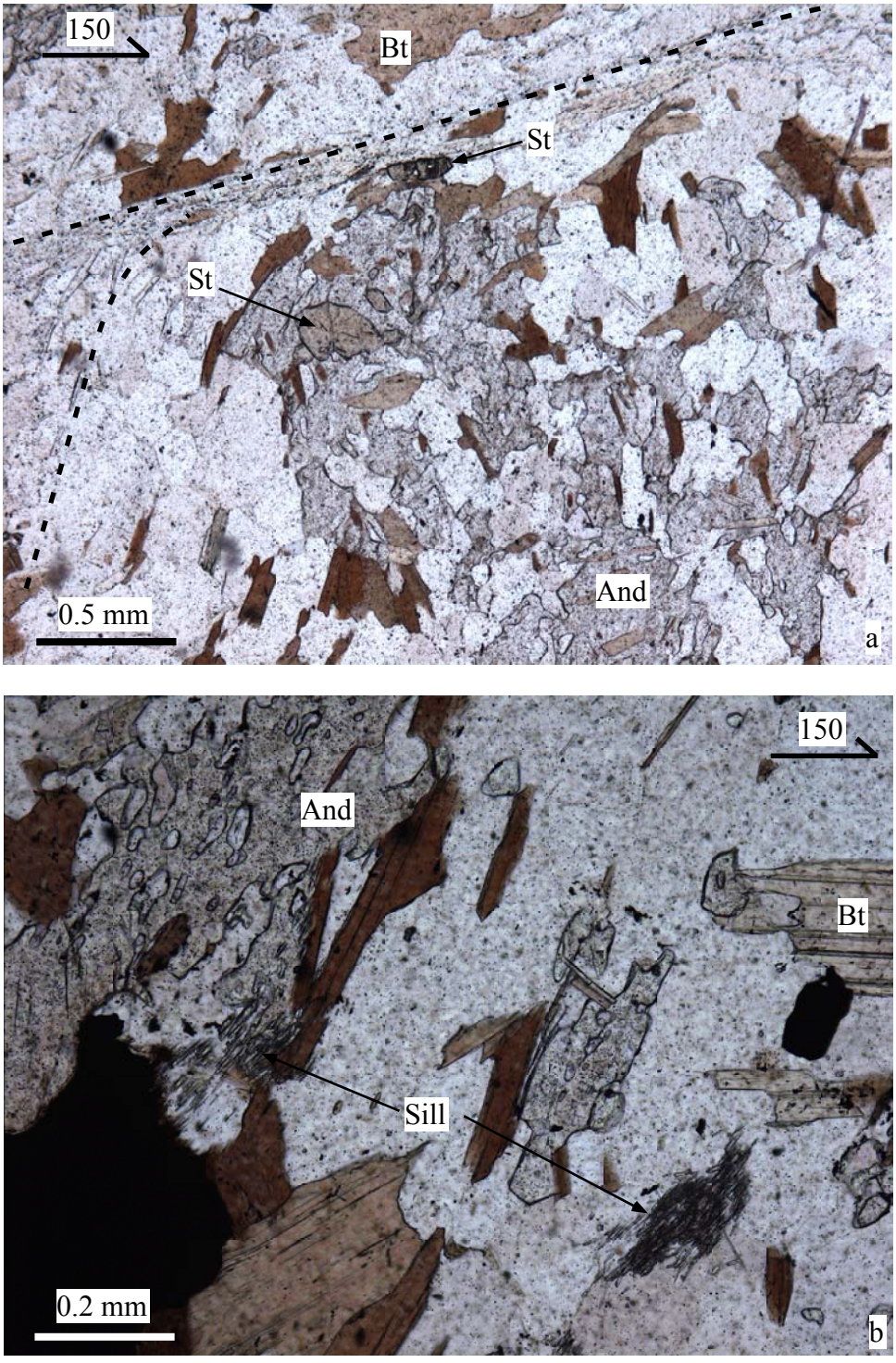

Figure 33. Photomicrographs from sample IS71 showing late andalusite. a) andalusite porphyroblasts replacing FIA5 staurolite porphyroblasts. Note the cleavage defined by muscovite that wraps around the andalusite suggesting that deformation continued after andalusite growth. b) small grains of prismatic sillimanite that nucleated in the matrix and in andalusite. Plane polarized light.

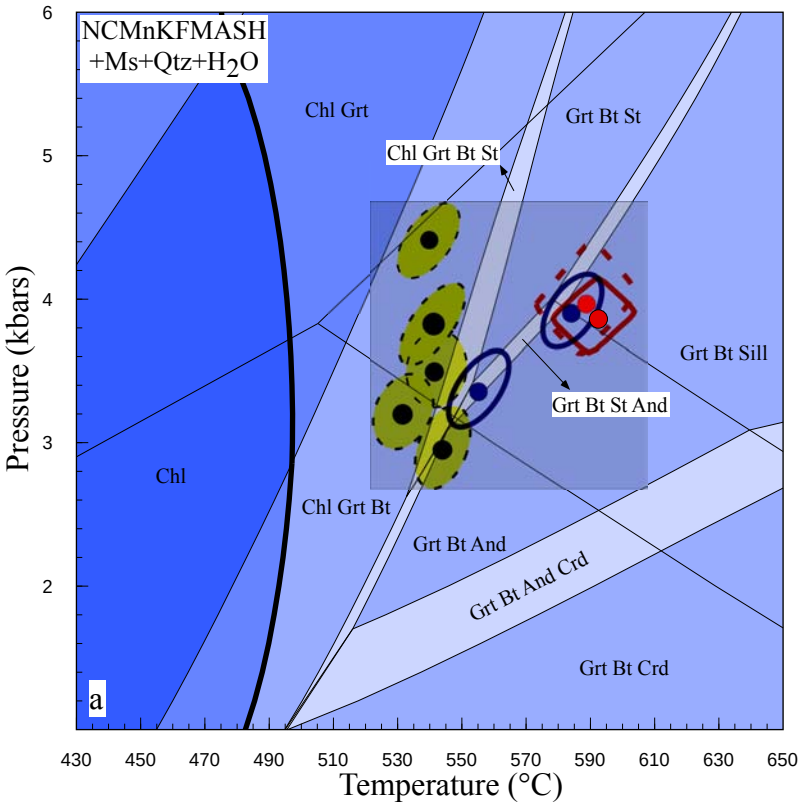
NCMnKFMASH
+Ms+Qtz+H2O
Chl Grt
Grt Bt St
Chl Grt Bt St
Grt Bt Sill
Grt Bt St And
Chl
Chl Grt Bt
Grt Bt And
Grt Bt And Crd
Grt Bt Crd
a
Pressure (kbars)
Temperature (°C)

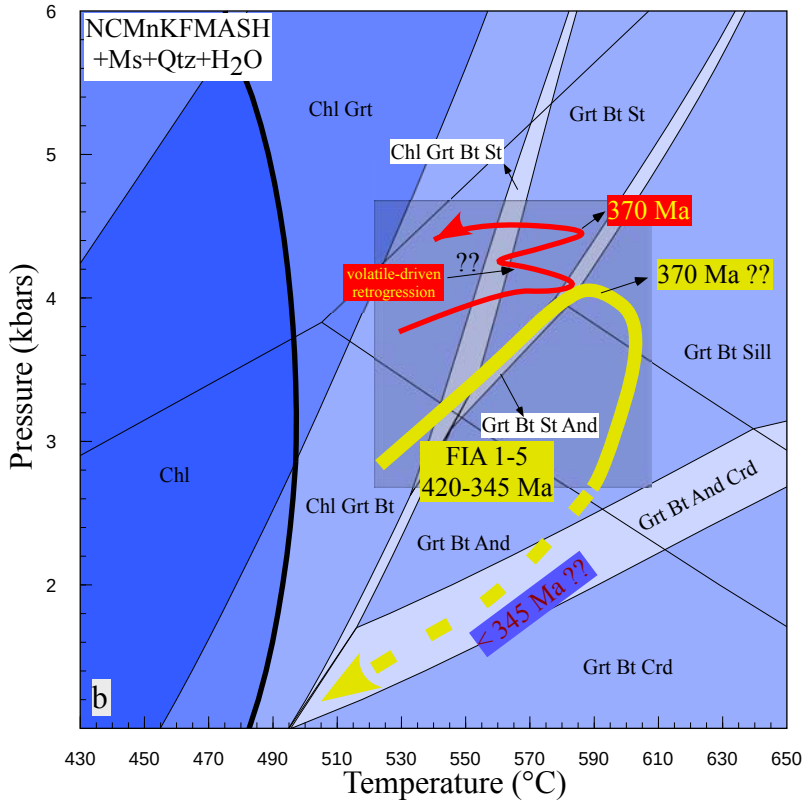
NCMnKFMASH
+Ms+Qtz+H2O
Chl Grt
Grt Bt St
Chl Grt Bt St
370 Ma
??
volatile-driven
retrogression
370 Ma ??
Grt Bt Sill
Grt Bt St And
FIA 1-5
420-345 Ma
Chl
Chl Grt Bt
Grt Bt And
Grt Bt And Crd
~345 Ma ??
Grt Bt Crd
b
Pressure (kbars)
Temperature (°C)

Figure 34. PT pseudosection calculated for the average composition showing the location of different PT estimates (a) and the possible PT paths (b) in the contact aureole of the Mooselookmeguntic pluton. a) The black dots with yellow ellipse show the location of garnet core isopleths for the five FIA sets; the dark blue dots with the blue error ellipse show the locations of the invariant points IP1 and IP2; the red dots with red error ellipse show the location of peak metamorphic conditions determined for sample IS104 (continuous line) and sample IS74 (dashed line). b) The red colored PT path after Johnson et al., (2003); the yellow colored PT path - this study.

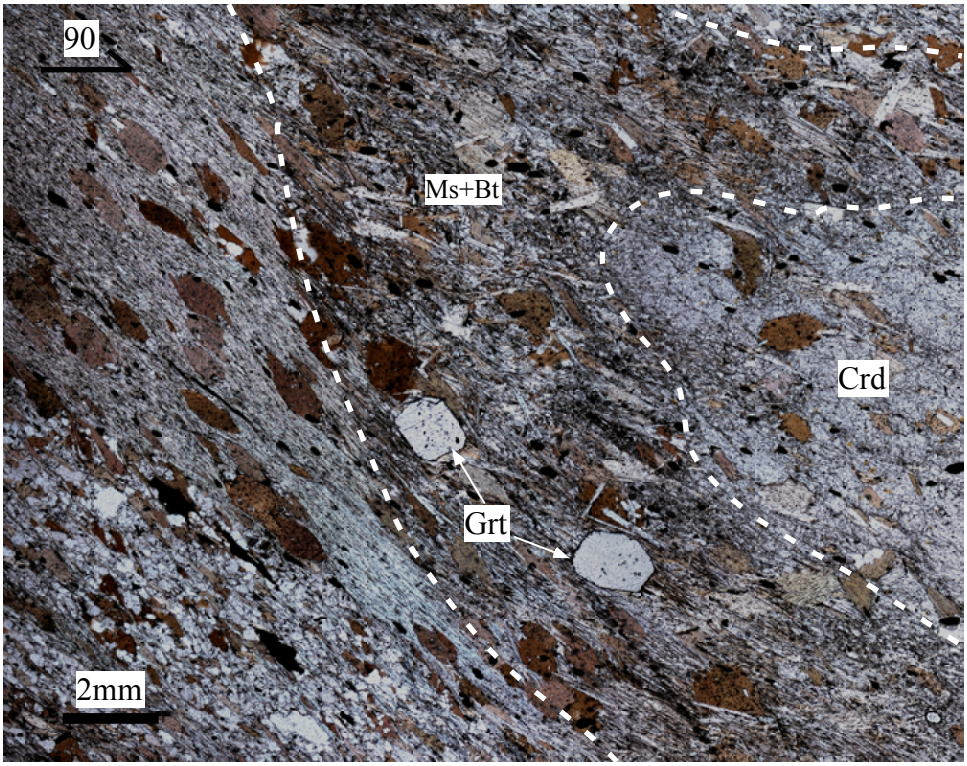

Figure 35. Photomicrograph from sample IS90 shows cordierite porphyroblasts breaking down to biotite and muscovite. Note the presence of porphyroblastic biotite inside the cordierite porphyroblasts, in the reaction rim that surrounds the cordierite porphyroblasts and in the matrix. The two garnet porphyroblasts located in the reaction rims have almost euhedral shapes. Plane polarized light.

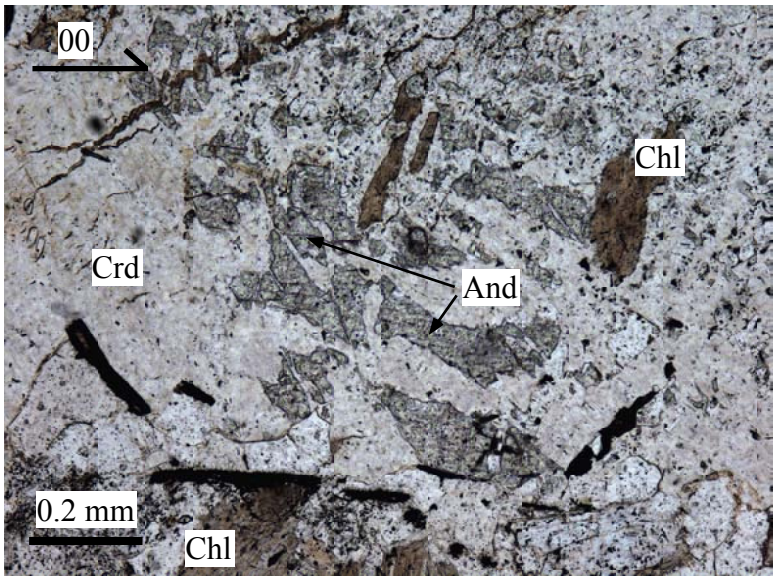

Figure 36. Photomicrograph from sample IS1 collected from about 2 km north of the area shown in Fig. 2. This photomicrograph shows andalusite relicts in a cordierite porphyroblast suggesting that decompression took place before retrogression occurred. Cordierite was partly replaced by chlorite. Plane polarized light.